**TECHNISCHE UNIVERSITÄT MÜNCHEN (TUM)**

Fakultät für Medizin

Institut für Medizinische Mikrobiologie, Immunologie und Hygiene

# Optimization of chimeric antigen receptor (CAR) therapy

Simon Paul Fräßle

Vollständiger Abdruck von der Fakultät für Medizin der Technischen Universität München zur Erlangung des akademischen Grades eines Doktors der Naturwissenschaften (Dr.rer.nat.) genehmigten Dissertation.

Vorsitzender: Prof. Dr. Ulrike Protzer

Prüfer der Dissertation: 1. Prof. Dr. Dirk H. Busch

2. Prof. Dr. Rudi F. Vogel

Die Dissertation wurde am 26.06.2020 bei der Technischen Universität München eingereicht und durch die Fakultät für Medizin am 06.10.2020 angenommen.

All truths are easy to understand once they are discovered.

the point is to discover them

*Galileo Galilei*

This thesis is dedicated to my family.

## Contributions to the field:

- Mulazzani M, **Fräßle SP,** von Mücke-Heim I, Langer S, Zhou X, Ishikawa-Ankerhold H, Leube J, Zhang W, Dötsch S, Svec M, Rudelius M, Dreyling M, von Bergwelt-Baildon M, Straube A, Buchhol VR, Busch DH, von Baumgarten . " Long-term in vivo microscopy of CAR T cell dynamics during eradication of CNS lymphoma" PNAS Nov 2019, 116 (48) 24275-24284; doi: 10.1073/pnas.1903854116

- Festag MM, Festag J, **Fräßle SP**, Asen T, Sacherl J, Schreiber S, Mück-Häusl MA, Busch DH, Wisskirchen K, Protzer U. „Evaluation of a fully human, hepatitis B virus-specific chimeric antigen receptor (CAR) in an immunocompetent mouse model "Mol Ther. 2019 Feb 10. pii: S1525-0016(19)30042-5. doi: 10.1016/j.ymthe.2019.02.001.

- Mohr F, Przibilla S, Leonhardt F, Stemberger C, Dreher S, Müller TR, **Fräßle SP**, Schmidt GP, Kiene ML, Stadler H, Busch DH., „Efficient immunoaffinity chromatography of lymphocytes directly from whole blood." Sci Rep. 2018 Nov 13;8(1):16731. doi: 10.1038/s41598-018-34589-z.

- Paszkiewicz PJ*, **Fräßle SP***, Srivastava S, Sommermeyer D, Hudecek M, Drexler I, Sadelain M, Liu L, Jensen MC, Riddell SR, Busch DH. „Targeted antibody-mediated depletion of murine CD19 CAR T cells permanently reverses B cell aplasia." J Clin Invest. 2016 Nov 1;126(11):4262-4272.

  *contributed equally

- Busch DH, **Fräßle SP**, Sommermeyer D, Buchholz VR, Riddell SR. „Role of memory T cell subsets for adoptive immunotherapy." Semin Immunol. 2016 Feb;28(1):28-34.

## Posters presented on international congresses

- **Simon P. Fräßle***, Cassie Chou*, Reed M. Hawkins, Rachel N. Steinmetz, Tinh-Doan Phi, Dirk H. Busch, Takahiro Miyazaki, Mario Marcondes, Stanley R. Riddell, Cameron J. Turtle "Effects of NKTR-255, a polymer conjugated human IL-15, on efficacy of CD19 CAR T cell immunotherapy in a preclinical lymphoma model." **ASCO, EHA**

# Contents

# List of Figures

## Abbreviations:

| | |
|---|---|
| µF | Micro Faraday |
| Ab | Antibody |
| ABT | Antibody based therapy |
| ACT | Adoptive cell therapy |
| ADCC | Antibody dependent cellular cytotoxicity |
| AICD | Activated induced cell death |
| ALL | Acute Lymphoblastic Leukemia |
| AML | Acute myeloid leukemia |
| APC | Antigen presenting cell |
| APC | Allophycocyanin / Antigen-presenting cell |
| BBB | Blood brain barrier |
| B-cell | B-lymphocyte |
| BCMA | B cell maturation antigen |
| BCR | B cell receptor |
| BSA | Bovine serum albumin |
| CAIX | Carboxy-anhydrase-IX |
| CAR | Chimeric antigen receptor |
| CD | Cluster of differentiation |
| CDC | Complement dependent cytotoxicity |
| CEA | Carcinoembryonic antigen |
| CEA | Carcinoembryonic antigen |
| CFU | Colony forming units |
| Ch | heavy chain constant region |
| Cl | Light chain constant region |
| CLL | Chronic lymphocytic leukemia |
| CML | Chronic myelogenous leukemia |
| CMV | Cytomegalovirus |
| CR | Complete response |
| CRS | Cytokine releasing syndrome |

| | |
|---|---|
| CSF | Cerebrospinal fluid |
| CTL | Cytotoxic T lymphocyte |
| Ctx | Cetuximab |
| d | Day |
| DC | Dendritic cell |
| $ddH_2O$ | Distilled, deionized water |
| DNA | Deoxyribonucleic acid |
| dNTP | Deoxynucleoside-triphosphate |
| *E. coli* | *Escherichia coli* |
| *EBV* | *Eppstein-Barr virus* |
| ecd | extracellular domain |
| EDTA | Ethylendiaminetetraacetate |
| FACS | Fluorescence activated cell sorting |
| FcRγ | Fc receptor  chain |
| FHCRC | Fred Hutchinson Cancer Research Center |
| FITC | Fluorescein-isothiocyanat |
| fl | Full length |
| FoxP3 | Forkhead box P3 |
| GATA3 | Trans-acting T-cell-specific transcription factor |
| GvHD | Graft versus Host Disease |
| GVT | Graft versus Tumor |
| *hCMV* | *Human Cytomegalovirus* |
| HER2 | human epidermal growth factor receptor 2 |
| *HIV* | *Human Immunodeficeny Virus* |
| HLA | Human leukocyte antigen |
| HSV-tk | Herpes simplex virus thymidine kinase |
| Icas9 | Inducible caspase9 |
| IFN | Interferon |
| IFNγ | Interferon gamma |
| Ig | Immunoglobulin |
| IL | Interleukin |
| ITAM | Immunoreceptor tyrosine activatory motif |

| | |
|---|---|
| ITIM | Immunoreceptor tyrosine inhibitory motif |
| kDa | Kilo dalton |
| LB | Luria-Bertoni Medium |
| $LB_{Amp}$ | Luria-Bertoni Medium + Ampicillin |
| LCK | Lymphocyte-specific protein tyrosine kinase |
| LN | Lymph node |
| LPS | Lipopolysaccharide |
| mAb | Monoclonal antibody |
| MART1 | Melanoma antigen recognized by T cells 1 |
| MCP-1 | Monocyte chemoattractant protein-1 |
| MHC-I/II | Major histocompatibility complex class I/II |
| MSKCC, NY | Memorial Sloan- Kettering Cancer Center, New York |
| NCI | National Cancer Institute |
| NHL | Non-Hodgkin Lymphoma |
| NK cell | Natural killer cell |
| NY-ESO | New York-esophageal squamous cell carcinoma-1 |
| OD | Optical density |
| PBS | Phosphate buffered saline |
| PCR | Polymerase chain reaction |
| PE | Phycoerythrin |
| PI | Propidium iodide |
| PI3K | Phosphoinositide 3-kinase |
| PRR | Pattern recognition receptor |
| RORI | Receptor tyrosine kinase like orphan receptor 1 |
| RORγ | RAR-related orphan receptor gamma |
| rpm | Rounds per minute |
| RT | Room temperature |
| Rtx | Rituximab |
| SAE | Serious adverse events |
| scFv | Single chain variable fragment |
| SDS | Sodium dodecyl sulfate |
| ST | Streptavidin |

| | |
|---|---|
| STAT | signal transducer and activator of transcription |
| STII | StrepTag II |
| TAA | Tumor associated antigen |
| TAP | Tumor associated protein |
| T-cell | T lymphocyte |
| TCR | T cell receptor |
| tEGFR | Truncated epidermal growth factor receptor |
| TEMED | N, N, N, N'-Tetraacetylethylenediamine |
| TIL | Tumor infiltrating lymphocytes |
| TLS | Tumor lysis syndrome |
| TNF$\alpha$ | Tumor necrosis factor alpha |
| TRAIL | Tumor necrosis factor- related apoptosis inducing ligand |
| Treg | Regulatory T Cell |
| TRFM | Time-resolved fluorescence microscopy |
| Tris | Tris-(Hydroxyl-methyl-) Aminomethane |
| UPenn, PA | University of Pennsylvania in Philadelphia |
| VEGF | Vascular epithelial growth factor |
| $V_h$ | Heavy chain variable region |
| $V_L$ | Light chain variable Region |
| Ω | Ohm |

# 1 Introduction

## 1.1 T cell immunity

The innate and adaptive immune system developed during evolution in vertebrates in order to protect the host against diseases from infectious pathogens and from other noxes [1]. The adaptive immune system consists mainly of antigen-specific B and T lymphocytes (B and T cells). T cells allow responses against a vast majority of antigens from different pathogens and have the unique feature to form immunological memory that was extensively studied in infectious diseases [2]. Nowadays, it is known that T cells are not only able to eliminate pathogens but also play a crucial role in recognizing and eliminating or controlling tumor cells by targeting tumor associated antigens (TAA).

Antigens associated with specific types of tumors are often 'self-antigens' and thus expressed also on healthy cells; therefore, T cell responses against this class of TAA less effective as a result of central and peripheral immune tolerance. Central tolerance presents a fundamental impediment for the effective targeting of tumor cells, since as a consequence of central tolerance most self-reactive high-avidity TCRs are clonally deleted in the thymus, which is a potential threat to health. In addition, peripheral tolerance can suppress effector functions of T cells while recognizing the TAA at the tumor site [3]. Peripheral tolerance is mediated by regulatory T cells or inhibitory myeloid cells like macrophages, as well as by the immunosuppressive milieu within the tumor. These immunosuppressive stimuli might trigger T cells to differentiate toward an exhausted phenotype, as highlighted by the expression of inhibitory receptors, e.g. CTLA-4 and PD-1 on the surface of tumor infiltrating T cells [4]. In line with that, the use of αCTLA-4 or aPD-1 monoclonal antibodies, so-called "checkpoint inhibitors", reduce or revert the development of non-functional and exhausted T cells within the tumor microenvironment and, remarkably, the re-activated T cells elicit potent antitumor responses (Nobel Prize Medicine 2018).

Another approach to overcoming peripheral and central tolerance and to further enhance T cell functionality is the adoptive transfer of genetically engineered T cells specific for a defined TAA.

T cells expressing a tumor-specific, high avidity T cell receptor (TCR) with optimal *in vivo* functionality or a synthetic receptor which combines the specificity of an antibody with the signaling capacity of the TCR receptor (chimeric antigen receptor - CAR) were developed. The adoptive transfer of suitable T cells, isolated from a donor (allogeneic) or a patient's own (autologous) T cells, is now emerging as an effective and long-lasting therapy against cancer and infectious diseases. The so far observed beneficial clinical responses of adoptively transferred T cells could perhaps be further improved by combination with other therapies like checkpoint blockage reagents ($\alpha$CTLA-4, $\alpha$PD-1). However, the exact in vivo behavior of genetically engineered T cells is not yet well understood and has to be carefully examined. The efficacy and safety of adoptive T cell immunotherapies must be further improved as well, especially T cell function, persistence, metabolism and immune regulatory mechanisms. Finally, to prevent unexpected toxicities and long-term side effects, it will be of paramount importance to develop strategies to specifically deplete the transferred and genetically engineered cells.

## 1.2 Development of B cell malignancies & current approaches

B cell malignancies are a heterogenous group of cancers that mostly derive from developing lymphocytes. The current World Health Organization (WHO) classified lymphomas as the fifth most common cancer in North America, where 90% are of B cell origin [5]. Approximately 1.5% (leukemia) and 2.1% (lymphomas) of all men and women will be diagnosed with one of these hematological cancers at some point during their lifetime (NIH, 2012-2014). Lymphoma and leukemia can occur if B cell differentiation and activation is disrupted. In normal B cells, proliferation is activated upon the recognition of the cognate antigen via the B cell receptor (BCR). Immature B cells generate the BCR with an initial VDJ DNA rearrangement in the bone marrow (BM). Mature B cells exit the BM expressing a functional BCR. Later, upon antigen encounter in the periphery, class-switch recombination (CSR) and somatic hypermutation (SHM) occur to further improve immune response plasticity. CSR creates immunoglobulin diversity in activated B cells and SHM adapts the antibodies towards the foreign antigen. Both mechanisms are based on a high somatic mutation rates and generate DNA breaks, which can lead to oncogenic chromosomal translocations leading to lymphoid malignancies. This results in blocked

differentiation, prevents apoptosis or promotes cell proliferation. For example, SHM is typically involved in chromosomal translocation at the typical position (t (8;14)) in endemic Burkitt lymphomas.

Lymphoid malignancies are divided into leukemia and lymphoma. Leukemia develops in the bone marrow where immune cell precursors undergo malignant transformations to then enter the peripheral circulation through the bloodstream; depending on the affected lineage, it can be further classified as lymphoid or myeloid leukemia, with acute lymphoblastic leukemia (ALL) and chronic lymphocytic leukemia (CLL) being the most common. Lymphomas are cancers of the lymphatic system and can be further divided into Hodgkin lymphoma (HL) and Non-Hodgkin lymphoma (NHL); these are the most relevant ones. So far, B cell malignancies have been treated with the complete eradication of the patient's immune system – by either irradiation or chemotherapy regimens – and its replacement with hematopoietic stem cells from HLA-matched donors. This treatment is associated with severe off-target toxicities due to T cells activated unspecifically towards host tissue, resulting in the development of graft-versus-host-disease (GvHD). As a result, complete remission and long-term, relapse-free survival is rarely achieved with common therapies, although hematological malignancies are the most curable ones compared with other cancers. Differences between normal and malignant B cells help to define strategies to treat these types of cancer. In particular, specific TAAs or lineage-specific antigens (LSA), which are normally expressed on malignant B cells, represent promising targets for immunotherapeutic approaches using Chimeric antigen receptor (CAR)-modified T cells. Two prime examples are the LSA CD20 and CD19 [6]. They represent an optimal compromise since the depletion of the endogenous B cell compartment is a manageable side-effect [7]. The CAR approach combines the antigen specificity of an antibody with the ability of T cells to mediate the killing of an antigen-expressing cell. These modified T cells can home actively and specifically to the tumor site and can persist long-term as memory cells *in vivo* by generating a long-lasting antitumor response in parallel to complete eradication of $CD19^+$ B cells [8]. Impressive clinical results were reported from the National Cancer Institute (NCI), Memorial Sloan-Kettering Cancer Center, New York (MSKCC, NY), the Abramson Family Cancer Research Institute at the University of Pennsylvania in Philadelphia (UPenn, PA) and the Fred Hutchinson Cancer Research Center

(FHCRC) in Seattle. These clinical trials followed the same overall protocols: isolation of human T cells from the donor, retro- / lentiviral transduction of human T cells, and finally expansion and reinfusion of the modified CAR T cells into the patient [7]. Clinical trials show varying outcomes between different centers [9]. Among the many variables to be taken into consideration, significant differences in CAR design (single chain variable fragment (scFv) clone; CD28 or 41BB costimulatory domain), conditioning regimen, intensity and selection of chemo-sensitive patients are crucial parameters, which differ between the centers. By now, various CAR T cells specific for other B cell surface markers such as CD22, CD30 and CD33 have been generated and will be tested for their potential as therapeutic targets for hematological malignancies [10].

## 1.3 Adoptive Cell therapy

For the treatment of B cell malignancies and other severe diseases new treatments using the immune system (-or parts of it) were developed. Adoptive cellular therapy (ACT) is defined as the infusion of immune effector cells (e.g. T lymphocytes) for the treatment and/or prevention of disease or cancer. The adoptive transfer of lymphocytes was first reported in rodent animal models over 60 years ago [11, 12]. It was shown that CD4 and CD8 T lymphocytes can recognize and kill cancer cells *in vitro* and *in vivo*. The improved understanding of cell and T cell biology, especially the activation of T cells and recognition of T cell targets, was very important. Indeed, the role of certain surface molecules and downstream signal transduction pathways involved in the regulation of T cell function, survival, and identification, as well as the discovery of T cell growth factors, lead to the feasibility to expand large numbers of T cells *ex vivo* for adoptive immunotherapy [13, 14]. The earliest used form of ACT was allogeneic hematopoietic stem cell transplantation (HSCT). It could successfully be shown that it was possible to treat a broad range of hematological malignancies such as leukemia, B cell malignancies or immunodeficiencies [15]. The therapeutic principle is to eliminate the patient's immune system and cancer with an intensive and high dose chemo/radiotherapy, and to restore impaired or lost immunological functions in patients through donor bone marrow transplantation. In detail, allogeneic HSCT is the transfer of hematopoietic stem cells between genetically non-identical individuals, which introduces new sets of human leukocyte antigens (HLAa) into the patient. Full or at least partial

match of HLA alleles between donor and recipient is required to minimize graft -versus-host-disease (GvHD). To prevent graft rejection, the patient must be immunosuppressed at the time of HSCT application. All these conditioning regimens are often associated with severe side effects, such as an increased risk of infection due to an impaired immune system during the post-transplantation time [16]. The donor lymphocytes have an enormous potential for preserving the recipient's health and having a curative effect. It was shown that the donor lymphocytes can mediate a strong anti-leukemic response driven by the alloreactive donor T lymphocytes, that was described as graft-versus-leukemia-effect (GvL) [17]. However, donor lymphocyte infusions (DLI) can also cause severe and life-threatening side effects due to the occurrence of GvHD mainly affecting liver, gut, skin, lung and bone marrow [18]. As GvHD is driven by donor T cells attacking the recipient's healthy cells, depletion of donor T cells reduced the risk of GvHD but increased the risk of a tumor relapse [19]. However, DLI could achieve durable clinical responses in patients with relapses of acute or chronic leukemia [20]. Since donor T cells that mediate GvHD respond to the recipient's HLA-peptide complexes like minor histocompatibility antigens (mHAg), which differ between each individual, it was important to identify tissue specific mHAgs, which are only expressed on hematopoietic stem cells (e.g. HA-1, HA-2). Based on this finding it is possible to minimize GvHD and support the GvL effect [21]. Clinical studies showed complete remission in some patients with a lower risk of GvHD [22]. These results suggest that the use of highly specific T cells for targeted tumor therapy can circumvent alloreactivity and unspecific side effects.

### 1.3.1 **Transfer of genetically unmodified antigen-specific T cells for ACT**

The first antigen-specific T cells transferred into patients were virus specific $\alpha/\beta$ T cells against Cytomegalovirus (CMV) or Epstein-Barr virus (EBV) derived antigens. Especially in the early period after allogeneic HSCT, severe deficiencies of NK cells, antibody producing B cells, and $CD4^+$, $CD8^+$ $\alpha/\beta$ T cells occur, and patients have an increased risk of severe and recurrent virus infection. Virus progression has proven to be problematic and life-threatening in immunodeficient patients [23, 24]. Because of the high prevalence of CMV and EBV in the population (depending on the geographical region up to 60-80%), seropositive healthy donors can serve as a source for virus-specific T cells with the ability to control and/or cure the virus infection after HSCT [25]. To demonstrate the functionality of virus-specific T cells, several preclinical and clinical studies were

performed. First studies mainly focused on effector functions and mechanisms, as well as providing the host with a protective response to acute infections and requirements for long-term *in vivo* survival of virus-specific transferred cells. The persistence and memory of the transferred cells is necessary to fight and specifically eliminate virally infected cells, also in case of latent virus reactivation [26]. Clinical studies showed protective immunity to CMV and EBV of patients who received CMV- or EBV-specific T cells [27].

T cells containing the $\alpha/\beta$ TCR chains are the major antigen-specific effector cells responsible for the recognition and elimination of virus-infected cells. Isolation, selection and expansion of these cells is crucial. In most cases, PBMCs derived from healthy donors are co-cultivated with professional antigen presenting cells (APCs) such as dendritic cells, which are pulsed with a specific viral peptide (e.g. pp65 for CMV); the *ex vivo*-expanded T cells are oligoclonal after the time of expansion [28]. Direct immunomagnetic selection based on pMHC-multimer technology or IFN$\gamma$ capture assay is possible. The pMHC-multimer approach could be further improved by using the so-called Streptamer technology, in which case the pMHC-multimer can be removed from the cell surface after selection to get untouched cells for downstream applications [29]. Overall, it was shown that the transfer of virus-specific T cells can lead to persistence and protectivity in patients even at very low doses, showing the enormous potential of this approach [30]. In a prophylactic setting, virus-specific T cells showed promising results to prevent severe infections after HSCT, BMT or solid organ transplantation when administered 28-115 days after HSCT [27]. For this approach, a mixture of virus-specific T cells against different viruses, e.g. EBV, CMV and Adenovirus, could be beneficial and could be rapidly produced with peptide libraries [31]. Off-the-shelf virus-specific T cells from seropositive third-party donor banks might be an approach to provide broad, fast accessible and feasible antiviral (CMV, EBV, BK virus, HHV6, AAV) prophylaxis and protection to recipients immediately after HSCT [32]. To optimize the transfer of virus-specific T cells, low numbers of healthy donor-derived memory subsets, especially central memory T cells ($T_{CM}$), are currently explored to restore the anti-viral immunity of the patient. $T_{CM}$ are used due to their lower risk of GvHD and the capability to persist long-term in the patient. Besides memory, they can give rise to effector T cells ($T_{EFF}$) able to effectively fight viral infections [33].

### 1.3.2 **TILs**

The possibility to isolate and expand antigen-specific T cells from tumor tissues improved the field of T cell immunology. These tumor-reactive T cells are called tumor infiltrating lymphocytes (TILs) and are usually a mixture of $CD4^+$ and $CD8^+$ positive T cells isolated from the patient's tumor. First findings demonstrating that TILs can lead to tumor regression in preclinical lung and liver models [34], supported the therapeutic potential of their adoptive transfer. The principle of this approach is that TILs are resected from a patient's tumor (mainly demonstrated in melanoma), expanded *ex vivo,* and reinfused in a high dose into the patient, exploiting the capability of specific autologous antitumor reactivity. However, generating a functional TIL product is challenging. First, it is difficult to recover enough tumor-specific T cells from often heavily pre-treated patients and to *ex vivo* expand them to high numbers suitable for re-infusion. Second, isolated tumor-specific T cells with a high affinity to their TAA are very rare. They are either eliminated during thymic selection, since most TAAs are self-antigens (central tolerance) or, after successful isolation, they tend to become exhausted during the laborious cultivation [35]. Highly variable clinical results showed on the one hand the feasibility of the approach and on the other hand the need for improvement, especially of the culturing and selection of tumor-reactive TILs.

Concerning culture conditions, TILs were initially extensively expanded (about 2 weeks) with a high dose of IL-2, resulting in high cell numbers [36]. Very early studies in metastatic melanoma patients showed limited success *in vivo*, since the IL-2 expanded TILs were unselected and had a low recognition potential against the tumor cells. They exhibited an exhausted phenotype and weak persistence caused by the extensive *in vitro* culture [37]. For this reason, culture conditions were improved to retain a non-exhausted phenotype and reactivity of the TILs after long-term culture. Especially the use of IL-21 or a combination of IL-7 and IL-15 [38, 39] showed superior culture conditions – with more memory-like T cells for better persistence, tumor reactivity, and regression in preclinical models [40].

Meanwhile, improved preconditioning regimens like non-myoablative lymphodepletion (Fludarabine, Cyclophosphamide) showed a superior engraftment and persistence of adoptively

transferred TILs in preclinical models, as well as in clinical observations. Less competition with endogenous cells, improved accessibility of homeostatic gamma chain cytokines (e.g. IL-7/15) and depleted immunomodulating cells like regulatory T cells/macrophages in the recipient contributed to the improved T cell product with better persistence and partially complete tumor remissions in some treated patients [41, 42]. With total body irradiation (TBI) a clinical response rate of 49-72% in metastatic melanoma patients could be achieved and more than 13% of the patients showed complete remission over years [43]. In some patients, administered T cells represented up to 80% of the $CD8^+$ T cells in circulation months after the injection. A comparative study combining reconditioning regimens is currently ongoing and results are pending (National Cancer Institute, NCI).

Once TILs are injected into the patient, they are also exposed to peripheral tolerance mechanisms at the tumor site. Peripheral tolerance should control and prevent tissue damage by self-reactive T cells, to which TIL-derived tumor reactive T cells might – at least partially - belong. Regulatory T cells can suppress effector functions of TILs in the periphery, whereas inhibitory myeloid cells like macrophages or dendritic cells (DCs) can inactivate TILs by clonal deletion or induction of anergy. The checkpoint inhibitors mentioned above can reduce peripheral tolerance and thereby enhance anti-tumor efficacy of TILs.

TIL therapy showed outstanding clinical benefit only in metastatic melanoma patients so far, with limited efficacy in other tumor types. In summary, the broader application of TIL therapy is currently limited by several factors: I) Tumor specimens are not available in many cancers, especially in metastatic settings where biopsies (like in the brain) cannot easily be taken; II) TILs are not reliably detectable due to the low frequencies and culture conditions; III) In vitro expansion is still very labor-intensive, expensive, time-consuming, variable and hard to standardize; IV) Current culture conditions are not feasible for all patients; V) Limited and compromised tumor-specific T cell repertoires caused by central host tolerance; and VI) Functionality and phenotypic properties might be changed due to long culture conditions and may revert to an immune-suppressed state after infusion.

### 1.3.3 **Genetic engineering of T cells**

The limitations and difficulties in culturing, expanding and the accessibility of TILs for many tumors have led to the development of new ACT approached [44] by which T cells can be genetically modified to be redirected against any tumor. The development of replication-defective lenti- or retroviral vectors provided new possibilities for adoptive cell therapies [45]. The limitations of TILs could be solved by repurposed *ex vivo* genetic modification combined with optimized culture conditions [46, 47]. T cells can be easily isolated from peripheral blood and redirected towards a TAA by introducing a α/β TCR or CAR into the genome via genetic engineering [48]. Redirection of a T cell using a conventional α/β TCR is constrained by the restriction of the HLA molecule that limits the treatment only in patients with the same HLA haplotype. CARs are modular synthetic receptors which are independent of the HLA complex. They usually consist of a TAA-specific monoclonal antibody single chain variable fragment (scFv), fused via a hinge to a transmembrane domain in frame with intracellular TCR signaling domains - capable of both T cell activation and antigen-specific binding. With this strategy, it is possible to rapidly generate anti-tumor T cells with a defined phenotype and functional qualities for different cancer types to improve therapeutic value, antitumor efficacy and safety. The overall functionality of TCRs and CARs can be optimized by modifying expression levels on the cell surface, signaling domains and tuning the receptors towards optimal affinity against specific TAA. The recently described genome editing technology CRISPR/Cas9 promises to be an efficient tool for T cell engineering of TCRs and CARs. It is possible to edit T cells by homologous recombination with an insert directly targeting the TCR $\alpha$ and $\beta$ locus [49]. This way, the endogenous TCR can be replaced by a newly integrated TCR or CAR, subsequently circumventing mispairing and expression under the natural promotor and regularity controls [50, 51].

#### *1.3.3.1 TCR engineering*

Typical canonical TCRs consist out of at least six polypeptide chains ($\alpha,\beta,\gamma,\delta,\varepsilon,\zeta$) assembled on the cell surface. One approach to redirect a natural α/β T cell towards a specific TAA is to introduce new α/β genes (chains) in the target cell and re-express the rearranged α/β TCR of a defined tumor specificity capable of forming a physiological TCR-CD3 immunocomplex. The

transfer of $\alpha/\beta$ chains into T cells was pioneered by Dembic and colleagues [52]. TCR sequences are for example isolated from TILs. After *in vitro* culture with peptide pulsed APCs, TILs can be characterized with specific MHC-multimer staining, verifying their epitope specificity. As alternative, direct isolation of antigen-specific T cells (e.g. from the patients' blood) via MHC-multimer staining is possible as well. After staining, antigen-specific T cells can be sorted as single cells by flow cytometry-guided sorting (FACS). Afterwards, genes for the $\alpha/\beta$ chain can be isolated via single cell PCR [53] or by the latest technologies such as Next Generation Sequencing (NGS) [54]. Retrieved $\alpha/\beta$ chains are cloned into viral vectors, re-expressed in PBMCs and characterized *in vitro* [55]. First studies in mice showed that recombinant TCR $\alpha/\beta$ expression was sufficient to re-direct antigen-specificity [52] and cytotoxicity [44]. These pioneering results demonstrated the proof of principle that the transfer of genetically engineered T cells is feasible, but more potent and specific TCRs are needed to overcome the consequences of central tolerance on TCR affinity. Therefore, approaches have been developed to obtain rare potent and high affinity TCRs. A recent approach could isolate human specific TCRs with optimal specificity and affinity by using antigen-negative humanized mice. These mice comprise a diverse human TCR repertoire that is able to recognize antigens of human origin when introduced into the mice. After immunization with human TAAs, optimal avidity T cells arise [56]. As a result of rising numbers of therapeutically relevant TAAs, optimal and most relevant TAAs have been published and listed by the National Cancer Institute (NCI) to accelerate the clinical translation for T cell immunotherapy [8]. However, the quantity of the listed antigens must be further enlarged as new 'optimal' TAAs are left to be discovered. Optimal targets for TCR therapy should be expressed on all transformed cancer cells and absent on normal cells to prevent outgrowth of TAA negative cells and side effects, respectively.

Another important feature of TCR-transgenic T cells is the so-called TCR avidity, determined by the TCR expression level and structural affinity [57]. It was shown that TCR avidity correlates with functionality against different viruses and tumors [58]. Tumor-specific TCRs isolated from TILs usually bind self-antigens with low avidity, because of central tolerance. Thus, mutations in complementary determining regions of the $\alpha$ and/or $\beta$ chain genes have been used to enhance TCR affinity [59], generating TCRs with a significantly higher avidity compared to their natural

counterpart. However, if the avidity is too high, the T cell cannot engage several TCR:pMHCs interactions, causing prolonged contact durations, which was shown to negatively influence T cell activation, especially when the target antigen shows a low expression pattern. In contrast, too low avidity leads to a weak and shorter binding and the T cell cannot be activated. This indicates that there is a certain range of optimal affinity TCRs. Besides the influence on T cell activation, TCR affinity modifications might come with the potential risk of new undesired and unpredicted specificities.

In summary, there are still many challenges for the clinical use of TCR-engineered T cells. The isolation of suitable optimal affinity α/β chain genes from tumor-experienced and specific T cells is improving due to new techniques like NGS and single cell RNA sequencing, as well as bioinformatic tools to predict specific binding. Improvements in designing gene cassettes for improved expression or replacing the endogenous TCRs are crucial to generate highly functional T cells. The limitation that TCR-modified cells recognize the cognate peptide only when presented by the HLA molecule on the tumor cell is still a main obstacle. TAAs must be presented and processed in the tumor in a proper manner to be accessible for the TCR-engineered T cells, which are often altered by various immune evasion mechanisms of the tumor cells.

#### *1.3.3.2 Chimeric antigen receptors (CARs)*

An alternative approach is to retarget T cells with artificial synthetic receptors specific for TAAs expressed on the cell surface. The basic concept of chimeric antigen receptors was introduced by Eshhar and colleagues in 1989 [60]. T cells were equipped with a new antigen specificity without affecting their effector function. CARs can mediate antigen-specific stimulation, IL-2, IFNγ, TNFα production and target cell lysis [61]. Introduced by gene transfer into T cells, the modular structure of CARs allows the combination of antibody-like specificities with the signaling characteristics of a TCR. Since the first description of the basic concept, many groups have evaluated the possibility of redirecting T cells with TAA specific scFvs. They were fused to the TCR CD3ζ or, especially in the beginning, Fc receptor γ (FCRγ) signaling domains, which were initially termed T-bodies, chimeric TCRs or later first-generation CARs. The advantage of CARs over TCRs is that they can bind their antigen and eliminate tumor cells in an HLA independent manner. HLA downregulation and altered peptide processing escape mechanisms of the tumor, which are

common immune evasion strategies, can be overcome [62]. CAR T cells can be triggered even with a low target epitope density on the cell surface due to their high sensitivity as a consequence of the high affinity receptor. Every target epitope might serve as a potential triggering event for T cell activation. In addition, since its modular structure, each component of the CAR backbone can be further modified for optimizing T cell functionality from the extracellular recognition domain through the hinge to the intracellular activation and signaling domains.

### 1.3.4 **Overview of clinical trials of TCR and CAR-engineered T cells**

#### *1.3.4.1 TCRs*

The first clinical results with TCR-engineered T cells was described in 2006 by Morgen and colleagues. Low affinity anti-MART1 (clone DMF4) HLA-A2 restricted T cells were used to treat metastatic melanoma patients. All patients were unresponsive to previous IL-2 therapy and had a poor survival prognosis. Patients showed low response rate and poor persistence of the engineered T cells was observed (<1 year) [63]. Another trial using high affinity TCRs targeting the same antigen (MART1 clone DMF5) or tumor antigen gp-100 resulted in a response in 25% of non-responder metastatic melanoma patients. Target toxicities were observed in this trial in 29 of 36 patients, resulting in hearing loss, erythematous skin rash, vitiligo and uveitis caused by the destruction of healthy normal tissue [64]. More and more clinical trials have been conducted over the last years, many of them targeting cancer testis antigens, which might be optimal targets for ACT since they are aberrantly expressed in various tumors and only present in germ cell but not healthy tissues. A prime example is NY-ESO (New York-esophageal squamous cell carcinoma-1), expressed in 80% of synovial carcinoma and in 30-40% of breast, melanoma, urothelial, esophageal, thyroid, prostate, hepatic, neuroblastoma and gastric cancers [65]. In subsequent clinical trials at the NCI, 4 out of 6 synovial sarcoma patients and 5 out of 11 melanoma patients showed a clinical response after the transfer of affinity-enhanced TCR-engineered T cells redirected against NY-ESO-1. Remarkably no toxicities were observed [66]. Several additional clinical trials started in 2011-2014 are ongoing, targeting NY-ESO-1 or MAGE-A3 in multiple solid tumors, and expecting results in 2019-2020 (NCI). Other TCR targets are being preclinically-

clinically evaluated. The most prominent targets are WT-1 [67], MDM-2 [68], tumor suppressor gene p53 [69] and HA1-specific leukemia antigen [70].

These clinical trials showed the general feasibility of ACT using TCR-engineered T cells. Nonetheless, the localization and expression of the targets is important and decisive whether the therapy is tolerated or might results in lethal off-target events that has been described for TCRs specific for MAGE-A3 or HER-2. As demonstrated in several clinical trials, the transfer of TCR-modified T cells can be well tolerated, but expansion, persistence and safety in the patients is still very limited and must be improved to observe better antitumor activity and safety to obtain a beneficial clinical outcome of the patients. Overall, the clinical trials using TCR engineered T cells are still not very consistent between different clinical centers. Different protocols, patient recruiting criteria and pre-conditioning regimens might lead to different outcomes, while using the same (enhanced) TCR transgenic T cells. The complexity as well as the clinical protocols must be adjusted to gather consistent and comparable patient data among each clinical center.

#### *1.3.4.2 CARs*

The clinical evaluation of CAR T cell-based ACT has exploded over the last years. Currently there are 227 open trials listed on the clinicaltrials.gov website (March 2020) that are recruiting for anti-CD19 CAR therapy with various CAR constructs. Most of them are recruiting patients with B cell malignancies and target the CD19 surface molecule, which showed outstanding clinical results in the latest results. Other clinical trials target other lineage markers or TAAs, such as human epidermal growth factor receptor 2 (HER2), CD20, CD22, B cell maturation antigen (BCMA), EGFR VIII, CD30, CD33, Carcinoembryonic antigen (CEA), or mesothelin to name couple of them. Initial clinical studies using first-generation CARs comprising only the CD3ζ activation domain introduced to treat lymphoma, neuroblastoma and ovarian cancer failed to mediate antitumor responses in patients. The lack of *in vivo* expansion and long-term persistence limited the clinical activity [71]. In two early studies, a CD19 or CD20-specific autologous CAR was used to treat NHL, mantle cell, or follicular lymphoma. Both studies used plasmid electroporation followed by an extensive *in vitro* culture, resulting in highly differentiated effector T cell phenotype. These cells could only be detected for a short period of time in patients' blood after transfer and no antitumor reactivity was observed. A different clinical trial used a CAR against

the carbonic anhydrase 9 (CAIX) to treat renal cell carcinoma resulting in short persistence, no antitumor effect and off-target toxicities in $CAIX^+$ epithelial cells in liver bile ducts. In addition, immune responses against the murine scFv were detected in patients that led to the rejection of the CAR T cells [72]. This finding was not surprising because prior studies showed immunogenicity of foreign transgenic products introduced in T cells for ACT. In summary, studies with first-generation CARs were disappointing and CARs needed to be improved by modifying signaling domains, improving gene transfer efficacy and reducing immunogenicity [73].

Second-generation CARs comprising an additional costimulatory domain upstream of the CD3ζ activation domain, such as CD28 or 41BB, showed better antitumor efficacy in preclinical models [74]. One clinical study compared the efficacy of first and second-generation CD19-specific CAR T cells. The second-generation CARs showed superior persistence and proliferation, as well as antitumor efficacy *in vivo* in comparison to the first-generation CARs only using the CD3ζ domain [75]. Recent outstanding clinical success has been achieved using second-generation CARs targeting hematological B cell malignancies, mainly targeting the CD19 B cell lineage antigen that is expressed in 95% of these cancers [76]. CD19 is a glycoprotein restricted to the B cell lineage and is a component of the signal transduction complex of mature B cells [77]. The absence of expression in healthy tissue other than B cells has made it an optimal target for CAR T cell therapy [78]. Infusion of CD19-specific CAR T cells was shown to be effective in different cancers such as ALL, CLL, NHL [79]. The first clinical trial using second-generation CARs was performed at the NCI, where patients received CD19-specific CARs containing CD3ζ and CD28 costimulatory domain. Significant tumor regression and partial remission of the first 8 patients was reported, accompanied with B cell aplasia [80]. Similar clinical results showing durable antitumor responses were demonstrated in other studies with CD19-CD28/CD3ζ-CARs in advanced, progressive B cell malignancies [81], follicular lymphoma [79] and ALL [82]. Outstanding results have been reported from the University of Pennsylvania in the setting of adult CLL [83] and pediatric ALL [84]. In these studies, CD19-41BB/CD3ζ CARs were modified with a lentiviral platform. CARs were expanded using anti-CD3 and anti-CD28 coated beads and infused into the patients two days after lymphodepletion. Using these settings, it was possible to eradicate large tumor burdens and mediate complete and long-term remission. CAR T cells were detected in the blood beyond 3

years in patients, showing an impressive persistence. Ongoing B cell aplasia indicates the long-term functionality of the CAR T cells. These clinical results could be reproduced and further improved and optimized by using optimal cell dosages and T cell subpopulations in other clinical trials, e.g. at the Fred Hutchinson Cancer Research Center (FHCRC) [85, 86].

Effective treatment with second-generation CARs, commonly accompanied by serious adverse events (SAE) like cytokine releasing syndrome (CRS) due to expansion of the CAR T cells *in vivo* or delayed tumor lysis syndrome (TLS), depends on the tumor burden and elevated cytokines. Elevated cytokine and chemokine levels including IFNγ, IL-6 and MCP-1 point to the systemic immune response by this potent therapy serving as risk factors for CRS. By using a clinically approved antibody against IL-6R (tocilizumab) or TNFα (infliximab), the impact of the cytokine cascade can be mitigated and symptoms clearly reduced [87]. CRS can be severe in some patients and clinical protocols have been established to reduce symptoms [88]. With the approval of tisagenlecleucel (Kymriah, Novartis) and axicabtagene ciloleucel (Yescarta, Kite) by the FDA in 2017, the first cellular therapeutics have been released for anti-CD19 CAR-based treatment, paving the way for more cellular therapies to come [89]. In order to further improve CAR therapy for blood-borne malignancies the observation of exhausted or dysfuctional CAR T cells lead to further modification of CAR T cells. Shang and colleagues for example, started a clinical trial using CAR T cells inheriting a PD-1 knockout. By that they want to achieve a more persistent and effective cell product that reveals a lower susceptibility to exhaustion in patients as the PD-1 protein is an activation/exhaustion relevant protein. Clinical trials combining CAR expression and knockout out of the endogenous TCR and/or exhaustion relevant proteins like PD-1 are promising strategies to ameliorate CAR T cell therapies. Another clinical trial tested an FDA-approved second-generation CAR including a 4-1BB costimulatory domain, modified by adding 15 amino acids from the native CD8a molecule to the CD8a transmembrane domain. The added amino acids changed the predicted structure compared to the FDA approved one and showed reduced production of inflammatory cytokines, reduced proliferation of T cells retaining the anti-tumor activity *in vitro*. In patients they could show impressive anti-tumor efficacies in six out of eleven patients pointing out no one of the patients developed CRS or neurotoxicities higher than grade 1 [90]. The ability to treat or cure end stage-patients who were relapsing or unresponsive to

conventional therapies and having a very poor prognosis shows the outstanding potential of the CAR therapy which is still in the beginning of its development.

In contrast to the outstanding clinical results using CD19-specific CARs, targeting solid tumors resulted in less-striking clinical outcomes. First-generation CARs have been used in solid cancers such as neuroblastoma with an anti-GD2 CAR where four out of eight patients responded to CAR therapy showing tumor necrosis or regression and, more importantly, no patients showed toxicities [91]. A specific mesothelin-specific CAR, another target for solid cancers, was used in different clinical trial. The CARs could be detected in the tumor, which shows the enormous migration capacity of the CAR T cells to the tumor cells through the tumor microenvironment. Unfortunately, only a transient tumor shrinkage of one lesion was observed. In an advanced study, 19 patients with sarcoma were treated using an improved anti-HER2 CAR with higher affinity towards HER2. Surprisingly, CAR T cells were detectable in several patients for over 6 weeks and no dose-limiting toxicities could be observed. But, again, no considerable antitumor activity was observed [92]. A very recent promising study showed that an anti-IL-13R$\alpha$2-specific CAR could mediate antitumor activity in three patients, leading to manageable temporary brain inflammation as the only toxicity – indirectly indicating the functionality of the intracranially infused CAR T cells [93]. Advanced clinical studies started using CAR T cells against bloodborne and/or solid tumors combined with checkpoint blockade inhibitors like anti-CTLA-4 or anti-PD(L)-1 monoclonal antibodies to enhance persistence, functionality, and anti-tumor efficacy in patients. These clinical trials are still recruiting and ongoing e.g. NCT03630159. More advanced clinical trials are to come and better treatment options for patients will be available in future.

In summary, these results indicate that overexpressed TAA on solid tumors can mediate antitumor activity and serve as CAR targets without off-tumor toxicities. Nevertheless, the main limitations of low persistence and functionality in patients [94] and poor antitumor activity [95] have to be addressed. Innovative approaches must be developed to broaden the applicability of CAR T cells.

Novel approaches must consider additional hurdles. Major hurdles which should be addressed are I) migration behavior and capability to actively home to the tumor site, especially if the tumor is hard to penetrate physically or actively inhibited by the tumor cells. II) CAR T cells have to overcome tumor suppression due to antigen downregulation or escape, as well as an immunosuppressive (hypoxic) microenvironment that can itself directly downregulate T cell activity in the tumor environment [96]. III) Improvement of proliferation and persistence with the optimal combination of costimulatory domains, optimal cell composition or cell dosage is necessary. IV) New tumor recognition mechanisms which might be more sophisticated and can lead to dramatic improvements in the ability to design therapeutic T cells might be able to effectively recognize target tumor cells and discriminate between malignant and healthy cells. Besides modifying CAR T cells, themselves, improving the preconditioning regimen of the patients using lymphodepletion, which is already implemented in clinical protocols, might lead to a better clinical response and outcome. New combinations/formulations of these regimens might be beneficial, too. Furthermore, the infusion of additional immunostimulatory cytokines such as IL-2 or IL-15 might lead to a better engraftment and/or expansion, potentially resulting in better clinical outcomes in specific scenarios [38].

### 1.3.5 **Composition of T cell product or memory T cells as optimal cell product for ACT**

Besides the definition of optimal targets and antigen receptors, it has become evident over the past years that T cell function, persistence and efficacy is influenced by many other parameters beyond antigen/CAR specificity. Especially the nature of the T cells, including the differentiation and phenotypical status as well as the dose/response relationship used in the clinic for ACT is highly correlated with clinical results [97]. ACT therapeutically transfers the defined T cell immunity of unmodified or genetically engineered T cells into patients. In the case of TCR or CAR T cell therapy, long-term maintenance of transferred cells is indispensable. Clinical studies performed with genetically modified T cells are highly heterogenous in their cell composition (bulk PBMCS, selected T cells), T cell subsets ($CD4^+$/$CD8^+$) and differentiation status of naïve ($T_N$), central memory ($T_{CM}$) and effector ($T_{EFF}$) T cell, making conclusive analyses of parameters and effects between different clinical trials challenging.

Detailed analyses determined different T cell subpopulations and their capability to confer tumor eradication and persistence after ACT. Besides the definition of optimal targets and antigen receptors, the differentiation status of transferred T cells is emerging as a crucial parameter for generating cell products with optimal efficacy and safety profiles. These findings are mainly focused on $CD8^+$ T cells observed in preclinical and clinical studies. In the T cell immunology field, $CD8^+$ T cells can be divided into $T_N$, $T_{CM}$ and $T_{EFF}$ T cell subsets. The differentiation status increases from $T_N$->$T_{CM}$->$T_{EFF}$ cells and is linked to a specific phenotype based on a unique expression of surface antigens. The phenotype of memory T cells is defined best as having the capability to proliferate after responding to homeostatic cytokines circulating in the blood. Memory T cells can be further subdivided by distinct patterns of adhesion molecules and chemokine receptors in $T_{CM}$, effector memory ($T_{EM}$) and tissue resident ($T_{RM}$) T cells [98]. These phenotypic differences can be translated into specific migratory characteristics. $T_{CM}$ have the ability to continuously re-circulate to lymphoid organs like $T_N$ cells, whereas $T_{EM}$ mainly migrate to non-lymphoid tissues [99]. The latest identified memory subset, the $T_{RM}$, resides locally in organs and might be further subdivided depending on the organ of residence, which adds more complexity to the memory compartment [100]. Specific combinations of different surface markers are necessary to determine a reasonably homogenous subset. Typical markers for the identification of the major subsets in humans are defined for $T_{CMs}$, $T_{EM}$s and $T_{RMs}$. Other surface markers or other marker combinations to determine a memory subset have been proposed as well [101]. Accordingly, the *in vivo* behavior of central and $T_{EMs}$ has been investigated. In a macaque study at the FHCRC, it was shown that $T_{EMs}$-derived CMV positive clones survived only a week in the peripheral blood. In contrast, $T_{CMs}$ were detectable four years after transfer in the peripheral blood, showing impressive longevity [102]. *In vitro*, no difference in functionality between the subsets was observed. Our laboratory showed that a repetitive transfer of single $T_{CM}$ cells over generations of mice can fulfill all criteria of tissue stem cells [103]. Another very interesting T cell subset is the $T_N$ cells. $T_N$ have the capability to repopulate all different memory and effector T cell subsets. We demonstrated that one single naïve antigen-specific T cell is sufficient to derive enough effector and long living memory T cells in immunocompetent mice upon immunization [104]. The enormous proliferative and differentiating potential of $T_N$ has been further evaluated in tumor

mouse models [105]. Using engineered T cells derived from $T_N$ resulted in superior antitumor activity, proliferation capacity and higher cytokine production compared to similar T cell numbers from memory T cells ($T_{CM}$ < $T_{EM}$) [106]. One limiting factor for the selection of a specific subpopulation is that patients are heavily pre-treated with chemo-radiotherapy to treat their malignancy. As a consequence, most patients are lymphopenic with decreased lymphocytes circulating in the blood and changed frequencies of $CD4^+$ and $CD8^+$ cells, as well as higher frequencies of $T_{EMs}$. Furthermore, the Riddell lab showed that a 1:1 combination of $CD4^+$ and $CD8^+$ engineered CAR T cells resulted in synergistic antitumor activity as well as enhanced proliferation capacity [85].

As already mentioned, the use of optimal cell subsets comprising a rapid and sustained *in vivo* proliferation, persistence and functionality is required to achieve a complete tumor eradication of large tumors. Preliminary data show that the selection of specific cell subsets is beneficial for patients and results in better engraftment and enhanced antitumor efficacy. Manufacturing a defined CAR T cell product (e.g. $CD4^+/CD8^+$ ratio) is feasible, highly reproducible and accompanied with a marked antitumor efficacy even when administered in a very low cell dose. Overall, the improvement in clinical cell selection methodology, improved cell culture conditions retaining the desired phenotype such as $T_N$, $T_{SCM}$ or $T_{CM}$, as well as the improvement in cell engineering may further enhance the functional properties of the engineered cells. This might facilitate large scale application of these therapeutic approaches.

## 1.4 CAR T cell therapy

CAR T cell therapy showed outstanding clinical results being commercialized in 2017. The evolvement of these constructs took over 20 years. Changes in structure and composition of these synthetic modular constructs was evaluated and is described in detail below.

### 1.4.1 **Structure: From the extracellular recognition site to the intracellular signaling cascade**

Generally, the extracellular antigen-recognition site consists of a scFv, comprising the heavy (VH) and light (VL) variable fragment of a TAA-specific monoclonal antibody joined by a flexible $(Gly4Ser)_3$ linker. Many monoclonal antibodies are readily available or can be generated with phage display libraries [107]. Over 100 different CAR specificities mainly using scFvs have been described [108]. Recognition sites expressed on the tumor cells have mostly been used to tackle mutated receptors like epidermal growth factor receptor (EGFR vIII), cell lineage antigens such as CD19, CD20, CD22 or developmental antigens like (receptor tyrosine kinase like orphan receptor 1) RORI and GD2. Overexpressed TAAs such as HER2, mesothelin and MUC16 are promising targets as well [109-111]. CARs can also be designed to use ectodomains of naturally occurring molecules for recognition of their counterparts like NKG2D. The stress-induced ligand NKG2D is upregulated on tumor cells and can be recognized [112]. A similar principle holds true for IL-13 and its binding to the IL-13 receptor, mainly expressed on glioblastoma [113]. However, the affinity of the CAR binding domain significantly affects the downstream signaling and functionality of the entire chimeric antigen receptor. The optimal affinity might be different depending on the target antigen and its composition, size, location, and expression level on the cell surface. Studies with different affinity scFvs (HER2, RORI and different clones) showed that stronger binding demonstrated superior antitumor activity, cytokine production and greater proliferation *in vitro* and in preclinical studies [114]. However, a very recent study of Amrolia and colleagues showed controversial data. They generated a CAR comprising an anti-CD19 scFv (CAT CAR) with a 40x lower affinity to its target compared to a clinically approved anti-CD19 CAR (scFv clone FMC63). *In vitro* and in the clinical trial (CARPALL, NCT02443831) they showed enhanced proliferation, cytotoxicity and persistence compared to the high affinity version of this CAR. It might be advantageous to use a CAR containing a scFv with a lower affinity. Serial triggering of multiple target cells and shorter duration of the CAR-target cell complex are proposed as mode

of action that might explain the ameliorated behavior [115]. Other studies argue that there might be an additional affinity threshold, especially when specific antigens are expressed in low levels on healthy tissue (e.g. HER2, EGFR) [116]. Low-affinity CARs are activated only when the target antigen is overexpressed on the tumor and not on normal tissue, which shows an enhanced selectivity. The behavior of affinity-tuned CARs still needs to be analyzed in more detail since most studies used different scFv clones. Affinity modification of a single scFv in more detail is crucial to address this question. Even non-binding parts of the scFv, e.g. the framework regions, can influence the functionality of the CAR. Some framework regions contribute to an antigen-independent 'clustering' of the CAR molecules on the cell surface which, in turn, leads to sustained tonic signaling resulting in early exhaustion, low secretion of cytokines and poor antitumor efficacy *in vitro* and *in vivo* [113]. It is known that several scFv clones for the same target antigen must be tested to generate a functional non-clustering CAR [117]. Grafting of CDRs into stable framework regions of the variable fragment can improve functional CAR expression [118]. ScFvs have therefore been screened for affinity of the antigen-binding and antigen-independent properties to further investigate the influence of the CAR affinity and resulting functionality.

The hinge region bridges the binding domain with the transmembrane and intracellular signaling domains. Common CAR hinge/spacer regions are derived from CD8$\alpha$, CD28 or immunoglobin (IgG1, IgG4, IgD) sequences and provide flexibility, positioning, dimerization and determine the distance between the CAR T cell and the target cell [119]. The length of the hinge/spacer domain influences the quality of the interaction depending on the location of the target epitope [120, 121]. The Riddell lab extensively investigated the length of the hinge/spacer region. They generated CAR T cells against RORI with a long ($CH_2/CH_3$), medium ($CH_3$) and small (9AA) hinge region derived from the IgG4 hinge. Interestingly, the short spacer was superior compared to the longer constructs *in vitro* but, contrarily, *in vivo* the situation changed, and the location of the epitope became crucial. For a membrane-proximal epitope, a long spacer was required for CAR T cell activation and target cell killing, whereas the short spacer was ineffective [114]. In line with that, several studies have shown that a lengthened spacer can improve the functionality, cytokine secretion and proliferation of the CAR when targeting a membrane-proximal epitope by adding

required flexibility to access these epitopes [122]. In contrast, lengthening the spacer for membrane-distal epitopes decreases the functionality and results in suboptimal T cell function. The location of the target epitope suggests the spacer length but since there is no specific rule to predict the best or optimal spacer length, this important issue requires empirical testing of multiple CARs against each epitope.

To efficiently translate the binding of the extracellular recognition domain to the intracellular stimulatory domain(s), a functional signal transmitting transmembrane domain (TM) is necessary. The transmembrane domain has been shown to be important by improving effective CAR expression on the cell surface. For that reason, many different TMs obtained from CD28 , OX40 [123], CD3ζ [124], FCRγ [125], CD8 [126] have been evaluated. Initial CARs fused the FcRγ or CD3ζ domain to the TM domain but, recently, most CARs in use comprise CD28 TM as incorporation of the CD28 TM showed superior expression compared to OX40 and CD3ζ [123].

These first-generation CARs containing only one single stimulatory domain could show lytic activity *in vitro* but failed *in vivo*, mainly due to limited persistence and poor antitumor activity [127]. In natural TCR signaling, two signaling events are necessary to achieve an adequate T cell response. First the CD3ζ TCR triggering event, followed by a second costimulatory signal, e.g. CD28[128]. This combination leads to CAR signaling which is independent of the endogenous TCR, as demonstrated in TCR α/β knockout T cells [129].

Inclusion of a second co-stimulatory domain (CD28 or 41BB) in cis-configuration led to the evolution of the more potent second-generation CARs [130]. Designing receptors comprising activation and co-stimulatory domains resulted in T cells capable of up to 20 times higher IL-2 secretion, proliferation after multiple antigen exposures, and superior antitumor activity, as well as increased antigen sensitivity *in vitro* [131].

Several co-stimulatory domains were introduced at the C-terminal of the CD3ζ domain. Incorporating inducible co-stimulators (ICOS), OX40 (CD134), 41BB (CD137) or CD28 [75] has been tested for their ability to support T cell survival, antitumor efficacy and long-term persistence [132] and CD28 and 4-1BB are the most common used. The CD28 co-stimulatory domain enhanced CAR T cell resistance against regulatory T cells [133]. On the other hand, compared to the CD28 co-stimulatory domain, the 41BB domain showed an increased *in vivo* persistence,

enhanced antitumor activity and tumor localization. Furthermore, 41BB co-stimulation likely initiates distinct signaling pathways, impacting different metabolic phenotypes and support $T_{MEM}$ formation [134]. These second-generation CARs are the backbone of the majority of current clinical CAR therapies. With the addition of more than one co-stimulatory domain, third-generation CARs have been generated. Using the CD3ζ activation domain combined with CD28 or 41BB and OX40 resulted in full activation of the complement, proliferation and survival signals for a further enhanced antitumor activity [135]. These CARs have a reduced signal threshold to a level at which the activation of T cells can occur without antigen stimulation. They might be triggered when binding to low avidity off-targets that can lead to a lethal or severe side effects [136]. Due to this, the CAR field avoids using third-generation CARs in the clinic, although some clinical trials have been started.

### 1.4.2 **Mode of action**

The mechanisms how CAR T cells signal and how this differs compared to normal T cells are not completely understood. Upon binding of the scFv, CARs cluster and dimerize on the cell surface followed by the phosphorylation of the intracellular ITAMs of the CD3ζ and CD28/41BB co-stimulatory domains. The CD3ζ domain recruits the endogenous components of the TCR downstream signaling mainly by the activation of ZAP70 [137]. CD28 multiplies the signaling strength with additional recruitment of LCK and PI3k. CAR T cells are still able to signal through the endogenous TCR, which makes it difficult to compare signaling intensities of the same cell. Signal intensities seem to be comparable if early signaling events like CD3ζ, ZAP70 and ERK are considered [138]. This was a surprising finding due to different binding properties since TCRs show a much lower binding affinity and require serial engagement of multiple pMHCs for full signal transduction, whereas CARs bind with high affinity and different binding kinetics and characteristics. One binding event might lead to full and sufficient signal transduction. By introducing point mutations in the costimulatory domains, selective activation of the CAR differences of 4-1BB and CD28 could be observed by Salter et. al using phosphoproteomic analysis. In brief, they showed that CARs containing a CD28 costimulatory domains are activated faster and with a higher magnitude in protein phosphorylation compared to CARs comprising a

4-1BB costimulatory domain. Additionally, they observed in 4-1BB activated CAR T cells more upregulated memory-associated genes compared to the CD28 costimulatory domain which is more effector-associated. This was related to the constitutive association of the LCK signaling protein to the CD28 costimulatory domain, that could be reduced by mutating CD28 phosphorylation sites [139]. These data could be extended by a recent study changing a single residue in the CD28 costimulatory domain resulting in less T cell exhaustion and enhanced persistence [140].

### 1.4.3 **Next Generation CARs**

CARs were developed against a variety of target molecules expressed on the cell surface. It is important that the candidate antigen is specifically expressed on the tumor and not on healthy tissue to circumvent off-target toxicities. Identified targets such as L1CAM, GD2, Her2, mesothelin, MUC16 and RORI serve as promising tumor targets, and tend not to be expressed on healthy tissues [143-148]. In contrast, the tumor target EGFRvIII bears a deletion in exon 2-7 and would be a true tumor antigen, but its heterogeneous expression on the tumor cells limits the antitumor efficacy [149]. Especially if the TAA is expressed on tumor and healthy cells there is a need for new strategies to approach complex situations.

For that reason, alternative concepts have been developed to bypass the above-mentioned limitations on the therapeutic value and antigen recognition. Several approaches aim to improve the selective recognition on the tumor cell. One approach was developed by using two different scFvs, allowing dual targeting and/or synergistic or inhibiting effects of these CARs [141]. The most advanced approach for the use of dual targeting CARs in the clinic is to prevent tumor escape, observed with a single scFv in several clinical trials. Using CARs expressing for example “CD19 and CD20” or “CD19 and CD123”, a relapse due to the loss of CD19 can be prevented and a tumor clearance is more likely [142]. Using logic-gated scFvs is another approach. Logic gates like AND/OR CARs could solve different purposes, such as improving the distinction between tumor and healthy tissue by targeting both the tumor and its microenvironment. In this case, either both tumor antigens have to be expressed, or only one correct binding leads to a tumor reactivity [143]. Examples of those CARs are dual CARs, TanCARs or iCARs [144]. Modifications of the modular structure of CARs generating a universal CAR that can theoretically recognize every

tumor antigen have been carried out and tested *in vitro,* as well as in pre-clinical models. One group showed a proof of concept study by using a CAR specific for the fluorochrome fluorescein isothiocyanate (FITC) molecule. By using FITC-conjugated antibodies specific for tumor-specific antigens, they could mark and eradicate tumors with the FITC-conjugated antibody [145]. Similar concepts have been described using either biotinylated antibodies and anti-biotin specific CARs, or using an anti-FC CAR which binds the FC part of human antibodies [146]. Recent relevant clinical studies have shown a similar principle by using a nucleoprotein tagged antibody, which bears a low immunogenicity, binding the tumor and the Tag-specific CAR [147]. These approaches, called switch-mediated CARs, showed promising results *in vitro* and in preclinical models but they must be further evaluated and tested in clinical trials. To overcome the limitation that CARs only recognize antigen expressed on the cell surface, TCR-like CARs have been developed. Antibodies against pMHC complexes have been generated via phage display and fused into the CAR backbone. CARs specific for gp100/HLA-A2, PR1/HLA-A2, and WT-1/HLA-A2 mediated antitumor activity *in vitro* and in preclinical mouse models. [148]. More sophisticated approaches to increase the potency of CAR T cells are chimeric co-stimulatory receptors (PD-1-CD28), or CARs co-expressing a synthetic Notch receptor which enables the activation of a specific transcription factor upon binding the target structure [149, 150]. This could be introduced into a pre-clinical solid tumor model using a logic gated RORI CAR. After recognizing EpCAM or B7-H3 on RORI positive tumor cells with a respective CAR a transcription Factor specific for the RORI CAR is activated and the expression of the RORI CAR is triggered. This strategy allows safe targeting of tumors which are separated from normal healthy cells [151]. Another approach improving CAR T cells is to prevent CAR T cells from exhaustion. A recent study could show that CAR T cells are resistant to exhaustion by overexpressing the transcription factor c-JUN which is a canonical AP-1 factor. This modification lead to improved proliferation, functionality, anti-tumor efficacy of the CAR T cells and more important CAR T cells were exhaustion resistant in citro and in preclinical mouse models [152].

All these innovative approaches are promising improvements in CAR T cell therapy. However, further investigations are required to address *in vivo* applicability, safety and persistence in patients. Knowledge about the function and characteristics of CAR T cells is accumulating and

CAR designs are further improved, demonstrating the enormous potential of synthetic receptor engineering and multiplexing enhancements. But it is unclear whether these observations can be translated into clinic applications.

## 1.5 Reported Toxicities in CAR therapy

The adoptive transfer of genetically engineered T cells, especially the use of CD19-specific CAR T cell immunotherapy for the treatment of bloodborne malignancies such as leukemias and lymphomas, has shown outstanding antitumor activity in clinical trials, as already mentioned. More importantly, durable remissions have been reported, suggesting that this treatment can be curative [153, 154]. However, there are several side effects and toxicities already reported which can be potentially life-threatening, often occurring during CAR T cell therapy and not yet fully understood. The extraordinary long-term persistence of up to 10 years in human trials bears potential toxicities [155]. The reported side effects can be very different, from immediately after infusion of the cell product to delayed, mild to severe, and persistent or temporary. It is important to investigate as well as manage these unique toxicities, which are distinct from those seen with traditional chemotherapies, monoclonal antibody therapy or small molecule-based therapies. Preventing or managing toxicities has therefore emerged as a key component in the successful clinical application of this novel technology. Ideally, the prediction of per-patient severity and onset would allow consideration of prophylactic therapy to guard against toxicity, resulting in improved management. In the following sections the most common toxicities occurring after CAR T cell therapy are described briefly.

### 1.5.1 **Cytokine releasing syndrome (CRS)**

The most commonly described toxicity after CAR T cell transfer is CRS, in which the infused CAR T cells themselves produce cytokines which stimulate macrophages and other immune cells to produce other cytokines in response to the initial cytokine boost. CRS includes more than one cytokine. A variety of cytokines including IL-6, IFN$\gamma$, TNF$\alpha$, IL-2, interleukin-8 (IL-8) and interleukin-10 (IL-10) are increased in the patient's serum. Subsequently the patients experience symptoms like fever, tachycardia, hypotension and some other toxicities on average within three

days after CAR injection [156]. Some reports correlate CRS with higher CAR T cell levels in the blood, as well as a higher tumor burden in the patient. Even though CRS is the most common toxicity after CAR T cell treatment, it is treatable and reversible in most instances, with only few cases of death reported. These cases mainly occurred in first clinical CAR trials due to very high cell numbers and suboptimal pre-conditioning of the patients. The intensity of CRS toxicity has been correlated with a beneficial antitumor response in CAR T cell trials carried out at multiple clinical research centers [129]. To counteract the cytokine storm, different cytokine antagonists and corticosteroids have been used as therapeutic agents [157]. In a study using a bi-specific antibody against CD19 and CD3 (Blinatumomab), a CRS was successfully treated by using an IL-6 receptor-directed monoclonal antibody (tocilizumab) [87]. Tocilizumab can block the activity of IL-6 and mitigate the inflammation. In a novel clinically relevant humanized mouse model, Norelli et al. showed that CRS was prevented by monocyte depletion or by IL-6 blockage with tocilizumab. These data show that monocytes are the main producer of IL-6 and are thus crucial drivers of CRS [158]. Corticosteroids act in a different manner by indirectly decreasing cytokine levels by reducing transduced T cell numbers and controlling the inflammation reaction. In addition to antagonists of specific cytokines (e.g. IL-6) and high-dose steroids, vasopressors and ventilatory support, as well as supportive care especially early on after T cell transfer, can circumvent severe toxicities. Predictive biomarkers, recommendations and practical guides based on serum cytokine levels (MCP-1 and IL-6) and fever within the first 36h have been developed for monitoring, grading and managing CRS and neurological toxicities in adult patients. These guidelines are capable of controlling and minimizing the toxicities of CRS after injection of the cell product. Latest reports describe a specific multi-parameter prediction model which can judge the severity and suggest a treatment plan [159].

### 1.5.2 **Neurological toxicities**

Neurological toxicities have been first reported in immunotherapies using high dose IL-2 for the treatment of solid tumors or in therapies with increased cytokine levels in the blood serum. In these cases, global encephalopathy was reported [160]. Neurological toxicities associated with the infusion of CD19 CAR T cells can be very diverse. CAR T cells can cause global encephalopathy, aphasia, tremor, ataxia, hemiparesis and cranial nerve palsies. These toxicities are similar to the

neurological toxicities observed with a bi-specific antibody (Blinatumomab). The incidence of neurological events is very variable [161]. Neurological toxicities occur usually at various times: simultaneously with CRS or delayed. There might be a link between the severity of the CRS and neurological toxicities. Severe CRS can be a risk factor for neurological toxicities by activating pericytes which trigger blood brain barrier (BBB) disruption, even if rare cases of CRS-independent neurological toxicities were reported CD19 CAR T cells could be found in the patient's cerebrospinal fluid (CSF), accompanied with increased levels of IL-6 in the CSF and a higher likelihood of neurotoxicities. However, the latest reports described possible mechanisms of neurological toxicities. One hypothesis is that the blood brain barrier (BBB) is affected due to the intense pre-conditioning of patients that allows CAR T cells to enter the CNS [162]. Other reports try to correlate the CRS grade with the appearance of neurological events, which seems to have some coherent mechanisms that must be addressed in more detail. A rare CD19 positive brain pericyte subpopulation recently identified with high resolution single-cell high resolution RNA-seq maps might play an important role for the integrity of the BBB, which is still under investigation and not published, yet.

### 1.5.3 **On-target/off-tumor toxicities (B cell aplasia)**

An ideal CAR target antigen is only expressed on the cell surface of the tumor cell and provides a critical signal for the malignant cell. Unfortunately, most CAR targets have shared expression on heathy tissues [163] providing the risk of tissue damage or organ failure because of CAR on-target/off-tumor toxicity. The severity of reported events ranges from lineage depletion (B-cell aplasia), which results in hypogammaglobulinemia, a state of 'immunocompromised', to life-threatening toxicities (death) [164]. This toxicity can be minimized by *in silico* target epitope prediction or safety studies in mouse models but cannot eliminate completely the risk of unwanted healthy tissue recognition before cell injection into patients. [136].

In an early clinical study, three patients were treated with CAR T cells targeting metastatic renal cell carcinoma (Carboanhydrase IX) CAIX. Patients had a grade 3-4 increase of alanine, aspartate aminotransferase or total bilirubin. After liver biopsies, cholangitis with T cell infiltration surrounding the bile ducts was identified. Unfortunately, it was found that the bile duct epithelial cells express CAIX, which was targeted by the CAR T cells [165]. Another severe example was

reported when an anti-ERBB (HER2/neu) CAR was used. The treated patient had acute respiratory distress and pulmonary edema and required mechanical ventilation. This patient subsequently died. Afterwards it was shown that normal lung tissue expresses the ERBB2 antigen [166].

To overcome those on-target toxicities by specifically eliminating only the TAA overexpressing tumor cells and not the TAA expressing healthy counterpart, affinity-modified CARs were generated. Using affinity-modified CARs led to better discrimination between tumor and healthy cells expressing the same TAA. More precisely, it was shown that CARs with lower affinity eliminate only TAA overexpressing tumor cells, whereas the healthy counterpart remains untouched [116, 167]. However, tumor cells which downregulate the TAA are able to evade and a complete tumor eradication is not possible. There are more strategies needed to overcome on-target toxicities.

## 1.6 Safeguard mechanisms for CAR T cell therapy

To prevent or reverse toxicities and side effects after CAR T cell therapy, it is important to include safeguard mechanisms in the cells to inactivate or remove toxicity-causing engineered cells. This means optimizing the CAR construct as well as introducing safeguard mechanisms that can alter the cell function. Several concepts have been proposed to ameliorate side effects and toxicities such as non-specific immune suppression or selective elimination and deletion of transferred gene modified cells with so called “safeguards, suicide, elimination genes or safety switches”, which follow different mechanisms that might be useful for different scenarios.

An essential component of the latest CAR evolution are suicide genes. These are integrated into the cells to allow for selective elimination or depletion of transferred CAR-modified cells. To date several mechanisms have been tested in pre-clinical or clinical studies. For example, after CD19 CAR transfusion, patients suffer from B-cell aplasia which is accompanied with hypogammaglobulinemia. Though it is a non-life-threatening event, treated patients are immunosuppressed. After complete and sustained tumor elimination, it might be beneficial for the patients to deplete CD19 CAR T cells with a safeguard mechanism to recover the normal endogenous B cell compartment to reverse B cell aplasia. The patients would regain their full immunocompetence and reduce the risk of unknown long-term off-target toxicities of the CARs.

In this scenario the speed of action is not important. However, in other reported toxicities like off-target toxicities where infused T cells attack healthy tissue, the speed and application of the safeguard mechanism is more important. Usually interventions should be done early after treatment to prevent further damage of the transferred cells. Taken together there is a need for different safeguard mechanisms to act on various levels. Differences in efficacy, speed and mode of action are required to cover as many toxicities as possible. Therefore, different safeguards, suicide or safety concepts have been evaluated. They can be subdivided into two groups: drug-induced suicide genes and antibody-based safeguard mechanisms.

### 1.6.1 **Drug-based suicide mechanism**

The first concept of integrating a safety mechanism involved introducing a herpes simplex virus thymidine kinase (HSV-TK) into genetically modified T cells. The expression of the HSV-TK makes the cells susceptible to treatment with the acyclic nucleoside analog ganciclovir, which is an antiviral drug used to repress viral replication [168]. By expressing the HSV-TK in modified cells, it catalyzes the phosphorylation of ganciclovir (active drug) that competes with endogenous guanosine DNA incorporation, resulting in the disruption of DNA polymerization and synthesis. The approach is effective as it is not recognized by the human thymidine kinase, making it very specific for the introduced cells. This strategy was successfully tested for controlling GvHD after allo-HSCT in highly immunosuppressed patients [169].

However, this approach also has some major caveats. The expression of HSV-TK leads to immunogenicity and subsequently the rejection of the transferred cells, as shown in immunocompetent patients [170]. Another disadvantage is that induction of cell death by the inhibition of DNA replication is delayed and might be not fast enough for adverse effects.

A more recent and more promising concept is based on dimerizable chimeric death molecules like inducible caspase9 (icasp9) and FAS. The chimeric elements are engineered to contain specific components of the FK-506 binding protein which cross links in the presence of a small molecule drug (AP1903). The bivalent small molecule is inert in the absence of the chimeric molecules and has no effect on healthy cells. The inducible FAS or casp9 dimerization leads to downstream activation of caspases, subsequently inducing apoptotic pathways and death of the target cells [171]. In a first proof-of-principal study, non-immunogenic icasp9 was introduced

into donor lymphocytes and was evaluated in a setting of haploidentical HSCT (DLI). Just a single dose of the small molecule dimerizer (AP1903) eliminated more than 90 % of the transferred cells containing the chimeric icasp9 molecule within 30 minutes. The fast clearance, which was observed without any adverse event, resulted in the reversal of GvHD in the patient without recurrence [172]. Nevertheless, translating these results into other scenarios might be different. When icasp9 is introduced in other genetically engineered T cell platforms, there might be some toxicities of cell populations which are unaffected by the AP1903 drug. Additionally, there is the possibility of tonic icasp9 dimerization in the absence of AP1903, which has been seen in engineered cell lines *in vitro;* subsequently, increased basal apoptosis might limit the clinical application [173]. Another bottleneck is the clinical availability of the small molecule that constrains the applicability for clinical use. Even if the proof-of-concept demonstrated impressive data, the exact efficacy of this suicide mechanism is not yet known. This approach might be limited, because in CAR T cell therapy a single surviving memory CAR T cell might be sufficient to drive the toxicity. A very recent Study could show that dasatinib could be repurposed for CAR T cell therapy and be used as a pharmacologic on/off switch. Dasatinib, a tyrosine kinase inhibitor interferes with LCK and inhibits the phosphorylation of the CD3z chain which is incorporated in current CAR constructs. By that the T cell receptor associated protein kinase 70kDa (ZAP70) is blocked as well. As a result, after the treatment with dasatinib (CAR) T cells are halted in a dose-dependet manner in cytotoxicity, cytokine secretion and proliferation. After clearance of dasatinib (CAR) T cells revert to normal function. In mouse studies CRS could be prevented by injecting dasatinib [174].

### 1.6.2 **Antibody-based safeguard mechanisms (elimination genes)**

Another idea is to introduce a selective marker expressed on the cell surface to deplete the genetically modified cell product. Using intracellular truncated cell surface markers which does not trigger any activation of the target cell but can be targeted by FDA-approved mAbs. Known clinically approved surface antigens are used (e.g. EGFR – Cetuximab (Ctx), CD20 – Rituximab (Rtx)). This would be a convenient strategy given the familiarity of clinicians with the use and safety profile of several FDA-approved mAbs. Cell death can then be triggered by infusing the corresponding mAb. The bound mAb will be recognized by NK cells and/or the complement

system and the marked cells will be eliminated [175]. Using surface markers as a safeguard mechanism is based on the antibody-dependent cellular cytotoxicity (ADCC via NK cells) or complement-dependent cytotoxicity (CDCC via complement system), which usually depends on the IgG Type and/or its glycosylation status [176]. Additional features of a known and specific surface marker are the ability to track the transferred cells *ex vivo* as well as select and purify genetically modified cells before transfer. To use these surface markers in CAR T cell therapy, it is crucial that the surface markers are co-expressed with the CAR or tumor targeting receptor. The choice of the surface marker is dependent on the situation. For example, T cells have been genetically engineered to express the full-length CD20 receptor or only the target epitope of the CD20 specific antibody Rituximab to mediate *in vitro* lysis of the modified T cells [177, 178]. It could be shown that binding Rituximab to the target cells leads to ADCC and CDCC and therefore to the elimination of the cells [179]. However, Rituximab treatment induces the depletion of endogenous $CD20^+$ B cells. CD20 is not a suitable safeguard mechanism to reconstitute endogenous B cells in the CD19 CAR T cell setting after successful CD19 CAR T cell therapy. Another synthetic surface marker is the Myc-tag, obtained from the nuclear protein c-Myc. The Myc-tag is directly fused to the recombinant receptor (CAR or TCR), which allowed targeted cell depletion by infusion of an anti-Myc-tag antibody and acted as a receptor-intrinsic safeguard mechanism in a preclinical autoimmune model [180]. Due to the human origin of the nuclear c-Myc protein, immunogenicity is supposed to be low. Even though the depletion is effective, the strategy is limited as no FDA-approved antibody is available.

Another promising safeguard mechanism is based on the non-immunogenic cell surface protein EGFR [181]. Natural EGFR consists of 4 extracellular domains, I-IV (distal-proximal), a transmembrane domain and an intracellular signaling domain. The natural EGFR was modified to an EGFR-like molecule that serves as a target for Ctx, a clinically approved IgG1 mAb. The developed EGFR-like molecule is truncated in the extracellular domains I and II and the intracellular signaling domain. In this case the truncated EGFR (EGFRt) can bind Ctx (EGF binding domains I and II are not necessary) and is functionally inert to inhibit signaling. This inert receptor can be co-expressed with any recombinant receptor such as TCR or CAR and mediates *in vivo* cell elimination.

In summary, adoptive T cell therapy showed astonishing results in clinical trials. The ability to modify T cells is increasing the scope and application of adoptive immunotherapy. However, the *in vivo* behavior of these "living drugs" is still not possible to predict and possible long-term toxicities are not known yet. Thus, including a safeguard mechanism is crucial to provide a safe, controllable therapy that can be terminated once the tumor is cured.

# 2 Aim of the thesis

In the recent years excitement is growing for immunotherapies utilizing a patient's immune system to combat certain types of cancer. Advanced cell therapy and adoptive cell transfer (ACT) involves genetic modification of patients' derived immune cells to recognize and attack tumors by introducing so called chimeric antigen receptors (CARs). CAR T cells showed outstanding results in clinical trials treating B cell malignancies leading to the first FDA-approved (CD19) CAR. However, for the treatment of solid tumors CARs have still major drawbacks. Main problems are severe adverse effects like CRS or neurotoxicity's which can be life threatening. A poor engraftment/persistence, in particular the solid tumors limit the success of CAR T cells for a broader application. Thereby it is crucial that CARs must be further improved and optimized for a more effective and more safe therapy. For that reason, in this thesis we investigated on the safety and optimization of CAR T cells.

i) First, we investigated on the functionality and completeness of the EGFRt safeguard mechanism under *in vivo* conditions. Specifically, we explored whether the EGFRt-based depletion strategy using the clinically available antibody Cetuximab is sufficient to prevent or reverse T cell-mediated side-effects such as B cell aplasia. ii) Secondly, we developed, designed and evaluated of a novel StrepTagII-based cellular safeguard mechanism. By generating an anti-STII specific CAR we were able to recognize and eliminate STII containing cells *in vitro*. iii) Thirdly, we aimed to get insights into the correlation of the binding affinity of the CAR (scFv) and its immunological function and biological behavior. Therefore, we generated scFvs and characterized CARs with reduced binding moieties and properties using the flow based $K_{off}$-rate assay developed in our laboratory. iiii) Since persistence and engraftment of CAR T cells are crucial parameters for effective therapy, especially for solid tumors, we investigated on the influence of a recombinant polymer conjugated IL-15 cytokine (NKTR-255) supplementation for optimal engraftment and persistence of CAR T cells *in vivo*. By supporting the CAR T cells with NKTR-255 *in-vivo* we could observe significantly improved engraftment and persistence as well as antitumor activity in a well-established NSG mouse model.

# 3 Material

## 3.1 Plastic & commodities

| item | manufacturer | |
|---|---|---|
| 15 ml Falcon tube Cell Star | Greiner bio-one | Heidelberg, Germany |
| 50 ml Falcon tube Cell Star | Greiner bio-one | Heidelberg, Germany |
| electroporation cuvette | Sigma Aldrich | Hamburg, Germany |
| 70 µm Nylon Cell Strainer | BD Falcon | Heidelberg, Germany |
| petri-dish | BD Falcon | Heidelberg, Germany |
| 1.5 ml Eppendorf tube | Eppendorf | Munich Germany |
| 1.0 ml Eppendorf tube | Eppendorf | Munich Germany |
| 2.0 ml Eppendorf tube | Eppendorf | Munich Germany |
| PCR tube | Eppendorf | Munich, Germany |
| Inject 5 ml | Braun | Melsungen, Germany |
| SuperRX | FujiFilm | Düsseldorf, Germany |

## 3.2 Plasmids

| epitope | parental clone | plasmid | Molecular Details |
|---|---|---|---|
| αCD19 CAR | FMC63 | pMP71<br>epHIV7 | Retroviral expression vector<br>Lentiviral expression vector<br>Selection marker: Ampicillin |
| αCD19 CAR SF wt<br>αCD19 CAR SF H35A<br>αCD19 CAR SF F108A | 4G7 | pMP71<br>epHIV7 | Retroviral expression vector,<br>Lentiviral expression vector<br>Selection marker: Ampicillin |
| αCD19 CAR scFv wt<br>αCD19 CAR scFv wt | FMC63<br>4G7 | pENTRY-IBA51 | Fusion vector, compatible recombination sites with pASG-IBA102 and pESG-IBA102 |

| | | | |
|---|---|---|---|
| αCD19 CAR scFv H35A<br>αCD19 CAR scFv F108A | | | Selection marker: Kanamycin |
| αCD19 scFv wt<br>αCD19 scFv wt<br>αCD19 scFv H35A<br>αCD19 CAR scFv F108A | FMC63<br>4G7 | pASG- IBA 102 (GGSC) | Periplasmic expression vector including N-terminal tandem *Strep*-tag and free cysteine<br>Selection marker: Ampicillin |

## 3.3 Antibodies

FACS Staining (All experiments were conducted with mAbs targeting murine epitopes)

| epitope | dye | clone | dilution | manufacturer | |
|---|---|---|---|---|---|
| CD19 | FITC/PE | HIB19 | 1:100 | eBioscience | San Diego, USA |
| FC-IgG | Biotin | polyclonal | 1:100 | Jackson Immunoresearch | Sata Clara, USA |
| EGFR | Biotin/PE/APC | AY13 | 1:300 | Roche | San Francisco, USA |
| CD3 | APC | OKT3 | 1:200 | eBioscience | San Diego, USA |
| CD8a | FITC/PE/APC | RPA-T8 | 1:200 | BD biosciences | San Jose, USA |
| CD45 | eF450/APC | HI30 | 1:100 | Biolegend | San Diego, USA |
| CD45RA | FITC/PECy-7 | HI100 | 1:100 | Biolegend | San Diego, USA |
| CD45RO | APC/PE/BV510 | UCHL1 | 1.50 | Biolegend | San Diego, USA |
| PD-1 | PECy-5.5 | eBioJ105 | 1:100 | eBioscience | San Diego, USA |
| Tim-3 | APC-Cy7 | F38-2E2 | 1:100 | Biolegend | San Diego, USA |
| Lag-3 | PE-Cy7 | 11C3C65 | 1:200 | Biolegend | San Diego, USA |
| CD62L | PE/APC | DREG56 | 1:100 | Biolegend | San Diego, USA |
| pSTAT5 | FITC | 47 | 1:100 | BD Bioscience | San Jose, USA |
| Anti-Human CD16/CD32 | purified | NA | 1:100 | BD Bioscience | San Jose, USA |
| CD4 | APC | RPA-T4 | 1:200 | Biolegend | San Diego, USA |
| CD69 | PE | FN50 | 1:200 | Biolegend | San Diego, USA |
| Streptavidin | PE/APC | - | 1:300 | Biolegend | San Diego, USA |
| Streptactin | PE/APC | - | 1:250 | IBA | Göttingen, Germany |

FACS Staining (All experiments were conducted with mAbs targeting murine epitopes)

| epitope | dye | clone | dilution | manufacturer | |
|---|---|---|---|---|---|
| CD19 | PE/Dazzle 594 | 6D5 | 1:300 | Biolegend | San Diego, USA |
| CD3 | FITC/eF450 | 17A2 | 1:200 | BD Bioscience | San Jose, USA |
| CD4 | PE/APC/PerCPCy5.5 | H129.19 | 1:250 | BD Bioscience | San Jose, USA |
| CD8 | BV510/eF450/PECy7 | 53-6.7 | 1:200 | Biolegend | San Diego, USA |
| CD45.1 | eF450 | 104 | 1:100 | Thermo Fisher | Waltham, USA |
| CD45.2 | APC | 104 | 1:200 | Biolegend | San Diego, USA |
| CD90.1 | eF450/APC/FITC | HIS51 | 1:200 | Thermo Fisher | Waltham, USA |
| CD90.2 | BV785 | 30-H12 | 1:100 | Biolegend | San Diego, USA |
| CD25 | PE | PC61 | 1:300 | Thermo Fisher | Waltham, USA |
| PD-1 | APC | J43 | 1:100 | Thermo Fisher | Waltham, USA |
| TIM-3 | APC | RMT3-23 | 1:200 | Biolegend | San Diego, USA |
| NK1.1 | PerCP-Cy5.5 | PK136 | 1:200 | Thermo Fisher | Waltham, USA |
| CD19/32 | purified | 2.4G2 | 1:300 | Biolegend | San Diego, USA |
| CD3 | purified | 145-2C11 | 1:1000 | BD Bioscience | San Jose, USA |
| CD28 | purified | 37.51 | 1:3000 | BD Bioscience | San Jose, USA |

Stimulation Assays (All experiments were conducted with mAbs targeting human epitopes)

| | | | | |
|---|---|---|---|---|
| αCD3 (OKT-3) | - | 1:250 | BD-Bioscience | Heidelberg, Germany |

Western blot (All experiments were conducted with mAbs targeting human epitopes)

| epitope | dilution | manufacturer | |
|---|---|---|---|
| pY-ZAP70 | 1:1000 | Cell signaling | Danvers, USA |
| pY-p42/44 | 1:1000 | Cell signaling | Danvers, USA |
| EGFR-Rituximab | 1:1000 | Roche | San Francisco, USA |
| αFc-IgG4 | 1:1000 | Jackson ImmunoResearch Laboratories, Inc. | Santa Clara, USA |
| αGAPDH | 1:4000 | Cell signaling | Danvers, USA |
| Goat anti-rabbit IgG-HRP | 1:5000 | Santa Cruz Biotechnology | Heidelberg, Germany |
| Avidin-HRP | 1:1000 | IBA | Göttingen, Germany |

## 3.4 List of used buffers

| | |
|---|---|
| PBS Dublecco | ready to use preparation |
| FACS buffer | PBS Dulbecco<br>0.5 % (w/v) BSA |
| PBT | PBS Dulbecco<br>0.5 % (v/v) Tween 10 |
| blocking buffer | PBT<br>0.5 % (w/v) milk powder |
| fixation-solution | 50 % (v/v) methanol<br>120 % (v/v) acetic acid<br>38 % (v/v) bi-distilled $H_2O$ |
| ethanol-solution | 50 % (v/v) ethanol (100 %)<br>50 % (v/v) bi-distilled $H_2O$ |
| Na-thiosulfate-solution | 10 % (v/v) Na-thiosulfate stock solution<br>90 % (v/v) bi-distilled $H_2O$ |
| Na-thiosulfate-stock solution | bi-distilled $H_2O$<br>2 % (w/v) Na-thiosulfate |
| Silver-nitrate solution | bi-distilled $H_2O$<br>0.4 % (w/v) silver-nitrate $AgNO_3$<br>0.76 % (w/v) formaldehyde (37 %) |
| EZ-Running buffer | 90 % (v/v) bi-distilled $H_2O$<br>10 % EZ-Running buffer stock solution (Fisher scientific) |
| Blotting buffer | 20 % (v/v) methanol<br>10 % (v/v) 10x Tris Glycin<br>70 % (v/v) bi-distilled $H_2O$ |
| Puffer P | 100 mM Tris/HCl pH8<br>500 mM sucrose<br>1 mM EDTA |
| Puffer W | 100 mM Tris/HCl pH 8<br>150 mM NaCl<br>1 mM EDTA |
| Puffer E | 100 mM Tris·Cl<br>150 mM NaCl<br>1 mM EDTA |

| | |
|---|---|
| | 2.5 mM desthiobiotin, pH 8 |
| Developer solution | $Na_2CO_3$ solution<br>0.2 % (v/v) Na-Thiosulfate stock solution<br>0.05 % (v/v) formaldehyde (37 %) |
| $Na_2CO_3$ solution | bi-distilled $H_2O$<br>6 % (w/v) dehydrated N $a_2CO_3$ |
| Lysis buffer | 20- 150 mM NaCl<br>1 mM DTT<br>1 mM $Na_2EDTA$<br>1 mM EGTA<br>0,5 % (v/v) Nonident P-40<br>10 % (v/v) Glycerol<br>20 mM beta-Glycerolphosphat<br>1 mM $Na_3VO_4$<br>0,4 mM PMSF<br>1 Tablet Protease Inhibitor Cocktail (EDTA free)<br>1 mM NaF |
| 5x loading dye | 200 mM Tris-HCl pH 6,8<br>400 mM DTT<br>10 % (w/v) SDS<br>16 % (v/v) Glycerol<br>2 g/l Bromphenolblue |
| CLM-Buffer | |

## 3.5 Oligonucleotides (5'-3' orientation)

Will be added

## 3.6 Solutions & Chemicals

| reagent | manufacturer | location |
|---|---|---|
| 30 % acrylamide/bisacrylamide 29:1 | Sigma-Aldrich | Taufkirchen, Germany |
| TEMED | Invitrogen, Paisley, | United Kingdom |
| APS | Sigma-Aldrich | Taufkirchen, Germany |
| SDS | Sigma-Aldrich | Taufkirchen, Germany |
| Agarose | Invitrogen, Paisley, | United Kingdom |
| AHT | IBA | Göttingen, Germany |
| BSA | Roth | Karlsruhe, Germany |
| Western Lightning Plus ECL | Perkin Elmer | Heidelberg, Germany |
| Methanol | Klinikum rechts der Isar, | Munich, Germany |
| Ethanol | Klinikum rechts der Isar, | Munich, Germany |
| $AgNO_3$ | Sigma-Aldrich | Taufkirchen, Germany |
| Formaldehyde | Sigma-Aldrich | Taufkirchen, Germany |
| D-biotin | Sigma-Aldrich | Taufkirchen, Germany |
| β-mercaptoethanol | Agilent Technologies, Inc., | Santa Clara ,USA |
| Ampicillin | Sigma-Aldrich | Taufkirchen, Germany |
| Bromphenol-blue | Roth | Karlsruhe, Germany |
| Dimethyl Sulfoxide (DMSO) | Sigma-Aldrich | Taufkirchen, Germany |
| Dithiothreitol (DTT) | Sigma-Aldrich | Taufkirchen, Germany |
| EGTA | Sigma-Aldrich | Taufkirchen, Germany |
| Rotisafe | Roth | Karlsruhe, Germany |
| G418 (Neomycin) | PAA | Karlsruhe, Germany |
| Glycerol | Sigma-Aldrich | Taufkirchen, Germany |
| Kanamycin | Sigma-Aldrich | Taufkirchen, Germany |
| Methanol<br>Magnesium chloride (MgCl2)<br>Magnesium sulfate (MgSO4)<br>milk powder<br>Sodium chloride (NaCl) | Roth | Karlsruhe, Germany |

| | | |
|---|---|---|
| Penicillin/Streptomycin | PAA | Pittsburgh, USA |
| TWEEN 20 | Sigma-Aldrich | Taufkirchen, Germany |

## 3.7 Cell Media

| Media | Ready to use preparation | manufacturer |
|---|---|---|
| HEK and Plat-A Media<br>(for adherent cells)<br>10 % FCS | 1 x DMEM<br>10 % (v/v) FCS<br>1 % (v/v) Penicillin-Streptomycin<br>1 % (v/v) Antibiotics/Antimycotics<br>0.035 % (v/v) -Mercaptoethanol | PAA<br>PAA<br>PAA<br>PAA<br>PAA<br>PAN |
| HEK and Plat-A Media<br>(for adherent cells)<br>2 % FCS (signaling) | 1 x DMEM<br>10 % (v/v) FCS<br>1 % (v/v) Penicillin-Streptomycin<br>1 % (v/v) Antibiotics/Antimycotics<br>0.035 % (v/v) β-Mercaptoethanol | PAA<br>PAA<br>PAA<br>PAA<br>PAA<br>PAN |
| K-562, K562-CD19, Jurkat, LCL, BLL, Raji, suspension cell Media<br>RPMI,<br>10 % FCS | 1 x RPMI<br>2 % (v/v) FCS<br>1 % (v/v) Penicillin-Streptomycin<br>1 % (v/v) Antibiotikum/Antimycotikum<br>0.035 % (v/v) -Mercaptoethanol | PAA<br>PAA<br>PAA<br>PAA<br>PAA<br>PAN |
| Freeze media | 10 % (v/v) DMSO 90 % (v/v) FCS | Sigma-Aldrich<br>PAA |

## 3.8 Media for bacteria

| Media | Ready to use preparation |
|---|---|
| $LB_0$(Luria-Bertani)- Medium | 10 g/l Bacto-Tryptone<br>5 g/l yeast extract<br>20 g/l Agar (for petri dishes)<br>10 g/l NaCl<br>pH 7,0 (NaOH)<br>Autoclaving |
| LB-Amp-Medium | See $LB_0$ + 50mg/l ampicillin |
| LB-Kana-Medium | See $LB_0$ + 10mg/l kanamycin |

## 3.9 Software

| Software | manufacturer | |
|---|---|---|
| Flowjo 10 | Treestar | Ashland, USA |
| MS Office (Word, Excel, PowerPoint) | Microsoft | Unterschleißheim, Germany |
| Prism | GraphPad | San Diego, Germany |
| Summit 4.3.01 | DakoCytomation | Golstrup, Denmark |
| Photoshop CS6 | Adobe | Adobe Systems Software Ireland |
| Illustrator CS6 | Adobe | Adobe Systems Software Ireland |

## 3.10 Organisms (Bacteria)

| Organisms | strain | manufacturer | |
|---|---|---|---|
| *E. coli* | *JM83* | IBA | Göttingen, Germany |
| *E.coli* | *XL-10* | Agilent | Santa Clara, USA |
| *E.coli* | *TOP10* | IBA | Göttingen, Germany |

## 3.11 Organisms (Cells)

| Organism | Type | Manufacturer, | ATCC number |
|---|---|---|---|
| *Human* | *Human Embryonic Kidney (HEK)* | ATCC, Teddington, UK | ATCC-Nr.CRL-1573 |
| *Human* | *K-562 (lymphoblast) chronic myelogenous leukemia (CML)* | ATCC, Teddington, UK | ATCC-Nr. CCL-243 |
| *Human* | *Jurkat (lymphocyte) acute T cell leukemia* | ATCC, Teddington, UK | ATCC-Nr. TIB-152 |
| *Human* | *Platinum A, retroviral packaging cells* | Cell biolabs Inc., San Diego, USA | - |
| *Human* | *Platinum E, retroviral packaging cells (mouse cells)* | Cell biolabs Inc., San Diego, USA | - |
| *Human* | *LCL, B-lymphoblast* | ATCC, Teddington, UK | ATCC-Nr.CRL-2371 |
| *Human* | *BLL, Typical human B cell leukemia* | ATCC, Teddington, UK | FHCRC |
| *Human* | *Raji, Burkitt lymphoma* | ATCC, Teddington, UK | ATC-Nr. CCL-86 |

## 3.12 Enzymes

| Name | Manufacturer | |
|---|---|---|
| Herculase II | Stratagene | London, UK |
| Benzonase | Sigma-Aldrich | Taufkirchen, Germany |
| Collagenase V | Sigma-Aldrich | Taufkirchen, Germany |
| DNase | Sigma-Aldrich | Taufkirchen, Germany |
| T4 DNA ligase | Thermo Fisher scientific | Waltham, USA |
| NHEI | Thermo Fisher scientific | Waltham, USA |
| EcoRI | Thermo Fisher scientific | Waltham, USA |
| NotI | Thermo Fisher scientific | Waltham, USA |
| RsrII | Thermo Fisher scientific | Waltham, USA |
| BamHI | Thermo Fisher scientific | Waltham, USA |
| HindIII | Thermo Fisher scientific | Waltham, USA |
| Phosphatase | Thermo Fisher scientific | Waltham, USA |
| Taq polymerase | Thermo Fisher scientific | Waltham, USA |
| NcoI | Thermo Fisher scientific | Waltham, USA |

## 3.13 Kit systems

| Name | manufacturer |
|---|---|
| SV Miniprep DNA Purification System | Promega |
| Wizard SV Gel and PCR Clean-Up System | Promega |
| SV Midiprep DNA Purification Systems | Promega |
| RNeasy mini kit | Qiagen |
| Effectene Transfection Reagent | Qiagen |
| Gibson assembly mix | New England Biolabs (NEB) |

## 3.14 List of machines

| Device | Name | Supplier |
|---|---|---|
| Thermocycler | T3 Thermocycler | Biometra, Göttingen, Germany |
| Thermocycler | T3000 Thermocycler | Biometra, Göttingen, Germany |
| spectrophotometer | NanoDrop | Kisker-Biotech, Steinfurt, Germany |
| flow cytometer | CyAn ADP | DakoCytomation, Golstrup, Denmark |
| FACS Sorter | MoFlo II | Beckman Coulter, Krefeld, Germany |
| power supply | Electrophoresis Power Supply EPS | Amersham, Freiburg, Germany |
| gel chamber | HE33 mini horizontal submarine unit | Amersham, Freiburg, Germany |
| gel chamber | SE250/260 | HOEFER, Holliston, USA |
| water bath | E100 | LAUDA, Königshofen, Germany |
| electroporator | pulse controller | Biorad, Munich, Germany |
| electroporator | gene pulser | Biorad, Munich, Germany |
| gel documentation system | Eagle Eye | Biorad, Munich, Germany |
| centrifuge | Sorvall 6+ Centrifuge | Thermo Scientific, Bonn, Germany |
| centrifuge | Multifuge 3 S-R | Heraeus , Hanau, Germany |
| bench top centrifuge | Biofuge fresco | Heraeus, Hanau, Germany |
| photometer | BioPhotometer | Eppendorf, Munich, Germany |
| photometer | Ultraspec3000 pro | Amersham *Bioscience*, Freiburg, Germany |
| radiographic cassette | radiographic cassette | Dr. Goos-Suprema, Heidelberg, Germany |

# 4 Methods

## 4.1 Molecular Methods

### 4.1.1 **PCR**

Polymerase chain reaction (PCR) was performed in a thermocycler T3 (Biometra, Göttingen). A typical PCR program included the following parameters:

| temperature [°C] | time [min:sec] | Cycle [count] |
|---|---|---|
| 1) 95 denaturation | 5:00 | x1 |
| 2) 95 denaturation | 1:00 | |
| 3) 48 annealing | 0:45 | X28/35 |
| 4) 72 elongation | 3-X | |
| 5) 72 synthesis | 3-X | x1 |
| 6) 4 storage | PAUSE | x1 |

Steps 4) and 5) were adjusted to the experiment and the different constructs. Step 2) to 4) were repeated from 28 to 35 times.

For common PCR following PCR reagents were used (Agilent PCR kit):

**Mutagenesis PCR Pipetting schematic according to Agilent manufacturers protocol**

| | Volume |
|---|---|
| Herculase II | 1 µl |
| Herculase-buffer | 10 µl |
| primer-forward [10µm] | 1.25 µl |
| primer-reverse [10µm] | 1.25 µl |
| dNTPs | 0.25 µl |
| DMSO | 0.25 µl |
| template (100ng) | 1 µl |

### 4.1.2 **Mutagenesis-PCR**

Mutagenesis polymerase chain reaction (PCR) was used to introduce directed point mutations in the framework regions of scFv of CAR constructs using specific forward and reverse primers. The method applied is based on the use of 5'-phosphorylated primers allowing the amplification of the whole plasmid including the subcloned GOI and the subsequent direct ligation of the amplicon. The primer contact site contains the site of mutagenesis.

### 4.1.3 **Gibson assembly PCR**

For subcloning of DNA fragments, Gibson assembly was used. This method is based on the joining of overlapping DNA fragments in a single isothermal reaction. For this primer were designed that allowed the amplification of the gene of interest including 20-30 bp overlap to the adjacent integration site. Further primers flanking the integration site allowed the linearization of the target vector [182].

The following reaction was set up (consequently on ice):

**New England biolabs (NEB) manufacturers protocol**

| | |
|---|---|
| 2-3 fragment Assembly | |
| Total Amount of Fragments | 0.02- 0.5 pmol X µl |
| Gibson Assembly Master Mix (2x) | 10 µl |
| Deionized $H_2O$ | 10- X µl |
| Total volume | 20 µl |

For the Gibson Assembly the reaction mix (see above) was incubated for 25 min at 50 °C in the thermocycler. Afterwards a heat-shock transformation with 5 µl of the Gibson assembly mix was performed as described.

### 4.1.4 DNA isolation via DNA Gel electrophorese

PCR amplified DNA fragments were electrophoretically separated using a 1-1.4 % agarose gel supplemented with rotisafe DNA dye (Roth). The agarose solution was prepared in 1x TAE–buffer, boiled, allowed to cool to 55°C then rotisafe (100 µl/l) was added. The solution was added to a horizontal gel chamber (Biorad) and allowed to polymerize for 20 min. PCR samples were supplemented with DNA loading dye (6x DNA Loading Dye, Fermentas) before run. For size reference 1 kb DNA marker (GeneRuler 1 kb DNA Ladder, Fermentas) was used. The gel run was performed at 130 V for 27 min. DNA fragment detection was done by UV–light at wave length 254 nm. Gels were documented and photographed with an Eagle Eye (Biorad).

### 4.1.5 Preparative DNA Gel

The desired DNA fragment of correct size was excised from the agarose gel using a sharp scalpel. The DNA was extracted from the gel slice using the Wizard SV Gel and PCR Clean Up System.

DNA quantification:

DNA concentration was determined photometrically by extinction at a wavelength of 260 nm. Extinction of 1 correlates with a concentration of 50 ug/ml. The Quotient 260/280 shows the purity of the DNA–

fragments. 1.8 is a very pure value which decreases with protein contamination. DNA quantification was performed using a NanoDrop ND-1000 (PeqLab)

### 4.1.6 Analytical restriction digest of DNA fragments

Restriction enzymes type II recognize specific palindromic recognition sites (4-8 bp). They produce sticky or blunt ends at the cutting side. These cutting sides can be ligated using a T4 DNA ligase. The restriction digest is done by at 37 °C and the following protocol is used.

2 µl 10 x Reaktionspuffer
1 µg DNA
0.5 µl 5'-Restriktionsenzym (10U/µl)
0.5 µl 3'-Restriktionsenzym (10U/µl)
add to 20µl $H_2O$bidest.

To degrade residual template DNA after a completed PCR run, methylated DNA (plasmid) was degraded using DpnI (1 U/PCR sample). The restriction enzyme was added to the PCR sample and the mixture was incubated for 1 h at 37 °C.

### 4.1.7 Ligation of DNA fragments

Ligation of compatible DNA endings was performed using the enzyme T4–DNA–ligase (Fermentas) according to the following protocol:

4 µl 5x *Rapid Ligation Buffer*
x µg Vector-DNA
y µg *Insert*-DNA
1 µl T4 DNA Ligase (1 U/µl)
ad to 20 µl $H_2O$ bidest.

The ligation was incubated at room temperature for 30 min and afterwards stored at-20 °C for further preparation. The ratio of vector and insert varied from 1:3 to 1:10 (v/i).

### 4.1.8 DNA sequencing

DNA sequencing was performed at GATC Biotech AG, Konstanz.

### 4.1.9 Heat shock transformation

For heat shock transformation chemical–competent *E. coli* (strain XL-10 (Agilent) or TOP-10 (IBA) were used. Competent *E. coli* were thawed on ice. 10-100 ng plasmid DNA (maximum volume 5 µl) were added to 50 µl *E. coli* suspension. The mixture was incubated on ice for 30 min then heat–shock was performed

for 45 sec at 42 °C followed by a 2min rest on ice. Then 1 ml $LB_0$ was added and the preparation was incubated at 37°C for 45 min under constant agitation. Then 100-200 µl of the suspension were plated on the respective selection media (ampicillin or kanamycin).

### 4.1.10 plasmid DNA extraction

The sample DNA was purified from previously prepared *E. coli* cultures using the PureYield Plasmid Miniprep System (Promega) according to the manufacturer's instructions. The DNA was eluted with 50 µl elution buffer. For the production of large amounts of plasmids, the SV Midipreps DNA Purification Systems (Promega) was used.

### 4.1.11 Production of electrical competent E. coli JM83

For production of electrocompetent *E. coli JM83,* bacteria were cultured in 5ml LB medium overnight at 37 °C under constant agitation (150 rpm). The next morning 1l $LB_0$ was inoculated with 5ml pre-culture and incubated (37 °C, 150 rpm) until an $OD_{600}$ of 0.5 to 0.6 was reached. Afterwards the cells were kept on ice for 10min and centrifuged (4000 x g; 15 min; 4 °C). The supernatant was discarded, and the pellet resuspended in 5ml ice-cold 1 mM HEPES buffer. After resuspension another 350 ml ice-cold 1 mM HEPES was added. The washing procedure was repeated twice. Afterwards the pellet was resuspended in 5ml ice-cold 10 % glycerin and centrifuged (4000 x g; 15 min; 4 °C). Finally, the pellet was resuspended in 2 ml ice-cold 10 % glycerin, divided into aliquots of 40 µl, shock frozen in liquid nitrogen and stored at-80 °C.

### 4.1.12 Periplasmic expression

For periplasmic expression one aliquot of the *E. coli* expression lineage *JM83* stock was thawed on ice and attenuated with 100 µl sterile bi-distilled $H_2O$. 80 µl of *JM83*-solution were transferred into a precooled 1.5 ml Eppendorf tube and 1 µl (100 ng) of target plasmid was added. After mixing the solution was transferred into an electroporation cuvette (optical path 1 mM (Sigma)) (. The cells were transformed with the target plasmid using electroporation (400 Ω 25 µF and 2.5 kV; Pulse Controller & Gene Pulser (Biorad). After electroporation bacteria were immediately supplemented with 1 ml prewarmed (37 °C) LB-medium and transferred to an Eppendorf tube. The cells were incubated for one hour at 37 °C to give the cells time to develop antibiotic resistance. Then 500 µl were transferred into 4ml $LB_{Ampi}$ (100 mg/L) and incubated under constant agitation (150 rpm) overnight at 37 °C. Next day 2 ml of overnight culture were transferred to a 200 ml Erlenmeyer flask and incubated for 24 h at 22 °C and 150 rpm. To start the main culture 25 ml were transferred into a two-liter flask which was then filled up to a total volume of one liter with $LB_{Ampi.}$

The bacteria were incubated at 22 °C and 150 rpm until an $OD_{600}$ of 0.5-0.6 was reached. For induction of protein expression AHT was added at a ratio of 1:10000. After incubation for another three hours the $OD_{600}$ was measured and the bacteria harvested. The cells were centrifuged at 5000 x g for 12 min at 4 °C and the pellet stored at-80 °C.

To extract the Fab-fragment the pellet was thawed and resuspended in 20 ml buffer P at 4 °C. After 30 min incubation on ice the cells were centrifuged at 15000 rpm for 15 min at 4 °C (Sorval 6+ Centrifuge SA300 rotor). The supernatant was transferred into a falcon tube and contaminating nucleic acids were enzymatically digested using Benzonase (125 U). The cells were kept on ice for 30 min and afterwards sterile filtered using a 0.22 µm filter. The filtered periplasmic extract was transferred onto a *Strep*-Tactin-Superflow column (IBA, Göttingen), which was previously equilibrated twice with 2.5 column volumes ice-cold buffer W. Afterwards the column was washed five times with buffer W. The Fab-fragment was eluted using buffer E. Three elution samples were collected (0.8 ml, 1.5 ml, 1.0 ml). The second elution sample having the highest protein content was dialyzed against sterile PBS pH 7.4 at a ratio of 1:1000000 using a cut off dialyses flexible tube (14 kDa). After dialysis the samples were analyzed for total protein content using a nanodrop device (Thermo scientific) and for their purity using SDS-PAGE and silver staining (8.6.). The Beer-Lambert equation (A = E x b x c) was used for all protein calculations to correlate absorbance with concentration.

A is the absorbance value ($A_{280}$), E is the wavelength-dependent molar absorptivity coefficient (or extinction coefficient) with units of liter/mol-cm, b is the path length in centimeters, c is the analyte concentration in moles/liter or molarity (M). The extinction ($A_{280}$) was measured by the Nanodrop. The molecular extinctions coefficient was calculated by Protparam using the amino acid sequences of the Fab-fragments. The path length used for calculation was 1cm, according to manufactures. The concentration was calculated by following equation:

Concentration: $c = \frac{E}{å \times d}$

### 4.1.13 **Dye conjugation of single chain variable fragments**

Ice cold degassed PBS at pH of 7.3 was added at a volume of 4 mL to purified single chain samples, before centrifuging at 3000 rpm (4 °C) with 10 kDa Amicon Ultracentrifugation filters (Merck, Darmstadt) until 500 µL was left in the upper chamber. The solution was transferred into an Eppendorf tube. 1 µL of the protease inhibitor DTT (154 mg in 10 mL H2O) was added to the sample and 2 µL of the Alexa488 dye were added for Maleimide conjugation. It was incubated overnight at 4 °C.

On the next day, a Gravity Flow column (GE) was equilibrated using 5 times of 5 mL PBS at pH 8.0. The sample was added to the column in a volume of 500 µL and washed with 500 µL PBS (pH 8.0). Eluted by using 4 mL PBS (pH 8.0) and 2 µL of each Leupeptin and Pepstatin were added, before using 10 kDa ultracentrifugation filters to concentrate the single chains at a volume of 500 µL by centrifuging at 3000 rpm, 4 °C. Dye was aliquoted and stored at -80 °C in the dark.

## 4.2 Protein biochemical Methods

### 4.2.1 **SDS-PAGE and analysis**

#### *4.2.1.1 SDS-PAGE*

To examine the purity of expressed protein constructs as well as for analysis of retrovirally transduced cells SDS-polyacrylamide-gel electrophoresis (SDS-PAGE) using a 12 % SDS gel was performed. After assembling the gel chamber the separation gel was casted into the gel chamber and covered with isopropyl alcohol. By covering the gel air bubbles are prevented and a clear horizontal top edge is formed. After polymerization of the separation gel the stacking gel was applied, and the comb was placed into the gel. The following reagents and volumes were used

**Table 1: components for 12 % SDS Gel**

| **12 % SDS-PAGE** | | |
|---|---|---|
| | Separation gel | Stacking gel |
| acrylamide | 12 ml | 2.6 ml |
| 1.5 M Tris-HCl pH8.8 | 7.5 ml | - |
| 2.0 M Tris-HCl pH6.8 | - | 1.25 ml |
| SDS 10 % (w/v) | 300 µl | 800 µl |
| $H_2O$ | 9.9 ml | 15.7 ml |
| TEMED | 15 µl | 20 µl |
| APS 10 % (w/v) | 150 µl | 100 µl |

For analysis 12 µl 5x loading buffer were mixed with 50 µl of the probe and boiled at 95 °C for 5 min. After a short spin (5 sec, to avoid concentration alterations due to condensation during boiling), 20 µl of the sample were loaded into the pocket of a prepared SDS Gel. 80 V of voltage were applied till the dye front reaches the end of the stacking gel; then the voltage was increased to 120 V. The gel run was stopped when the 10 kDa marker band reached the bottom edge of the gel.

#### *4.2.1.2 Silver staining*

Silver staining is a sensitive procedure to detect trace amounts of proteins in SDS-PAGE gels. It is possible to identify or quantitatively determine the components of protein mixtures. Silver staining was used to analyze the purity of expressed Fab-fragments after purification. The SDS-gel was incubated in the fixation solution for 30min and afterwards washed three times for 15 min in the ethanol solution. After discarding the ethanol solution, the gel was incubated in the thiosulfate-solution for one minute. After washing the gel three times in bi-distilled $H_2O$ for 20 sec each, the silver nitrate solution was added, and the gel was incubated for 20 min. After washing the gel twice in bi-distilled $H_2O$ for 30 sec, the developer solution was added. The staining process was stopped by adding the fixation solution when an optimal staining intensity was achieved. For conservation stained gels were incubated in sealing buffer for 10min and finally sealed between two layers of cellophane.

#### *4.2.1.3 Coomassie Blue staining*

Gel of SDS-PAGE separation was fixated for 10 minutes at room temperature in destaining solution. It was then stained for 0.5 – 2 hours at room temperature to get a uniform blue color of the gel. It was then destained for several times and overnight. A photo was taken for analysis.

### 4.2.2 **Western blot analysis**

#### *4.2.2.1 Semi dry- blot*

For the detection of a protein using a specific antibody western blot analysis was performed. In detail the gel was applied on two layers of Whatman paper (7 cm x 18 cm for a large gel and 7 cm x 9 cm for a small gel) wetted with blotting buffer and a layer of nitrocellulose membrane (6x18 cm for large gels, 6x9 cm for small gels). After adding a small volume of blotting buffer, the gel was trimmed smooth to the surface and another two layers of Whatman paper soaked with blotting buffer were applied on top. The blotting chamber was assembled and connected to the power supply. The power supply was set to a maximum of 25 V and 1.2 A/$cm^2$ gel, the transfer time was limited to 1 h 40 min. Afterwards the gel and the Whatman

paper were disposed, the nitrocellulose membrane was blocked in blocking buffer for one hour at 4 °C and subsequently washed twice in PBT for 2 min each. After washing the nitrocellulose membrane was transferred into a falcon tube containing 2 ml of the primary antibody solution. The primary mAb was diluted as recommended by the manufacturer (usually in a ratio 1:5000 anti-CD3ζeta) and incubated at 4 °C overnight on a rolling incubator. The next morning the membrane was washed three times in PBT for 10 min each, followed by secondary mAb incubation for one hour. After incubation the membrane was washed four times in PBT for 5 min and two times in PBS for 5 min. After washing the membrane was incubated for one min with Western Lightning ECLplus (enhanced chemiluminescence lightning solution) and stored in a radiographic cassette. X-ray films were exposed for different time intervals on the membrane in the darkroom and afterwards developed.

## 4.3 Cell biological methods

### 4.3.1 **Cultivating of adherent cells**

Cultivation of adherent cells was done in 15 cm cell culture petri dishes in DMEM adherent cell medium 10 % FCS at 37 °C, 5 % $CO_2$ and 95 % humidity. The cells were cultivated until a confluence of 80-90 % was reached and then splitted. First the cells were washed once with 5 ml PBS then trypsinized with 5 ml 1x trypsin in PBS to detach the cells from the culture plate. The trypsin digest was stopped by adding DMEM 10 % FCS media, resuspended and centrifuged for 5 min at 1500 x rpm. About 20 % of the cells were added to a new culture plate for further cultivation.

### 4.3.2 **Cultivation of suspension cells**

Suspension cells were cultivated in 25cm$^2$ or 75cm$^2$ culture flasks standing in the incubator with RPMI 10 % FCS media, 37 °C, 5 % $CO_2$ and 95 % humidity. For further cultivating and expanding of the cells the media was sucked up to a rest volume of the media by 2ml and fresh RPMI 10 % FCS media was added. If necessary, a new or additional culture flask was used.

### 4.3.3 **Freeze and thaw cells**

Cells were prepared as described before and instead of sawing those out on a new culture plate the cells were resuspended in 4ml of the freeze media and aliquoted in cryo- conserving tubes. First the cells were stored in-20 °C for 2 h, and then transferred to-80 °C. After 24 h cells were transferred to liquid nitrogen for permanent storage. For thawing, cells were warmed quickly in a water bath at 37°C. The cell suspension was then added to about 30 ml of cell medium (RPMI or DMEM) containing 10 % FCS. The cells were washed twice by centrifugation 1500 x rpm for 6 min. After washing the cells were resuspended and seeded in an appropriate volume and cultured at 37 °C and 5 % $CO_2$.

### 4.3.4 **Transfection**

For transfection the Effectene® Transfection Reagent (Qiagen) was used according to the suppliers' instructions. In this case a high transfection efficacy and low cytotoxicity is reached. In this kit the plasmid DNA is first condensated then a complex was formed with the lipids in the solution, diluted and finally added dropwise to the cells. This facilitates the cellular uptake of DNA. The transfection efficacy is cell line dependent and thus requires adjustment of the protocol to the different cell lined used.

### 4.3.5 **Retroviral transfection**

The retroviral transfection is a method to transfer DNA in cells with retroviruses. After infection of the target cells the retroviral RNA is reverse transcribed to dsDNA and integrated into the host genome allowing the stable expression of the gene of interest. Special envelope proteins (envelope) bind to surface associated receptors and thus induce receptor specific uptake into the target cell. Here an amphotronic cell line (Plat A) was used which can infect almost every cell type.

### 4.3.6 **Production of retroviral particles**

The Plat A cell line is stably transfected with the viral protein coding genes (env, gag, pol). If these cells are transfected with a retroviral vector which contains a ψ packaging signal the production and secretion of retroviral particles is induced. For virus particle production 2 x $10^6$ Plat A cells were seeded in 10 ml DMEM 10 % FCS in a 10cm petri culture dish. After 12 h the plasmid of choice was transfected using Effectene® Transfection Reagent (Qiagen). 24 h and 48 h after transfection retroviral particles were harvested by partial media exchange. The supernatant which contains the retroviral particles was filtered through a 45 µm filter. To complete the transduction, mix polybrene was added to a final concentration of 5 µg/ml.

### 4.3.7 **Production of lentiviral particles and transduction**

293T Lenti-X cells (Clontech) were cultured in Dulbecco's modified Eagle's medium (Gibco) supplemented with 10% fetal bovine serum, 1 mM l-glutamine (Gibco), 25 mM Hepes (Gibco), and penicillin/ streptomycin (100 U/ml; Gibco). K562 (CCL-243) and Raji (CCL-86) cells were obtained from the American Type Culture Collection and cultured in RPMI 1640 (Gibco) supplemented with 5% fetal bovine serum, 1 mM l-glutamine, 25 mM Hepes, and penicillin/streptomycin (100 U/ml). Primary human T cells were cultured in CTL medium consisting of RPMI 1640 supplemented with 10% human serum, 2 mM l-glutamine, 25 mM Hepes, penicillin/streptomycin (100 U/ml), 50 µM β-mercaptoethanol (Sigma), and human IL-2 (50 U/ml; Prometheus). All cells were cultured at 37°C and 5% CO2 and tested bimonthly for the absence of mycoplasma using the MycoAlert Mycoplasma detection Kit (Lonza).

To prepare CAR T cells, Lenti-X cells were transiently transfected with the HIV7 CAR vector, as well as psPAX2 (Addgene plasmid no. 12260) and pMD2.G (Addgene plasmid no. 12259) packaging plasmids. One day later (day 1), primary T cells were activated using Dynabeads Human T-Activator CD3/CD28 (Thermo Fisher Scientific) and cultured in CTL supplemented with IL-2 (50 U/ml). On the next day (day 2), lentiviral

supernatant was harvested from Lenti-X cells, filtered using 0.45 um polyethersulfone (PES) syringe filters (Millipore), and added to activated T cells. Polybrene (Millipore) was added to reach a final concentration of 4.4. g/ml, and cells were spinoculated at 800g and 32°C for 90 min. Viral supernatant was replaced 8 hours later with fresh cRPMI supplemented with IL-2 (50 IU/ml). Half-media changes were then performed every 48 hours using cRPMI supplemented with IL-2 (50 U/ml). Dynabeads were $CD8^{+}EGFRt^{+}$- removed on day 6; transduced T cells were FACS (fluorescence-activated cell sorting)–purified on a FACS AriaII (BD Biosciences) on day 9. To prepare K562/CD19 cells, Lenti-X cells were transiently transfected with psPAX2, pMD2.G, and an HIV7 lentiviral vector encoding CD19. To prepare K562 cells, Lenti-X cells were transiently transfected with MLV g/p, 10A1, and an mp71 retroviral vector encoding ROR1. To prepare Raji/ffluc cells, HEK293 cells were transiently transfected with psPAX2, pMD2.G, and an HIV7 lentiviral vector encoding GFP and firefly luciferase. Two days later, viral supernatant was filtered using a 0.4 um PES syringe filter and added to K562 or Raji cells. Five days later, transduced cells were stained with mAbs specific for CD19 (HIB19, BioLegend) or ROR1 (2A2, Miltenyi Biotec) and FACS-purified on a FACS Aria II to greater than 97% purity.

### 4.3.8 Lenti - retroviral transduction of K-562 and Jurkats (cell lines)

For lenti- retroviral transduction 1-1.5 $x10^6$ target cells were seeded in a 12-well plate and 3 ml of the virus preparation was added. To further enhance transduction efficacy 4 mM $CaCl_2$ were added. After adding the supplement spin transduction was performed 24 h and 48 h ($1^{st}$. $2^{nd}$ harvest) for 90 min, 1000 x g to enhance the transduction efficacy. The polykation in this case increases the interaction between virus particle (glycoprotein) and target cell receptor [183, 184]. Fresh virus supplement was added twice. 12 h after the last administration of virus supplement the cells were centrifuged (1000 x g, 5 min) and resuspended and seeded in RPMI 10 % FCS.

### 4.3.9 Preparation of cell lysates for proteo-chemical analysis

For analysis of protein content or phosphorylation status cells were lysed using a detergent containing buffer. For detection of activation of ZAP-70 or p42/42 the cells were serum starved for 24 h in DMEM 2 % prior to stimulation. After harvest the cells were washed once with ice cold PBS and centrifuged (2000 x rpm, 5 min, 4 °C). The cell pellet was resuspended in 50 µl 150 mM NaCl lysis-buffer and incubated on ice for 20min. Then the lysate was centrifuged one more time (13000 x rpm, 5 min, 4 °C) to remove cell debris and membrane fragments. The supernatant was transferred to a new 1.5ml tube and

supplemented with 5x sample buffer. Lysates were either directly subjected to western blot analysis or stored at-20 °C (see SDS-Page).

#### *4.3.9.1 RNA extraction*

For RNA extraction a maximum of 2 x $10^5$ cells was used. The mRNA was isolated using the RNeasy Mini Kit (Qiagen). Briefly the cells were lysed, and the DNA digested using DNase I and the mRNA was bound to an anion column washed and later eluted.

#### *4.3.9.2 cDNA synthesis*

The isolated RNA was reverse transcribed according to the protocol of Agilent (AccuScript PfuUltra II RT-PCR Kit). For that the mRNA was first incubated at 65 °C for 5 min with the following master mix:

4.9 µl of RNase-free water (not DEPC-treated water)
1.0 µl of 10× AccuScript RT reaction buffer
0.6 µl of oligo (dT) primer or random primers or a gene-specific primer
(100 ng/ µl)
1.0 µl of dNTP mix (10 mM each dNTP)
1.0 µl of RNA (see table below for guidelines on RNA quantity)

#### *4.3.9.3 RNA Quantity*

Total RNA, target <2 kb 10–200 ng
Total RNA, target >2 kb 200–500 ng
mRNA (all targets) 0.1–10 ng
Next the reaction mix was cooled down to room temperature in about 5min to allow primer annealing. Then 1 µl of 100 mM DTT and 0.5 µl AccuScript High-fidelity RT were added to the reaction. The reaction was incubated for 30- 50 min at 42 °C for cDNA synthesis. After synthesis the cDNA was used as PCR template to amplify the gene of interest.

### 4.3.10 **In vitro-killing assays**

#### *4.3.10.1 xCelligence cytotoxicity assay*

Blanks of E-Plates (ACEA) containing DMEM medium were measured by xCelligence instrument. CD19 presenting Human embryonic kidney cells (HEK293-$CD19^+$) or Raji ($CD19^+$) cells were counted. 2x$10^4$ HEK293-CD19+ cells were transferred to E-Plate and cultivated for 1 day. Transduced T cells were added

to have the highest E:T ratio of CAR cells of 10:1 or 5:1 and were subsequently diluted 1:1. Plates were incubated for 3 days while measuring impedance for monitoring killing capacity. Specific killing was determined using following formula: %Specific release= (Maximum release (counts)-Spontaneous release (counts)/ Experimental release (counts)-Spontaneous release (counts)) x100.

#### *4.3.10.2 Europium cytotoxicity assay*

Target cells were labelled at a cell number of 5x105 Raji cells. They were washed with 10 mL Europium medium with 10% heat-inactivation and no indicator and resuspended in 200 µL medium. 1 µL of the BATDA Reagent of the Kit was added and incubated for 30 minutes at 37 °C with the falcon lid off. Solution was resuspended every 10 minutes for homogeneous labeling. Effector cells were plated in a 96 well plate in a volume of 100 µL with the highest ratio being 30:1 of effector to target cells.

Target cells were washed three times in 10 mL fresh Europium medium containing 1x Sulfinpyrazone and centrifuged at 1500 rpm, 20 °C for 3 minutes. Target cells were resuspended in 10 mL medium with Sulfinpyrazone and added in a volume of 100 µL to the plated effector cells.

Samples were measured as triplicates and the following controls were added:

Medium control: medium with stabilizer was mixed 1:1 with medium without stabilizer

Raw spontaneous value: target cells in medium with Sulfinpyrazone were added to an equal volume of medium without stabilizer

Maximum value: target cells in medium with Sulfinpyrazone were added to an equal volume of medium containing 2% Triton X-100 without Sulfinpyrazone. Plate was spun down at 300 rpm for 3 minutes and then incubated for 4 hours at 37 °C.

Afterwards the plate was mixed for 30 seconds and samples of maximum control were pipetted up and down. Plate was spun down at 800 rpm for 3 minutes and supernatant used. 200 µL of a 1:5 diluted Europium solution was mixed with 25 µL of the supernatant and incubated on a plate shaker for 5 – 15 minutes. Plate was put into the plate reader and Europium program was started. Specific lysis was calculated using following formula

Equation 2: calculation of specific lysis for europium killing assay

%lysis = 100*((raw value-spontaneous value))/ ((maximum value-spontaneous value))

#### *4.3.10.3 Chromium$^{51}$ (51CR) cytotoxicity assay*

Functionality of clinically relevant anti-CD19 CAR T cells was tested using chromium release assay. The K562 cell line, and K562-CD19-overexpressing cell lines were used as target cells that were labeled with radioactive chromium (51Cr) at 37°C for 90 minutes. Excess chromium was removed by washing radiolabeled cells twice with PBS. Effector cells had been generated from PBMCs separating $CD8^+$ cells. $CD8^+$ CD19 CAR transduced cells were added to the radiolabeled target cells at different E:T ratios, while keeping the number of target cells constant at 1000 cells/well on a round-bottom 96-well plate. After centrifugation at 800rpm for 3 minutes, cells were coincubated at 37°C for 4 hours. Spontaneous and maximum release was determined by adding medium or a detergent (2% Triton-X) to the target cells instead of effectors. All samples were run in triplicates. After co-incubation of target and effector cells, 30µL of the supernatant were transferred to solid scintillator-coated lumaplates that were then dried overnight. Chromium release was measured as counts per minute (cpm) by analyzing samples with the TopCount scintillation counter. The specific lysis was calculated by using the following formula: % specific lysis = (mean sample release - mean spontaneous release) ÷ (mean maximum release - mean spontaneous release) x 100.

#### *4.3.10.4 Co-incubation assays*

For the in co-culture vitro killing assay effector and target cells were co-incubated at different ratios e.g. E:T (3:1, 2:1, 1:1). Untransduced cells served as a negative control whereas transduced CAR positive cells represented the functional effectors. Target cells were CD19 or STII positive cells. The cells were co-incubated for 24 h or 48 h. Afterwards a FACS staining was done as described. In that case the CD19 surface molecule was stained to determine the frequency of CD19 or STII positive cells in the cell suspension. To normalize the data the total cell number per well was usually counted manually.

### 4.3.11 **In vitro cytokine secretion assay**

CAR T cells were cocultured with mainly K562, K562/CD19, or corresponding target cells at a T cell–to–tumor cell ratio of 2:1 in a 96 well format. In some experiments, CAR T cells were also incubated with control cells in a similar E:T ratio. Cytokine concentrations in cellular supernatant were quantified by ELISA (Thermo Fisher Scientific) 24 hours after stimulation/co-incubation. T cell proliferation was quantified by staining CAR T cells with a 0.2 µM solution of CFSE or CTV dye (Thermo Fisher Scientific) and incubating CAR T cells with K562/ CD19 cells or control target cells for 72 hours.

### 4.3.12 **TM-LCL expansion**

After transduction, cells were counted and analyzed by flow cytometry or FACS sorted. The numbers of CAR positive T cells were calculated. CD19 expressing LCL cells were harvested, calculated, irradiated and added to the CAR T cells in an E:T ratio of 1:7 for the LCL cells, supplemented by 50 U/mL IL-2 in 20mL cRPMI media. Cells were incubated for 7 days changing the media every second day. On day 7, fold of expansion was measured, and cells were phenotyped.

### 4.3.13 **Fluorescence microscopy**

T cells from healthy donors were transduced as previously described. Instead of FACS purification on day 9, cells were imaged on a DeltaVision Elite microscope (GE Healthcare). At least eight cells were visualized per condition. Raw images were subjected to a linear adjustment of brightness and contrast using ImageJ (NIH).

## 4.4 Flow cytometry

### 4.4.1 **CFSE/CTV staining**

Isolated lymphocytes were diluted to $2x10^6$ cells/ml in PBS at room temperature and the designated amount of cells was transferred into a 15 ml falcon tube. Carboxyfluorescein diacetate succinimidyl ester (CFDA-SE) or CellTraceViolet (CTV) was added to a final concentration of 1.5 µM, vortexed gently and kept in the dark at room temperature for 8min. During this time the CFDA-SE or CTV was taken up and intracellular esterases removed the acetate groups and convert the molecule to Carboxyfluorescein succinimidyl ester (CFSE), a fluorescent ester. CFSE covalently couples to amino groups of intracellular molecules mostly proteins via its succinimidyl group [185]. After 3 min cells were filled up with RPMI (10 % FCS) medium and incubated at 37 °C in a water bath for 10min. During this time CFSE efflux occurred and thereby prevented additional labeling and damaging of the cells. The cells were centrifuged for 6min at 1500rpm and the supernatant was discarded. The cells were then washed two more times with 1 ml PBS per $10^6$ cells. After the last washing step, the cells were resuspended in an appropriated amount of FACS buffer for further use.

### 4.4.2 **Intracellular cytokine staining (ICCS)**

Cells were rested overnight without IL-2 supplement. As target cells, 5x104 Rajis were seeded at highest cell number in a volume of 50 µL and diluted further for titration profile of cytokine production. As

negative control a 1 to 10 dilution of DMSO was added in a volume of 20 µL to the respective well. For the positive control the stock solutions of PMA (mM)and Ionomycin (mM) were diluted 1:540 and 1:67 in RPMI respectively and added at a volume of 20 µL. Effector cells were counted and 5x104T cells were added per well in a volume of 100 µL. The mix was incubated for 30 minutes at 37 °C before 40 µL of a 1:300 dilution of Golgi-Plug solution was added and incubated for 4h at 37 °C.

Cells were transferred into a V-bottom plate and centrifuged at 1500 rpm, 4 °C, for 3 minutes. Supernatant was removed and cells were washed in FACS buffer. Life/dead staining with 2 µg/mL EMA solution for 20 minutes was performed. After washing first staining reagent, containing the biotinylated anti-EGFR antibody was incubated with the cells for 20 minutes. Cells were washed and resuspended. Second master mix for surface staining for 20 minutes was added. We then resuspended cells in 100 µL Cytofix/Cytoperm (BD Bioscience) and incubation for 20 minutes on ice in the dark. Buffer was exchanged with 1x Perm Wash buffer (BD Bioscience) and cells were centrifuged for at 567g, 5 minutes, 4 °C. The supernatant was aspired carefully with a pipette. After two washing steps with Perm Wash buffer, cells were incubated with staining mix for intracellular cytokines Interferon-y, Interleukin-2 and Tumor necrosis factor-alpha for 20 minutes on ice. FACS analysis was performed washing.

### 4.4.3 **Flow cytometric analysis and cell phenotyping**

Conventional flow cytometry systems have emerged as important tools in modern biological laboratories. The cytometer creates a hydrodynamically focused stream of cell suspension which is analyzed using a laser beam and an array of photodetectors. Fluorescent labels are attached to one or more cell types in a heterogeneous suspension and the cells are analyzed or sorted individually based on how they scatter the incident laser light and the wavelength of light they emit.

For flow cytometry cells were stained after cell culture. In the standard staining protocol $5x10^6$ cells were resuspended in 50 µl FACS-buffer and transferred to a 96-well plate. The staining procedure was performed at 4 °C and as dark as possible. Each fluorochrome used in the actual experiment also had to be displayed as a single color. For single-colors $2x10^6$ cells were stained with a single antibody carrying the needed fluorochrome needed for compensating spectra interference between some fluorochromes. The mAbs were added to the 50 µl cell solution according to their titrated dilution. For staining with antibody was incubated with 3 µl *Strep*-Tactin coupled with a fluorochrome (either PE: ST-PE or APC: ST-APC). After addition of the dye-labeled staining reagent cells were incubated for 20 min at 4 °C in the dark. Afterwards the cells were centrifuged at 2000 x rpm at 4 °C for 3 min, the supernatant discarded and

resuspended 200 ml FACS-buffer. The cells were centrifuged at 1500 rpm at 4 °C for 3 min. The washing step was repeated once. For analysis cells were resuspended in 200 ml FACS-buffer and transferred to FACS-tubes. Before measurement 100 µl PI (final concentration 1 µg/ml) were added for differentiation of living and dead cells. Fluorescence was measured on a CyanADP flow-cytometer. The acquired data were analyzed using the FlowJo software.

### 4.4.4 **CAR $K_{off}$-rate assay**

0.5 – 1x$10^6$ fresh or thawed PBMCs were incubated with 5 – 10 µL dye conjugated single chain variable fragments for 20 minutes at 4 °C. Streptactin-APC was added after washing cells for another 20 minutes in a ratio of 1:15 to the cells, staining the cells for CD3 and CD20 positive populations as well. Cells were resuspended in 200 µL FACS buffer. A $K_{off}$-rate tube was prepared, the three ways valve was washed with 200 µL FACS buffer, before adding the sample to the tube and loading the valve with 0.5 - 1 mL 2 mM D-Biotin. Sample was loaded into the instrument. After 30 seconds of acquisition D-Biotin solution was added to the sample. It was measured for 15 minutes. Dissociation of the single chain was detected by gating on the CD20/CD19 positive population and monitoring the APC and FITC signaling of the Streptactin and the single chains.

### 4.4.5 **Fluorescence-activated cell sorting (FACS)**

For sorting transduced cells were sorted by FACS. Cells were stained with and incubated in 50µL FACS buffer at 4°C for 30 minutes. Optionally after a washing step, a second antibody staining was directly added to the cell suspension and incubated at 4°C for another 20 minutes, including PI during the last 3 minutes. Cells were washed with 6mL FACS buffer and any cell aggregates were removed by passing stained cells through a sterile 30µm filter. The whole procedure was performed on ice and under sterile conditions. Cells were sorted on a MoFloII or Aria cell sorter to obtain living cells. Sorted cells were collected into tubes with 1mL FCS and 1mM D-biotin for release of the EGFR Fab Streptamer.

### 4.4.6 **Adoptive T cell transfer into C57BL/6 mice**

Mouse splenocytes were retrovirally transduced with constructs that encoded the CAR/EGFRt as described in. The phenotype and transduction efficiency was determined by flow cytometry. Transduced splenocytes were expanded for 2-3 days and enriched for EGFRt-expressing cells by fluorescence-activated cell sorting (FACS) as indicated for individual *in vivo* studies in the result section. One day before cell transfer, wildtype C57BL/6 mice were sublethally γ-irradiated with 6 Gy. EGFRt- or mock-transduced cells were pooled, washed twice with PBS and subsequently transferred into mice by intravenous (i.v.) injection at 200µL/mouse. Cetuximab or Rituximab as a control mAb was infused intraperitoneally (i.p.) at 1mg/mouse at specified time points. Mice were challenged by i.v. application of modified vaccinia virus Ankara expressing ovalbumin (MVA-OVA) at $1x10^6$ pfu/mouse. MVA-OVA was kindly provided by Andreas Muschaweckh and Ingo Drexler.

### 4.4.7 **Analysis of blood and serum samples**

At different time points during the course of in vivo studies, approximately 100µL blood was obtained from the tail vein. On the final days of experiments, mice were sacrificed and 200-400µL blood was collected by heart puncture. Heparinized blood was incubated in 10mL ACT buffer at room temperature for 10 minutes for erythrocyte lysis. After centrifugation at 1500rpm for 6 minutes, residual erythrocytes were lysed again with 5mL ACT buffer for 5 minutes. Lysis was stopped by adding 10mL FACS buffer. After another centrifugation step, cells were transferred to a V-bottom 96-well plate for flow cytometry stainings. During experiments in the HBV mouse model, an additional blood sample was obtained and incubated at room temperature for at least 30 minutes. To retrieve serum, the blood samples were centrifuged at 5000g for 10 minutes.

### 4.4.8 **Isolating and processing of organs**

At the end of each experiment, mice were sacrificed by cervical dislocation and spleens, lymph nodes, and bone marrow were obtained in addition to blood. Isolation of spleens was described in. Cervical, axillary, brachial, mesenteric and inguinal lymph nodes were collected and squeezed through a 100µm cell strainer to obtain a single-cell suspension.

Mouse splenocytes were isolated from spleens of wildtype or OT-I transgenic C57BL/6 or NSG mice. The spleen was transferred to a sterile 70µm cell strainer that had been placed in a 3cm petri dish with 5mL

cRPMI. After squeezing the spleen through the cell strainer with the plunger of a syringe, the splenocytes were filtered through another 70µm cell strainer to bring them into single-cell-suspension. Collected splenocytes were centrifuged at 1400rpm for 6 minutes. The pellet was resuspended with 3mL ACT buffer and incubated at room temperature for 3 minutes for lysis of the erythrocytes. Lysis was stopped by adding cDMEM and 15mL and centrifuging again. Splenocytes were then transferred into a T-25 flask with 10mL cDMEM, supplemented with 100U/mL of IL-2, and stimulated over night with anti-mouse CD3 (clone 145-2c11) and anti-mouse CD28 (clone 37.51) at a dilution of 1:500. Cells were centrifuged at 1400rpm for 6 minutes and washed with 10 mL cRPMI. No erythrocytes

Bone marrow was harvested by isolating the femur and transferred it to a sterile 70µm cell strainer that had been placed in a 5cm petri dish with 5mL cRPMI. Bone morrow was flushed three times with 3mL cRPMI media and bone marrow cells were squeezed through a cell strainer with the plunger of a syringe. Cell pellet was subsequently resuspended in FACS buffer and prepared for flow cytometry staining (see section 4.4.2).

Lymph nodes, lungs and livers were processed in a similar manner as described for the spleens, including the erythrocyte lysis. The total cell number was acquired, and frequencies of transferred and endogenous cell subsets were assessed by flow cytometry staining. Absolute cell numbers could be subsequently calculated for individual cell subsets based on frequency and total cell number.

### 4.4.9 **T cell transfer into NSG mice**

Transfer of T cells in NSG mice Six- to 8-week-old male or female NSG mice were obtained from the Jackson Laboratory or bred in-house. Mice were engrafted via tail vein $10^5$ $CD19^+$ with 5xRaji/ffluc cells and, 7 days later, injected intravenously with PBS or a defined product of purified and CD19-specific CAR T cells mixed together in a 1:1 $CD8^+/CD4^+$ ratio. Bioluminescence imaging was performed as described [85]. Mice were either followed for survival or sacrificed on day 20 for analysis of T cell frequencies and phenotypes by flow cytometry. Peripheral blood was extracted, red blood cells were lysed using ACK Lysing Buffer (Thermo Fisher Scientific), and remaining cells were stained with fluorochrome-labeled mAbs. Bone marrow was isolated from hindlimbs by mechanical disruption, followed by red blood cell lysis, and staining with fluorochrome-labeled mAbs. Mice handlers were blinded to group allocation. The FHCRC Institutional Animal Care and Use Committee approved all experimental procedures.

# 5 Results

## 5.1 Truncated epidermal growth factor receptor (EGFRt) as a safeguard mechanism for adoptive cell therapy

The truncated EGFR (EGFRt) was first published by Wang et al. and was developed in the Jensen Lab (Seattle Children's Hospital). It is derived from the human full-length EGFR that consists out of four extracellular domains I-IV, a transmembrane domain and an intracellular signaling domain. The EGFR is truncated by removing the extracellular domains I and II as well as the intracellular signaling domain (Fig. 1A). These changes lead to a functionally inert receptor, which cannot bind its natural ligands, the epidermal growth factor (EGF) and the transforming growth factor a (TGF$\alpha$). Moreover, the removal of the intracellular signaling domain abolishes the capability to signal to tyrosine kinases. The residual sequence of the EGFRt is comprised of the amino acids (aa) 310-644 of the mature wildtype human EGFR. Additionally, a GM-CSF leader peptide (22aa) was fused to 5' of the EGFRt to ensure adequate expression on the cell surface.

EGFRt serves various purposes. It could be shown that it can be used as a tracking marker for *ex vivo* population as well as a selection marker for engineered (T) cells. Further, it could be shown that EGFRt can be used to deplete engineered (T) cells via antibody-dependent cellular cytotoxicity (ADCC) [181]. In this thesis, we wanted to explore whether EGFRt expression can be used to deplete engineered CAR T cells *in vivo* in order to terminate a successful CAR T cell therapy and reverse B cell aplasia.

### 5.1.1 **Proposed depletion mechanism *in vivo***

The proposed depletion mechanism based on binding the EGFRt can mediate very efficient T cell elimination by recruiting endogenous cytolytic effector pathways including ADCC as wells as CDC. When using the anti-EGFRt antibody Cetuximab (Erbitux$^{TM}$, Merck KGaA), which is an IgG1 antibody, natural killer cells (NK cells) are thought to bind to the Fc part of the antibody and eliminate the marked target cells. In this case, it is important that enough antibodies bind and NK cells recognize the marked cells. Generated *in vitro* data supported this notion when using

high expressing EGFRt positive cells. However, low expressing cells were not completely depleted. As we could show that EGFRt is stably expressed on the cell surface and can be targeted via Cetuximab, we further wanted to investigate the mechanism and completeness of the depletion *in vivo*, which is close to the clinic situation, mimicking the situation in a real patient as much as possible.

### 5.1.2 **Stable co-expression of the EGFRt with a murine anti-CD19 CAR (mCD19 CAR)**

EGFRt can be implemented in various expression systems such as retro- or lentiviral vectors. Michel Sadelain kindly provided us with a murine anti-CD19 CAR construct. Daniel Sommermeyer from the Riddell lab (FHCRC) further engineered the construct by adding a CD28 co-stimulatory domain, a P2A ribosomal skip element for equimolar expression and the truncated EGFR. In order to use the EGFRt as safeguard mechanism *in vivo*, we decided to co-express a murine anti-CD19 CAR (mCD19) with the EGFRt (Fig. 1B). Prior to *in vivo* testing, we examined the killing efficacy of mCD19 CAR T cells *in vitro*. The full construct was cloned into the γ-retroviral pMP71 vector (kindly provided by the Uckert lab, Berlin). To confirm killing activity of the modified construct

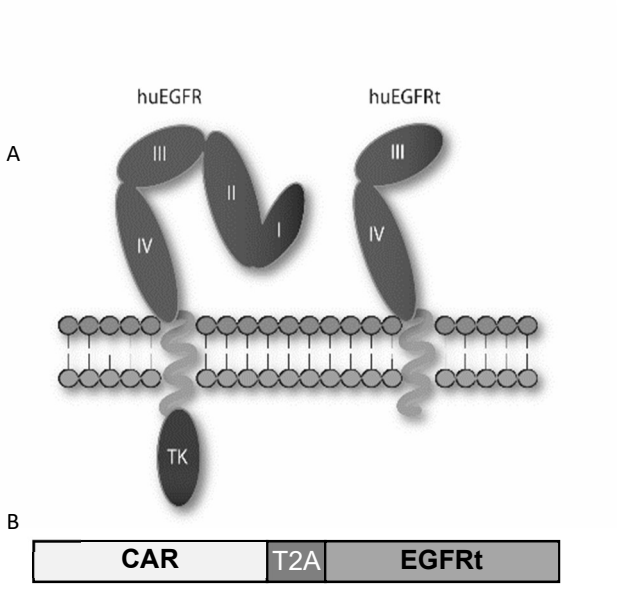


**Figure 1: Structure of the human full-length/truncated EGFR and application in a bicistronic gene cassette.** (A) Schematic representation of the human full-length EGFR (huEGFR) and the truncated EGFR (huEGFRt) lacking extracellular domains I and II as well as the intracellular tyrosine kinase signaling domain (TK). (B) Representative gene cassette encoding a transgenic receptor (CAR), a ribosomal T2A skip element for equimolar co-expression and the EGFRt.

against $CD19^{+}$ target cells, we performed a co-incubation killing assay, which demonstrated functionality of the m1928E CAR (see doctoral thesis of Paulina Paszkiewicz).

### 5.1.3 *In vivo* depletion of mCD19 CAR T cells and sustained B cell recovery at early and late time points

After modifying the m1928E CAR we could show that the killing capacity is maintained. Next, we transferred m1928E CAR T cells into WT C57Bl/6 (Bl/6) mice to first induce complete B cell aplasia and subsequently deplete the m1928E CAR T cells by the administration of Cetuximab targeting the EGFRt to see whether it is possible to promote B cell recovery. This scenario represents a clinically relevant situation for the use of a safeguard mechanism to recover endogenous B cells in treated, B cell depleted patients who underwent a successful CAR T cell therapy.

#### *5.1.3.1 Functional in vivo depletion of mCD19 CAR T cells*

It has been described in a syngeneic preclinical mouse model that m1928E CAR T cells are able to efficiently eliminate endogenous B cells as well as $CD19^+$ tumor cells long term. Not only the endogenous B cells in the blood were affected, also B cells in the spleen and bone marrow (BM) were depleted over months [186]. We wanted to use the mouse model to generate m1928E CAR T cell-mediated B cell aplasia followed by the depletion of the engineered T cells upon Cetuximab administration and consequent recovery of the endogenous B cell compartment. Only upon complete depletion recovery of the endogenous B cells will be possible. In a first *in vivo* experiment, we retrovirally transduced congenic $Thy1.1^+$ splenocytes with the m1928E CAR construct to target $CD19^+$ B cells in the mice. Therefore, we transfected the γ-retroviral pMP71 vector (Uckert lab, Berlin) into Platinum Ecotropic cells (Plat E). $Thy1.1^+$ splenocytes were derived from $Thy1.1^+$ transgenic mice, activated with anti-CD3 and anti-CD28 mAb, subsequently transduced with m1928E CAR. After transduction, splenocytes were kept in culture for 3 days and injected ($1.2x10^6$ per mouse, intravenously (i.v.)) into sublethally irradiated (6Gy) wt Bl/6 Thy1.2 mice. Control mice received mock transduced splenocytes. Endogenous B cells and m1928E CAR T cells were monitored over time in the blood by flow cytometry (Fig. 2A). On day 50 and 55, anti-EGFR specific mAb Cetuximab (Ctx) or an irrelevant human anti-CD20 specific mAb, Rituximab (Rtx), were administered intraperitoneally (i.p.). To be able to eliminate all m1928E CAR T cells, a relatively high dose of mAb (1mg/mouse) was used. Blood was

continuously monitored to see the depletion efficacy as well as the recovery of endogenous CD19⁺ B cells. Mice were monitored up to 180 days.

Representative flow plots of transduced m1928E CAR T cells prior to injection and *ex vivo* staining 43 days after injection are shown in Figure 2B. Injected m1928E CAR T cells showed a transduction efficacy of 83.2% indicated by EGFRt staining, which correlates with CAR expression. Thy1.1 staining, indicating the congenic marker, enabled us to track adoptively transferred cells; on day 43 after m1928E CAR T cell transfer, Thy1.1⁺ EGFRt⁺ cells were still detectable in the blood. Monitoring of the endogenous B cell compartment is shown in Figure 2C. We observed efficient B cell depletion in all mice that received m1928E CAR T cells, whereas control mice which received

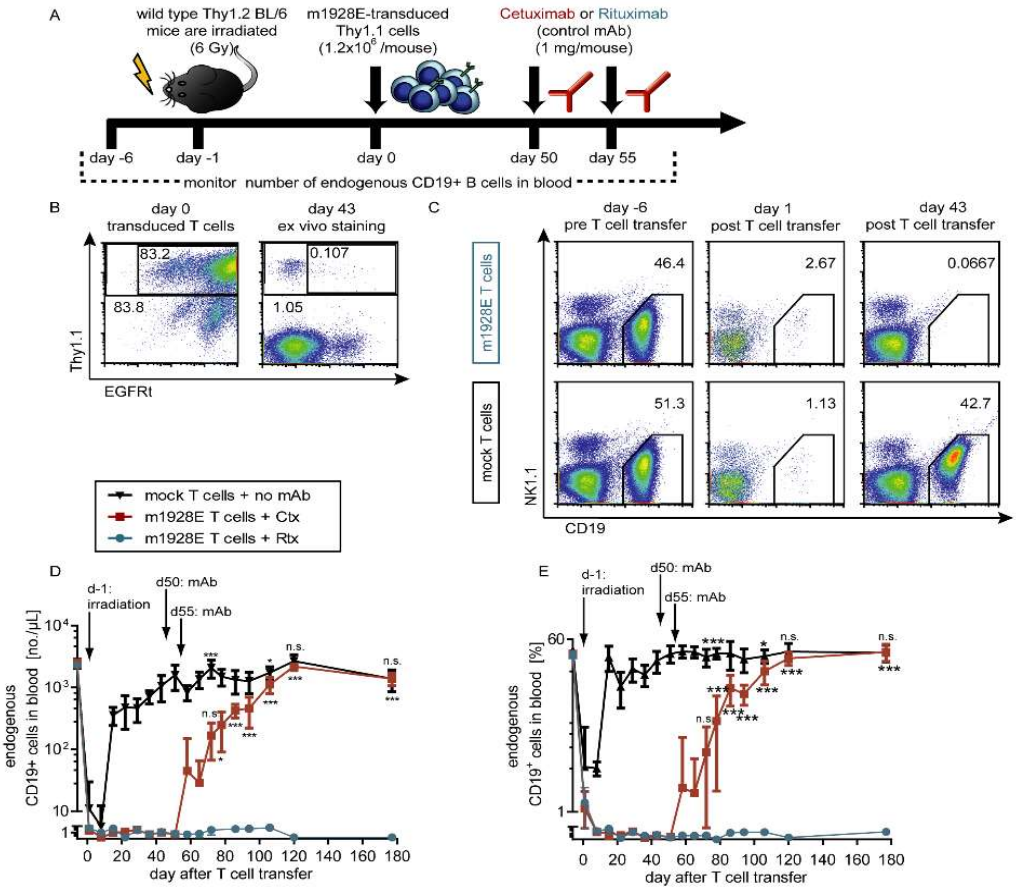


**Figure 2: Cetuximab-mediated in vivo depletion of m1928E⁺ T cells allows for B cell recovery in vivo.** (A) Experimental layout of in vivo depletion experiment based on the transfer of m1928E-transduced cells targeting endogenous CD19⁺ B cells. (B) Thy1.1⁺ mouse splenocytes were γ-retrovirally transduced with the m1928E CAR construct. After transfer of 1.2x10⁶ m1928E-transduced (unsorted) T cells, EGFRt⁺ cells were detected by ex vivo EGFR staining in a blood sample on day 43 after injection. (C) Mice were irradiated on day –1 and received m1928E⁺ T cells or mock T cells on day 0. Numbers of endogenous CD19⁺ B cells were monitored in the blood before T cell transfer (day –6) and 1 or 43 days after T cell transfer. Endogenous B cells and NK cells were detected in representative samples for each group with anti-CD19 and anti-NK1.1 mAbs, respectively. Gates were set on CD19⁺ B cells among Thy1.1– living lymphocytes, and numbers indicate B cell frequencies. (D, E) Numbers per microliter or frequencies of living endogenous CD19⁺ B cells in the blood were acquired for each mouse group over the time course. Time points of irradiation and the two mAb infusions are indicated by arrows. Means ± SD are shown; n=6 mice per group. Two-way ANOVA followed by Bonferroni post-test was used for statistics.

identical numbers of mock-transduced T cells had rapid recovery of B cell numbers and frequencies to normal levels after temporary irradiation-induced lymphopenia. Figure 2C shows B cell frequencies over time of mock group and m1928E CAR treated group by staining for CD19 and NK1.1 at three different time points. Frequencies and absolute cell number of B cells gathered from blood are indicated over time. Only after administration of Ctx the endogenous B cells recovered rapidly and reached normal B cell numbers and frequencies, indicating a complete eradication of transferred mCD19 CAR T cells. Rtx-treated control group stayed B cell depleted long-term and did not recover endogenous B cells (Fig. 2D and E).

In a separate experiment using the same experimental setup as in Figure 2, we performed the Cetuximab-mediated depletion at a later point on day 158 and 162 to test the system for the reliability and robustness especially for the clinical situation where CD19 CAR T cell depletion might be considered at later time point after adoptive T cell therapy to ensure complete tumor eradication preventing a tumor relapse. Therefore, we tested whether endogenous B cells can be restored also after long-term B cell aplasia. We transferred $8x10^6$ transduced, unsorted Thy1.1$^+$ cells into irradiated WT Bl/6 mice. Endogenous B cell numbers and frequencies were monitored as in the previous experiment and Ctx was administered on day 158 and 162. Representative FACS plots show transferred Thy1.1$^+$ congenic m1928E$^+$ CAR T cells on day -6, 1, 43 and 157 (Fig. 3B). CAR T cells persist long-term in the blood of the mice in low cell numbers.

Despite the low circulating levels, the mice show B cell aplasia, indicating the functionality of the transferred CAR T cells, even at later time points like day 157 (Fig 3B). – one day prior to late time point Ctx administration. After Ctx injection we monitored B cell recovery at a later time point. Like in the previous experiment endogenous B cells recover and reach normal B cell numbers and frequencies similar to the mock-treated group (Fig. 3C).

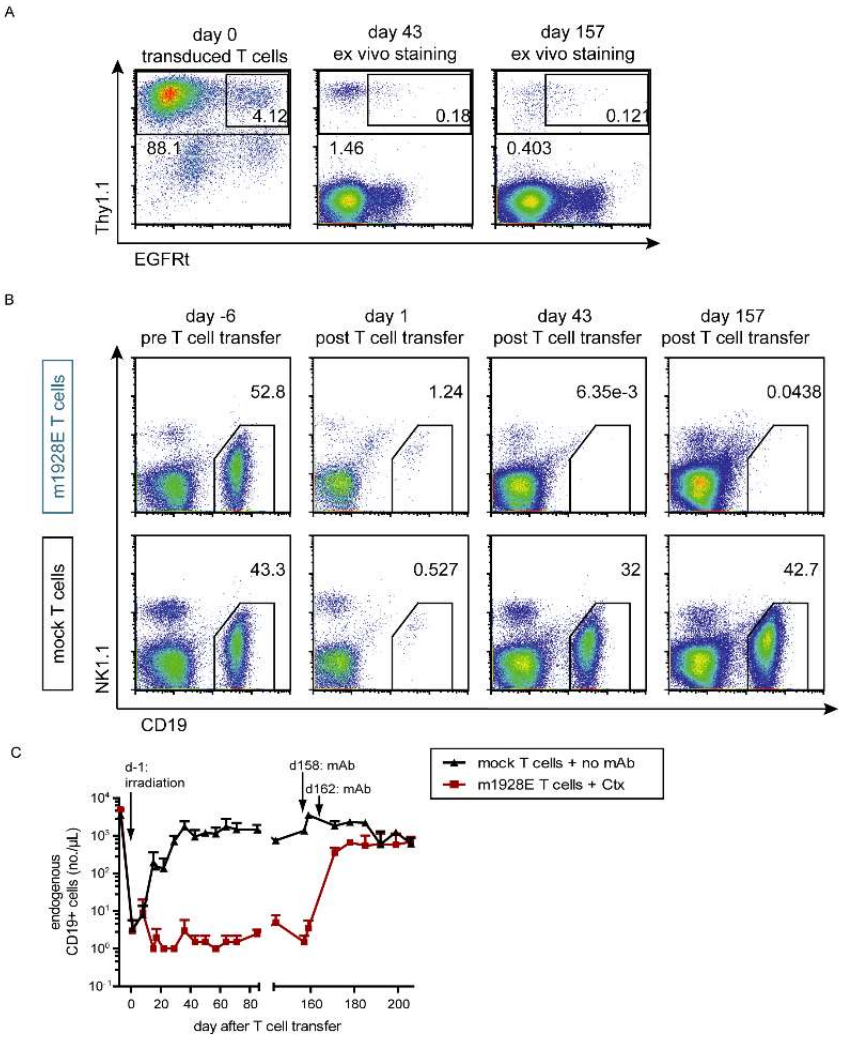


**Figure 3: Late Cetuximab-mediated in vivo depletion.** In a separate long-term experiment, 8x10$^6$ m1928E-transduced, unsorted Thy1.1$^+$ cells were transferred into irradiated WT Bl/6 mice. Cetuximab infusions were performed at late time points (days 158 and 162). (A) After transfer of 8x10$^6$ m1928E-transduced (unsorted) T cells, EGFRt+ cells were detected by ex vivo EGFR staining in a blood sample on day 0, 43 and 157 after T cell transfer. (B) Endogenous B cells and NK cells were detected in representative samples for each group with anti-CD19 and anti-NK1.1 mAbs, respectively. Gates were set on CD19$^+$ B cells among Thy1.1– living lymphocytes, and numbers indicate B cell frequencies. (C and D) Numbers per microliter or frequencies of living endogenous CD19$^+$ B cells in the blood were acquired for each mouse group over the time course. Time points of irradiation and the 2 mAb infusions are indicated by arrows. Means ± SD are plotted. n=3 mice per group.

### *5.1.3.2 The functionality of recovered endogenous CD19$^+$ B cell compartment*

Next, we wanted to test whether the recovered B cells were fully functional. We performed vaccination of m1928E CAR T cell treated mice after Ctx-mediated B cell recovery. We used the chicken Ovalbumin (OVA) protein in alum for vaccination. We injected a mixture of OVA and Alum into the mice and harvested the blood serum after 7 (Fig. 4A) and 14 (Fig. 4B) days after injection and performed an OVA-specific IgG ELISA. With that assay, we were able to confirm a B cell-dependent response by quantifying and detecting OVA-specific IgG antibody titers in the mice.

OVA-specific IgG antibody titers reached similar levels after *in vivo* depletion of m1928E CAR T cells compared with control mice that received mock-transduced T cells. Mice treated with Rtx,

which did not affect B cell aplasia and persistence of m1928E CAR T cells, failed to generate and mount detectable OVA-specific antibody responses to the given vaccination. Ctx treated mice in contrast, could mount an antibody response comparable to control mice, which were not B cell depleted at any time point. These data demonstrate that *in vivo* depletion of m1928E CAR T cells via co-expressed EGFRt with Ctx can revert numerically and functionally endogenous B cell deficiency.

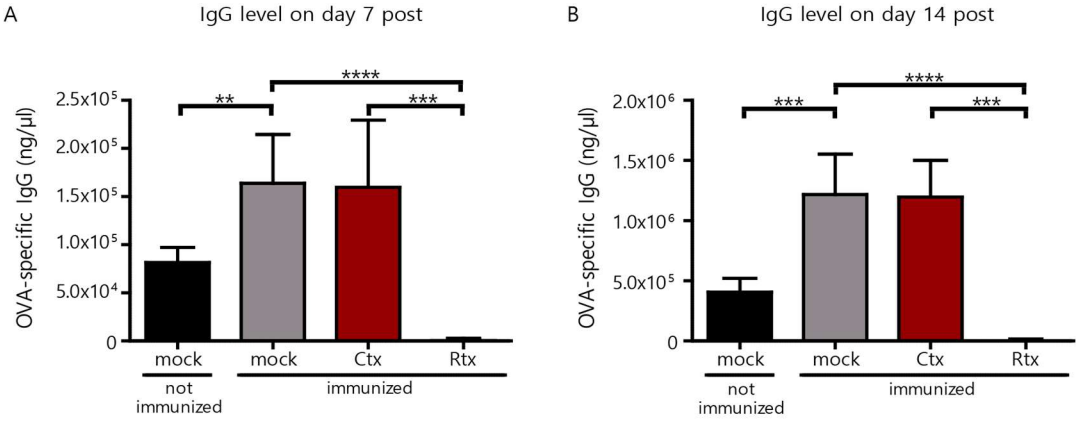


**Figure 4: Ova-specific Immunization after mCD19 transfer.** (A and B) After recovery of normal B cell numbers, mice were immunized with OVA protein (100 µg/mouse) mixed 1:1 with Imject alum on day 245 after CAR T cell infusion. One mouse group had received mock T cells and was not immunized as a negative control. OVA-specific IgG levels in the blood plasma were measured by ELISA 7 days (F) and 14 days (G) after immunization. Means ± SD are shown for 2 independent experiments; P values were calculated by unpaired 2-tailed Student's t test; n = 5 for immunized mock, Ctx, and Rtx groups; n=7 for not immunized mock group. **P ≤ 0.01, ***P ≤ 0.001, ****P ≤ 0.0001.

#### *5.1.3.3 Persistence of functional CD19 CAR T cells causes sustained depletion of endogenous CD19⁺ B cells and hypogammaglobulinemia.*

Ongoing B cell aplasia is associated with reduced levels of Immunoglobulins like IgG, IgM, and IgA [164, 187]. Low levels of immunoglobulins in the blood is called hypogammaglobulinemia. We could observe markedly reduced levels in the mouse study already in the first month after m1928E CAR T cell transfer, which is consistent with findings in human patients. For measuring the serum Immunoglobulins, we collected with each blood draw the serum (50 ul) and analyzed all serum samples after finishing the experiment. We could show that all serum Immunoglobulin levels (IgG1, IgG2b, IgG3, IgM, IgA) were remarkably reduced already one month after injection of m1928E CAR T cells. Control groups did not show any effect. After administration of Ctx on day 50 and 55 post CAR T cell transfer, serum Immunoglobulins did increase that were linked to the endogenous B cell recovery, indicating functionality of recovering B cells. The reappearance of B cell numbers after Ctx treatment was associated with normalization of immunoglobulin levels in

the blood. Rtx treated control group did not show any effect and showed hypogammaglobulinemia throughout the experiment. Overall the recovery of serum cytokines took about 3 weeks to be detectable and about 5 weeks until reaching normal serum levels compared to mock control group (Fig. 5).

#### *5.1.3.4 Ctx-mediated in vivo depletion of mCD19 CAR T cells does not increase tumor relapse in a murine B-ALL model*

In murine B-ALL model, we investigated the risk of tumor relapse after eliminating tumor-reactive mCD19 CAR T cells after administration of Ctx. The eradication of malignant B cells by the CAR T cells must be complete to prevent a recurrence of malignant B cells after Ctx-mediated depletion of mCD19 CAR T cells. In detail, we evaluated whether elimination of mCD19 CAR T cells increased the risk of relapse in mice bearing the rapidly growing and progressive B cell leukemia EuALL01, which is radio-resistant *in vitro*. In these experiments, we used a m19-41BB-EGFRt CAR (m19BBE), as 41BB CARs achieved a very high rate of complete remission in human clinical trials [161], and we wanted to be as close as possible to this clinical situation. For the experiment, $CD45.1^{+}$

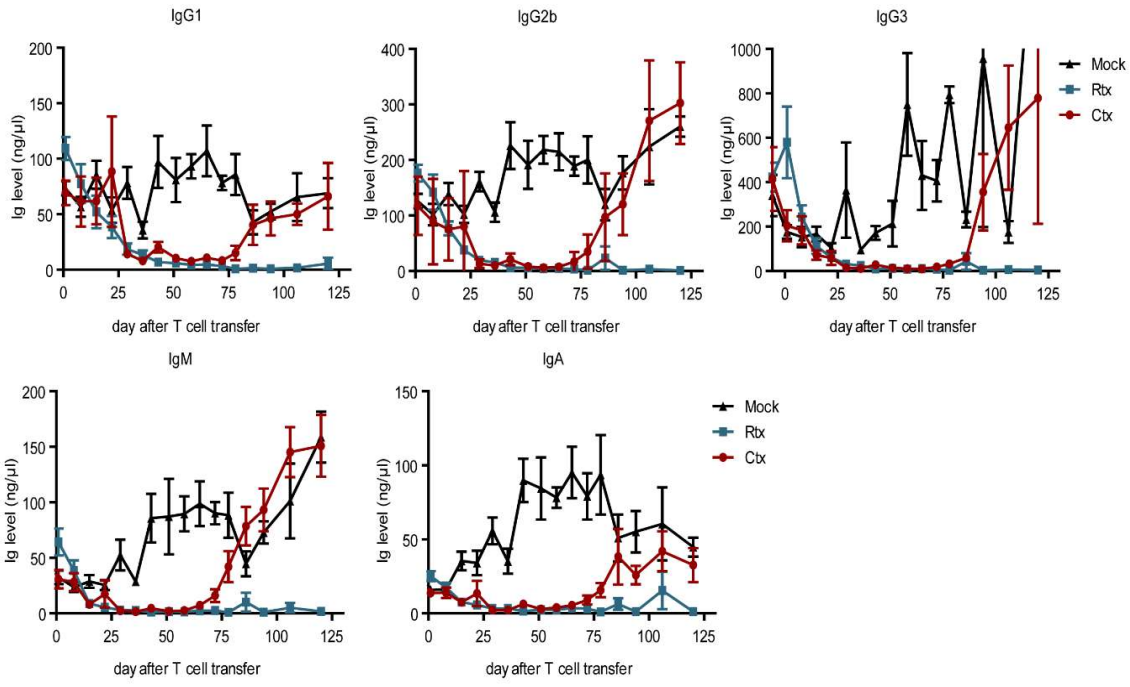


**Figure 5: Murine CD19 CAR T cells cause hypogammaglobulinemia.** Serum was collected and was analyzed with Luminex multiplex assay. Values were normalized and serum cytokines levels plotted over time for each group. Luminex multiplex assay was done with frozen serum samples and indicated Immunoglobulins were tested. n=6 mice per group. Means ± SD are plotted.

congenic BL/6 mice were inoculated i.v. with $1x10^6$ $CD45.2^+$ congenically marked Eu-ALL01 tumor cells. All mice were sublethally irradiated (5 Gy) and were either left untreated or treated one day later with $3x10^6$ congenic $CD45.2^+CD8^+$ CAR T cells. Three weeks after CAR T cell infusion mice were treated with two doses of Ctx (1mg/mouse) one week apart (Fig. 6A). Blood screening was performed weekly. CAR T cells reached the peak of expansion in the blood on day 7 after cell transfer. After administration of Ctx, m19BBE CAR T cells became undetectable in treated groups (Fig. 6B) and Ctx-treated mice recovered normal endogenous $CD19^+$ B cell numbers. Mice receiving Rtx control mAb had persisting CAR T cells in the blood and remained B cell-deficient (Fig. 6B and C). Eu-ALL01 leukemic cells were readily detected in the blood of mock-transduced control mice that did not receive CAR T cells and subsequently died from progressive leukemia after 27-31 days after tumor inoculation (Fig. 6D and E). In contrast, Ctx-treated mice remained leukemia-free and their survival was similar to Rtx-treated mice (Fig. 6E). Next, spleens and BM were harvested two weeks after tumor inoculation and analyzed with low cytometry. Eu-ALL01 tumor cells were stained using congenic $CD45.2^+$ marker and CD19 surface marker. Initial engraftment and detection of tumor cells is clearly shown in the blood staining (Fig. 6F, upper left). Ctx-treated group failed to show residual leukemia cells in all mice. Tumor cell frequencies were below the detection limit (similar to control non-tumor bearing mouse-group). The successful depletion of m19BBE CAR T cells, as well as the recovered $CD19^+$ B cell compartment, was nicely detected only in groups treated with Ctx (Fig. 6F). These data show that in this Eu-ALL01 mouse model Ctx-mediated elimination of mCD19 CAR T cells efficiently reverses B cell aplasia without increasing risk of leukemia relapse.

In summary, all these experiments could show that cetuximab-mediated *in vivo* depletion of EGFRt-coexpressing mCD19 CAR T cells efficiently reverses B cell aplasia and provides a sustained recovery of the whole $CD19^+$ B cell compartment and their function, including normalization of serum immunoglobulin levels and the induction of isotype-switched antigen-specific antibodies upon vaccination. Further, elimination of mCD19 CAR T cells does not increase the risk of tumor relapse showing clinical relevance of the safeguard mechanism. EGFRt is therefore a suitable safeguard mechanism to terminate CAR T cell therapy after complete tumor eradication. In the scenario of CD19 CAR T cell therapy, B cell aplasia in patients can be reversed restoring their full

immune system. For acute side effects, however, EGFRt targeting is probably not the best choice due to endogenous EGFR upregulation on the inflammation site of healthy tissue.

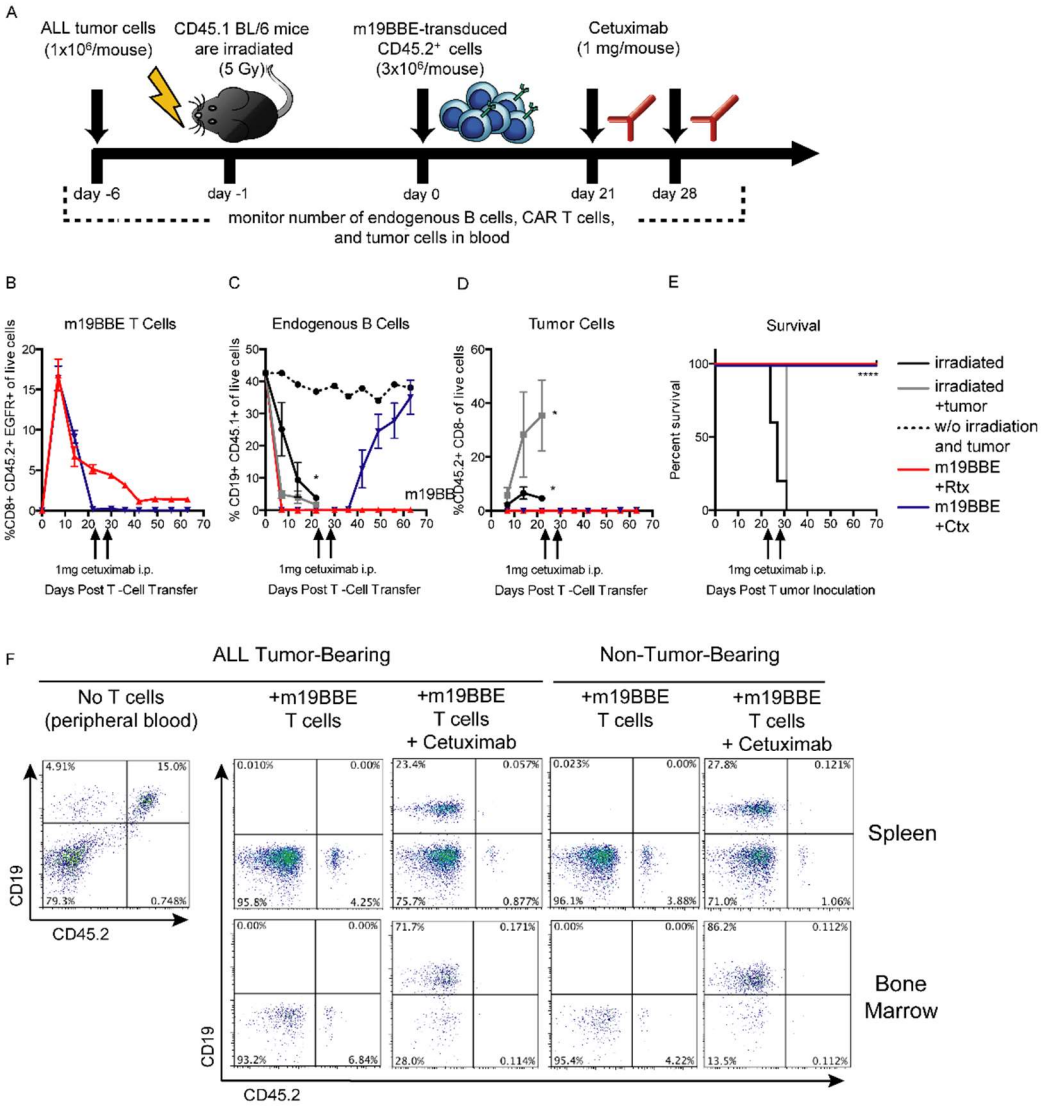


**Figure 6: Cetuximab-mediated in vivo depletion of m19BBE⁺ murine T cells does not increase tumor relapse in a model of B cell ALL.** (A) Experimental layout of depletion experiments based on the transfer of m19BBE-transduced cells targeting CD19⁺ ALL tumor cells. Mice were inoculated with $1\times10^6$ ALL tumor cells i.v.; 6 days later they were sublethally irradiated (5 Gy), and 24 hours later they received $3\times10^6$ CD8⁺ m19BBE CAR T cells. Cohorts of mice were left untreated or treated with 2 doses of 1 mg cetuximab on day 21 and day 28 and bled weekly to monitor T cell, normal B cell, and tumor cell frequency. (B–D) Summary of flow cytometry analysis of CD45.2⁺CD8⁺EGFR⁺ m19BBE mouse T cell frequency (B), CD45.1⁺CD19⁺ endogenous normal B cell frequency (C), and CD45.2⁺CD19⁺ tumor cell frequency (D) in the peripheral blood of mice with ALL tumors left untreated (black), mice irradiated with 5 Gy (gray), mice irradiated and treated with m19BBE CAR T cells (red), or mice irradiated and treated with m19BBE CAR T cells followed by cetuximab depletion (blue). Non–tumor-bearing WT mice are shown for comparison (dotted black line). Means ± SEM are plotted. n=6 per group. (E) Kaplan-Meier survival analysis of mice inoculated with ALL tumor cells and left untreated (black), irradiated with 5 Gy (gray), treated with m19BBE T cells (red), or treated with m19BBE T cells and cetuximab (blue). Statistical significance was determined using log-rank Mantel-Cox test; *P ≤ 0.05, ****P ≤ 0.0001. n = 6 per group. (F) Representative flow cytometry data from peripheral blood of ALL tumor-bearing mice (left) 2 weeks after tumor inoculation and spleens and bone marrow of m19BBE/cetuximab-treated mice (middle) or WT non–tumor-bearing mice (right) 10 weeks after T cell transfer. Plots are gated on live CD19⁺ cells.

## 5.2 Novel cellular based safeguard mechanism

In consequence, there is a need for further safeguard strategies that can rapidly and specifically eliminate adoptively transferred CAR T cells when side effects occur. As mentioned in the section above, in the case of inflammation and acute side-effects, EGFRt might not be the optimal safeguard due to the upregulation of EGFR gene in inflamed tissues as well as the poor capability of mAbs to penetrate dense (cancer-) tissue. To terminate CAR T cell therapy when severe side effects like CRS, neurological toxicities or chronic toxicities occur, we explored the possibility of a novel cellular-based safeguard mechanism. The advantages of using a cellular-based safeguard mechanism are the high sensitivity, specificity, and capability to penetrate each type of tissue (see details in ***table 1***). For realizing the idea of a cellular safeguard mechanism, we need a specific, non-immunogenic target structure expressed on the target cell which can be attacked by the new cellular safeguard.

**Table 1: Comparison of mAb and cellular-based safeguard mechanisms:** Predicted functionality of different categories.

| | **mAb-based Safeguard mechanism** | **cellular based safeguard mechanism** |
|---|---|---|
| **Application** | several injections | single injection |
| **Specificity** | high | very high |
| **Sensitivity** | high | very high |
| **Half-life [$t_{1/2}$]** | short | long |
| **Tissue penetration** | Ok/good | Very good |

### 5.2.1 **Evaluation of a specific target structure which can be implemented in current CAR designs**

Finding a specific target sequence which can be implemented into current CAR designs is crucial for maintaining or ideally improving the functionality. The current structure of CAR T cells includes a scFv, a spacer domain, a transmembrane domain and intracellular signaling domains to trigger effector functions. However, current designs lack sequences which allow rapid selection, *in vivo* tracking and regulation of CAR T cells. In cooperation with Stan Riddell from the

FHCRC we could find a StrepTagII (STII) based target sequence which can be used for implementation into CAR T cells. Stan Riddell's group could show that the inclusion of the STII sequence into the current design of CARs for immunotherapy can improve their functionality. Inclusion of the STII, an eight amino acid sequence (WSHPQFEK), into the hinge region of the CAR not only enhanced CAR functionality and flexibility, but it could also be used for *in vitro* activation/expansion, selection and *in vivo* tracking of $CAR^+$ cells using StrepTactin or anti-STII mAbs [188]. This multi-functional CAR contains a target structure, the STII sequence, which we can target with a CAR T cell containing an anti-STII scFv, originating from a mouse "anti-StrepTagII classic" monoclonal antibody generated by cooperating company IBA. The STII sequence can further be introduced in all current CAR designs as well as in TCR transgenic cells, giving us a very broad range of applications.

### 5.2.2 Principle and proposed mode of action of the novel cellular StrepTagII based safeguard mechanism

The principle of the proposed mechanism is that the anti-CD19 STII containing CAR (19ST CAR) serves as a target being recognized by the newly generated anti-STII "classic" (name of the commercial anti-STII mAb) containing scFv CAR (aCARCARc). The 19ST CAR possesses three repetitions of the STII linked with a common G4S linker to improve target recognition. After recognition of the STII sequences through the aCARCARc, effector functions are triggered and subsequent killing of the 19ST CARs takes place as described for any functional CAR T cell (Fig. 7).

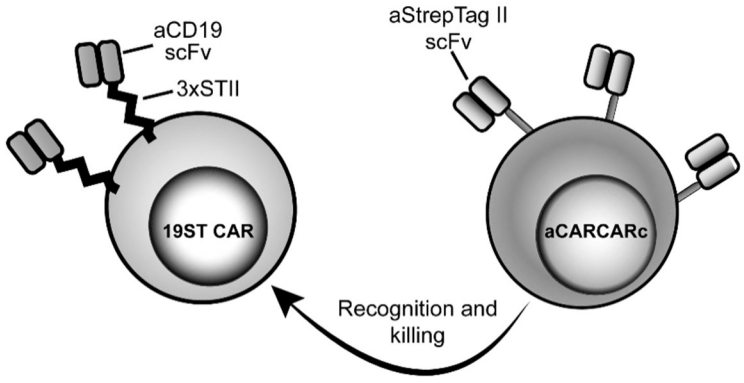


**Figure 7: Proposed mechanism of the novel cellular safeguard mechanism.** Target 19ST-CAR T cell (left) contains a triple StrepTagII (3xSTII) serving as a target structure. Anti-StrepTagII CAR (aCARCARc, right) containing the STII recognizing scFv. Ideally the aCARCARc is able to recognize and kill the StrepTagII containing target 19ST CAR T cell.

### 5.2.3 **Generation and expression of novel anti-StrepTag CAR in human T cells**

Anti-StrepTagII CAR (aCARCARc) was generated based on current clinical CAR constructs. In detail, the construct contains an anti-StrepTag scFv (classic), $CH_2CH_3$ IgG4 hinge domain, CD28 transmembrane and co-stimulatory domain fused to the CD3ζ TCR signaling domain. Additionally, the EGFRt transduction marker was added with a T2A ribosomal skip element which allows equimolar expression of CAR and EGFRt. For evaluation of the aCARCARc, we used an anti-CD19 CAR containing a triple STII target sequence in the hinge region and a 41BB co-stimulatory domain as described in above and Liu et al. 2016 (19ST CAR) (Fig. 8A). We cloned the constructs into the γ-retroviral vector pMP71 and transfected RD114 amphotropic packaging cell lines. Human primary T cells were isolated out of PBMCs and transduced with the corresponding virus. Five days after transduction, the transduction efficacy was measured with flow cytometry. The EGFRt was stained and served as a transduction marker. Representative plots gated on living $CD3^+$ lymphocytes are shown (Fig. 8B). Untransduced lymphocytes do not show a genetic modification (2,31%) and serve as a control. Transduced constructs show a transduction efficacy of 79,3% (19ST CAR) and 94,4% (aCARCARc). Due to the high transduction efficacy, enrichment or selection of transduced cells was not necessary and cells could be used immediately for experiments.

With the genetically modified cells, cytotoxicity assays were performed to validate the proposed mechanism. First, an xCELLigence impedance-based cytotoxicity assay was performed. For this, adherent HEK cells were modified and sorted for expressing the 19ST CAR construct to serve as a target cell line (HEK-19ST). In a 96 well E-plate 25.000 target cells per well have been seeded on day 0. Effector cells were added on day 1 in different effector to target (E:T) ratios (3:1; 1,5:1; 0,7:1), followed by impedance monitoring for 20h and specific lysis was calculated (Fig. 8C). For determining the dose-dependent killing capacity, 10h time-point after addition of effectors was chosen and plotted in different E:T ratios. The newly generated aCARCARc eliminated HEK-19ST target cells in a dose-dependent manner (Fig. 8D). In a separate Europium-based cytotoxicity assay, we performed the killing assay with human primary effector T cells and target cells. Target cells were labeled with DELFIA® BATDA labeling reagent and co-incubated with effector cells for 6h; labeling reagent was released from lysed target cells and measured with time-resolved

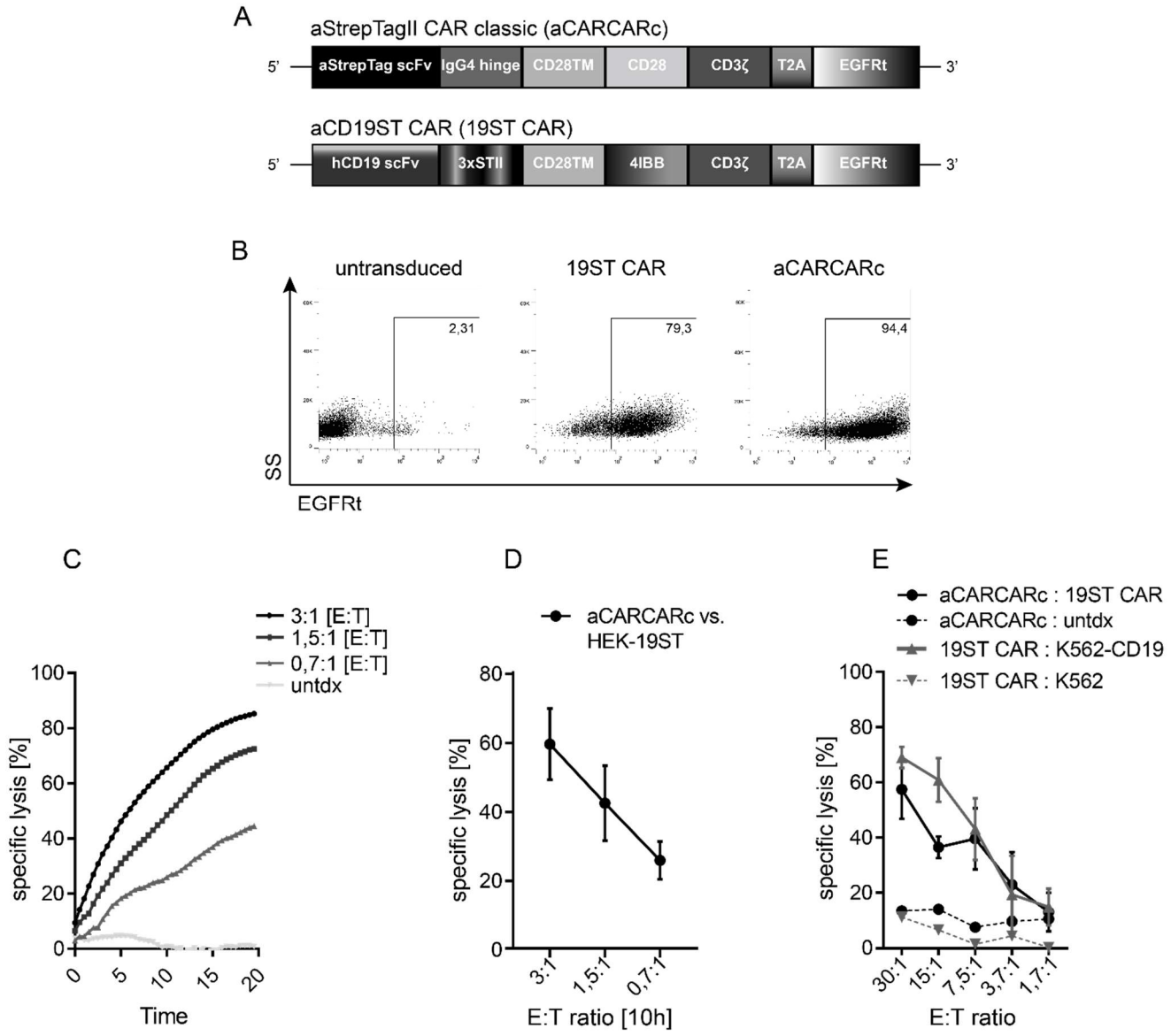


**Figure 8: Generation and Functionality testing of the newly generated aCAR-CAR.** (A) Retroviral vector designs for the aSTII CAR (aCARCARc) and the 19ST CAR. Both CAR constructs based on a human CAR backbone. CARs containing beside the scFv an IgG4 hinge or a triple STII as a hinge followed by a CD28 transmembrane domain. Intracellularly a CD28 or 41BB domain is fused to the CD3z signaling domain. As a transduction marker the EGFRt is fused via a ribosomal T2A skip element which is expressed equimolar. (B) Transgene expression 5 days after retroviral transduction. Only CAR transduced cells show transgene expression indicated by the EGFRt expression. Pregated on living lymphocytes (C) xCELLigence cytotoxicity assay was performed with HEK cells transduced with the 19ST CAR construct that serves as a target cell line. aCARCARc cells were added in different E:T ratios. Killing was measured via impedance monitored for 20h. (D) Killing capacity was qualitatively quantified 10h after addition of the effectors. (E) Europium cytotoxicity assay was performed with freshly transduced human primary T cells shown in (B). Target cells were labelled with DELFIA® BATDA labeling reagent. Different E:T ratios were used for determining the killing capacity. N=2 independent experiments, all cytotoxicity assays have been performed in quadruplicates. Means ± SD are plotted.

fluorescence measurement (TRFM). Gathered data were normalized and specific killing capacity was calculated. Untransduced human primary T cells or K562 cells served as controls. 19ST CAR T cells were co-incubated with K562-CD19 cells showing a potent killing capacity, serving as positive control. Co-incubated aCARCARc with 19ST CAR T cells showed a slightly lower killing capacity. However, compared to negative controls, both co-incubations led to a very effective killing of target cells. The killing of the aCARCARc was effective against both adherent HEK-19ST

cells and primary 19ST CAR T cells. These data confirm the cytotoxicity of the aCARCARc which indeed can recognize the STII containing cells *in vitro*.

### 5.2.4 **Further investigation of the functionality of the aCAR-CARc**

It has been described that CAR T cells containing an STII sequence in the hinge region can be stimulated thereby. We therefore investigated in more detail whether the binding of the aCARCARc to the STII stimulates the 19ST CAR. In the previous performed killing assays we additionally either labeled target cells or used adherent HEK-19ST tumor cell lines as targets. In a co-culture experiment, we monitored the frequency and absolute numbers of both effector and target cells. By that, we got more insights whether 19ST CAR T cells are stimulated and proliferate or whether they are killed immediately after binding of the aCARCARc. The experimental layout is shown in (Fig. 9A-B). Human $CD3^+$ cells from the same healthy donor were transduced on day 0 and co-culture was started on day 5 for 24h and 48h, followed by flow cytometry analysis. Target cell populations were stained with specific markers like aSTII mAb (19ST CAR) or EGFRt (aCAR-CARc) (Fig.9C). The experiment was performed in a 96-well format. Different E:T ratios were tested ranging from 1:1 up to 30:1. In Figure 9D, a significant killing in the low E:T ratios were observed. By measuring the absolute cell number, we detected a reduction of 19ST CAR T cells compared to the co-incubation with untransduced $CD3^+$ cells, which should not have any effect. The aCARCARc population showed an increase in absolute cell numbers compared to the control, suggesting stimulation and proliferation upon antigen encounter (Fig. 9E). The proliferation also increased with higher E:T ratios. In a similar experiment we performed a co-incubation with 10:1 E:T ratio subsequent stained for target populations. Same co-culture settings have been used as before. After 48h co-incubation control sample showed a maintained E:T ratio of 10:1. After 48h only 0,14% of target cells ($STII^+$) could be detected (Fig. 9F and G). These results confirm the killing capacity of the aCAR-CARc when co-cultured with 19ST target cells *in vitro*, due to vanished 19ST CARs. Nevertheless, we cannot totally exclude that the 19ST CAR is stimulated after binding of the aCAR-CARc. Additional experiments have to be done to confirm the data.

For further investigation of the functionality of the aCARCARc, we needed to test them in a clinically relevant mouse model.

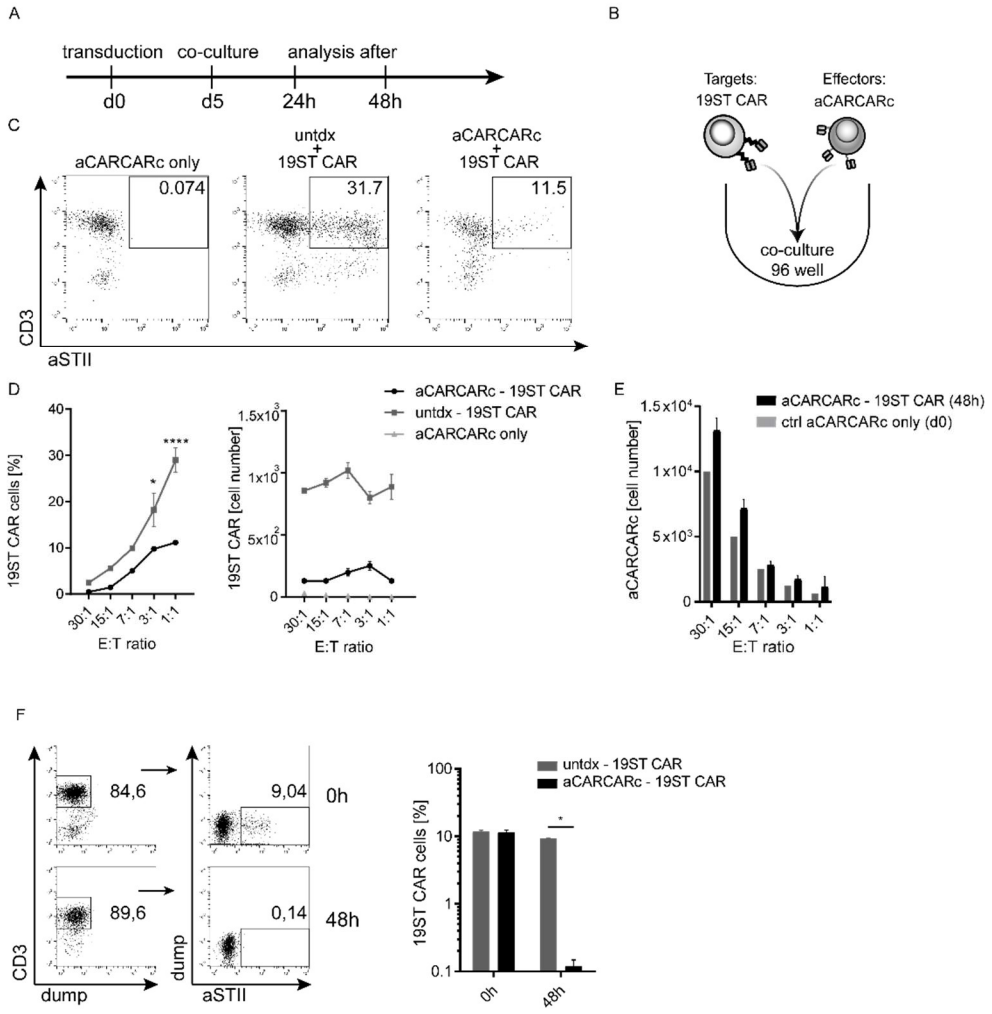


**Figure 9: Co-culture of 19ST CAR and aCARCARc.** (A-B) Experimental setup indicating transduction, start and analysis of the co-culture. (C)Representative FACS plots pregated on living lymphocytes showing control groups (aCARCARc only (left) and untransduced cells incubated with 19ST CAR (middle) and aCARCARc cells incubated with 19ST CAR (right) stained with CD3-eF450 and StrepTag-FITC. (D) Percentage and absolute number of 19ST CAR cells after co-incubation. Control groups such as untransduced cells incubated with 19ST CAR (dark grey) and aCARCARc only (light grey) and sample aCARCARc incubated with 19ST CAR (black) are shown. (E) Absolute cell number of aCARCARc on day0 (grey) and after 48h (black) for the different E:T ratios. Another co-incubation experiment shown in (F and G). Cells were pregated on $CD3^+$ and target population was stained via StrepTag staining. E:T ratio of 10:1 was used. Results are quantified in (G). Untransduced cells incubated with 19ST CAR are indicated in dark grey, incubation of aCARCARc and 19ST CAR in black. Data of two different experiments are shown. Statistical analysis with Two-way Anova; **** $P \leq 0{,}0002$; * $P \leq 0{,}05$. Means ± SD are plotted.

## 5.3 *In vivo* testing of aCARCARc safeguard mechanism

### 5.3.1 Generation, expression and functional testing of novel anti-StrepTagII CAR in murine cells for mouse studies

After testing the 19ST CAR recognizing the human CD19 antigen and the aCARCARc recognizing the STII in the hinge region of the 19ST CAR, we transferred the STII containing constructs into γ-retroviral vectors for a murine syngeneic setting. Constructs specific for the murine situation enabled us to perform more clinically relevant *in vivo* studies. Therefore, we introduced the three repetitions of the STII into the hinge region of the murine aCD19 CAR (m19-ST-28z_E CAR) backbone and the aStrepTagII scFv (classic) into the same murine aCD19 CAR backbone (mCARCARc). Both constructs consisted out of CD8α hinge and transmembrane domain fused to the intracellular CD28 costimulatory and CD3ζ TCR signaling domain (Fig. 10A). Both constructs

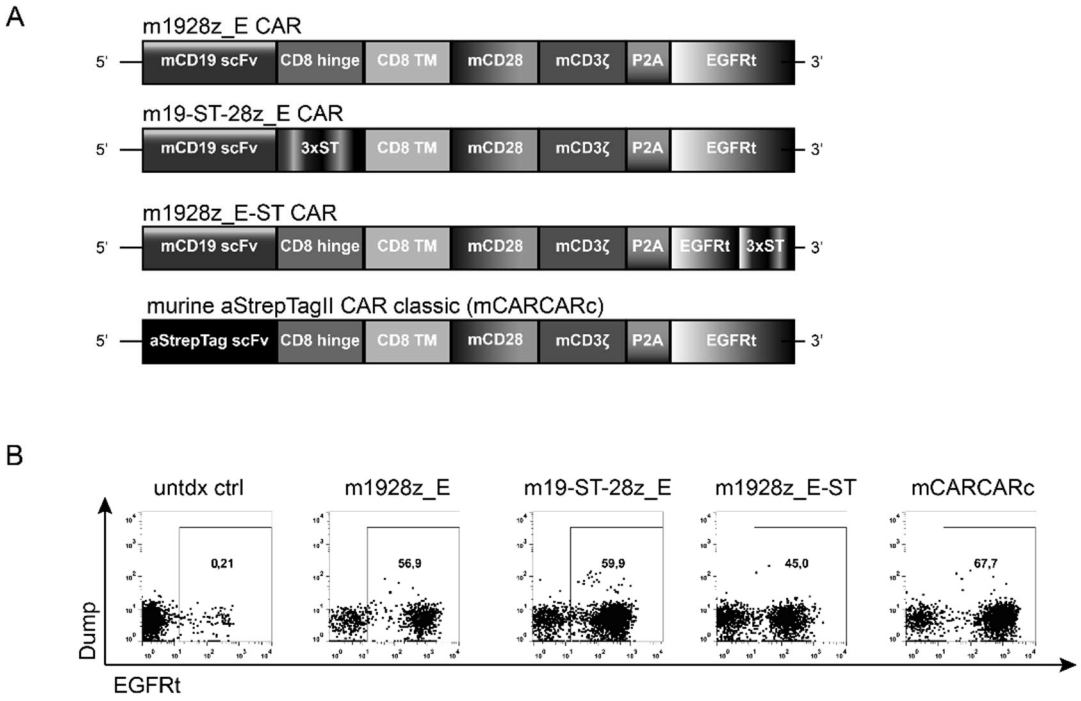


**Figure 10: Generation and expression of novel murine constructs.** Different vectors shown in (A). Vectors comprising a anti murine CD19 scFv

**Figure 11: Generation and expression of novel murine constructs.** Different vectors shown in (A). Vectors comprising a anti murine CD19 scFv All (1-3 from top) or an aStrepTag classic scFv (bottom). As a hinge a triple StrepTag (3xST, second from top) or a CD8a hinge region is used. All$_{3z)}$ vectors containing a CD8 transmembrane (CD8 TM), murine CD28 costimulatory domain (mCD28), a murine CD3 zeta stimulatory domain (mCD3z)$_{ıce}$ linked to a P2A cleaving peptide followed by the truncated EGFR receptor (EGFRt). The vector m1928z_E_ST contains a triple StrepTag sequence$_{ıgs}$ (3xST) N-terminal of the EGFRt. Transduction efficacies of generated retroviral vectors are shown in (B). Representative Flow cytometry stainings$_{:ral}$ for the transduction marker EGFRt are shown. All samples are pregated on living lymphocytes. Irrelevant fluorescence channel with no spectral overlap was used as dump channel. Untransduced control sample shown on the very left. All generated constructs are expressed.

additionally contained the truncated EGFRt, which is equimolarly expressed with the CAR itself, for selection and tracking. Cloning was done via Gibson assembly. Correct clones were confirmed by Sanger sequencing and multiplied with a plasmid maxi preparation.

As a first pilot experiment, we performed γ-retroviral transduction to confirm proper CAR expression. We transfected PLAT E cells with the retroviral vectors and the generated virus supernatants were used to transduced murine splenocytes, stimulated with anti-CD3 and anti-CD28 mAbs during the previous 24h. For analysis, cells were stained for the transduction marker EGFRt and for PI to distinguish living and dead cells. All constructs showed transduction efficacies ranging from 45,0% (m1928z_E-3ST) to 67,7% (mCARCARc). Due to the fact that the CAR should be co-expressed with the transduction marker, we considered the CAR to be expressed accordingly (Fig. 10B). In a follow-up experiment, we performed a co-culture experiment similar to the co-culture experiment we performed with the human constructs (see Fig. 9). At day 0, we transduced murine splenocytes with either mCD19 CAR constructs containing or not the STII target site (m1928z_E, m19-ST-28z_E or m1928z_E-ST) or mCARCARc construct; the co-culture started on day 1 with final analysis 48h later (Fig. 11A). We had three different conditions for each construct. First, we cultured only mCD19 CAR splenocytes, second, we cultured mCD19 CAR splenocytes co-incubated with $CD19^+$ TBL-12 tumor cells and in the third condition, we cultured the CD19 CAR splenocytes, tumor cells and additionally added mCARCARc cells. When adding all three components a mixture of 1:1:1 was used. As a readout, we used the frequency of endogenous B cells which are naturally present in murine splenocytes. When incubated with murine anti-CD19 CARs (m1928z_E, m19-ST-28z_E or m1928z_E-ST) no B cells were detected in all samples after 48h (Fig. 11B). This demonstrated the expression and functionality of the murine anti-CD19 CARs. In the second set where also TBL-12 tumor cells were present, aCD19 CAR T cells efficiently eliminated both tumor and B cells. In a third sample, we additionally added mCARCARc cells to see whether mCARCARc cells can prevent STII containing aCD19-CAR T cells from killing B or tumor cells. Indeed, the mCARCARc cells clearly inhibited the killing of B and tumor cells only when the anti-CD19 CAR T cells comprised an STII sequence. When mCARCARc cells recognized aSTII containing CAR either anti-CD19 CAR cells have been eliminated or their killing capacity was inhibited. Of note, we could not differentiate between tumor cells and B cells. No effect was

observed when mCARCARc was co-incubated with m1928z_E CAR (Fig. 11B). All controls showed $CD19^+$ populations (B cells or/and tumor cells) after co-culture. Controls co-cultured with tumor cells showed the biggest $CD19^+$ population due to the fast proliferation of the tumor cells. Controls without tumor cells showed lower frequencies of $CD19^+$ cells because of suboptimal culturing conditions for the B cells. In this experiment, we showed that anti-CD19 CAR T cells are fully functional and the mCARCARc can inhibit the killing of $CD19^+$ cells *in vitro*. However, we cannot clearly tell whether anti-CD19 CAR T cells are inhibited or eliminated by the mCARCARc cells.

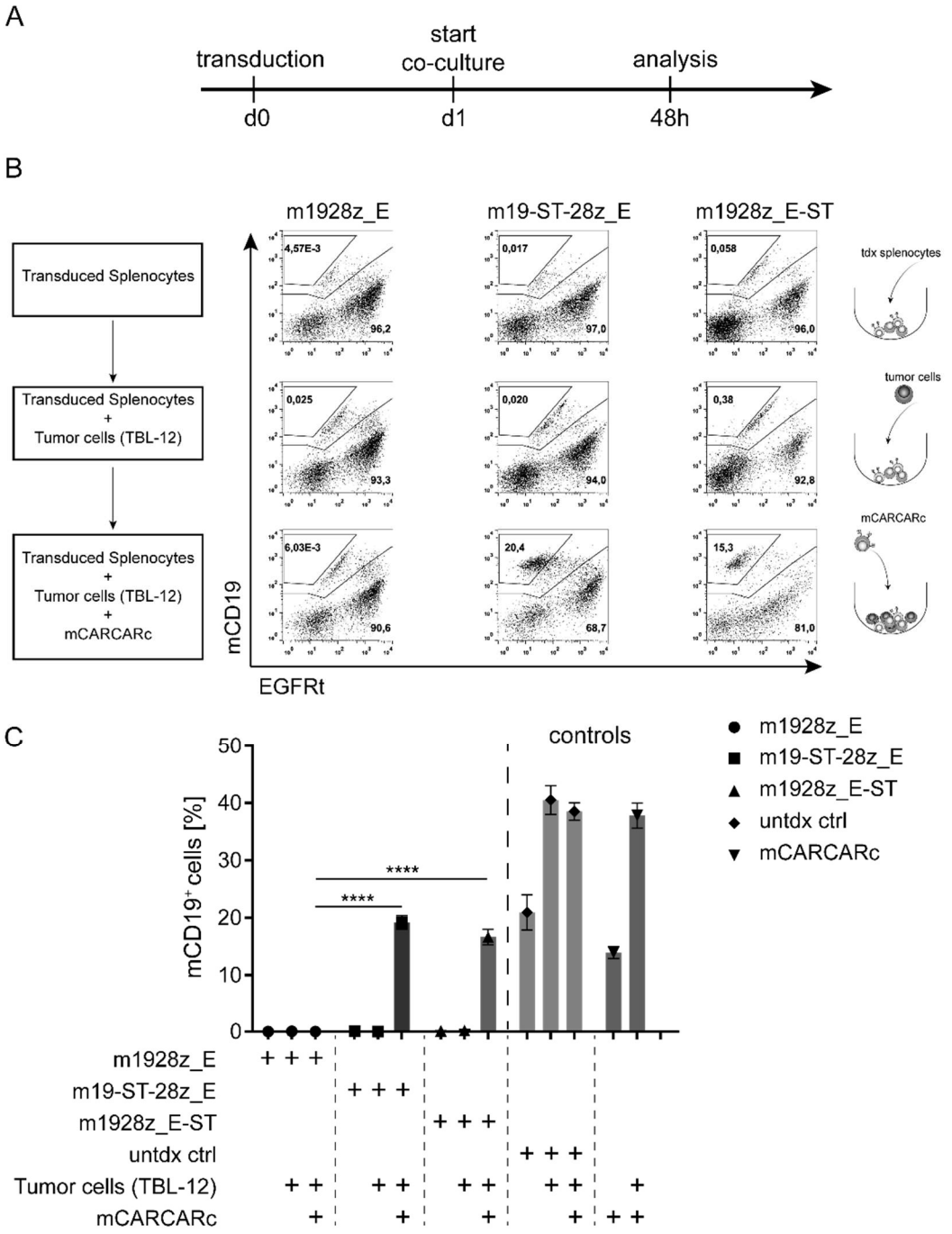


**Figure 12: Functional co-culture assay.** Experimental setup is shown in (A). Representative flow cytometry plots are of each group is shown in (B) pregated on living splenocytes and CD19 and EGFRt positive cells. First row represents transduced splenocytes, in the second-row tumor cells are added additionally and the third-row tumor cells and mCARCARc cells are added. Mouse CD19 positive cells are quantified including controls (C). m1928z_E (black circles), m19-ST-28z_E (dark grey quadrants), m1928z_E-ST (grey triangles), untransduced control (untdx., light grey diamonds) and mCARCARc (dark grey triangles). Crosses indicating added cell populations. Dashed lines separating samples from controls. n.t. = not tested. Data observed out of three independent experiments. Statistical analysis was done with Two-way ANOVA; **** $P \leq 0{,}0002$. Means ± SD are plotted.

We further wanted to gather functionality data on the behavior of the mCARCARc as a safeguard mechanism *in vivo*. For the first *in vivo* experiment, we used WT BL/6 CD45.2 congenic mice like in previous experiments. As a functional readout, we used the endogenous CD19 positive population. Our hypothesis was that the anti-mCD19 CARs (m1928z_E, m19-ST-28z_E or m1928z_E-ST) should be able to first eradicate the endogenous $CD19^+$ compartment leading to B cell aplasia in mice as described by Davila et al. Subsequently, we wanted to test if B cell aplasia after injection of mCARCARc cells could be reversed by eliminating mCD19 CAR cells. Retroviral transductions were performed with the MP71 retroviral vector with constructs described in the previous figure (Fig. 12A). Mouse splenocytes were derived from CD45.1 transgenic mice, stimulated with anti-CD3 and anti-CD28 mAbs and transduced with desired virus supernatants. Four days after transduction, $1x10^6$ mCD19 CAR T cells per mouse were injected (i.v.) into irradiated Bl/6 WT 45.2 congenic mice. Injected cells engrafted well and were monitored by weekly blood draws and flow cytometry analysis. On day 26 post mCD19 CAR T cell transfer, B cell aplasia was observed in all groups confirming *in vivo* functionality of all mCD19 CAR constructs (Fig. 12B). After steady B cell aplasia, we injected $3,5x10^6$ transduced CD90.1 congenic Bl/6 wt mCARCARc cells intravenously. The mCARCARc cells were generated as described for mCD19 CAR T cells and injected i.v. into mice. Transferred cells engrafted well and were detected with flow cytometry but, unfortunately, mCARCARc cells could not reverse B cell aplasia (Fig. 13B and C). Due to the fact that mCARCARc cells were not able to reverse B cell aplasia, we injected a second dose of mCARCARc cells trying to enhance the functionality and absolute number in mice. Transduction was performed with BL/6 WT CD90.1 congenic OT-I cells. All OT-I cells express a chicken ovalbumin (OVA) specific TCR, which can be triggered by injection of modified vaccinia virus Ankara expressing OVA (MVA-OVA). OT-I mCARCARc cells failed again after the second injection to reverse B cell aplasia. We then triggered the OT-I specific cells with an MVA-OVA vaccination and the cells overall expanded *in vivo*. Still, we could not observe an increase in the endogenous B cell population in all mCD19 groups (Fig. 12B). Besides monitoring the endogenous B cells, we monitored also transferred T cells which can be distinguished by congenic markers and EGFRt expression (gating strategy is shown in Figure 13D). Frequencies of mCD19 CAR T cells and mCARCARc cells in different mouse groups are shown in Figure 13E, albeit the frequencies

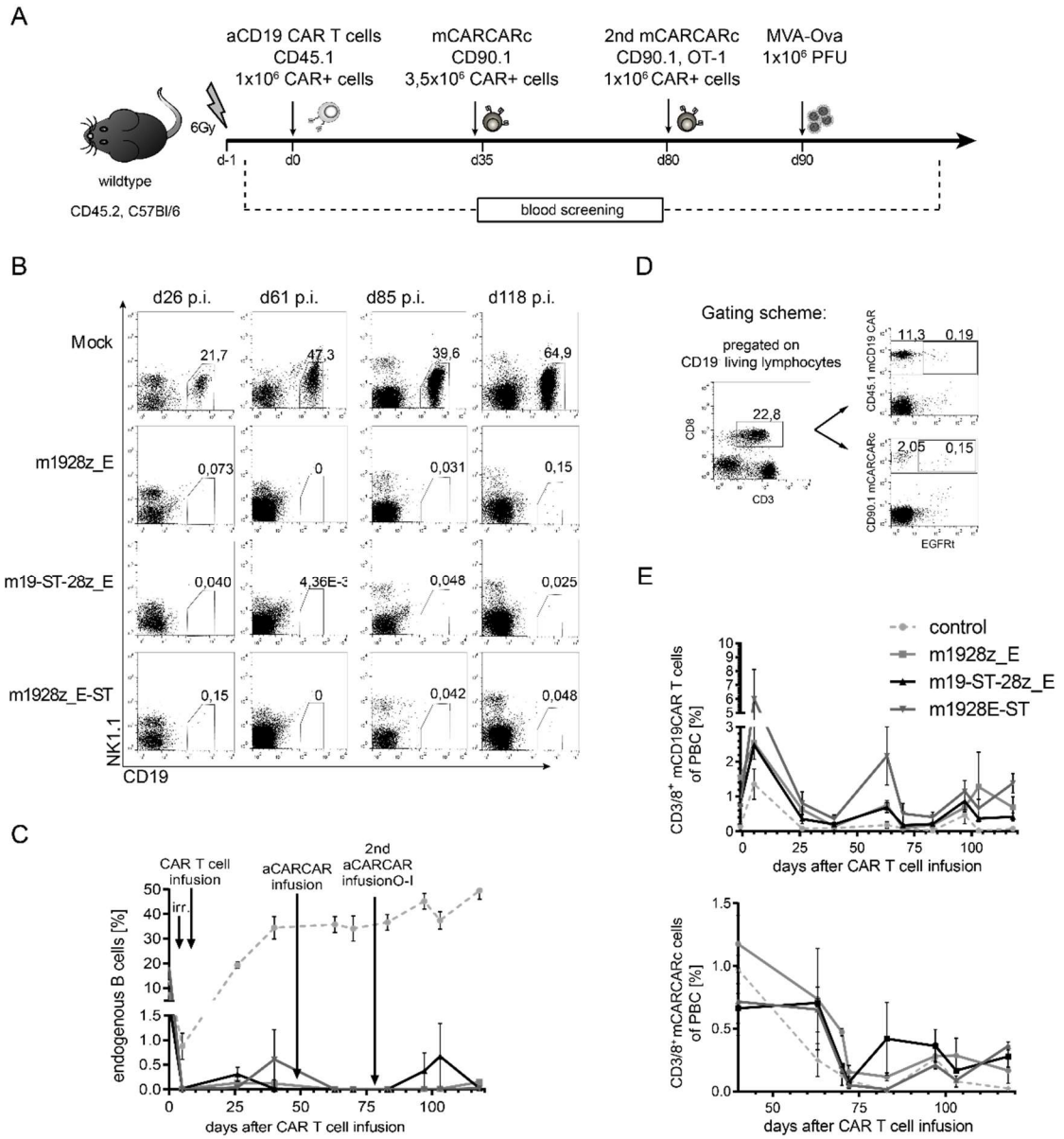


**Figure 13: In vivo functionality of mCARCARc cells.** Experimental layout is shown in (A). Chronological representative flow cytomertry stainings for CD19 positive cells for each group are shown in (B). Frequencies of endogenous B cells are quantified in (C) over time. Mean of each group (n=3 mice) is shown as well as all interventions. Gating strategy is shwon in (D), pregated on living lymphocytes. Freqencies of tranferred transgenic mCD19 and mCARCARc $CD3^+/8^+$ cells in blood are shown over time in (E). Mean (S.D.) of each group is shown, indicated by error bars.

of mCD19 CAR T cells in peripheral blood were in all groups very low. Similar findings we observed already in previous experiments. However, the frequency of mCARCARc cells was low as well.

Surprisingly, the OT-I transgenic mCAR-CARc cells which were $EGFRt^+$ did not expand post-MVA-OVA challenge. For that reason, we performed a final blood draw and tissue analysis of spleen, lymph nodes, and BM. Interestingly, after 7 days of MVA-OVA challenge, we could only observe an expansion of $CD8^+$ OT-I mCARCARc cells that were $EGFRt^-$ (Fig. 13A). Next, we tested whether the transgenic $CD8/EGFRt^+$ cells are exhausted due to both TCR and CAR signaling, since additional TCR signaling can lead to T cell exhaustion [139]. We determined exhaustion by

staining the Programmed cell death protein-1 (PD-1, CD279). Intriguingly, we found a significant PD-1 upregulation in OT-I mCARCARc EGFRt$^+$ cells (Fig. 13B). Unfortunately, this higher PD-1 expression in mCARCARc EGFRt$^+$ was detected in blood, spleen and BM of all groups (Fig. 13C and D). even in control groups where no STII containing mCD19 CAR was injected. These findings do not completely support the hypothesis that OT-I mCAR-CARc were exhausted due to dual CAR and TCR triggering. However, bone fide exhaustion is better defined through the co-expression of more inhibitory molecules or loss of effector functionality. We therefore cannot completely decipher whether it is real exhaustion of the transgenic cells, and/or if non-transgenic (EGFRT$^-$) cells simply outcompeted EGFRt$^+$ transgenic cells (Fig. 13E).

In summary, we validated a new mechanism of cellular safeguard using an STII containing CAR and an anti-STII binding safeguard CAR in human primary cells and in murine cells. Newly generated constructs performed as expected *in vitro*, where anti-STII CARs could recognize and eliminate CARs possessing an STII in their hinge region. First *in vivo* experiments did not confirm the findings we observed *in vitro* and additional experiments are currently ongoing in order to elucidate the reasons behind the not observed *in vivo* functionality (i.e. lack of preconditioning

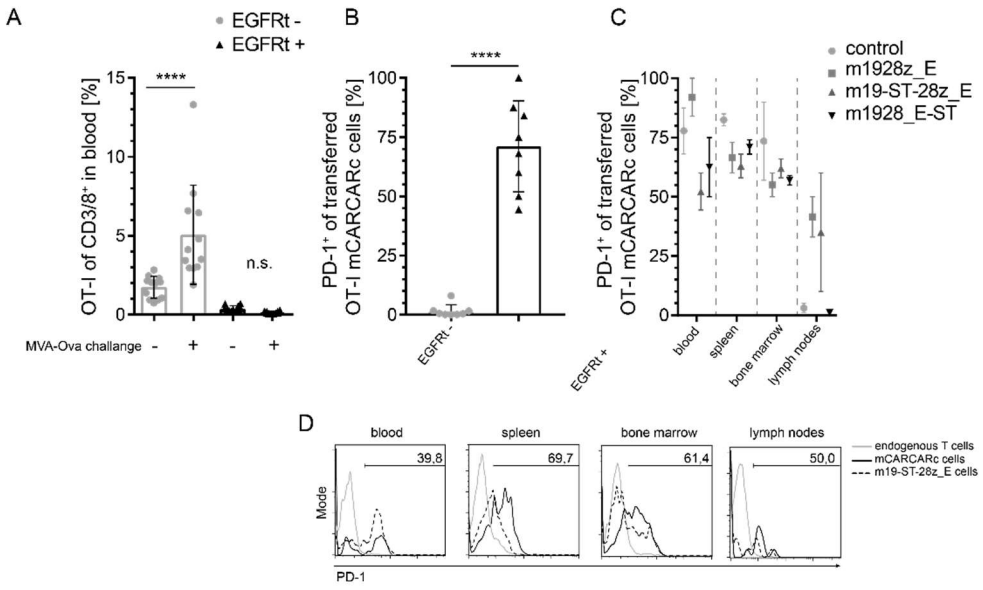


**Figure 14: Exhaustion of transgenic EGFRt$^+$ cells.** Experimental setup (A). CD3$^+$/CD8$^+$ transgenic EGFRt positive cells in the blood after 7 days of MVA-OVA challenge are shown in (B). Cross indicates MVA-OVA challenge or EGFRt$^+$. EGFRt$^-$ (grey) and EGFRt$^-$ (black) cells are indicated for each mouse. PD-1$^+$ of congenic EGFRt$^-$ (grey circles) or EGFRt$^+$ (black triangles) cells in the blood (C) and in tissues (D) for each mouse group are shown. (E) Representative histograms indicating PD-1 expression in different tissues. Living, CD3$^+$/CD8$^+$ endogenous T cells (grey line), m19-ST-28z_E (black dashed line) and OT-I mCARCARc (black line) cells are shown. Statistical analysis used: Unpaired t-test **** P ≤ 0,0001; n.s.=not significant. n=3 mice per group. Means ± SD are plotted.

before aCARCAR infusion). First promising data have been already collected by Lingfeng Liu (Riddell lab) and Mortimer Svec (Busch lab).

## 5.4 Affinity modified CAR T cells for improvement of CAR T cell therapy

Another optimization strategy to improve CAR T cell therapy, we hypothesized, could be to modulate the affinity of the scFv to its target antigen. We therefore exchanged single amino acids in the scFv by alanine via mutagenesis PCR. Most frequently, amino acids in close proximity to the framework region were mutated, as these positions were found to be important for the binding kinetics of Fab fragments without completely interfering with the Fab specificity to its target [189].

One aim of this thesis was first to generate reagents that can be used to measure CAR binding affinity using the $K_{off}$-rate assay developed in our laboratory. This assay allows the measurement of receptor-ligand affinity under natural conditions (e.g. expression and cell surface distribution of the respective receptor). In its original design, the $k_{off}$-rate assay was established to measure TCR-MHC I interactions and, thereby, the structural avidity of TCRs. Here the MHC I molecule, by itself of only low affinity, was fluorescently labeled and multimerized via its recombinantly fused StrepTag on a StrepTactin-backbone. Upon administration of D-biotin, the multimer complex is disrupted and the MHC molecules dissociate spontaneously from the cell surface. Their dissociation rate can be measured via the loss of fluorescence on the cell surface [58]. Whereas the original method is based on pre-enriched cells that were measured using confocal microscopy, the latest developmental stage is based on a flow-based system [190]. We aimed to transfer this elegant and sensitive technology to measure the affinity of the scFv of CARs. To perform any kind of affinity measurement at least one interaction partner has to be available in a soluble form. Unfortunately, there was no soluble CD19 protein commercially available which was suitable for the $K_{off}$-rate assay. We failed expressing the soluble, natural monomeric CD19 protein by ourselves (data not shown). Therefore, we decided to design and express soluble scFvs

mimicking the CAR receptor to perform a physiological $K_{off}$-rate assay using natural $CD19^{+}$ tumor cells.

### 5.4.1 **Generation of affinity modified scFvs for optimal affinity and functionality**

Our laboratory could show that specific point mutations in the framework or complementary determining regions (CDR1-3) of Fab fragments led to significant reductions in binding affinity [191]. This technique was established for Fab-fragments by the STAGE cell therapeutics group. For the generation of affinity-modified anti-CD19 scFvs we set specific point mutations in the CDR1 (H35A, predicted by Kabat) and in the CDR3 region (F108A, predicted by Kabat). Previous findings could show that these point mutations led to a significant reduction in binding affinity when introduced into the human anti-CD19 Fab-fragment (parental CD19 antibody 4G7, IBA). The company could show that the exchange of amino acids at positions H35A and F108A of the heavy chain resulted in a low-affinity Fab fragment spontaneously dissociating from the cell surface. For the Fab fragment it is shown that the mutation CD19-H35A has a lower affinity as the CD19-WT Fab but higher than the CD19-F108A Fab (unpublished data, former STAGE cell therapeutics). For that reason, our first aim was to generate soluble scFvs for affinity determination and data comparison.

### 5.4.2 **Generation of soluble scFv-binding domains**

For generation of the anti-CD19 scFv derived from the anti-CD19 Fab fragment (parental CD19 antibody 4G7) we designed specific primers for the variable light (VL) and variable heavy (VH) chain comprising a GST-linker in-between. We then cloned the scFv construct into the pENTRY-IBA 51 plasmid. The described pENTRY-IBA51 vector was used for subcloning of the inserts in the final expression vector (pASG-IBA102-GGSC). By recombinase-based integration in this vector, the insert is N-terminally fused with a signal peptide for periplasmatic expression in E. *coli* as well as C-terminally equipped with a Twin-StrepTag followed by a free cysteine (-c) (Fig. 14). The StrepTag is used for affinity purification and for multimerization of the construct on a StrepTactin-backbone. The C-terminal cysteine is needed for the covalent coupling of a fluorescence dye which is crucial for the $K_{off}$-rate assay measurement. For introducing point-mutations, we exchanged the amino acid Histidine (H) to Alanine (A) at position 35 and the amino acid Phenylalanine (F) to again Alanine (A) at position 108 in the heavy variable chain of the scFv by mutagenesis PCR (Fig. 15A).

### 5.4.3 **Expression and staining of soluble scFv fragments**

For expression, the respective scFvs were cloned into the periplasmic expression vector (pASG-IBA102-GGSC) and electroporated into the electrocompetent *E. coli* strain JM83. ScFvs contain disulfide bonds stabilizing their folding, therefore a reducing milieu for correct folding in the

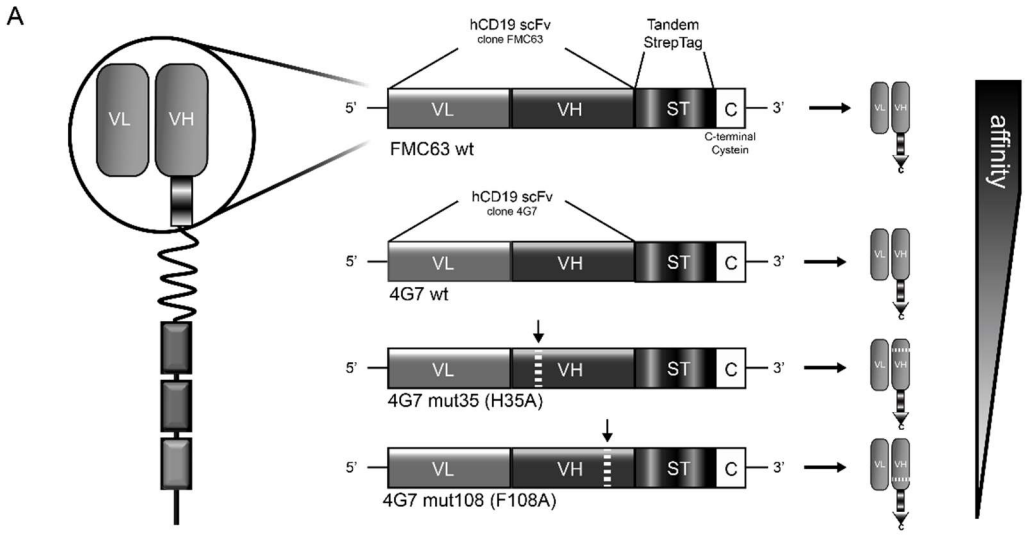


**Figure 15: Schematic illustration of soluble scFvs isolated from a CAR using two scFvs clone FMC63 and clone 4G7 WT.** Variable light (VL) is linked to variable heavy (VH) chain fused to a tandem StrepTag domain (ST) coupled to a N-terminal exposed Cysteine (C) for purification and dye coupling. Two point mutations (alanine exchange) set in scFv clone 4G7 on position 35 and 108 for affinity modification in the VH chain (vertical arrow, dashed line). Correct folded soluble scFvs are illustrated on the right.

periplasm is crucial. Expressed scFvs were purified by periplasmatic extraction followed by purification with StrepTactin gravity flow affinity column. Quantitative analysis, verification of correct proteins and purity analysis were performed with Bioanalyzer, SDS-Page and silver staining (Fig. 15A - C). In details, expressed scFv proteins were detectable in an SDS-PAGE at a size of 28 kDa after 30 seconds exposure by probing the membrane with StrepTag-classic-HRP (Fig. 16A) and the high purity of the periplasmatic expressed scFvs was further corroborated by sensitive silver staining (Fig. 16B). The concentration of purified proteins was finally measured with Bioanalyzer. For all constructs reasonable concentrations could be detected (4G7 WT (127,7 ng/µl), 4G7 mutant 35 (99,7 ng/µl), 4G7 mutant 108 (90,3 ng/µl) and FMC63 WT (370 ng/µl)) indicated by the peak in the electrogram (arrow) (Fig. 15C). However, batch-to-batch variation was also observed after each recombinant protein expression.

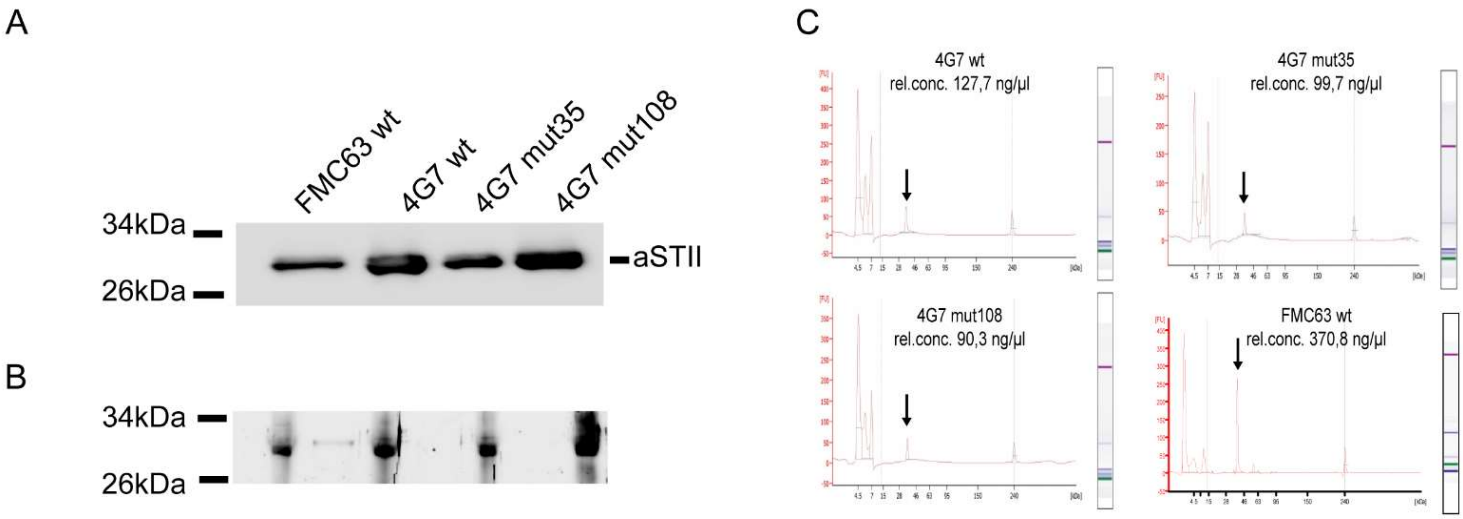


**Figure 16: Periplasmic expression and purification of soluble scFv fragments.** (A) Detection of recombinant scFvs with an SDS-PAGE using anti-StrepTag-classic-HRP mAb. Proteins were obtained from a E.coli culture after induction of protein expression with AHT. Silver staining conforming expression and purity of recombinantly expressed scFvs (B). Electropherogram generated with Bioanalyzer and measured relative concentrations of expressed proteins are indicated. Arrows indicate peak of recombinant proteins (C).

Next, we used the purified recombinant scFv proteins for staining $CD19^{+}$ LCL cells and test whether the scFvs recognize specifically the CD19 surface protein. To detect staining by flow cytometry, scFvs were multimerized on StrepTactin-PE (ST-PE) (Fig. 16A). Titration of 0,1 µg, 0,5 µg and 1 µg protein multimerized with 0,2 µg ST-PE was performed and controlled with ST-PE background staining. Control staining with ST-PE only was negative whereas staining with FMC63 wt and 4G7 wt scFvs was clearly positive even in low scFv concentrations. Stainings with 4G7 mutant 35 and 4G7 mutant 108 was possible only in higher protein concentrations, with 4G7 mutant 35 staining. We observed a brighter staining intensity of 4G7 mutant 35 compared to 4G7 mutant 108 which might be due to its higher affinity (Fig. 16B).

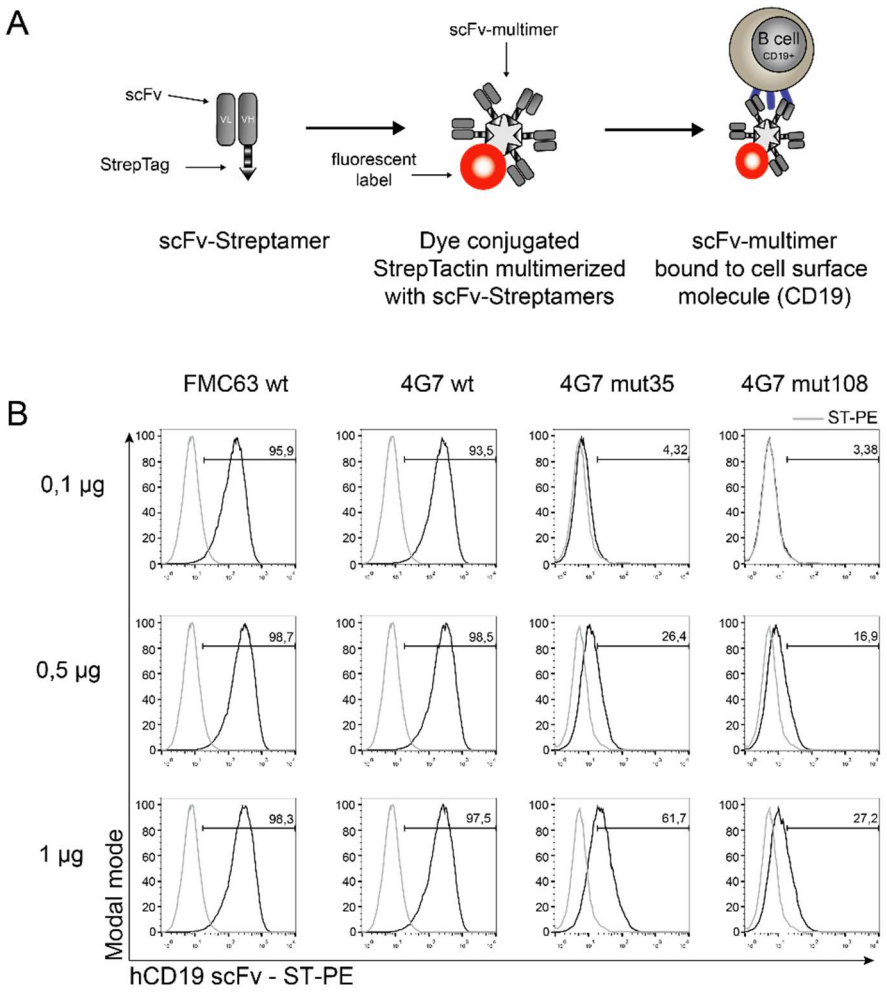


**Figure 17: Titration and staining with expressed scFvs.** (A) Scheme of standard staining procedure using scFv-Streptamer multimerized with StrepTactin-PE for staining CD19⁺ LCL cells. (B) Staining-titration using different protein amounts of scFvs by keeping the amount of ST-PE constant are shown. Top 0,1µg, middle 0,5µg, bottom 1,0µg. ST-PE background staining is shown in grey, staining with scFvs in black. Percentage of stained cells is indicated by gated frequency. At least three independent experiments performed.

To improve the staining intensity, we investigated different protocols. We either pre-multimerized before the staining scFv proteins with StrepTactin or stained the LCL-cells with scFvs first and StrepTactin afterwards. In the other procedures, we simultaneously added scFv proteins and StrepTactin to the cells or first added scFvs and washed them prior to StrepTactin addition. After analyzing the staining via flow cytometry, we observed consistently good stainings for the 4G7 wt in all protocols but variable staining intensities for the mutant scFvs. Overall, we got the best staining results when using the last two-step procedure first staining the scFvs, adding the Streptactin after a washing step (very right panel in Fig. 17). However, for the mutant 108 the staining was still weak, so we decided to perform additional stainings with more relevant human PBMCs isolated from healthy donors. The LCL cell line might not be the optimal target to test the staining of CD19 due to the homogeneity of CD19 cell surface protein expression. An

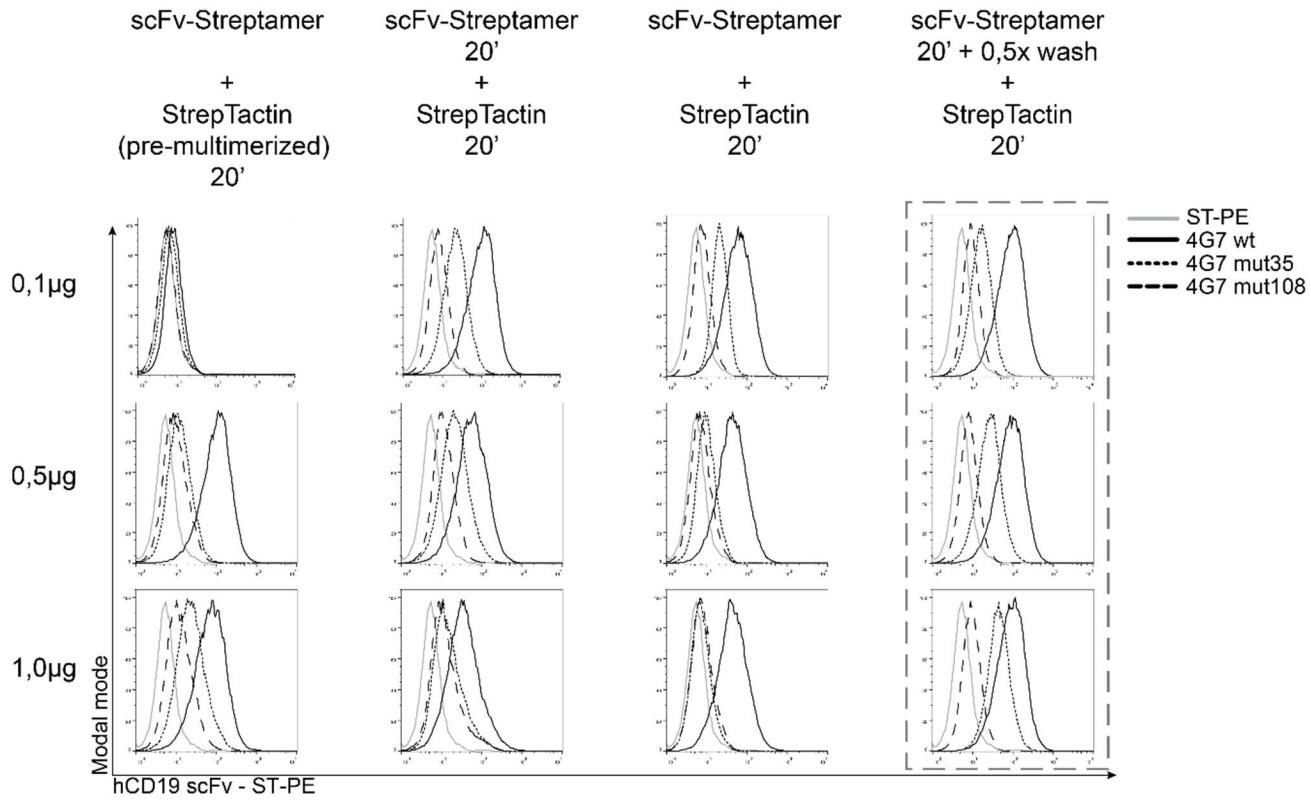


**Figure 18: Optimization of the scFv staining protocol.** Different staining procedures were tested, staining details indicated on top. Concentration of used scFv protein is indicated on the left, 0,1µg; 0,5µg; 1,0µg from top to bottom. ST-PE background staining is indicated (grey), 4G7 wt (black solid), 4G7 mutant 35 (black dotted line) and 4G7 mutant 108 (black dashed line). Staining procedure which resulted in the best staining result is indicates by the dashed box.

advantage of using human PBMCs is the presence of CD19 negative cells such as T cells. Very distinct stainings, which are important for further experiments, were observed. For the stainings we gated on living lymphocytes and differentiated between T and B cells using the surface markers CD3 (T cells) and CD19 (B cells) (Fig. 18A). We analyzed all stainings with histograms gated on living lymphocytes including $CD19^+$ and $CD3^+$ cells. With that additional information, we were able to judge the specificity of the CD19 surface protein staining. As a negative control, we used an ST-PE control staining to determine the unspecific background staining. As a positive control, we used a commercially available anti-CD19 mAb conjugated to the same fluorophore PE to define the target population (Fig. 18B). Additionally, we performed another dose titration of different protein concentrations to validate previous results with human PBMCs. We observed for all scFv proteins similar percentages of $CD19^+$ cells compared to the control mAb confirming the specific binding to the CD19 surface molecule expressed on human B cells (Fig. 18B middle). We identified that mutants 35 and 108 showed a lower staining intensity compared to FMC63 WT and 4G7 WT in all protein concentrations (Fig. 18B bottom). We assume that it is the result

of the reduced affinity of the mutants which might be limited to bind to the similar amount of CD19 surface proteins compared to the WT proteins. Another possibility could be that the amount of correctly folded proteins of the mutants might be lower resulting in less scFvs binding to the CD19 surface protein, which is hard to address. However, all recombinantly expressed scFvs specifically stained the CD19 surface proteins on human B cells.

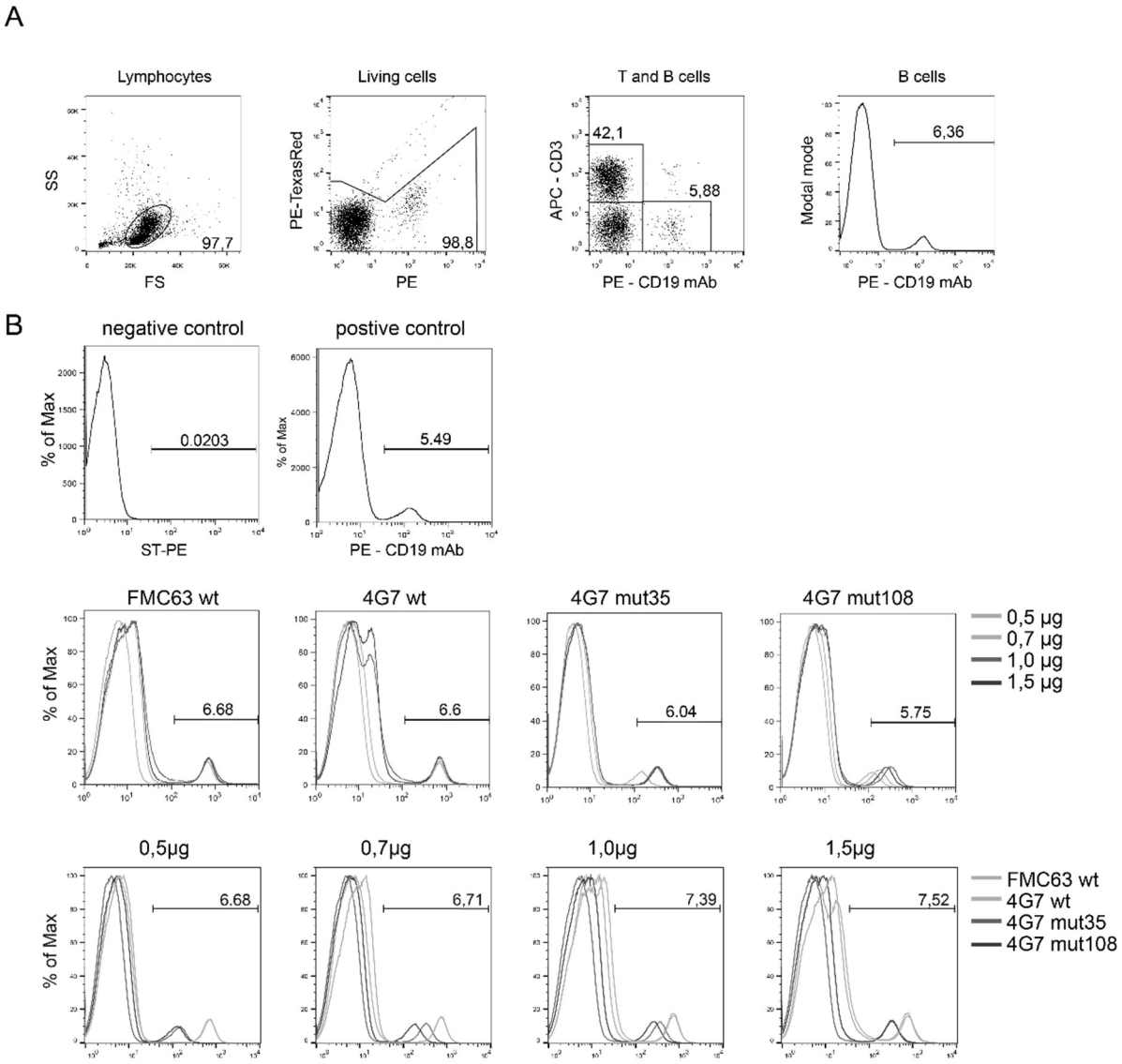


**Figure 19: Staining of human PBMCs with generated scFvs.** Gating scheme is shown in (A). All samples are gated on living, single, lymphocytes. Histograms showing CD19⁺ fraction of gated cells. Frequencies of CD19⁺ cells are indicated. (B) Negative control (ST-PE background staining) and positive control (PE-CD19 PE mAb) are displayed in top row. Middle row showing titration of used scFv proteins 0,5µg (light grey), 0,7µg (grey), 1,0 (dark grey) and 1,5µg (black). Bottom row different scFvs are overlaid in ascending concentration from left to right ranging from 0,5µg to 1,5µg. FMC63 (light grey), 4G7 wt (grey), 4G7 mutant 35 (dark grey) and 4G7 mutant 108 (black). Frequencies of gated cells are indicated in percentage.

### 5.4.4 **Reversible staining of recombinantly expressed scFvs**

Finally, the reversibility of the recombinantly expressed scFvs was analyzed in a flow cytometry-based assay. ScFvs were multimerized on a fluorescent labelled StrepTactin backbone and the resulting Streptamer used to stain target cells. After adding D-biotin, the scFv-StrepTactin multimer is disrupted and the fluorescent signal vanishes. To control for the residual cell-bound scFv monomers, cells are re-stained after washing with the StrepTactin-PE (Fig. 19A). Compared to the WT scFv FMC63 and 4G7, the mutant 35 and 108 should have a lower binding strength to its target, potentially resulting in a spontaneous dissociation from the cell surface and lower or absent restaining. To test the reversibility of the different scFvs we first stained human PBMCS with scFvs only (Fig. 19B, first column) or in combination with ST-PE (Fig. 20B, second column). Disruption of the complex after adding of 2mM D-biotin (Fig. 19B, third column) and the examination for residual scFv monomers on the cell surface was measured by re-probing the samples with ST-PE (Fig. 19B, fourth column). In the first column, no fluorescence signal was detected since monomeric scFv are not dye conjugated. After adding ST-PE, a distinct CD19 positive population was detected in a comparable range (14,3-10,2 %; second column). Addition of 2mM D-biotin disrupted as expected the scFv-ST-PE complex resulting in a loss of staining signal in all samples (third column). To test whether the scFv proteins spontaneously dissociated from the cell surface, cells were re-stained with ST-PE. In stainings with WT 4G7 or FMC63, remaining scFvs were detected on the cell surface in a comparable manner. The population size was decreased probably due to the washing steps in between. Interestingly, cells stained with the mutants did not show remaining scFvs on the cell surface, indicating spontaneous dissociation from the cell surface due to the reduced affinity to the target antigen. These results corroborated our hypothesis that the mutants have a reduced affinity to the target antigen compared to the parental clone 4G7 in a quantitative manner.

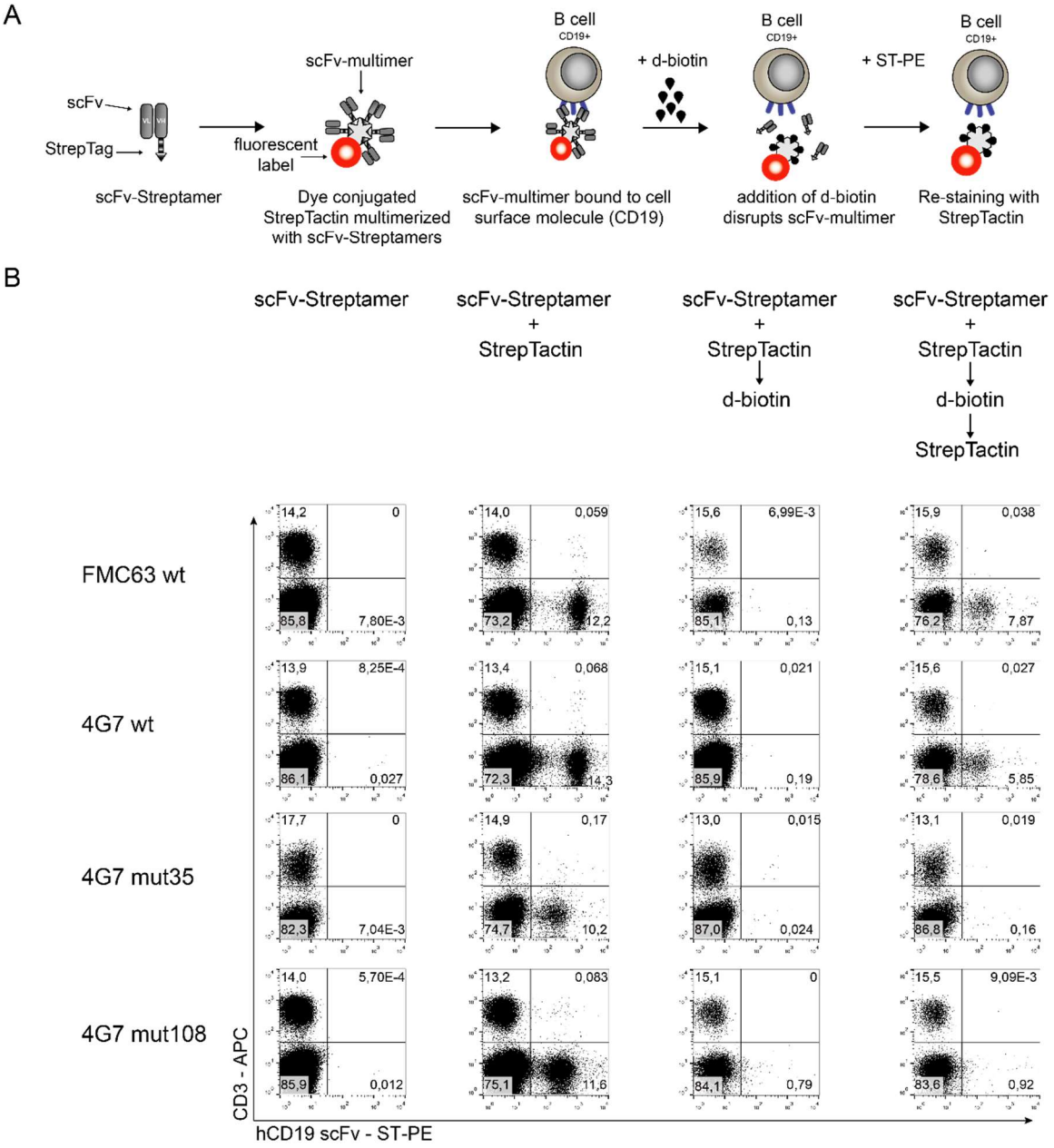


**Figure 20: Reversibility staining of scFvs.** Schematic procedure of reversibility staining is illustrated in (A). ScFv-Streptamers multimerized with StrepTactin-PE and CD19+ from PBMCs were stained for 20 min. After each step an aliquot has been taken for analyzing. Addition of 2mM Biotin disrupted the multimer complex and remaining scFvs on the cell surface have been measured after washing (PBS) and ST-PE restaining. (B) Analyzed PBMC aliquots are stained for CD3 and CD19. Timepoint of taken aliquots are indicated above. Different scFv are shown FMC63 wt (top row), 4G7 wt (seconds row), 4G7 mutant 35 (third row) and 4G7 mutant 108 (bottom row).

### 5.4.5 **Dye-labelling of the scFvs for $K_{off}$-rate assay measurement**

For $K_{off}$-rate assay affinity measurements, it is necessary to couple a dye to the free C-terminal cysteine of the scFvs. For that, we wanted to label the scFv proteins with an Atto488 dye using the C-terminal cysteine via a maleimide reaction. By labeling only a single cysteine per scFv, we achieve a monomeric staining pattern later where the fluorescence can directly be linked to the intensity (Fig. 20A). After the process of covalent maleimide conjugation, we performed fluorescence microscopy to test if the dye conjugation was successful. We incubated the scFvs to colorless StrepTactin-bound agarose beads. As a positive and negative controls, we coupled the same StrepTactin agarose beads with Atto488-dye conjugated MHC proteins and without any additional protein, respectively (Fig. 20B). As an internal control, we used for each scFv a dye conjugated and a non-dye conjugated protein. We measured a relatively high intensity in the FITC channel when agarose beads were incubated with the positive MHC control and no signal when

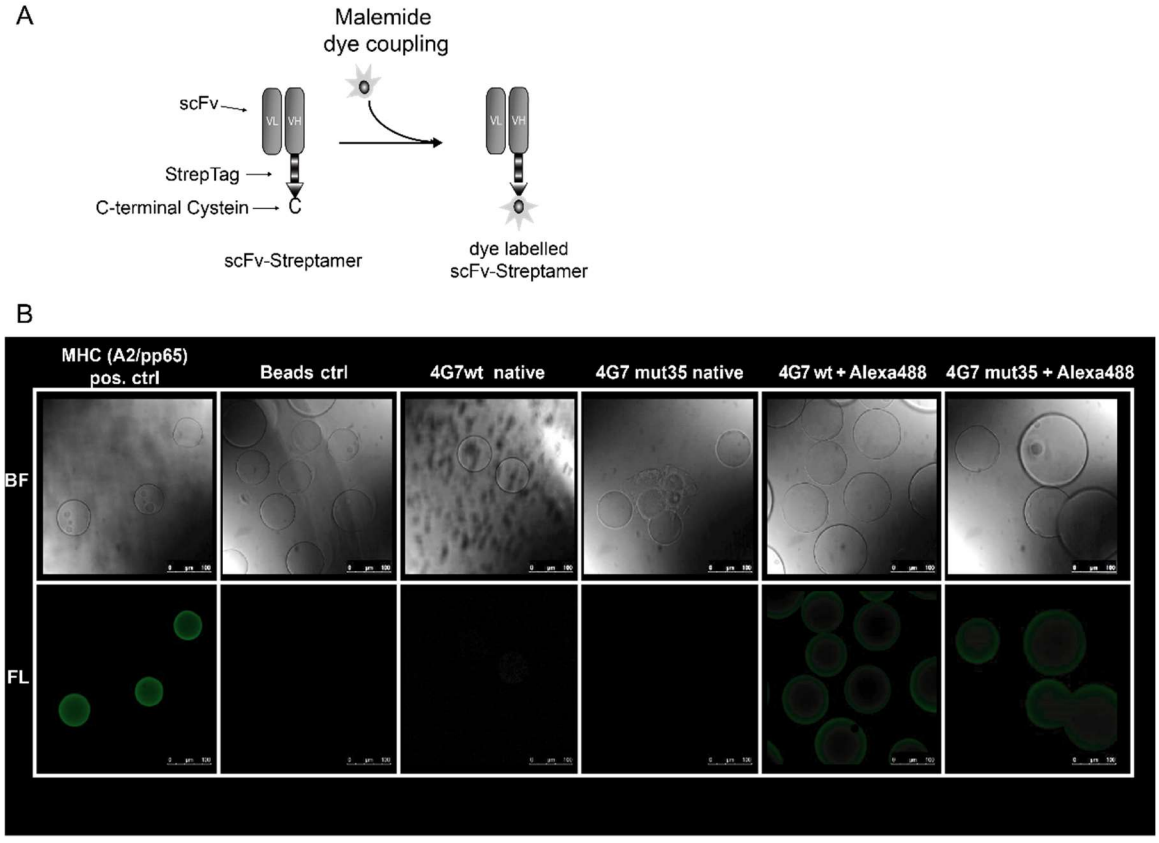


**Figure 21: Specific scFv maleimide dye coupling.** (A) Schematic mechanism of Atto488 maleimide dye coupling using scFv-Streptamer containing an accessible and reactive cysteine on the C-terminus. (B) Upper row showing Brightfield microscopic pictures of StrepTactin agarose beads. Bottom row displaying 488nm Fluorescence channel. Green Agarose beads indicating Atto488 conjugated MHC-Streptamers bound to the agarose beads (left). Uncoupled (second from left) and unconjugated scFvs of 4G7 wt (third from left) and 4G7 mutant 35 (forth from left) serving as negative controls. Dye-coupled 4G7 wt scFvs (second from right) and 4G7 mutant 35 (right) confirming successful dye conjugation representative for all scFvs generated. Bottom left of each microscopic picture scale is included.

using agarose beads alone. We also detected an Atto488 signal when we incubated agarose beads with dye-conjugated scFvs – and not for the unconjugated scFvs (Fig. 20B). Nevertheless, the fluorescence intensity for the dye conjugated scFvs was slightly lower compared to the MHC protein which is probably a result of a lower dye coupling efficacy. The fluorescence intensity should be sufficient for measuring downstream $K_{off}$-rate assay measurements.

After proving successful dye conjugation, we performed flow based $K_{off}$-rate assay affinity measurements. The workflow is shown in Figure 21A. In brief, dye-conjugated scFvs are multimerized with the StrepTactin backbone. The formed scFv multimer exhibits two fluorescence labels when binding to CD19 positive LCL cells. After addition of d-biotin, the scFv-multimer is disrupted and the StrepTactin backbone dissociates from the cell surface. This is the starting point of the monomeric scFv dissociation kinetics. How fast the scFvs spontaneously dissociate from the cell surface can be measured in real-time by the decrease of the Atto488 fluorescence intensity (Fig. 21A). The measurement is started after complete dissociation of the StrepTactin backbone (intensity of the APC signal), indicated on the left y-axis (Fig. 21B). Dissociation of scFvs is indicated by the decrease of the FITC signal intensity shown on the right y-axis (Fig. 21B). Summary of measured $K_{off}$-rate assay half-life is indicated in seconds in Figure 22C. As expected, the half-life of the FMC63 WT (748,5s) and 4G7 WT (627,3) is pretty high indicating a high affinity towards the target antigen CD19. Contrarily, the half-lives of mutant 35 (167,5s) and mutant 108 (61,5s) were lower. These findings indicate that the WT scFvs possesses a higher half-life compared to the mutants and it seems that mutant 35 possesses a higher half-life compared to mutant 108.

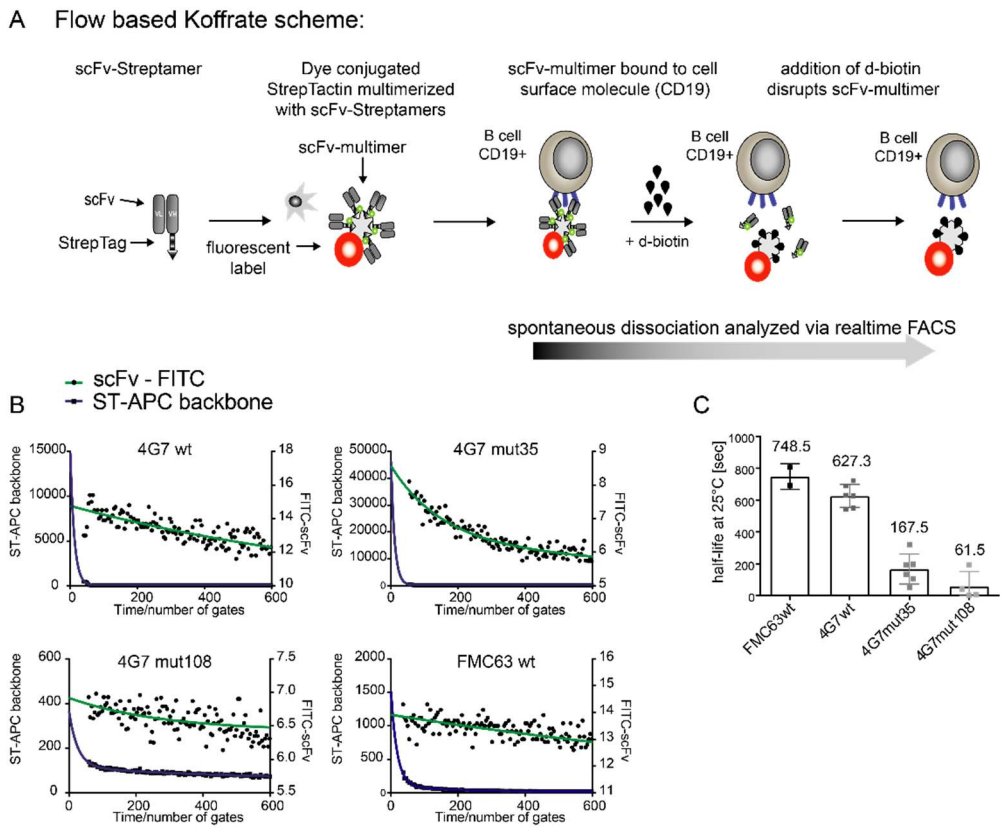


**Figure 22: $K_{off}$-rate measurements of affinity modified scFvs.** (A) Illustration of real-time flow based $K_{off}$-rate assay. Dye conjugated scFvs are multimerized and CD19⁺ LCL cells are stained. After addition of d-biotin ST-APC backbone is disrupted, and spontaneous dissociation is measured via flow cytometry. (B) Representative analyzed flow plots over time are shown for each scFv. Time was subdivided into 200 equal gates. Green line indicates dissociation of the Atto488 coupled scFvs by monitoring the FITC signal. Blue line indicates dissociation of the APC backbone disruption by monitoring the APC signal. Half-life was calculated by fitting a one-phase decay curve after complete disruption of the backbone. (C) Summary of calculated half-lives of all experiments and different scFv batches. No statistical analysis was done due to high batch to batch variation.

## 5.5 Generation of CAR constructs containing the affinity modified scFvs

Tested 4G7 scFvs (WT, mutant 35, mutant 108) were afterwards cloned into a γ-retroviral (pMP71) and lentiviral vector (epHIV7) containing a parental clinically relevant CAR construct containing the FMC63 wt scFv, kindly provided by Stanley Riddell from the FHCRC. After successful cloning, all CARs possess the same domains. Besides the scFv, they consist out of a hinge region including a triple STII (3xST), a CD28 transmembrane and a 41BB costimulatory

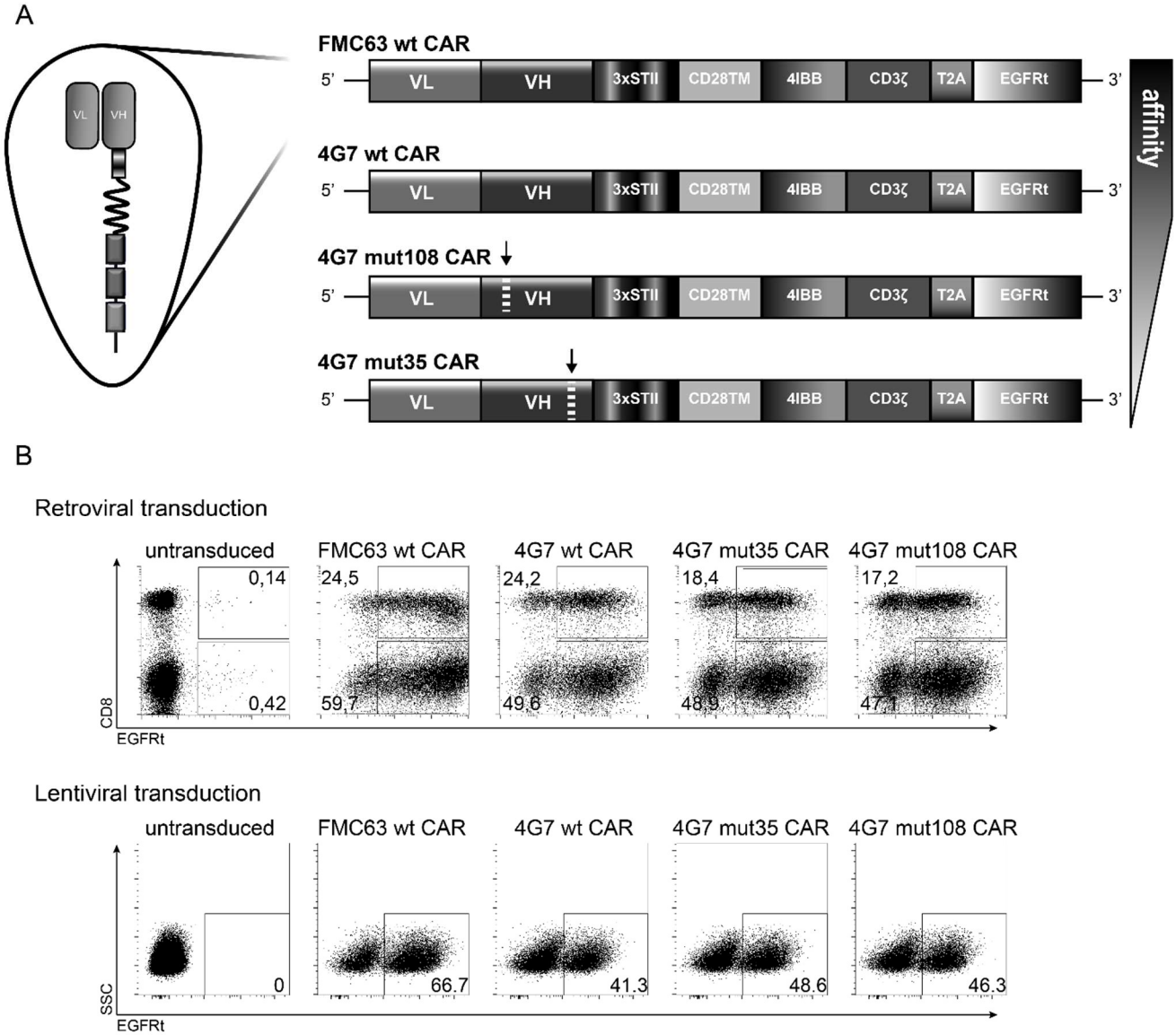


**Figure 23: Introducing of point mutations and expression of generated CAR T cells.** (A) Generated CAR constructs are shown. FMC63 wt scFv (top), 4G7 wt (upper middle), 4G7 mutant 35 (lower middle) and 4G7 mutant 108 scFv (bottom). All constructs containing a triple StrepTag (3xST) in the hinge a CD28 transmembrane (CD28TM), 41BB costimulatory (41BB) and a CD3 zeta (CD3z) domain fused to a T2A cleavage peptide (T2A) followed by the transduction marker and safeguard mechanism EGFRt. Assumed affinity is indicated on the right – from high (top) to low (bottom). (B) Expression in human PBMCs (top row) and $CD8^+$ (bottom row) are shown. Top row showing retroviral transduction bottom row indicating lentiviral transduction. Untransduced cells used as a control. CAR constructs indicated above are used.

domain followed by a CD3ζ TCR signaling domain. An EGFRt transduction marker was also included into the CAR constructs separated by a ribosomal T2A element for equimolar expression (Fig. 22A). Retroviral transduction was performed using a RD114 retroviral packaging cell line producing high titer retroviral particles released into the supernatants. For a generation of lentiviral particles, HEK293T-LentiX cells were used. Cells were transduced via spinoculation and analyzed 5 days after transduction. Retro- and lentiviral transductions resulted in high transduction efficacies using human T cells. Both $CD4^+$ and $CD8^+$ T cells could be transduced equally (Fig. 22B).

To get enough transgenic cells for *in vitro* functionality assays, we performed a CD19 specific expansion co-culturing CAR T cells with $CD19^+$ LCL cells in a 7:1 ratio for 7 days. The expansion was done with both $CD4^+$ and $CD8^+$ cells. As shown in Figure 23A and B, $CD4^+$ CAR T cells expanded better than $CD8^+$ cells overall. We could also observe that affinity-reduced CAR T cells, mutant 35 and mutant 108, expanded not as well as the WT , especially in $CD8^+$ cells, in line with the hypothesis that the affinity reduced CAR T cells are not getting as much stimulation as the WT. Looking at the phenotype of the CAR T cells after expansion using CD62L and PD-1 as activation markers [192], we observed minor differences by that the $CD8^+$ mutants showed a reduced PD-1 expression and the $CD4^+$ cells showed a lower upregulation of CD62L. All cells were $EGFRt^+$ (>95%), CD62L positive and PD-1 positive. Affinity reduced CAR T cells mutant 35 or mutant 108 showed slightly lower expression of CD62-L and PD-1 for CD4 cells. These results can be explained by the lower stimulation intensity due to the reduced binding affinity to the target antigen. The EGFRt expression of the mutant CARs was slightly higher compared to their wt after expansion.

It is known that upon strong CAR stimulation the CAR itself and the linked EGFRt can be downregulated to reduce cell stress and exhaustion (Fig. 23C).

After successful expansion of CAR T cells, we performed functional assays with generated affinity modified CAR T cells. We first performed an antigen-specific CFSE proliferation assay to test how and if the CARs proliferate upon specific CD19 antigen stimulation in an E:T ratio of 1:10. We performed the assay with CFSE labeled $CD4^+$ and $CD8^+$ CAR T cells stimulated with irradiated LCL or Raji cells for 72h followed by flow cytometry analysis. We observed that both wt CAR T cells (FMC63 and 4G7) proliferated more compared to the mutants in both $CD4^+$ and $CD8^+$ CAR T cells. It seems that the mutant 108 proliferates even a bit more than mutant 35, which is surprising regarding the affinity data (Fig.24A). Calculation of the proliferative index (all cell

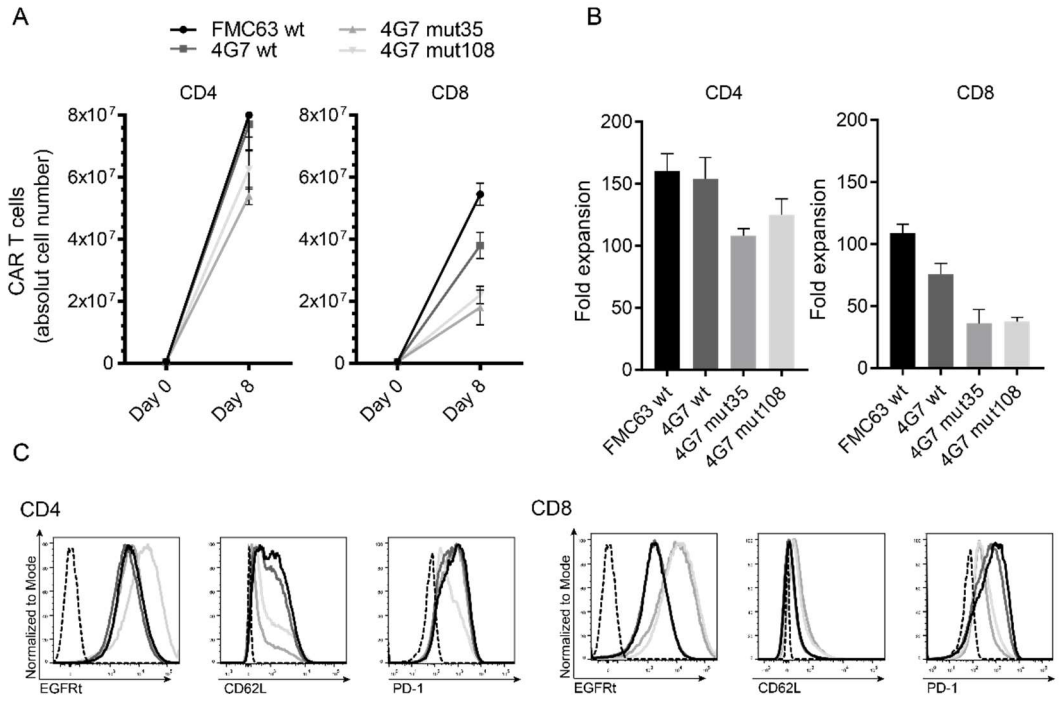


**Figure 24: Expansion and phenotype of newly generated CAR T cells.** (A) Absolute numbers of expanded CD4 (left) and CD8 (right) CAR T cells on day 0 and day 8 are shown. Fold expansion was calculated based on initial cell numbers of CD4 (left) and CD8 (right) cells are presented (B). Observed phenotype staining in histograms for EGFRt (left), CD62L (middle) and PD-1 (right) are displayed in (C). Left panel demonstrating CD4, right panel $CD8^+$ CAR T cells. Two independent experiments were performed.

divisions/experiments) showed that both FMC63 and 4G7 completed equal amounts of cell divisions whereas the mutants divided less frequently. Another interesting finding was that the mutants proliferated slightly better when antigen-specific cells expressed more target antigen on

the cell surface (Fig. 24A and B). The affinity reduced mutants might need more target antigen on the cell surface for getting activated.

After the CFSE proliferation assay, we performed two different killing assays. We first performed an xCELLigence killing assay which is based on measuring the impedance of the adherent target cell line (see Figure 8). We first generated a $CD19^+$ HEK293 adherent cell line expressing the CD19 surface antigen. After seeding the $CD19^+$ HEK293 cell line, we added effector $CD8^+$ CAR T cells in different E:T ratios ranging from 5:1 to 1,25:1. The advantage of the xCELLigence is the use of low and more physiological E:T ratios, the sensitivity and the long incubation time during which the killing capacity can be monitored in real-time. Using the ratio of 5:1, WT FMC63 and 4G7 eliminated the target cell line better and faster compared to the mutant 35 and 108. Nonetheless, the mutants are able to eliminate target cells, with mutant 35 being slightly better than mutant 108 after 20h (Fig. 24D). The second killing assay was performed in a short-term Europium cytotoxic assay. Target cells were labeled with the BATDA fluorescence enhancing ligand, co-incubated with effector CAR T cells for 5h and the BATDA ligand signal in supernatant used to quantify target cell lysis. The WT CAR T cells (FMC63 and 4G7) showed an effective killing in all E:T ratios ranging from 30:1 to 3:1 whereas, according to xCELLigence assay, the mutants showed a lower killing capacity. Overall, these data confirmed that all constructs are able to kill $CD19^+$ target cells and that FMC63 and 4G7 WT had a higher killing capacity compared to the mutant 35 and 108.

To complete functional *in vitro* testing of the generated CAR constructs, we performed a flow cytometry-based intracellular cytokine staining (ICCS) and a cytokine-specific ELISA upon stimulation of $CD19^+$ target cells. For the ICCS assay, we co-cultured CAR T cells with Raji cells in E:T ratios from 5:1 to 1:1.2 for 4h. After co-culture, we analyzed the CAR T cells by staining them for the effector cytokines IFN$\gamma$, IL-2 and TNF$\alpha$ (Fig. 25A). We observe similar patterns gathered from prior experiments. Again, the WT CARs produced most cytokines, although 4G7 WT produced less IL-2 and TNF$\alpha$ compared to the FMC63. Still, the 4G7 WT produced more cytokines compared to the mutants, which show lower cytokine production for all three cytokines, though always clearly above the untransduced control indicating a real and specific cytokine production (Fig. 25B). These results were validated and completed with a cytokine-specific ELISA. For the ELISA $CD4^+$ or $CD8^+$ CAR T cells were incubated with irradiated Raji cells in an E:T ratio of 1:5 for

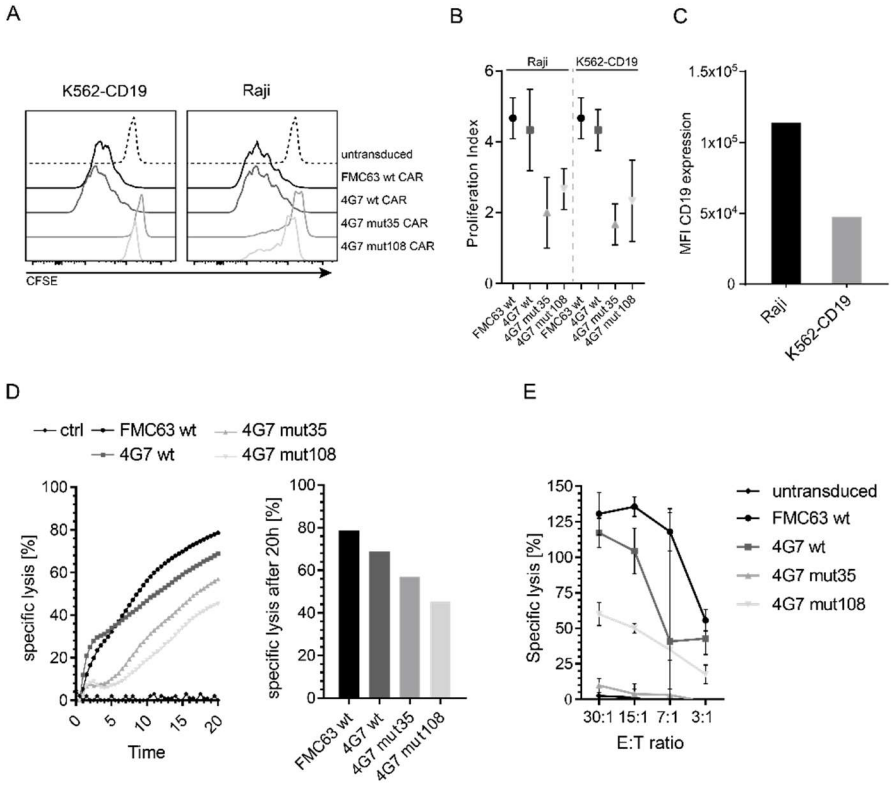


**Figure 25: In vitro proliferation and cytotoxicity of CAR constructs.** (A) Representative CFSE dilution plots showing the proliferation using Raji (left) and K562-CD19 (right) cells for stimulation are used. Untransduced cells are used as a control. CAR constructs are indicated on the right. Proliferation Index was calculated in (B) by dividing all cell division by the number of experiments for Raji and K562-CD19 cells. MFI of target cells (Raji and K562-CD19) was measured with flow cytometry (C). XCELLigence cytotoxicity assay was performed and impedance was monitored over time for 20h. Specific Lysis was calculated with described formula. Specific lysis after 20h is shown in the right graph. Representative data are shown. (E) Europium cytotoxicity assay is displayed. Target cells are labelled, and specific lysis was calculated using different E:T ratios ranging from 30:1 to 3:1. Means ± SD are plotted.

24h and the secreted cytokines were calculated to background control (fold over control). The FMC63 WT again produced most cytokines especially when $CD8^+$ cells were used. When using $CD4^+$ cells both FMC63 and 4G7 showed similar amounts of cytokines. 4G7 WT produced even more TNF$\alpha$. The mutants secreted less cytokines, with mutant 35 producing more than mutant 108. Both mutants produced more cytokines than the background control validating previous findings.

In summary, these *in vitro* data suggest a reduced affinity of modified CAR T cells with mutant scFvs. The affinity of FMC63 WT is slightly higher than the affinity of 4G7 WT, and the affinity of

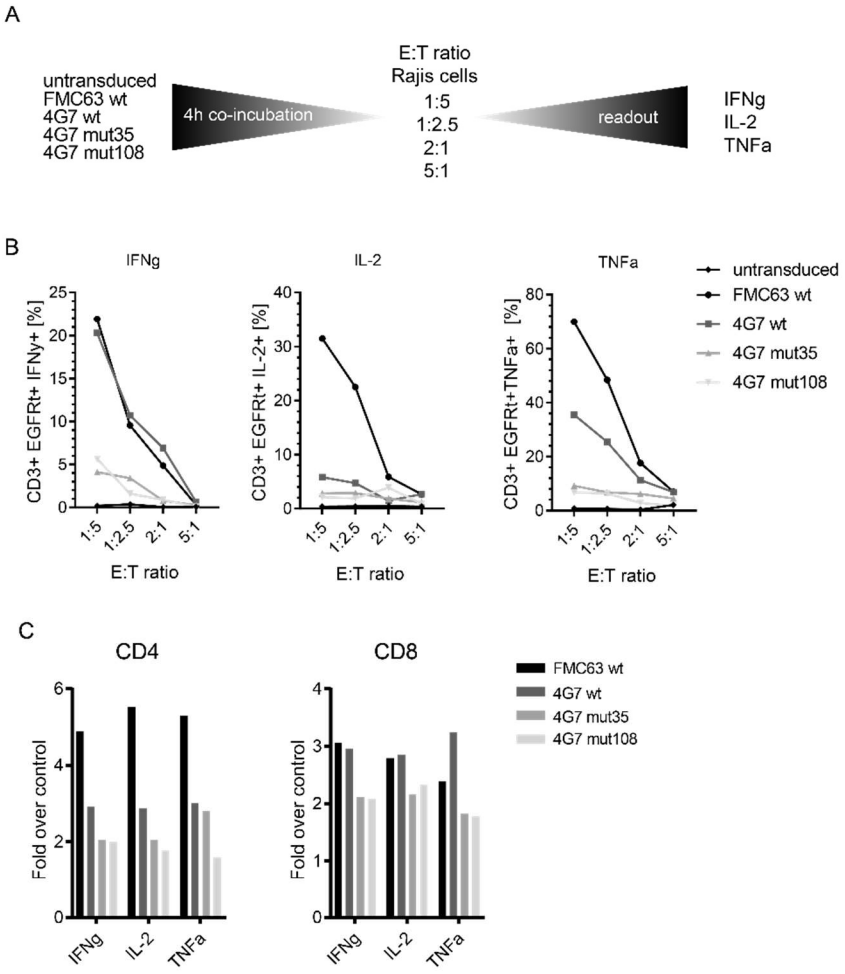


**Figure 26: In vitro cytokine expression and secretion.** (A) Experimental setup illustrated performing the flow cytometry based intracellular cytokine staining (ICCS) assay. (B) Representative ICCS flow stainings of $CD3^+$ positive cells transgenic for the indicated CAR construct are displayed for IFN$\gamma$, IL-2 and TNF$\alpha$. Different E:T ratios were used as indicated. (C) Representative data of secreted cytokines detected via ELISA demonstrated for $CD8^+$ (left) and $CD4^+$ (right) CAR T cells. Concentration of secreted cytokines is shown by fold over control (irrelevant stimuli).

mutant 35 seems to be slightly higher than the affinity of mutant 108, but differences are rather subtle compared to the affinity differences between WT and mutant constructs. Affinity reduced CAR T cells could be a promising tool for clinical application by producing less cytokines despite being able to specifically kill target cells. The killing itself is not as efficient as the wt, but that may actually be an advantageous feature to circumvent adverse toxicities in patients with high tumor burden, circumventing aggressive target cell lysis driving CRS.

### 5.5.1 *In vivo* functionality testing of newly generated affinity modified CAR T cells

To further test these findings, we used a clinically relevant well-established xenograft NSG-Raji mouse model to evaluate the *in vivo* behavior of the generated affinity modified CAR T cells. In Figure 26A the experimental setup is displayed. In brief, NSG mice were used and $5x10^5$ Raji-GFP-ffluc tumor cells were injected on day -6, followed by injection of $1,0x10^6$ (sub-optimal dose) or $2,0x10^6$ (curative dose) of CAR T cells on day 0. CAR T cells in a CD4/CD8 ratio of 1:1 were used to obtain optimal *in vivo* effects as described [85]. Tumors were imaged and blood was collected on indicated time points. Blood samples were stained and analyzed via flow cytometry. Up to day 21 blood serum was collected and analyzed for serum cytokines with a Luminex multiplex assay (Fig. 26A). In this experiment, bulk T cells were transferred and CAR T cell numbers calculated based on the EGFRt expression (Fig. 26B). Previous experiments (not shown in the thesis) showed

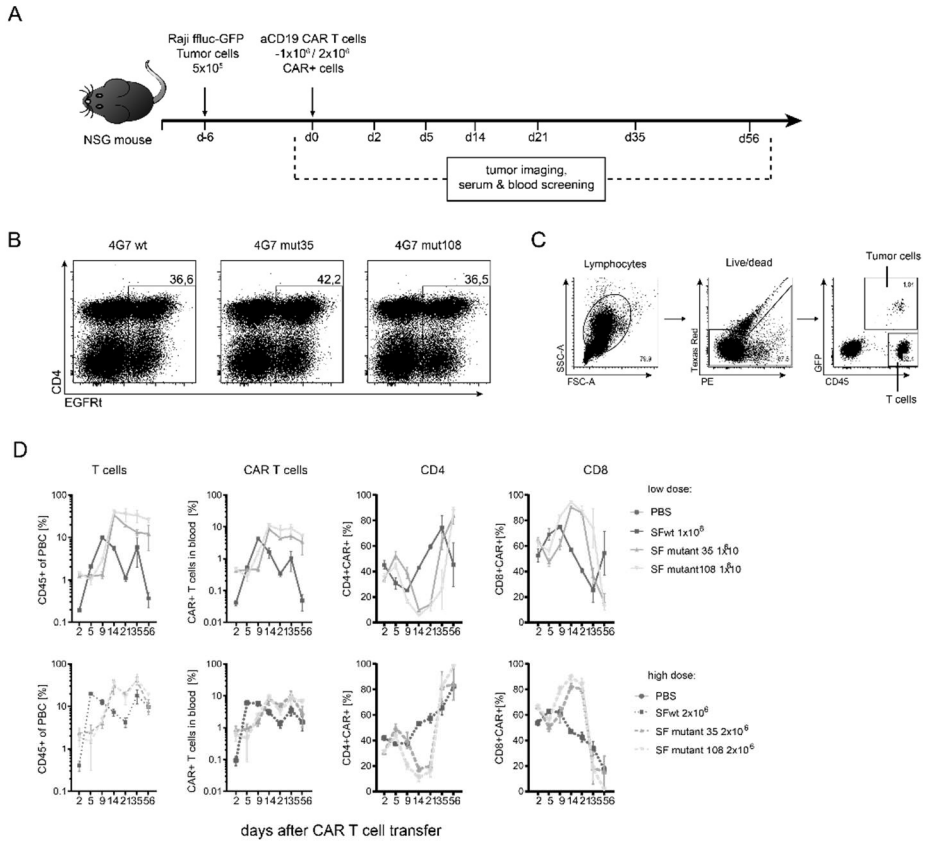


**Figure 27: In vivo functionality of newly generated CAR T cells.** Experimental layout for testing the in vivo functionality of generated CAR constructs in a Raji-NSG mouse model. Human $CD4^+$ and $CD8^+$ T cells were lentivirally transduced with generated CAR constructs. $1.0×10^6$ or $2.0x10^6$ transduced CAR T cells ($EGFRt^+$) were injected ($CD4^+$:$CD8^+$, ratio 1:1). (B) Transduction efficacies are displayed by staining for EGFRt (x-Axis) and CD4 (y-axis). (C) Gating hierarchy is demonstrated for blood screens. (D) T and CAR T cell frequencies in the blood are plotted over time. CAR constructs indicated on the right. n=4 mice per group. Means ± SD are plotted.

that the FMC63 and 4G7 wt had similar antitumor activity *in vivo*. Based on those data, we used CARs consisting of the scFv originating from the clone 4G7 (WT, mutant 35, mutant 108). Gating strategy for flow cytometry analysis of the blood is displayed in Figure 26C to distinguish between tumor cells ($CD45^+$, $GFP^+$) and transferred T cells ($CD45^+$, $GFP^-$). Expansion and persistence of transferred T cells are indicated in Figure 26D. We observed in both WT groups ($1x10^6$, $2x10^6$) a faster expansion and contraction or homing into the tumor residing BM compared to mutant 35 and 108. Both mutants expanded similarly. Additionally, we observed that $CD8^+$ CAR T cells had an earlier peak of expansion compared to the mutants which could indicate a faster tumor recognition and eradication driven by $CD8^+$ cells observed in the blood. Indeed, we tracked a faster tumor clearance and elimination in WT groups by analyzing tumor burden in the blood and tumor radiance (Fig. 27A and C). Very interestingly, the mutants acted delayed. The measured tumor burden in both mutants critically increased until day 9 to be subsequently controlled by the CAR T cells over time. CAR mutant 35 showed a more potent antitumor activity compared to mutant 108. When using the curative dose, all mice which received CAR mutant 35 controlled the tumor over time whereas only 50% of mice which received CAR mutant 108 controlled the tumor in both dosages (Fig. 27C). Surprisingly, the survival curve of mice treated with WT CAR T cells and mutant 35 CAR T cells looked identical. With both, suboptimal and curative dosages, a single mouse died in each group. Nonetheless, mice treated with the mutant 35 CAR still showed detectable tumors until the end of the experiment. The same is true for mice treated with mutant 108 CAR, while here 50% of the mice were actually lost due to high tumor burden (Fig. 27B). Furthermore, we observed intriguing results when analyzing the serum of the mice. As expected, the 4G7 WT CAR T cell treated mice show very high levels of IFN$\gamma$ and TNF$\alpha$, pinpointing high antitumor activity. In contrast, mice treated with 4G7 mutant 35 or mutant 108 CAR T cells, show much lower cytokine levels in the blood serum confirming *in vitro* data shown in Fig.26B (Fig.27D). High frequency of mutant 35 and 108 CAR T cells in the blood over time and little-increased serum cytokine level until day 21 was noticed, albeit being in a low range supposedly not leading to any cytokine-related toxicities.

In summary, generated affinity modified CAR constructs recognized $CD19^+$ Raji tumor cells *in vivo*, expanded and proliferated upon antigen encounter, followed by tumor eradication or tumor

regression. 4G7 WT CAR T cells showed the fastest expansion and very potent antitumor efficacy leading to 5 cured mice out of 8 not showing any remaining tumor. Two mice still showed remaining tumor when treated with the suboptimal dosage. Surprisingly, 7 out of 8 mice treated with the mutant 35 CAR survived until day 50, despite showing a high tumor burden when treated with suboptimal dosage, and still detectable tumors when treated with the curative dosage. CAR mutant 108 could control the tumor over time leading to tumor regression while 50% of the mice were lost, in which tumor burden could not be controlled.

We next wanted to investigate if affinity-modified CAR T cells are truly of lower affinity, or if differential CAR expression levels could also contribute to our findings. After staining for the CAR itself with an anti-STII mAb (Seattle) we recognized an equimolar expression of the EGFRt and the CAR on the cell surface only when WT FMC63 or 4G7 were stained. The mutants 35 and 108

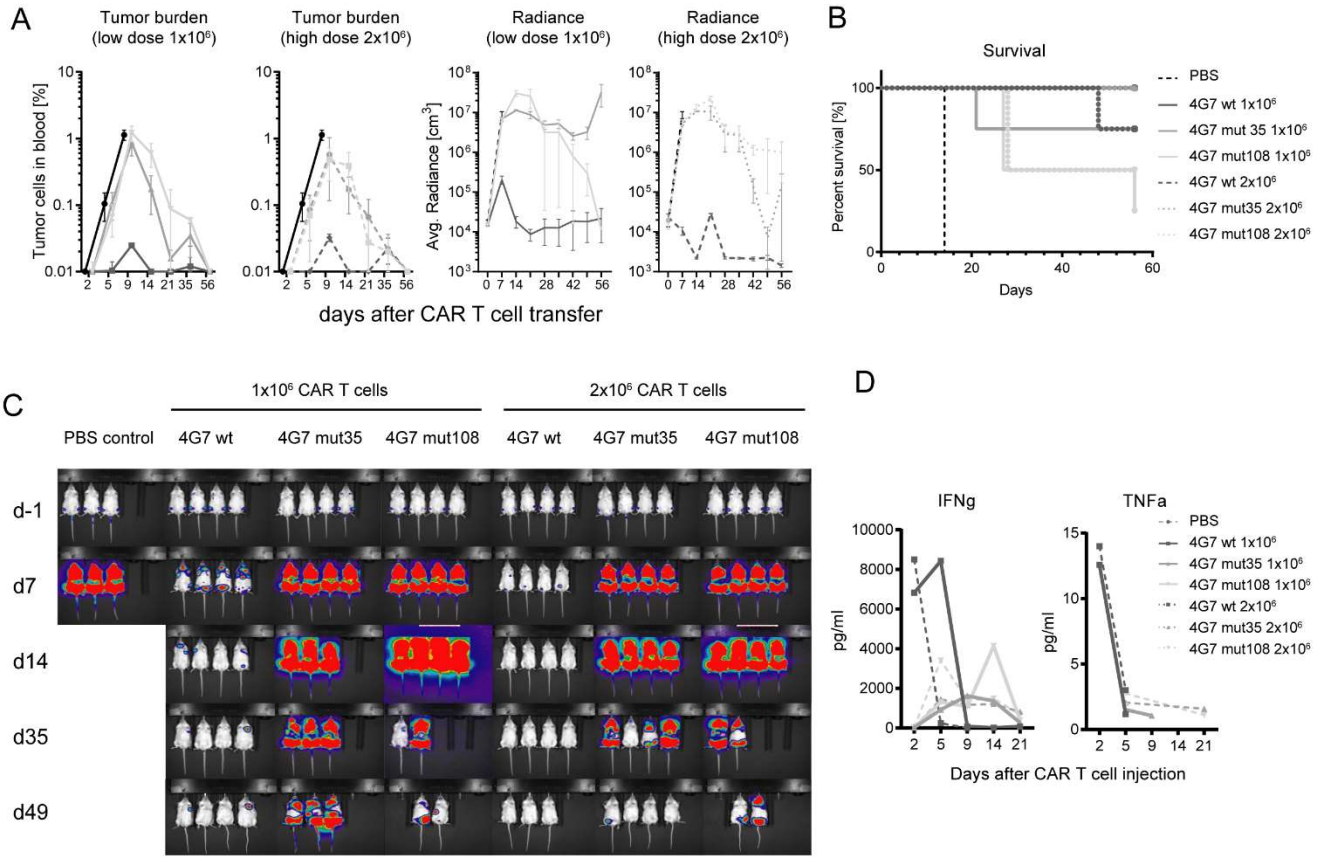


**Figure 28: In vivo functionality of newly generated CAR T cells.** (A) Tumor cells circulating in blood of mouse groups are shown over the period in the two left graphs. Average tumor radiation (cm³) after tumor resulting from tumor imaging are presented in the right graph. (B) Survival analysis over the period is displayed for all mouse groups. (C) Tumor pictures recorded chronological with IVIS (PerkinElmer) and analyzed with Living Image software (PerkinElmer). (D) Serum cytokine levels measured via Luminex multiplex assay at indicated time points after CAR T cell transfer. n=4 individual mice for each experimental group. N=4 mice per group. Means ± SD are plotted.

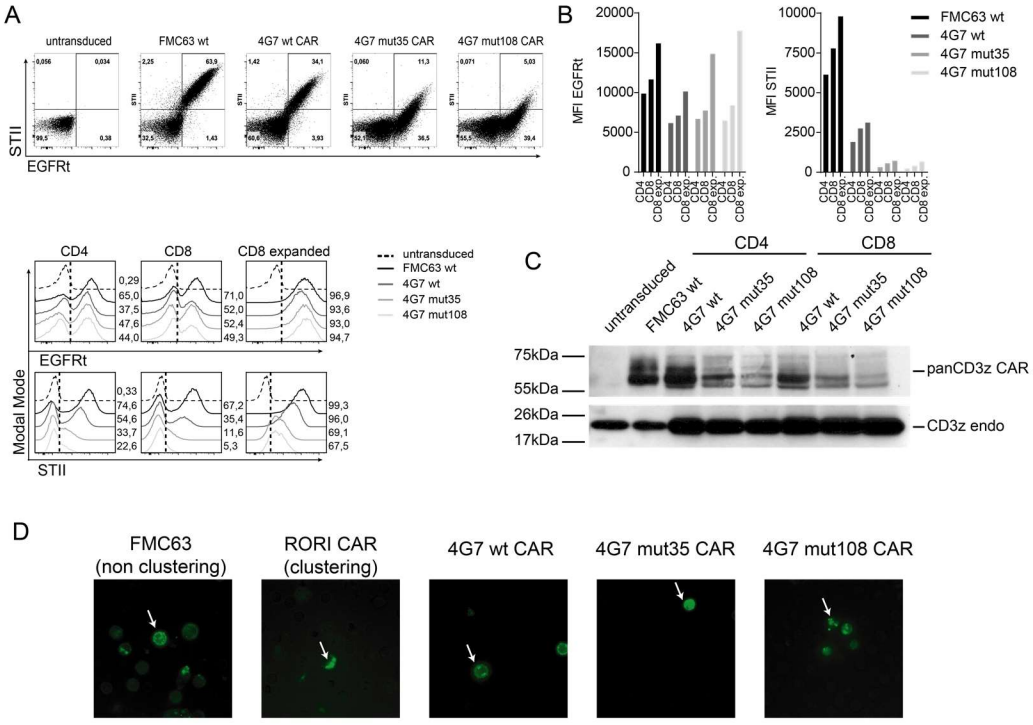


**Figure 29: Impaired CAR expression on the cell surface.** (A) Flow cytometry staining of both EGFRt and StrepTag (STII) are displayed. Cells were pregated on single, living lymphocytes (top panel). Additional histograms for CD4$^+$, CD8$^+$ and LCL expanded CD8$^+$ cells specific for EGFRt (upper) and STII (lower) is shown. (B) Overall MFI of EGFRt and STII expression are illustrated. CD3zeta specific SDS-PAGE for CD4$^+$ and CD8$^+$ cells is shown in (C). SDS PAGE using 5x10$^6$ EGFR$^+$ cells are used for detection of endogenous CD3 zeta (CD3z endo), band detected at the size of 18,7kDa. CAR containing CD3 zeta domain is detected at 72kDa. (D) Fluorescence microscopic images of CAR-CD3z-EGFP fusion constructs are illustrated. Described and representative cells are indicated with white arrow.

in contrast showed a similar EGFRt staining and a very low CAR staining (Fig. 28A). We compared non-expanded CD4$^+$ and CD8$^+$ CAR T cells as well as expanded CD8$^+$ CAR T cells and observed similar data. EGFRt expression is similar after all three procedures whereas the STII staining of the mutants is highly impaired. We detected a weaker expression of the 4G7 wt as well but only in the MFI which may be caused by lower numbers of integration sites. The frequency of EGFRt and STII positive cells is comparable with the FMC63 WT CAR (Fig. 28B). Using molecular biology methods, we performed an SDS-PAGE of transduced CAR T cells probing for the endogenous CD3ζ protein and the CD3ζ domain linked to the CAR construct. Similar amounts of CAR T cells were lysed (5x10$^6$ CAR T cells) and protein concentration was adjusted. Untransduced cells were used as a negative control and FMC63 WT was used as positive control. We detected similar amounts of endogenous CD3ζ but less CD3ζ of the CAR in the mutant samples (Fig. 28C). Explanations for that could be that the CAR is clustering or misfolded on the cell surface. Another explanation might be ubiquitinoylation or glycosylation of the mutant CARs intracellularly leading to denaturation. To exclude that the mutant CARs cluster on the cell surface we generated CAR-

GFP fusion constructs by fusing EGFP covalently to the CD3ζ domain of the CAR. This technique has been used to identify CAR clustering [193]. After transduction, constructs were analyzed via a fluorescence microscope. As a positive control, we used the non-clustering FMC63 CAR. As a negative control, we used a CAR which is described to cluster on the cell surface (RORI-specific CAR, provided by A. Salter, Riddell lab). Representative microscopic pictures in Figure 28D show that the 4G7 WT CAR and the CAR mutant 35 did not cluster, whereas the CAR mutant 108 clustered slightly on the cell surface. The clustering was not as strong as for the RORI-specific CAR. Taken together, these data cannot satisfyingly explain the low CAR expression on the cell surface. Due to the fact that the mutants are not being equimolarly expressed on the cell surface, we cannot conclude that the *in vitro* and *in vivo* findings are based on a merely reduced affinity. Other issues might play a confounding role such as glycosylation of misfolding of mutant CARs. More experiments must be performed to address this question in more detail. Mutated CARs might be still clinically relevant due to low cytokine secretion upon antigen encounter and delayed tumor eradication which can be used for combinatorial therapies.

## 5.6 Superior engraftment and persistence using polymer conjugated IL-15 (NEKTAR)

For further improvement of CAR T cell therapy, optimal engraftment and persistence of CAR T cells after antigen encounter is highly desired as these features been shown to directly correlate with patients' outcome [79] . A very promising strategy is to use the cytokine IL-15 for promoting the CAR T cells *in vivo*. IL-15 was identified by the NCI as one of the most promising immune-oncology agents due to its biological activity and index. IL-15 is a common γ-chain cytokine that activates and provides survival benefit for memory T and NK cells, and plays a key role in the formation and maintenance of immunological memory. The IL-15 receptor is a heterotrimeric receptor consisting of the IL-15 receptor α subunit and IL-2/IL-15 receptor β, γ subunits. Exploiting the therapeutic value of native IL-15 has been challenging due to its unfavorable pharmacokinetic properties. Especially the serum half-life of natural IL-15 in humans averages about 2 h, which is very unsuitable for clinical application.

There is an urgent need to improve the pharmaco-kinetic (PK) and the pharmaco-dynamic (PD) to sustain IL-15 activity to achieve a larger PD effect without the need for hourly or daily dosing. Binding to the IL15Ra must be maintained for having all advantages and the full spectrum of the IL-15 biology without alterations or solubility problems of the IL-15Rα which has been described to result in major drawbacks [194]. Taking all these criteria into consideration, NKTR-255 was developed by NEKTAR pharmaceuticals. NKTR-255 is a polymer-conjugated human IL-15 that retains binding affinity to the α subunit of the IL-15 receptor and exhibits reduced clearance to provide sustained pharmacodynamics (PK and PD). It could be shown that the half-life of NKTR-255 is highly improved compared to the native IL-15 in mice and non-human primates (NHP). Native IL-15 shows a half-life of 2-4 h in NHP whereas NKTR-255 increases the half-life up to 30 h when using a high dosage (unpublished data, NEKTAR therapeutics; Fig. 29A). NKTR-255 is therefore the first potential medicine to access the IL-15 pathway by preserving receptor binding to IL-15Rα with antibody-like dosing. In this thesis, we investigated the biological effect of NKTR-255 on CAR T cells in respect to the persistence and antitumor effect in tumor-bearing NSG mice.

### 5.6.1 **Stimulation of CAR T cells with NKTR-255**

First, we investigated the activity and stimulation capacity of NKTR-255 on CAR T cells. We stimulated clinically relevant CD19 CAR T cells (scFv clone FMC63, CAR construct without STII in the hinge, performed in Seattle, FHCRC) using different concentrations of native IL-15 or NKTR-255. It was already known that native IL-15 is about 5,5x more potent than NKTR-255 which has been tested with human PBMCs ($CD4^+$ and $CD8^+$ cells). For that reason, we adjusted the concentrations for stimulation (suggested by NEKTAR therapeutics). We transduced and expanded purified CD19 CAR T cells prior to the assay and froze them. For the stimulation, we thawed CD19 CAR T cells and rested them for 2 h on starving media followed by stimulation for 10min with different concentrations of either native IL-15 or NKTR-255. After stimulation, we fixed the cells with 4% formaldehyde and performed methanol-based intracellular staining for pSTAT5 overnight. The percentage of pSTAT5 positive cells are shown for each condition in Figure 29B. A dose-dependent stimulation is observed for both $CD4^+$ and $CD8^+$ positive CAR T cells. To compare the observed data with previous experiments performed by NEKTAR we calculated the EC50 value. As a reference, we use data where conventional $CD8^+$ cells have been stimulated with native IL-15 or NKTR-255. The gathered EC50 values are comparable between $CD8^+$ CD19 CAR T

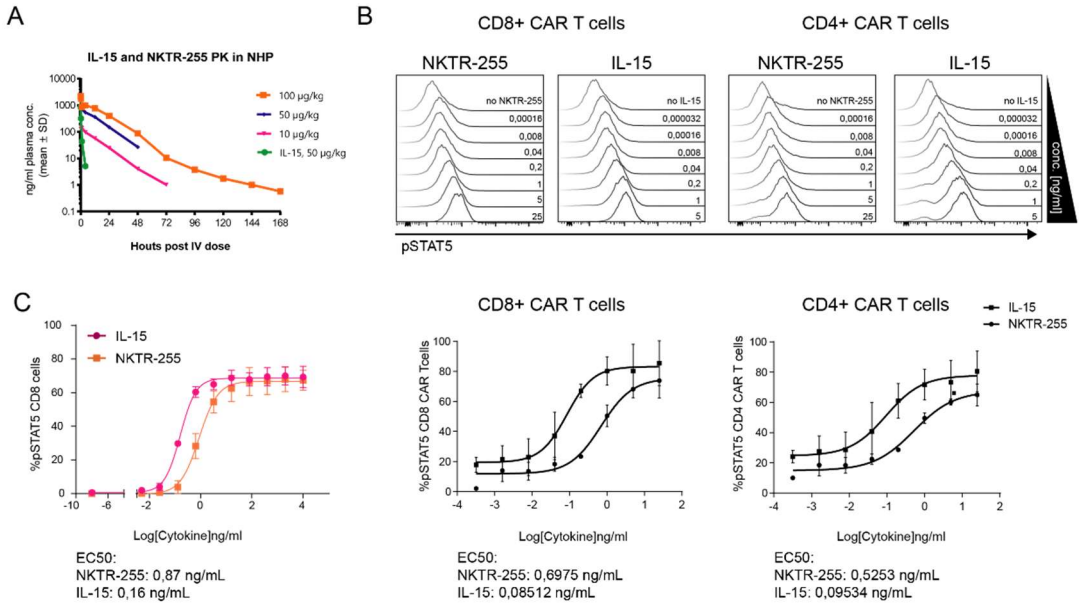


**Figure 30: Stimulation of CAR T cells with native IL-15 and NKTR-255.** (A) Plasma concentration of native IL-15 and NKTR-255 indicated in hours post i.v. dosing. (B) Stimulation of $CD4^+$ and $CD8^+$ CAR T cells with either native IL-15 or NKTR-255 analyzed by the percentage of %STAT5 expression. Concentrations indicated in the stainings. (C) EC50 values calculated after normalizing the data gathered from stainings specific for STAT5. EC50 value for $CD8^+$ cells (left) stimulated with native IL-15 or NKTR-255. EC50 values for $CD4^+$ (middle) and CD8 (right) CAR T cells shown in the right panel. n=3 independent experiments. Means ± SD are plotted.

cells and CD8⁺ cells from the blood. The same is true for CD4⁺ cells (Fig. 29C). In the performed experiments we needed 8,1x and 5,7x more NKTR-255 for CD8⁺ and CD4⁺ CD19 CAR T cells compared to native IL-15. This shows that native IL-15 is more potent compared to NKTR-255, but NKTR-255 can fully stimulate CD4⁺ and CD8⁺ CD19 CAR T cells *in vitro*.

### 5.6.2 *In vitro* functionality testing of clinically relevant CD19 CAR T cells

Before testing the effect of NKTR-255 in an *in vivo* Raji NSG tumor model (experimental setup similar to Fig. 26A), we functionally tested and characterized clinically relevant CD19 CAR T cells *in vitro* for validating functionality. This CD19 CAR construct differed from previous constructs not exhibiting a STII in the sequence. We performed lentiviral transduction and subsequently sorted and expanded the CD19 CAR T cells. Transduction and purity of expanded cells are shown in Figure 30A, by staining for EGFRt. Characterization of CAR T cells was done by staining for transgene expression (EGFRt) and staining of activation markers like CD25 and PD-1. Both CD4⁺ and CD8⁺ CAR T cells showed a similar phenotype and state of activation by being positive for CD25, PD-1 positive as well as the transgene (Fig. 30B). Prior to injection into the mice we

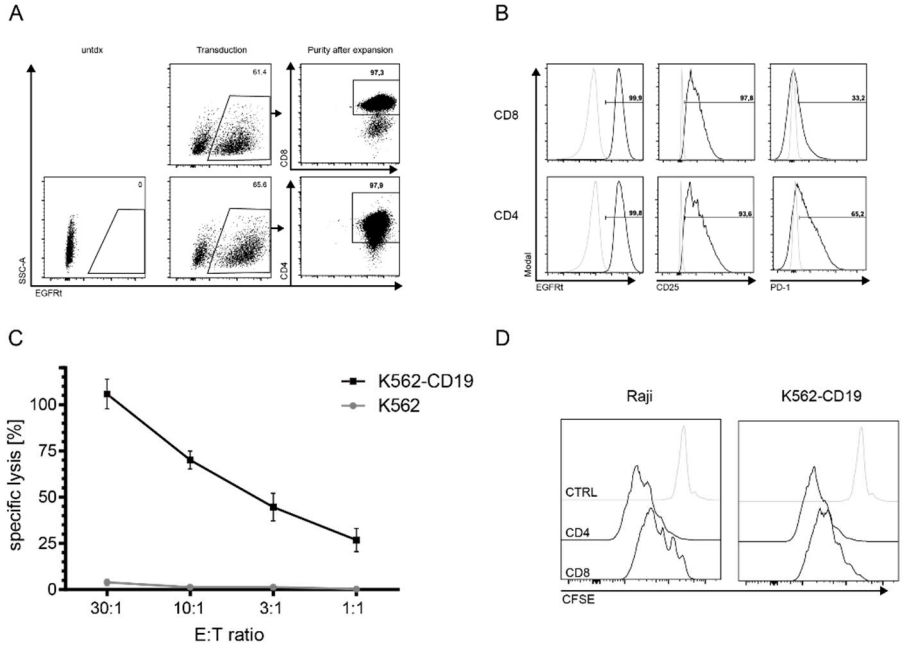


**Figure 31: Functionality of clinically relevant CD19 CAR T cells.** (A) Generated CAR T cells are shown after transduction (middle panel) and after sorting and expansion (right panel) stained for the transduction marker EGFRt. Untransduced cells serve as a control (left). (B) Highly pure CAR T cells are stained for transgene expression (EGFRt), activation markers CD25 (middle) and PD-1 (right). Both CD4⁺ and CD8⁺ CAR T cells show similar expression patterns. (C) Chromium release assay using K562-CD19 target cells or K562 control cells in different E:T ratios ranging from 30:1 to 1:1. (D) CFSE proliferation assay using Raji (left) or K562-CD19 (right) target cells. Untransduced cells serve as a control and CD4⁺ and CD8⁺ CAR T cells are used as effector cells. Means of technical quadruplicates ± SD are plotted (C).

performed a cytotoxic chromium release assay to determine the specific lysis of target cells. For this assay, we used K562-CD19$^+$ cells as targets and K562 as control cells. Different E:T ratios were tested ranging from 30:1 to 1:1. We observed a dose-dependent killing capacity of the generated CAR T cells against the target cells, but not against control cells (Fig. 30C). Additionally, we performed a CFSE proliferation assay. In this assay, we stimulated the CAR T cells with K562-CD19$^+$ cells or as a control with K562 cells. CD4$^+$ and CD8$^+$ CAR T cells proliferated only when incubated with K562-CD19 target cells and did not when incubated with K562 control cells (Fig. 30D). These results showed that the CD19 CAR T cells are functional and can be used for further *in vivo* testing.

### 5.6.3 *In vivo* effect of NKTR-255 on CD19 CAR T cells in a clinically relevant mouse model

In the first *in vivo* study, we used the same Raji NSG tumor model we used in previous experiments (Fig.31A). First, we injected on day -6 5x10$^5$ Raji-GFP-ffLuc cells into the mice and injected NKTR-255 cytokines in different concentrations one day prior to CAR T cells (day -1), and every seven days from then on (0.3, 0.1 and 0.03 mg/kg). On day 0 we injected 0,8x10$^6$ CAR T cells in a CD4:CD8 ratio of 1:1. This is a suboptimal CAR T cell dose for which it is shown that the CAR T cells reduce the tumor in the early phase but cannot completely clear the tumor later leading to tumor relapse after about 3 weeks. However, there might be some variables which can affect the outcome due to different donor T cell quality. We monitored the mice performing weekly tumor scans and blood draws analyzed with flow cytometry. Additionally, we took and analyzed blood serum samples on day 0, 3 and 6 to monitor serum cytokine levels (GM-CSF, IFN$\gamma$, and TNF$\alpha$) hinting to any kind of toxicities such as CRS. Detected CAR T cell frequencies in the blood showed an NKTR-255 dose-dependent order. In the group that received the highest dosage of NKTR-255 (0.3 mg/kg) we observed the highest frequency of transferred CAR T cells pregated on lymphocytes and stained for GFP negativity and CD45 positivity. The medium dose (0.1 mg/kg) ranged a little below and the low dose (0.03 mg/kg) showed clearly lower CAR T cell frequencies in the blood, nevertheless being higher compared to the control group (CAR T cell only) over time. Comparing CD4$^+$ and CD8$^+$ CAR T cells in more detail we noticed that especially CD8$^+$ CAR T cells are stimulated by NKTR-255 compared to the control. Over the period of time, a large CD8$^+$ CAR T cells population was detected in the blood (Fig. 31B). The tumor burden in the blood of the

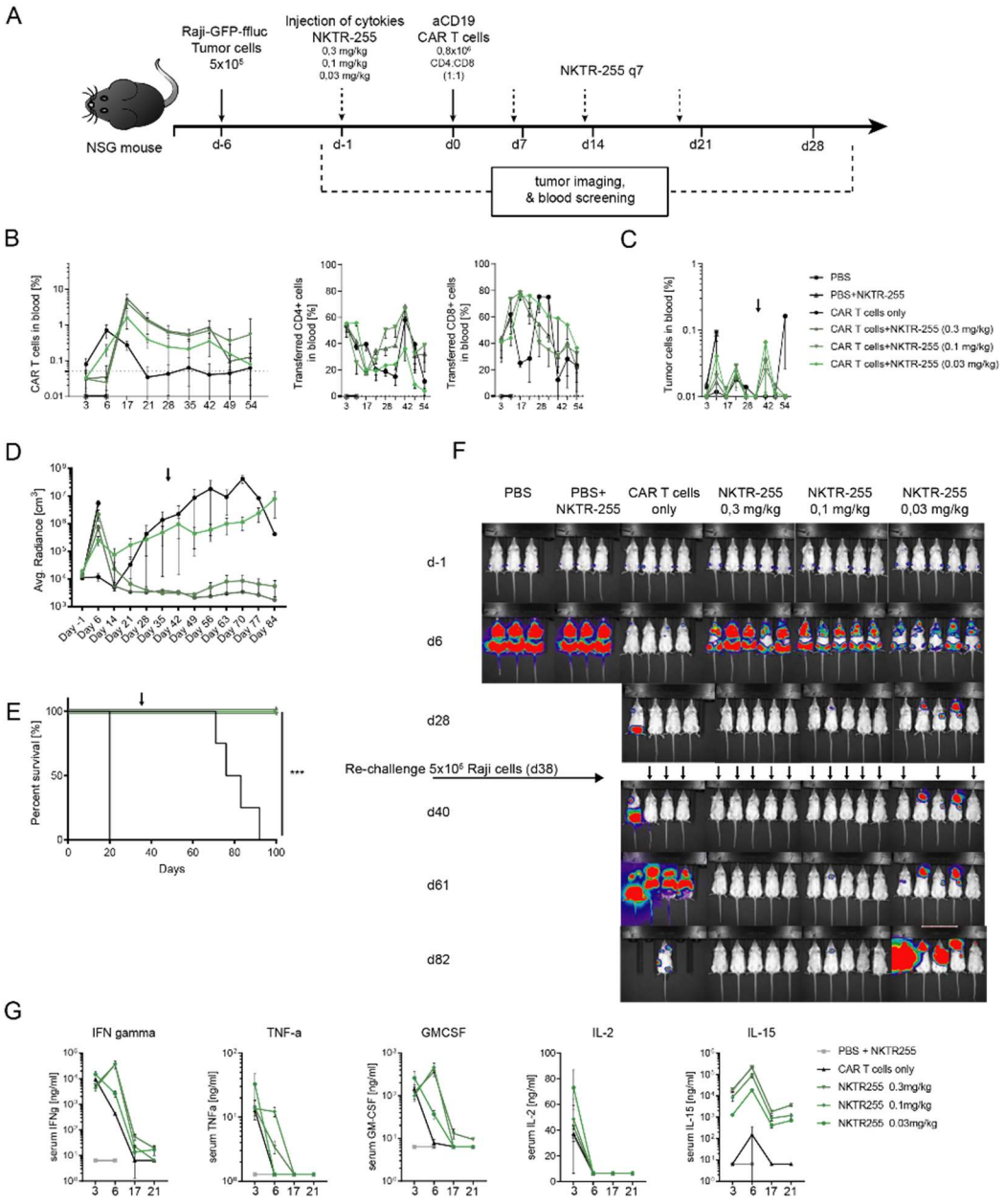


**Figure 32: NKTR-255 supports CAR T cells in vivo.** (A) Experimental layout for testing NKTR-255 in-vivo. (B) Frequencies of transferred CAR T cells (left) and $CD4^+$ (middle) and $CD8^+$ (right) CAR T cells displayed over time. CAR T cells pregated on living $CD45^+$ lymphocytes and GFP negativity. (C) $CD45^+$ $GFP^+$ tumor cells monitored in the blood are shown. (D) Average radiance of measured tumor via luminescence (IVIS, PerkinElmer) is illustrated over time. (E) Survival analysis (percent survival) of different mouse groups over time is shown. (F) Normalized tumor images for representative time points are displayed and separated in different groups. Re-challenge with $5x10^5$ Raji-GFP-ffluc tumor cells is indicated (long arrow). All tumor free mice received a re-challenge are marked by a bold arrow. Mice showing tumor did not receive a re-challenge. Statistical analysis: Log-rank Mantel-Cox test; *** $P \leq 0.0002$, n=5 mice per group. Means ± SD are plotted.

control groups treated with PBS and PBS+NKTR-255 increased fast and mice died after 21 days, as expected in this model. All other groups treated with CAR T cells revealed a decrease in tumor cells in the blood. After controlling the tumor in all mouse groups, we decided to re-challenge all tumor-free mice with an additional dose of $5x10^5$ Raji-GFP-ffluc tumor cells. After re-challenge of tumor-bearing mice on day 35, we recognized an increased frequency of tumor cells in the blood which is expected (day 45). Only NKTR-255 treated groups could clear the tumor a second time

whereas the control group relapsed, and mice were sacrificed (Fig. 31C). Analyzing and quantifying the average radiance per $cm^3$ we could observe similar results. Surprisingly, tumor radiance was initially (d 6) higher when NKTR-255 was additionally applied compared to control group (CAR T cells only). After an initial drop, control and low dose NKTR-255 group showed high tumor burdens compared to groups treated with medium or high dose NKTR-255 not showing any radiance. Over time high dose NKTR-255 was accompanied with slightly higher T cell frequencies and lower tumor burden in the blood compared to the low dose. Investigating survival, we see a highly significant survival benefit of NKTR-255 treated and control mice. NKTR-255 clearly enhances CAR T cell persistence and promotes the antitumor effect without any sign of toxicity (Fig. 31E). Representative tumor pictures are chronologically displayed in Figure 31F. Especially the high dose of NKTR-255 showed a complete and impressive tumor clearance even after re-challenge. Interestingly, when we tested serum cytokines in the blood within the first 21 days, we observed similar cytokine levels on day 3, however they decreased the subsequent days in the control group (CAR T cells only) and increased in the NKTR-255 treated groups. Especially, when injected a high or middle dose of NKTR-255 serum cytokines peaked on day 6, three days later compared to control group. Low dose NKTR-255 behaved similar to control group. We assume, that the cytokine peak of the control group occurred earlier and the NKTR-255 treated mice have their peak delayed which is in line with the delayed antitumor effect in the beginning. Serum cytokines IL-2 and IL-15 served as controls (Fig. 31G).

Recognizing that NKTR-255 is promoting especially $CD8^+$ CAR T cells, we next performed a similar experiment using only $CD8^+$ CAR T cells. The experimental setup was otherwise the same as before. We analyzed CAR T cells in the blood and observed similar behavior as in the previous experiment. All NKTR-255 treated groups exhibited increased CAR T cell frequencies in blood compared to the control group. The frequencies again correlated with the NKTR-255 dosage. No tumor cells in blood were detected in NKTR-255 treated groups whereas the control group showed a fast and lethal outgrowth of tumor cells detectable in the blood (Fig. 32B). After re-challenge on day 70, low frequencies of tumor cells were detected in groups treated with medium and low dose of NKTR-255 in the blood. Both groups subsequently cleared the tumor cells in the blood (Fig. 32B). We noticed the same finding when analyzing the tumor radiance per

$cm^3$. All NKTR-255 treated groups showed detectable radiance (Fig. 32C). Survival analysis illustrates significant survival benefit when combining NKTR-255 with clinically relevant CD19 CAR T cells even when using only $CD8^+$ CAR T cell (Fig.32D). Tumor images are displayed in Figure 33E emphasizing rapid death of control groups and longevity of groups when treated with NKTR-255. Only at the last time point little radiance was seen in two mice treated with a low dosage.

In summary, both experiments showed the clinical potential of NKTR-255 improving CAR T cell expansion, persistence, and efficacy in a clinically relevant mouse model. Mice treated with NKTR-255 showed significantly better survival compared to control groups. However, initial NKTR-255 injection reduced the antitumor efficacy within the first 7 days compared to control group in all experiments. We hypothesize that exhaustion or proliferation-linked apoptosis as it has been described in NHP might be the mechanism [195]. To investigate this initial drawback, we performed a further experiment injecting the NKTR-255 one week later (d 7) after CAR T cell transfer.

Apart from the omitted first dose of NKTR-255, the experimental setup was the same as before (Fig. 33A). T cell frequencies of CAR T cells in the blood were similar between groups on day 7, but after injection of NKTR-255 the overall frequency of CAR T cells increased in a dose-dependent manner. The frequency of $CD4^+$ T cells was likewise increased in the blood whereas the $CD8^+$ frequency was a bit lower in the blood until day 21 compared to control (Fig. 33B). At this time point, the $CD8^+$ cells might have migrated more into organs like BM where most tumor cells are expected. After day 21, the $CD8^+$ CAR T cells were increased in peripheral blood and

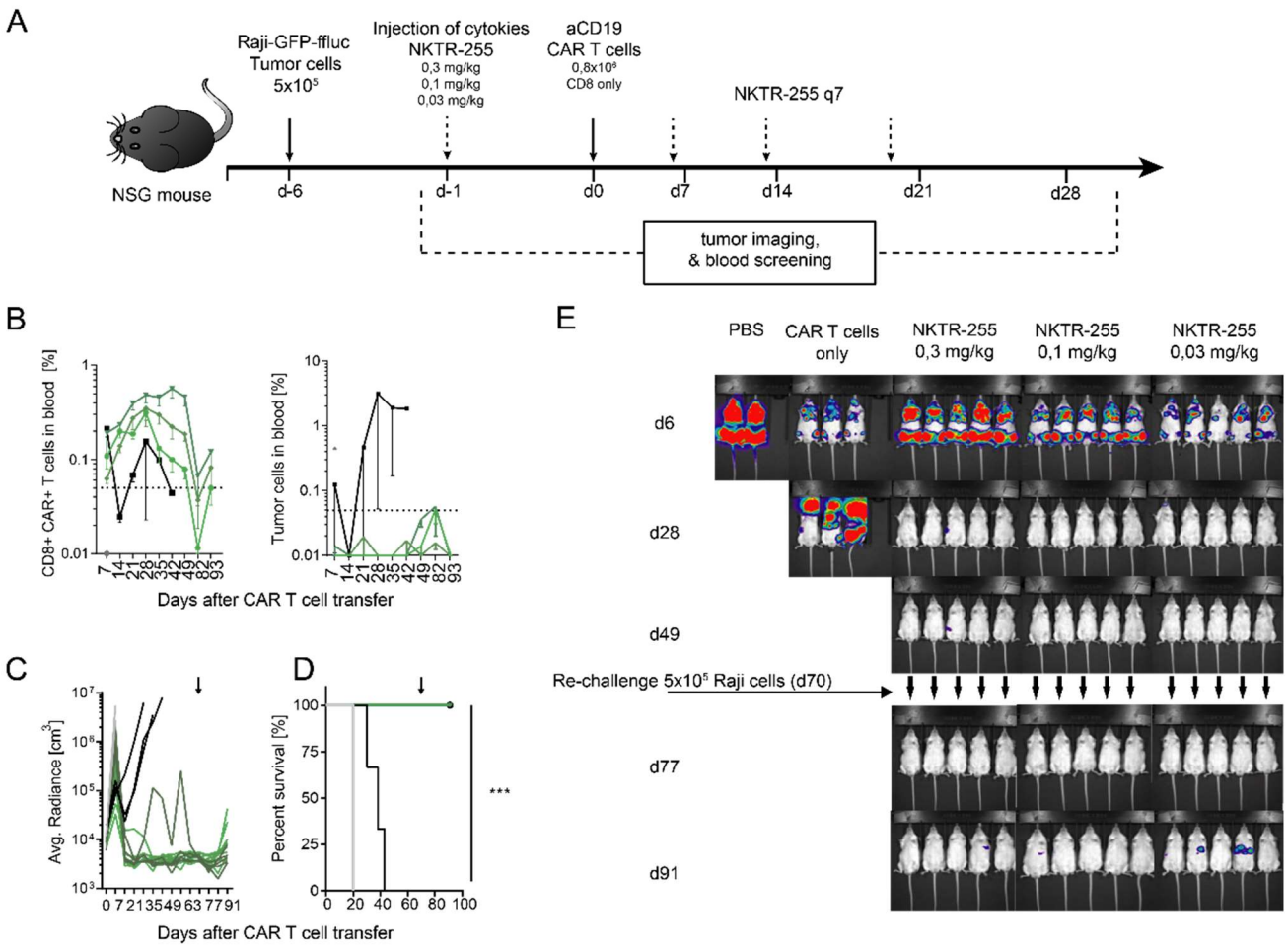


**Figure 33: NKTR-255 supports CD8⁺ CAR T cells in vivo.** (A) Experimental layout for evaluation NKTR-255 in-vivo. (B) Frequencies of transferred CD8⁺ CAR T cells displayed over time (left) and tumor cells detected via flow cytometry in the blood (right). CAR T cells pregated on living CD45⁺ lymphocytes and GFP negativity, tumor cells gated on CD45⁺ and GFP positivity. (C) Average radiance (cm³) measured via luminescence (IVIS, PerkinElmer) for each mouse illustrated over time. (D) Survival analysis (percent survival) of different mouse groups over time is shown. (F) Normalized tumor images for representative time points are displayed and separated in different groups. Re-challenge with 5x10⁵ Raji-GFP-ffluc tumor cells on day70 is indicated (long arrow). Tumor free mice received re-challenge are marked with short arrow. Statistical survival analysis done with Log-rank Mantel-Cox test; *** P ≤ 0.0002, n=5 mice per group. Means ± SD are plotted.

showed a better persistence compared to the control. Tumor cells in the blood could not be detected until day 21. On day 28, an increased tumor burden in the blood was observed in the control group, but not in the NKTR-255 treated groups. Similar findings were observed when measuring the tumor burden via luminescence. Starting on day 28, tumor radiance increased dramatically in control groups followed by rapid death. NKTR-255 treated groups did not show any increase of tumor radiance until re-challenge on day 90 (Fig. 33C). After late re-challenge on day 90 NKTR-255, treated mice could not eliminate the tumor completely. This resulted in a dose-dependent tumor relapse whereas the low-dose-treated group relapsed first, followed by the medium and high dose of NKTR-255. However, relapse was slowed down, and mice died rarely until day 120, which was the end of the experiment (Fig. 33C). Highly significant survival benefit of mice treated with NKTR-255 can be shown in Survival curves in Figure 34D within the first 90

days. After re-challenge on day 90, mice died slowly in a dose-dependent manner, which indicates a beneficial effect of NKTR-255 on CAR T cells. Tumor pictures measured over time show similar findings. Interestingly, tumor burden on day 7 was similar compared to the control group. We delayed the NKTR-255 injection in this experiment (day 6), and we were able to circumvent

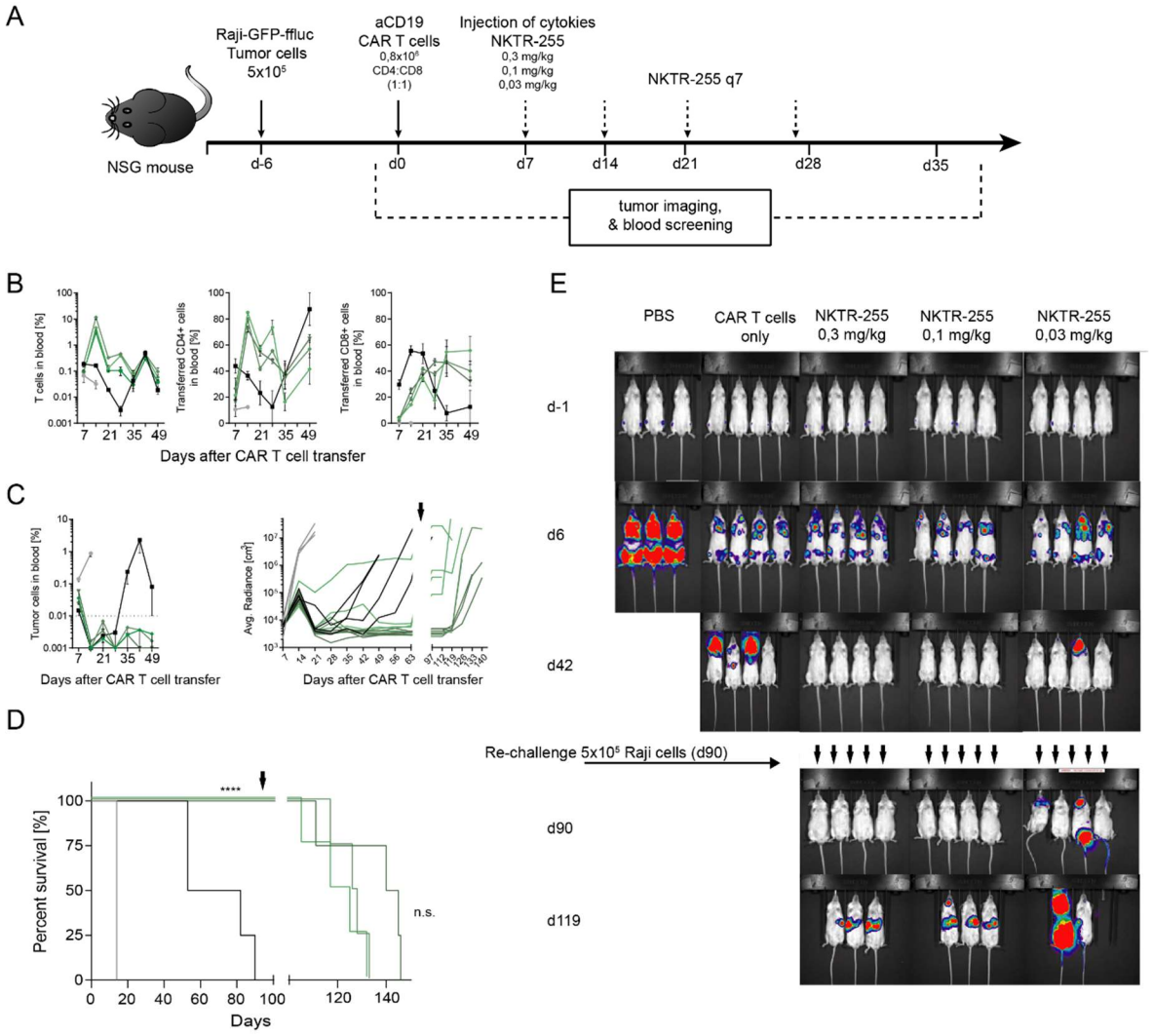


**Figure 34: Optimal time-point for NKTR-255 injection for supporting of CAR T cells.** (A) Experimental layout for evaluation NKTR-255 in-vivo. (B) Frequencies of transferred CAR T cells (left) and $CD4^+$ (middle) and $CD8^+$ (right) CAR T cells displayed over time. CAR T cells pregated on living $CD45^+$ lymphocytes and GFP negativity. (C) Tumor cells detected in the blood via flow cytometry are indicated (left). Tumor cells gated on $CD45^+$ and GFP positivity. Average radiance ($cm^3$) measured via luminescence (IVIS, PerkinElmer) for each mouse illustrated over time. Re-challenge on day 90 is shown by the interruption of the x-axis. (D) Survival analysis (percent survival) of different mouse groups over time is shown. Interruption of the x-axis indicated the re-challenge. (F) Normalized tumor images for representative time points are displayed and separated in different groups. Re-challenge with $5x10^5$ Raji-GFP-ffluc tumor cells on day90 is indicated (long arrow). Mice received tumor re-challenge are marked with short arrow followed over time. Statistical survival analysis done with Log-rank Mantel-Cox test; **** $P \leq <0.0001$, n=4 mice per group. Means ± SD are plotted.

the delayed tumor-activity we observed in experiments when NKTR-255 was injected on day -1 (Fig. 33E).

### 5.6.4 **Investigating on the delayed antitumor effect initially**

We wanted to look further into the disadvantageous effect when injecting NKTR-255 early, 1 day prior to CAR T cell injection, and performed an additional experiment trying to clarify whether the CAR T cells get exhausted or die. We used a similar experimental setting as in initial experiments by injecting Raji-GFP-ffluc tumor cells on day -6, injecting only the high dosage of NKTR-255 (0.3mg/kg) on day -1 and transferring 1,6x$10^6$ $CD4^+$ and $CD8^+$ CAR T cells (ratio 1:1) on day 0. We additionally labeled transferred CAR T cells with CTV giving us insight into the proliferation behavior and used double amounts of CAR T cells being able to detect CAR T cells in the blood and tissues later on. We performed blood draws and performed tumor imaging on day 3 and harvested blood, spleen and BM on day 7 (Fig. 34A). Increased proliferation was observed when analyzing the CTV labeled CAR T cells in the blood on day 3. All NKTR-255 treated mice showed a faster proliferation of CAR T cells compared to control. After segregating the CTV histograms, we observed that more than 51,3% of the NKTR-255 treated CAR T cells and only 13,5% of the control group proliferated. NKTR-255 treated CAR T cells divided up to four times whereas the control CAR T cells only completed two cell divisions (Fig. 34B). On day 7 CTV labeled cells could not be detected anymore as it was diluted. Confirming previous finding we detected a delayed antitumor effect on day 7. Control group showed lower tumor radiance compared to NKTR-255 treated group (Fig. 34C). Tumor cells in the blood were lower as in the control group on day 3, whereas on day 7 NKTR-255 showed a lower frequency of tumor cells in the blood (Fig.35D). After harvesting tissues on day 7 we observed higher frequencies of CAR T cells in the BM when treated with NKTR-255. In blood and spleen, we did not observe any difference. In respect of $CD4^+$ and $CD8^+$ CAR T cells we observed no differences in $CD4^+$ cells, whereas $CD8^+$ cells were slightly increased in all tissues (Fig. 34E). Staining the transferred CAR T cells for exhaustion markers such as PD-1, TIM-3 and Lag-3 in combination gave some insights. We observed higher expression of the mentioned markers in the NKTR-255 treated group. Especially in the BM we detected more ‘exhausted’ or highly ‘activated’ $CD8^+$ CAR T cells when treated with NKTR-255. This might be due to a delayed antitumor effect whereas the control group already cleared the tumor in the BM on day 7 hinted by a lower activation status of PD-1, Lag-3 and Tim-3 (Fig. 34F). Another hypothesis could be that high expressing CAR T cells when treated with NKTR-255 died

off and remaining cells start to proliferate strongly and clear the tumor delayed. Nonetheless, more experiments have to be done to get a clear picture and a detailed mechanism. However, we could overcome the weaker antitumor effect by injecting NKTR-255 one week later leading to an improved and maybe optimal time point for injecting the NKTR-255 in a clinical setting.

In summary, we pinpointed NKTR-255 is a very potent and safe supplement for the improvement of CAR T cell therapy. We demonstrated *in vivo* that the expansion and persistence of both $CD4^+$ and $CD8^+$ CAR T cells are superior compared to the common therapy without NKTR-255. After re-challenge, NKTR-255 had a highly beneficial effect by maintaining the functional CAR T cell population and clearing the tumor which could not be achieved with the common experimental setup. More experiments have to be done, however, NKTR-255 is a very promising engineered T cell stimulating cytokine engaging the IL-15 pathway, inducing long-term CAR T cell activation and persistence for optimal therapeutic outcome.

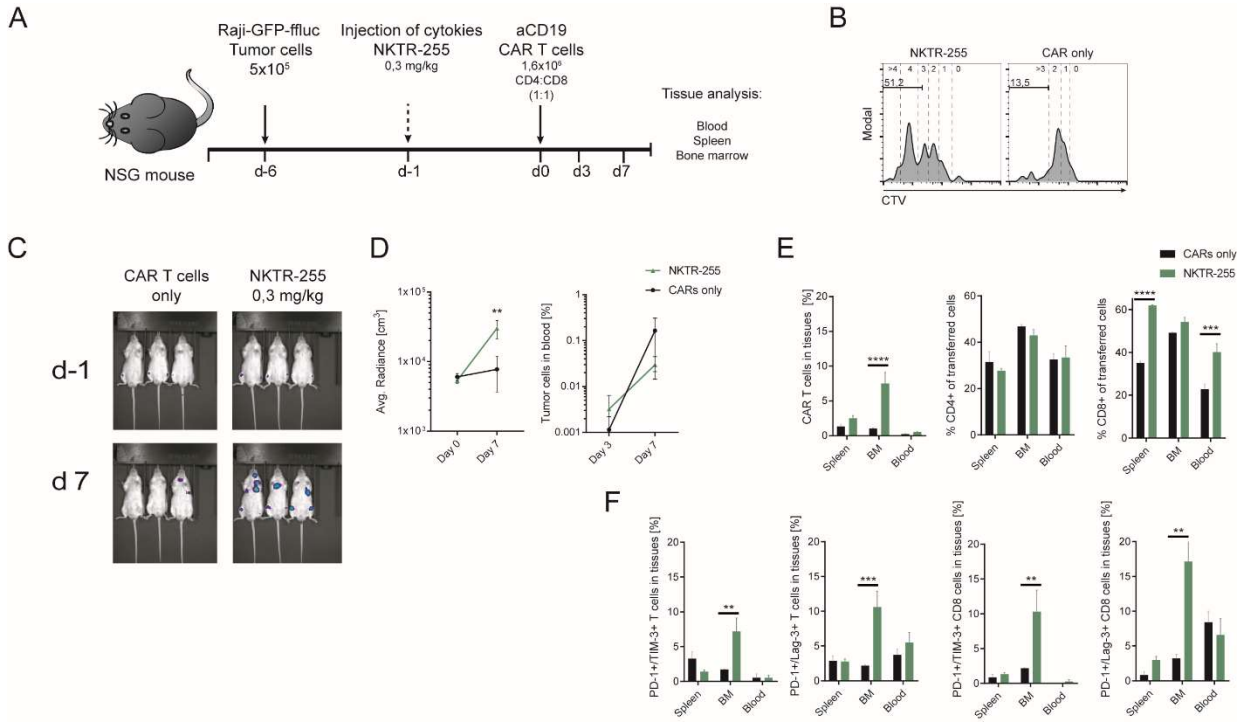


**Figure 35: Delayed antitumor effect when NKTR-255 is injected on day-1.** (A) Experimental setup and treatments are illustrated. (B) Proliferation of CellTraceViolet (CTV) labelled CAR T cells 3 days after transfer. Mice treated with NKTR-255 (left) and non-treated mice (right). Representative histograms are displayed. Separated fractions indicate divisions of the CAR T cells in vivo (dashed lines). (C) Normalized tumor images recorded on day-1 and day7. (D) Quantification the average radiance ($cm^3$) of tumor images shown in (C, left). Percentage of tumor detected in the blood are presented (right). Tumor cells are detected via flow cytometry and were pregated on living lymphocytes and gated on $CD45^+$,$GFP^+$. (E) Percentage of transferred CAR T cells (left) as well as $CD4^+$ (middle) and $CD8^+$ (right) CAR T cells detected in different organs are presented. CAR T cells are pregated on living lymphocytes and CD45 positivity. (F) Frequencies of PD-$1^+$/TIM-$3^+$ CAR (left) or PD-$1^+$/Lag-$3^+$ (left middle) and $CD8^+$ PD-$1^+$/TIM-$3^+$ (right middle) or PD-$1^+$/Lag-$3^+$ (right) CAR T cells in different tissues are shown. Statistical analysis done with 2way ANOVA; ** $P \leq 0.002$ *** $P \leq 0.0002$, **** $P \leq 0.0001$, n=3 mice per group. Means ± SD are plotted.

# 6 Discussion

Adoptive cell therapy using genetically modified CAR T cells specific for a desired antigen is a promising approach in cancer immunotherapy. Outstanding pre-clinical and clinical results have been generated for anti-CD19 CARs. However, the safety and efficiency of this new approach is highly dependent on the chosen target specificity and the structure of the CAR. High activity after target antigen encounter can lead to life threatening adverse effects. Furthermore, transferring this approach to other (solid-) tumors persistence and engraftment of CAR T cell manifest a major hurdle. To improve CAR therapy concerning safety, optimal affinity and engraftment in this thesis we studied in detail the truncated EGFRt marker as a safeguard mechanism for adoptive CAR T cell therapy. Rapid cell specific and complete depletion with Ctx of target cells could be observed *in vivo* with a clinically approved antibody. However, some disadvantages, which will be discussed below in further detail, may limit the clinical use of a depleting antibody, therefore we investigated a novel cellular safeguard mechanism based on the StrepTagII technology. We could show functionality of this cellular safeguard mechanism *in vitro*, but further *in vivo* experiments have to be done to validate the clinical relevance. To further improve and optimize CAR T cell therapy, we investigated the effect on the CAR binding affinity towards the target antigen CD19 *in vitro* and *in vivo*. In addition, we studied the effect of NKTR-255, an engineered IL-15 cytokine, on the expansion and persistence of anti-CD19 CAR T cells *in vivo*. Taken together the work of the thesis focused on four main aspects. I) EGFRt as a clinically relevant safeguard mechanism evaluated *in vivo*. II) Design, development and generation of a novel cellular safeguard mechanism. III) Design, generation and characterization of affinity modified CAR T cells *in vitro* and *in vivo.* IV) The influence of NKTR-255 on the expansion, persistence and antitumor efficacy of clinically relevant anti-CD19 CAR T cells *in vivo*.

## 6.1 EGFRt as a safeguard mechanism

EGFR targeting drugs, which are usually therapeutic monoclonal antibodies, can re-direct immune effector mechanisms. Most prominent effector mechanisms are ADCC and CDC after binding of EGFR. EGFR specific antibodies have been linked to ADCC as well as the inhibition of

the EGFR signaling and receptor downregulation [196]. Besides Ctx, Panitumumab is a widely used anti-EGFR mAb in the clinic. Comparing both mAbs, Ctx possesses an IgG1 and Panitumumab a IgG2 FC part. We can assume that Ctx is more potent due to the high affinity of the IgG1 to the FC receptor of effector cells whereas IgG2 has a low affinity [197]. Overall IgG1 antibodies such as Ctx are most effective to trigger ADCC via the FC receptor [181]. Therefore, Ctx was chosen for *in vivo* studies as the most suitable reagent for eliminating $EGFRt^+$ cells.

Before we started evaluating the EGFRt as a safeguard mechanism we evaluated the stable expression on the cell surface of the EGFRt and the transgenic receptor. The use of a T2A linker allows for concordant expression of both the EGFRt and another transgene, which can be e.g. a CAR or another reporter protein (Fig. 1A). We could show that implementing the EGFRt in lentiviral or retroviral constructs allows for robust and simple detection of gene-modified cells. The stability of EGFRt expression was studied under resting as well as stimulatory conditions *in vitro* and *in vivo*. For example, CAR/EGFRt-transduced T cells were activated through their CD19-CAR *in vitro* by co-incubation with $CD19^+$ target cells. Importantly, the expression of the EGFRt was not affected (doctoral thesis Paulina Paszkiewicz).

## 6.2 T cell depletion in a clinically relevant mouse model

### 6.2.1 **B cell aplasia can be reversed by eliminating mCD19 CAR T cells**

In clinical trials it has been described that a long-term side effect such as B cell aplasia occurs after CAR T cell therapy is terminated [198]. However, it is not a very severe side effect and can be treated by supplementing the patients with serum donated by healthy donors. Interestingly, an immunocompetent mouse model mimicking this side effect was developed by [186]. After injecting mCD19 CAR T cells into the syngeneic mouse model not only the tumor cells (Eμ-ALL01) were eradicated, but the mice additionally showed a long-term B cell aplasia seen previously in patients. To adopt the model for depleting EGFRt expressing CAR T cells after Ctx infusion, we modified the mCD19 CAR to possess a CD28 costimulatory domain and the EGFRt surface marker separated by a P2A ribosomal skip element for equal co-expression. Congenic murine splenocytes were transduced with the m1928E CAR and injected into recipient mice. Recipients were

sublethally irradiated before cell transfer to simulate a situation close to the clinic and enhance the engraftment of transferred cells. In the control group, receiving mock-transduced cells, B cells recovered rapidly to normal levels after an initial drop caused by irradiation. Recovery was prevented in mice injected with m1928E CAR T cells for 3 months after cell transfer, indicating functionality of m1928E CAR T cells *in vivo*. After administration of the aEGFRt antibody Ctx, we detected recovery of the endogenous B cell compartment to normal levels within 6 weeks. Recovery was not observed when an irrelevant control antibody Rtx was infused (Fig. 2D and E). In a separate experiment we injected Ctx to a later time point (day 158 post CAR T cell transfer) and observed similar kinetics of the B cell recovery (Fig. 3B and C). These data suggest that Ctx is an efficient and more important complete depletion reagent of functional m1928E CAR T cells. However, we could not follow the detection of the CAR/EGFRt$^+$ population upon Ctx administration due to inhibition of the EGFRt staining. A reagent specific for the scFv of the CAR as well as a murine CD19 FC fusion protein for binding the scFv were not available. As we used the CD8$\alpha$ hinge we were able to stain the CD8$\alpha$ but were not able to distinguish between hinge region of the CAR and natural CD8 hinge expression. In summary, however, these data show that for terminating CAR T cell therapy after successful and complete eradication of the malignant B cells to reverse B cell aplasia, Ctx is a very promising tool.

Next, we tested whether the recovered B cell compartment is fully functional. We performed an OVA-specific immunization of the mice with OVA-Imject alum on day 0 and performed an OVA specific IgG ELISA on day 7 and day 14. We showed that the recovered B cell compartment in Ctx-treated mice can generate an OVA-specific antibody response similar to the vaccinated mice that never received mCD19 CAR T cells (mock group). As additional control, non-vaccinated mock and Rtx-treated groups could not mount any antibody response (Fig. 4A). However, the mock group showed a little background signal, which is probably due to unspecific binding. These results hold true for day 14. As the recovered B cells could mount a specific IgG antibody response, we concluded that isotype switch was performed. During the course of B cell aplasia and mAb treatment, we took weekly serum samples and measured the serum cytokine levels over time. During stable B cell eradication, the serum cytokines were decreased to then, upon Ctx infusion, slowly recovered in the blood to normal levels comparable to the recovered B cell compartment.

Due to the fact that we froze and thawed all serum samples before analysis we cannot completely exclude effects caused by freeze-thaw cycles. Nonetheless, functional IgG antibodies indicated that recovered B cells were functional. To further investigate the functionality of the recovered B cell compartment, a specific immunophenotyping would be interesting to determine the clonality and differentiation status of the recovered B cells [199]. Interestingly, we observed a drop of serum cytokines which could not be prevented by plasma cells supposedly being CD19 negative [200]. Changes in the structure of germinal centers and its B cell zone would additionally be interesting to look at – to evaluate whether recovered B cells can repopulate and reorganize these structures.

### 6.2.2 **Ctx-mediated *in vivo* depletion of mCD19 CAR T cells does not increase risk of tumor relapse in a model of B cell ALL.**

Based on the previous results we modified the mouse model and additionally transferred murine ALL tumor cells before irradiation. We evaluated whether elimination of mCD19 CAR T cells increases the risk of relapse in mice bearing the rapidly progressive B cell leukemia Eμ ALL01, which is radioresistant *in vitro*. In these experiments we used a m19BBE CAR, because we and others achieved very high rates of complete remission in clinical trials with the human CD19-41BB CAR. We inoculated congenic Eμ ALL01 tumor cells, irradiated the mice subsequently, inoculated m19BBE CARs and monitored the mice over time. Ctx was infused on day 21 and 28 after the endogenous B and tumor cells were eradicated, whereas the control group received Rtx. The mice treated with Ctx recovered to normal B cell numbers whereas the control group stayed B cell deficient. Tumor cells were detected in the blood of mock-control groups, subsequently followed by rapid death of the mice caused by the high tumor burden. Ctx treated group remained leukemia free after B cell recovery and the survival of mice was similar to control group receiving no tumor (Fig. 6A-E). No residual tumor was detected when sensitive flow cytometry was performed in spleen and BM (Fig. 6F). These data show that in this model of B cell ALL, the elimination of mCD19-CAR T cells can reverse B cell depletion without increasing leukemia relapse. Taken together, our data in a murine B ALL model show that CAR T cells can be depleted one month after adoptive transfer, allowing the recovery of normal B cells without leukemia relapse. This should not be taken to conclude that elimination of CAR T cells in patients will

definitely not increase relapse, since a variety of factors, including type of malignancy, tumor burden, and susceptibility to T cell eradication, may determine the risk of relapse [82]. Even if relapse occurred after CAR T cell ablation, it could potentially be managed by a repeated infusion of CAR T cells, after Ctx is cleared.

A potential limitation of antibody based depletion strategies is that it may not be sufficiently rapid to reverse severe toxicity resulting from cytokines released by activated T cells or to reverse serious toxicity to cells that cannot be easily replenished. We did observe efficient reduction of T cell numbers within 24 hours after the second mAb infusion, including T cells residing in secondary lymphoid organs or other vital organs, which may be the site of unexpected acute adverse effects [136, 201]. The rapidity of T cell elimination might be improved by enhancing the Fc portion of anti-EGFR mAbs to improve ADCC; thus, it is conceivable that EGFRt could be used to rapidly counteract even acute side effects. Combination of different anti-EGFR antibodies triggering ADCC and CDC could further improve the efficacy and speed of T cell elimination.

In summary, we demonstrated that the EGFRt marker is stably expressed on T cells and can be targeted with Ctx to eliminate CAR-modified T cells after adoptive transfer. This safeguard mechanism can be integrated in genetically engineered T cells that target other tumor-associated molecules and pathogens and may therefore be broadly applied to enhance control over highly potent cell therapeutics.

## 6.3 Development of a novel cellular safeguard mechanism

### 6.3.1 **Proposed strategy of novel cellular safeguard mechanism**

To overcome limitations of an antibody based safeguard mechanism we designed and developed a novel cellular safeguard mechanism based on the StrepTagII technology. The Riddell lab (FHCRC) could show that inclusion of a STII in the hinge region of an anti-CD19 CAR leads to flexibility, superior functionality as well as the possibility to *in vitro* specifically stimulate engineered T cells through the CAR itself. *In vivo* tracking and detection is possible as well. Based on these data we hypothesized it would be advantageous to use this STII sequence as a target structure being recognized by a novel safeguard mechanism. We designed an anti-STII binding

CAR to test whether it is possible to eliminate STII containing CAR T cells *in vitro* and *in vivo* (Fig. 7). A CAR as an active and living safeguard mechanism, we hypothesize, has several advantages compared to a passive mAb safeguard mechanism. Proposed advantages are the ability to actively home through tissues, high sensitivity, longevity and the ability of forming memory (Table 1). It is described that the sensitivity of a CAR is much higher than of passive mAbs, which are dependent on ADCC or CDC [202]. We additionally equipped the anti-StrepTagII CAR (aCARCARc) with the EGFRt marker to be able to select and track generated aCARCARc cells.

### 6.3.2 **Expression and functionality of STII specific aCARCARc**

Initially we generated CAR constructs for genetic engineering of human primary cells (Fig. 8A). We retrovirally transduced human PBMCs with viral particles specific for either the STII containing CAR (19ST CAR) or the aCARCARc. Performed cytotoxicity assays confirmed the STII recognition of the aCARCARc followed by elimination of the 19ST CARs in a dose dependent manner performed with two different cytotoxicity assays (Fig. 8C-F). After demonstrating the killing capacity and the recognition of the STII, we evaluated whether any kind of stimulation of the 19ST CAR due to STII binding is occurring [203]. To address this question, we performed a co-incubation assay with 19ST and aCAR-CARc CAR T cells. Again, the aCAR-CARc cells eliminated StrepTagII containing 19ST CAR cells. Interestingly, we did not observe a stimulation or proliferation of the 19ST CAR cells, although admittedly the experimental layout was not ideal for testing the stimulation or proliferation of the 19ST CAR T cells. Ideally 19ST CAR T cells should be labeled with proliferation dyes (CTV or CFSE) and monitored over time. Nevertheless, we observed an increase of aCARCARc cells after 48h indicating aCARCARc cells were stimulated and proliferated upon antigen encounter (Fig. 9E). We demonstrated STII recognition and elimination of 19ST CAR T cells by the newly generated aCARCARc T cells. Additional experiments like cytokine secretion and proliferation assays should be performed to characterize aCARCARc cells in more detail allowing the judgement for (pre-) clinical use. Nonetheless, cytotoxicity data motivated us to design and generate corresponding murine constructs for further *in vitro* and *in vivo* functionality in a clinically relevant mouse model.

### 6.3.3 **Design and expression of murine anti-STII CARs**

We designed and generated STII containing CARs using the murine CAR backbone we used in previous experiments. We added a triple STII (3xSTII) either in the hinge region of the CAR or C-terminally of the EGFRt resulting in a fusion EGFRt-STII protein. Introduction of the anti-STII scFv into the same murine backbone resulted in a murine anti-STII binding CAR (mCARCARc) (Fig. 10A). When transduced into murine splenocytes, all constructs were expressed, based on the EGFRt staining assuming equal expression between EGFRt and CAR (Fig. 10B). To test the cytotoxic functionality of the newly generated constructs we co-cultured, in different combinations, T cells engineered with murine anti-CD19 CAR constructs either without or with a STII recognition site (m1928z_E, m19-ST-28z_E, m1928z_E-ST), the aCARCAR T cells and CD19-expressing TBL-12 tumor cells. When the transduced mCD19 CAR T cells were incubated with murine splenocytes and/or tumor cells , all mCD19 CAR constructs were fully functional and eliminated all $CD19^+$ cells including endogenous B cells as well as TBL-12 tumor cells, similarly to what described for the original m1928z CAR [186]. For functionality testing of mCARCARc we added tumor cells to mCD19 CAR transduced splenocytes and added additionally mCARCARc cells (Fig. 11B and C). With this setting we wanted to see whether mCARCARc cells are able to eliminate mCD19 CAR T cells containing a STII either in the hinge or fused to the EGFRt. We could not detect direct killing activity of the mCARCARc cells, but we observed an indirect killing or inhibition of the mCD19 CAR T cells by analyzing the frequency of $CD19^+$ cells like B- and tumor cells. Remarkably, we observed a distinct population of $CD19^+$ B- or tumor cells only in the groups in which mCD19 CAR T cells contained a STII recognition sequence. Differences due to STII location were not observed. With that indirect measurement of mCARCARc cell activity, we argued that the aCARCARc is functional, but we could not conclude whether it was inhibition of the mCD19 ST containing CAR T cells or direct killing (Fig. 11B and C). To test the killing capacity, we would need to perform a separate direct killing assay as performed in the human setting. We could not incubate the cells longer than 48h because the endogenous B cell compartment did not survive longer using T cell favored culturing conditions. We also did not congenically or fluorescently label the mCARCARc and mCD19 CAR T cells – which would have made the experiment more informative. However,

to determine the functionality of the newly generated constructs this experiment was sufficient and cytokine secretion and direct killing assays should follow.

### 6.3.4 *In vivo* functionality of the murine anti-STII CAR

In a first *in vivo* experiment, we used a similar experimental setup as we did to investigate EGFRt as a safeguard mechanism (see Fig. 2A). We irradiated the mice, followed by injection with congenically (CD45.1) labeled mCD19 CAR T cells on day 0. After observing established B cell aplasia, which confirmed the functionality of generated mCD19 CAR T cells, we injected a medium dose ($3{,}5x10^6$) of mCARCARc cells. We did not purify mCARCARc cells due to practicability. We expected a recovery of the endogenous B cell compartment like we observed after administration of Ctx. Unfortunately, mice stayed B cell depleted even after three weeks after mCARCARc injection.

While mice still maintained a B cell aplasia, we decided to inject a second dose of mCARCARc cells. This time we injected $1x10^6$ mCARCARc cells which are congenic for CD90.1 and possess a transgenic OT-1 TCR receptor enabling us to vaccinate the mice later and trigger specific expansion of the secondly injected mCARCARc cells via a TCR specific stimulus. Unfortunately, we again did not detect an indirect effect of the endogenous B cell population demonstrating mCD19 CAR elimination – even after additional vaccination of secondly transferred OT-I mCARCARc cells by injection of $1x10^6$ PFU MVA-OVA. By monitoring endogenous B cell frequencies, we observed no effect at all (Fig. 12B-E). Interestingly, 7 days after vaccination we performed a blood staining to see whether OT-I specific mCARCARc cells expanded after MVA-OVA challenge. We observed that exclusively $EGFRt^-$ cells responded to MVA-OVA vaccination, but not the $EGFRt^+$ mCARCARc cells. Additionally, we stained for PD-1 expression of $EGFR^-$ and $EGFRt^+$ OT-I mCARCARc cells. Remarkably, all $EGFR^+$ cells exhibited high PD-1 expression on the cell surface. Contrarily, $EGFR^-$ cells did not show any PD-1 expression at all. That was consistent in all mice. After sacrificing the mice, we analyzed the tissues and observed PD-1 positivity in all tissues of OT-I mCARCARc cells. Surprisingly, in mice which received mCD19 CAR T cells without STII the mCARCARc OT-I cells also showed a PD-1 positive phenotype.

It is described for CD19 CAR T cells that they cannot engraft when they are injected into non-irradiated or non-preconditioned mice [186, 204]. Preconditioning provides an environment supporting CAR T cell expansion and proliferation by lowered competition and better accessibility of homeostatic cytokines such as IL-15 or IL-2 [102]. This may explain the missing proliferation and functionality of mCARCARc cells after injection, as no preconditioning was performed before transfer of mCARCARc cells. At the same time the preconditioned immune system tolerates foreign gene products like the human EGFRt which can trigger cell rejection due to immunogenicity in mice. When injecting genetically engineered CAR T cells later without a preconditioning regimen, it is hard to engraft functional CAR T cells in the organism [204]. To overcome this problem, an additional preconditioning of the mice using chemotherapeutic reagents, or a second irradiation might be advantageous. Very preliminary data generated in Seattle at the FHCRC support this hypothesis. Besides that, not having the migration capacity to specifically home to target tissues as mCD19 STII containing CARs could be another issue. However, when analyzing the organs of the mice we could equally find mCARCARc and mCD19 CAR T cells. A defective migration capacity is therefore unlikely. After MVA-OVA challenge the additional stimuli through the TCR may have led to hyperactivation and subsequent exhaustion of mCARCARc cells, which has been described in detail also for CD19 CAR T cells [205]. Unspecific recognition of endogenous surface proteins continuously triggering the mCARCARc joint with MVA-OVA vaccination might lead to exhaustion and non-functionality as well.

Another reason could be the mCARCARc construct itself, combined with the accessibility of the target-epitope localization which plays a crucial role for CAR functionality *in vivo*. The aCARCARc exhibits a relatively short CD8$\alpha$ hinge domain which might be not ideal. The STII recognition site, when used in the hinge domain, is in close proximity to the cell surface which might indicates the need for a longer spacer (e.g. $CH_{2/3}$) for optimal accessibility and functionality. The importance of the hinge domain has been described by the Riddell lab (FHCRC), evaluating the optimal spacer length for CAR T cells recognizing novel and known TAAs [122]. In brief, they showed that TAAs being proximal to the cell surface (e.g. RORI) need a long spacer to be recognized and eliminated *in vivo*. Interestingly, *in vitro* the short spacer was functional, whereas *in vivo* no functionality was observed due to inaccessibility.

Suboptimal presentation of the CAR on the cell surface leading to clustering on the cell surface might lead to exhaustion through continuous tonic signaling described for various scFv clones. Therefore, each scFv clone must be tested empirically to gain proper surface expression. Ligand independent tonic signaling leading to CAR exhaustion is also reported and might be a reason for these findings [117]. To investigate these aspects in more detail additional experiments must be done to elicit the optimal spacer length and scFv to evaluate the most effective construct for further *in vivo* studies. In combination with an improved mouse model this might be key to prove the cellular safeguard mechanism and its efficiency.

In summary cell-based immunotherapies like CAR T cell therapy gained a lot of interest after several astonishing clinical trials demonstrating the benefit of T cells that were genetically engineered to recognize and specifically eliminate tumor cells. Enhanced functionality of engineered cells lead to a higher risk of therapy related adverse effects. Observed effects include on-target and off-target toxicities that can occur unexpectedly, or adverse effects are transient like CRS or long-term. The living cellular safeguard mechanism is a very promising system to improve safety of adoptive therapies more sensitively and independent of ADCC/CDC. Ideally, different safeguard mechanisms can handle a variety of adverse effects under different circumstances.

### 6.3.5 **Safeguard mechanisms**

The EGFRt-based cell-specific safeguard mechanism as a complete depletion marker needs to be addressed in a clinical study. In an NHP pilot study performed by the FHCRC, no signs of toxicity within the first three weeks was observed. No toxicities concerning the EGFRt modified T cells and no toxicities after infusion of the Ctx depletion reagent were observed. In this study, it could not clearly be shown that the loss of EGFRt modified cells was caused by Ctx-mediated depletion or by an immune response of the NHP against the EGFRt which was of human origin. This caveat could be overcome by using an EGFRt version which is of NHP origin. Rejection of the human EGFRt we observed in a mouse model as well [204]. As the EGFRt is already included in the clinical CD19-CAR construct and being evaluated in clinical studies at the FHCRC, no issues have been reported so far. From other studies using Ctx as an antitumor reagent, only minor side effects

have been described like skin rash [206]. In CAR T cell therapy the use of Ctx for terminating the therapy is possible due to the outstanding results after CAR therapy. Nevertheless, no Ctx-based depletion of engineered cells has been reported so far. Ethical aspects play a certain role. In our mouse studies, we could show that there is no increased risk of relapse after Ctx infusion. However, patients may not want to lose their anti-cancer CAR cells, since living tumor free without the B cell compartment is possible accompanied with only minor constraints.

As the EGFRt-based safeguard mechanism reveal limitations, which were mentioned earlier, we developed a cellular StrepTagII based safeguard mechanism. The possibility to recognize engineered cells inheriting a short target sequence (STII) might overcome these. Using a living safeguard mechanism might extend the range of applications for this unique cellular safeguard. Yet, all described safeguard or safety mechanisms are passive like mAb/drug-based systems. The therefore need to be infused multiple times and exhibit a limited duration of action. As we validated the cellular safeguard *in vitro* and in preliminary *in vivo* studies, further experiments must be done to achieve a clinically relevant safeguard mechanism. If the proposed advantages, ability to home through tissues, possessing high sensitivity, longevity and forming memory hold true this would be an ideal safeguard mechanism for cell therapy. Especially when adoptive cell therapy reaches solid tumors a living safeguard might be superior compared to others. Nonetheless, this has to be proven and further be tested and evaluated.

Taken together, both safeguard mechanisms are valuable for clinical translation possessing advantages and limitations. It may thereby prove most important to have different safeguard mechanisms that can be well adjusted to different situations and circumstances accompanied by the lowest risk of adverse effects.

## 6.4 Generation and characterization of affinity modified anti-CD19 CAR T cells

Adoptive cell therapy with genetically modified CAR T cells specific for a desired TAA is a promising approach in cancer immunotherapy. The safety and efficiency is highly dependent on the chosen target and the specificity of the CAR. High activity upon target antigen encounter can lead to toxic responses. The CRS is a systemic adverse effect commonly reported for treatment

of B cell malignancies with anti-CD19 CAR T cells. As most of the current clinical studies are performed with high affinity CAR T cells, the potential of CARs exhibiting a lower affinity has yet to be determined. Therefore, we aimed to functionally characterize CARs with different affinities newly developed in our laboratory. We will focus on the cytotoxicity and cytokine production of the engineered T cells, as well as the determination of their target antigen binding affinity by using the $K_{off}$-rate assay developed in our laboratory. We aim to complete the data set in a clinically relevant *in vivo* xenograft NSG tumor model.

### 6.4.1 Generation and expression of soluble scFvs for affinity determination

To investigate whether a CAR can specifically be modified in its affinity and to measure biochemically and functionally the effects of such modifications, in this thesis different mutations were set in the newly introduced scFv (clone 4G7) of the CAR construct. Soluble scFv domains crucial for affinity measurements were generated in addition. With the affinity modified scFvs (WT, mutant 35 and mutant 108), we were aiming to measure the affinity by using the flow based $K_{off}$-rate assay developed in our laboratory for pMHC-TCR avidity determination [190, 191].

Usually, the TCR is naturally or transgenically expressed on the cell surface and the natural pMHC ligand is recombinantly expressed. In the CAR $K_{off}$-rates we performed it the other way around as we failed initially to generate enough soluble CD19 protein (data not shown; no other lab has so far succeeded in generating soluble CD19 protein). CD19 is the natural ligand of the anti-CD19 CAR. It exhibits IgG-like domains and is therefore hard to be expressed. Having both counterparts (soluble scFv and soluble CD19) we could have performed $K_{off}$-rate measurements in various combinations (solid vs. soluble). However, we only succeeded in expressing and purifying the soluble scFvs for affinity measurements (Fig. 14; Fig. 15). Expression yield was good, albeit varying from batch to batch. For higher protein yield a mammalian expression system might be advantageous as it has been recently described specifically for scFvs [207].

### 6.4.2 Specificity testing of newly generated soluble scFv proteins

The expressed scFv proteins were tested for specificity by staining $CD19^+$ LCL tumor cells. LCL cells were stained with all expressed scFvs, albeit having a higher staining intensity when using WT scFvs FMC63 and 4G7. Mutants showed lower intensity supporting a reduced affinity which

is in line with findings in our group observed using low avidity TCRs. We confirmed specific CD19 binding of the scFvs by using human PBMCs and detected a more distinct staining pattern (Fig. 18). Finally, we performed a reversibility staining developed in our lab for testing affinity modified Fab fragments and observed no reversibility of WT FMC63 and WT 4G7 whereas mutant 35 and 108 showed reversibility (Fig. 19A). These results confirmed previous findings in our lab that mutations, set in the parental Fab fragments on position 35 and 108 in the heavy chain possess a lower affinity (data not shown, STAGE cell therapeutics). The reversible staining protocol gives a rough estimate whether a scFv is of high or low affinity. No residual scFv were detectable on the cell surface indicating low affinity scFvs.

### 6.4.3 $K_{off}$-rate measurements of affinity modified scFvs

We continued to dye label the scFvs via the accessible C-terminal cysteine for $K_{off}$-rate measurements. The maleimide dye-conjugation efficiency to Atto488 was lower compared to dye-labeled pMHC proteins previously generated in our laboratory, i.e. A2pp65 pMHC (Fig. 20B). Reason for that was probably the labeling process itself or an unknown abundance of misfolded scFvs that are not easily detectable [208]. Nevertheless, $K_{off}$-rate assays could be performed which was not the case when scFvs were labeled with other conjugation methods like Chromeo488-Ni-NTA to a 6xHis-Tag C-terminally (data not shown, IBA). We measured several $K_{off}$-rates of all expressed scFvs and observed slow dissociation kinetics for WT FMC63 and 4G7 and fast dissociations for mutant 35 and 108. Mutant 35 showed a slightly lower half-life compared to mutant 108 (FMC63 > 4G7 > mutant 35 > mutant 108). $K_{off}$-rate measurements overall resulted in variable half-lives.

Since CARs do bear a higher affinity than TCRs we performed the assay at room temperature (25°C) to accelerate the dissociation. The dye-conjugated scFvs showed initially a weak fluorescence intensity leading to variable half-lives. Due to this variability, we decided to qualitatively separate the scFvs in possessing a high, medium or low binding strength. For further experiments the fluorescence intensity must be improved to gather more robust and accurate $K_{off}$-rate data; the higher the initial fluorescence intensity the more precise the $K_{off}$-rate data. Therefore, another dye conjugation technique using a multifunctional TubTag, which has already

been established for the TCR-pMHC $K_{off}$-rate measurements in our laboratory, might improve the fluorescence intensity and sensitivity of the CAR $K_{off}$-rates [209]. On the contrary, transferring this technique bears some risks as well. It is known that the expression of Fab fragments or scFvs is challenging to allow correct and proper folding of the proteins. Adding a new TubTag C-terminally of the scFvs might alter the expression (yield and purity) and/or behavior of the tested scFvs. An interference within the modular structured protein consisting out of "scFv-tandem-StrepTag-TubTag" might be problematic and has to be tested empirically. The abundance of misfolded scFv proteins might additionally affect the dissociation and the resulting half-life. Standardizing protein quality is therefore crucial to receive reliable results and minimizing batch to batch variation. This being said the assay is sufficient to characterize CARs with the identical scFv clone of high, medium and low affinity, which is unique in the field of CAR T cells. To date, differences in the binding strength of CAR T cells only have been described using different scFv clones. By using different clones, different characteristics and functional properties are inherited [114].

### 6.4.4 **In-depth characterization of affinity modified CAR T cells *in vitro* and *in vivo***

After defining the affinity range of the scFvs, we introduced the scFvs into a STII containing CAR backbone kindly provided by Stan Riddell (Fig. 22A). We were able to express these CAR constructs in primary human cells (Fig. 22B and C). CAR expressing $CD4^+$ and $CD8^+$ cells were FACS purified, subsequently expanded and stained for activation markers CD62L and PD-1. CARs having low affinity receptors (mutant 35 and 108) lead to a lower activation status (Fig. 23). In line with that, we measured a faster proliferation of the WT FMC63 and 4G7 compared to mutant 35 and 108 when co-cultured with either K562-CD19 or Raji target cell lines (Fig. 24A). Remarkably, the mutants proliferated slightly faster when stimulated with Raji cells bearing a higher CD19 expression on the cell surface compared to K562-CD19 (Fig. 24C). WT CARs showed similar proliferation rates, independent of the CD19 expression level (Fig. 24A). In cytotoxicity assays, WT constructs showed faster and more effective killing compared to the mutants (Fig. 24D and E), with mutant 35 showing a slightly better killing capacity compared to mutant 108 which fits to previous affinity measurements.

To complete the *in vitro* functional dataset, we tested the CARs for cytokine secretion (ICCS and ELISA) an important parameter for defining functionality (Fig. 25). Similar to the proliferation and cytotoxicity assays, we observed that WT CARs showed higher cytokine secretion compared to mutants. Affinity reduced mutants showed a drastic decrease in cytokine secretion as it has been described for affinity modified genetically engineered CAR and TCR cells [116, 167]. Overall, the killing capacity and cytokine secretion of the CARs correlated with the affinity of the binding domains - the higher the affinity the better the cytotoxicity and cytokine secretion.

Confirming the *in vitro* behavior of the CAR constructs we conducted experiments in an *in vivo* xenograft NSG mouse model. It is an aggressive and clinically relevant lymphoma model used for CAR evaluation well-established in the Riddell lab (FHCRC) [85]. Using two mouse groups receiving a low and a high dose of CAR T cells, we observed comparable CAR T cells kinetics in blood over the time course, although higher CAR T cell numbers resulted in better antitumor efficacy. Remarkably, we observed a similar behavior of the CARs *in vivo* as seen *in vitro*. WT CAR T cells showed superior antitumor activity and faster proliferation upon antigen encounter compared to mutant 35 and 108. Frequencies of WT CARs dropped after tumor clearance whereas CAR frequencies of both mutants stayed high in the blood indicating tumor presence (Fig. 26D). After peak of expansion of the mutant CAR T cells a decrease of tumor burden was observed, but tumor clearance was not achieved within the experiment (Fig. 26 and 27). Using a high CAR T cell dose, mutant 35 could continuously decrease the tumor burden over time, whereas mutant 108 could only decrease tumor burden initially but again complete tumor eradication was not achieved.

Interestingly, we observed a great advantage of the affinity modified CARs when measuring the serum cytokines within the first 21 days after CAR T cell infusion in the blood. Serum cytokines were drastically lower compared to the WT CARs. The WT CARs showed a high initial peak for IFN$\gamma$ and TNF$\alpha$, indicating a rapid and effective T cell activation which led to antitumor effect that, however, could be accompanied by a high risk for severe CRS or neurological side effects [156]. In contrary, mutant 35 and 108 showed a drastically reduced cytokine release pattern for IFN$\gamma$ and TNF$\alpha$ (Fig. 27D).

In line with these findings (*in vitro* and *in vivo*) it is described that there is a certain threshold to be exceeded to get a proper activation and proliferation of CAR T cells. Using an anti-CD20 CAR it is described that high affinity CAR T cells need several hundred target antigens expressed on the cell surface to trigger activation. In contrast, low affinity CAR T cells need for activation several thousand target antigens on the cell surface [202]. Low affinity CAR T cells need then a higher threshold for full activation and are more dependent on a high TAA expression on the target cells [116, 167]. We observed similar findings with the generated CARs (data not shown). Low affinity CAR T cells show a lower activation status which is correlated with lower expansion, killing capacity and cytokine secretion as it is described by several groups [114, 116, 210]. Another typical characteristic which has been described is that high affinity CAR T cells have a higher sensitivity compared with low affinity CAR T cells. By that, target molecule expression must be strictly negative on healthy tissue circumventing adverse effects and off-tumor recognition [136]. In contrast, using affinity modified CAR T cells sensitivity is decreased whereas selectivity is increased; high TAA expressing tumor cells can be eliminated whereas the low expressing natural counterpart remains untouched [116]. Within the proliferation assay we observed similar results by getting more proliferation using target cells expressing more target antigen on the cell surface. These data mirror data using high and low avidity TCR modified transgenic cells [211].

A clinically relevant advantage of using affinity modified CAR T cells is the proposed lower cytokine secretion after cell infusion [116, 167]. Remarkably, we observed similar findings in our preclinical lymphoma model. WT CAR showed a high peak of cytokines like IFN$\gamma$ and TNF$\alpha$ whereas low affinity CAR T cells showed drastically lower cytokine secretion. Considering that CRS is the most common adverse effect after CAR T cell infusion, the initial use of affinity modified CARs to reduce the tumor burden with a desirable low cytokine secretion would be beneficial [156]. This may not only circumvent CRS, as neurological toxicities often occur in parallel or in consequence these adverse effects might be reduced as well. Subsequent infusion of high affinity CAR T cells to complete therapy could drastically improve CAR T cell therapy and safety.

Transferring affinity modified/reduced CAR T cells to solid tumors minimizing off-tumor toxicity against physiological expression of the TAA in natural tissues could be prevented. The improved selectivity of affinity reduced CARs provides the ability to distinguish between tumor and healthy

tissue [116, 212]. Our technique specifically reducing the affinity of scFvs can be transferred to any other CAR independent of the clone and the organism of origin of the scFv – or nanobodies. We believe that lower binding affinities could have unique, and potentially complementary, advantages to high affinity CARs. High affinity CAR T cells possess an unnatural slow $K_{off}$-rate compared to natural offrates natively found between TCR and pMHC [213]. Such a high off rate might hamper T cell characteristics like serial killing and instead trigger exhaustion and AICD. Similar findings were described between high affinity TCR-pMHC interactions [214]. Future CAR designs should cover a range of affinities to adjust the optimal CAR characteristics to different scenarios.

### 6.4.5 **Impaired expression of modified chimeric receptors**

Unfortunately, when looking closer into the expression of the CAR and the EGFRt itself, we observed dramatic differences between the WT FMC63 or 4G7 and the mutants 35 and 108. WT constructs showed correlating double stainings; mutants showed an impaired CAR expression, whereas EGFRt expression was similar (Fig. 28A). After LCL expansion the expression of the CAR was slightly improved, but still lower compared to WT situation. (Fig. 28A and B). Interestingly on protein level we detected a high CAR expression in WT CARs, a low CAR expression in mutant 35 and 108. We additionally observed an additional protein band above the CAR-CD3ζ (Fig. 28C). To exclude clustering, we covalently fused EGFP C-terminally to the CD3ζ domain of the CAR. We expressed and performed fluorescence microscopy with all constructs (Fig. 28D).

The impaired CAR expression cannot be easily explained. Being able to increase the STII staining slightly after expansion might be due to the selection of well-CAR expressing cells as it is seen for CD19 CARs after expansion. The unexpected protein band in the SDS-Page hints towards glycosylation of the CAR intracellularly. The Riddell lab observed similar patterns expressing a fully humanized CAR. Using PNGase they could inhibit the glycosylation and get rid of the additional protein band [193]. Degradation of the CARs intracellularly has not been described so far. In our scenario, it might be an explanation which must be tested. Tonic signaling which leads to exhaustion of CAR T cells due to misfolded CARs on the cell surface might also be relevant [117]. Accordingly, we tested all our constructs for tonic signaling via SDS-Page and did not

recognize any signs for tonic signaling (data not shown). In line with these data, the fluorescence microscopy indicated no CAR clustering on the cell surface subsequently leading to tonic signaling which could be confirmed by SDS-PAGE (data not shown).

The accessibility of the STII tag in the hinge region, which was used for CAR staining, might be hampered using mutant CAR constructs. This might be caused by formation of a different tertiary structure of the scFv. ScFv interactions causing CAR aggregation or scFv swapping on the cell surface might be possible as well. Unfortunately, there is no idiotype mAb for the 4G7 scFv clone available to directly stain the scFv on the cell surface. Why the STII staining/expression is impaired still needs to be clarified – otherwise we can't link the observed data strictly to the affinity. It is hard to tell whether the gathered data are based on impaired expression or modified affinity. However, if the mutants were linked to affinity reduced CARs, the data would strikingly fit to findings observed in the TCR research field and for other low affinity CARs.

## 6.5 Effect of NKTR-255 on clinically relevant anti-CD19 CAR T cells

### 6.5.1 *in vitro* effect of NKTR-255 on $CD4^+$ and $CD8^+$ CAR T cells

Another approach to improve and optimize CAR T cell therapy is to increase the expansion capacity and persistence of CAR T cells after transfer into the patient. Low cell numbers correlate with lower adverse effects whereas a better antitumor efficacy even with low numbers of CAR T cells is desirable [215]. A very attractive drug for realization is IL-15 named by the NCI to be one of the most promising immune-oncology reagents. Unfortunately, the native cytokine has poor drug-like properties with an unfavorable half-life of about 2h in mice. NEKTAR therapeutics developed a novel immunotherapeutic agent consisting of polymer-engineered IL-15 (NKTR-255) designed to optimally engage the IL-15 receptor complex alpha (IL-15R$\alpha$) and provide durable downstream pathway activation. Thereby NKTR-255 has a greatly improved plasma half-life (mouse and NHP) and positively induce T cell activation, proliferation and superior persistence *in vivo* (Fig. 29A, NEKTAR data not shown). To confirm bioactivity of NKTR-255 on $CD4^+$ and $CD8^+$ CAR T cells we performed a stimulation assay inducing phosphorylation of STAT5 (pSTAT5) upon NKTR-255 treatment. It was known from previous data that NKTR-255 is 5,5x less potent

compared to native IL-15. For that reason, we adjusted the used NKTR-255 concentration and observed comparable stimulation of native IL-15 and NKTR-255 (Fig. 29B). We calculated the EC50 value for both $CD4^+$ and $CD8^+$ CAR T cells. As, expected the native IL-15 was 5,5x - 8x more potent compared to NKTR-255. Adjusting the NKTR-255 concentration, NKTR-255 was stimulating the cells similarly compared to native IL-15. These data confirmed previous data using $CD8^+$ T cells. Next, we generated CD19 specific clinically relevant $CD4^+$ and $CD8^+$ CAR T cells, FACS sorted and LCL-expanded them gathering a pure and activated CAR T cell product (Fig. 30A and B). Before performing *in vivo* studies, we functionality tested them *in vitro* and observed a dose dependent cytotoxicity and an antigen specific proliferation with both $CD4^+$ and $CD8^+$ CAR T cells (Fig. 30C and D).

We confirmed that NKTR-255 engages the STAT5 pathway indicating activation and proliferation of CAR T cells as described for $CD8^+$ and $CD4^+$ T cells as well as for NK cells [216]. However, NKTR-255 is about 5,5x less potent compared to native IL-15 which can be overcome by adjusting the concentration without observing saturation or any alterations of CAR T cell stimulation *in vitro*. Further, NKTR-255 preserves sustained IL-15 receptor pathway engagement in T and NK cells and improves IL-15 receptor agonist exposure (NEKTAR, unpublished). Due to the increased half-life, it is the first potential medicine accessing the IL-15 pathway by preserving receptor binding to IL-15R$\alpha$ with antibody like dosing. It also could be shown that $CD8_{EM/CM}$ are more sensitive to NKTR-255 which is in line with findings using native IL-15 [217]. To demonstrate more relevant data of NKTR-255 on CAR T cells, NKTR-255 has to be tested in a clinically relevant mouse model.

### 6.5.2 *in vivo* effect of NKTR-255 on CAR T cells

In the first *in vivo* titration experiment, we used the Raji-NSG lymphoma model (as described in 1.5.4.). One day prior CAR T cell injection we injected different NKTR-255 doses (0.3; 0.1; 0.03 mg/kg) followed by repetitive infusions every 7 days. We observed a delayed CAR T cell expansion within the first 6 days followed by a drastic increase in NKTR-255 treated mice in a dose dependent manner. Looking at T cell subsets we recognized that NKTR-255 favors the expansion of $CD8^+$ CAR T cells (Fig. 31B). Tumor cells were cleared rapidly in the blood within the first 14 days in control and NKTR-255 treated mice. Interestingly, mice that received NKTR-255

had a lower initial antitumor activity in a reverse dose depended manner compared to the control group. As the initial antitumor effect was curative, we decided to re-challenge all tumor-free mice on day 38 to see whether NKTR-255 is beneficial for persistence and antitumor activity of CARs. Indeed, we observed rapid death of control mice, whereas NKTR-255 treated mice (high dose) could clear the tumor completely. For mice receiving the low dose of NKTR-255 a slow tumor outgrowth was recognized (Fig. 31D-F). Analyzing serum cytokine levels within the first 21 days, a delayed peak of effector cytokines like IFN$\gamma$, TNF$\alpha$ and GM-CSF was seen. Overall the NKTR-255 treated mice behaved like control mice (CAR T cells only). We repeated the same experiment, using $CD8^+$ CAR T cells only (Fig. 32). Again, we observed an NKTR-255 dose dependent CAR T cell frequency in the blood (high > middle > low) and tumor cells were cleared rapidly in mice treated with NKTR-255, but not in control mice which died rapidly (CAR T cells only). Again, we recognized a delayed antitumor effect in mice treated with NKTR-255 in a dose depended manner initially. To see whether NKTR-255 supported CAR T cells have a better persistence and functionality at a later time-point we re-challenged the mice on day 70. Strikingly, mice which received high and middle dose NKTR-255 could clear the tumor again, whereas mice which received a low dose could not (Fig. 32C-E).

Based on the initially delayed antitumor effect, we decided to inject NKTR-255 on day 6 after CAR T cell infusion. Astonishingly, all mice showed similar tumor radiance on day 7. As expected, CAR T cells drastically expanded in the blood upon NKTR-255 infusion in a dose dependent manner. Control group died rapidly whereas NKTR-255 treated mice cleared the tumor completely, except for a single mouse receiving a low dose of NKTR-255. After tumor clearance, we decided to re-challenge the mice at a very late time-point on day 90. Interestingly, after re-challenge, we detected a slow relapse of the tumor in a reverse dose depended manner (low > middle > high) (Fig. 33).

To address the initial drawback of NKTR-255 we used a similar experimental setup as previously and injected a high dose of NKTR-255 on day -1 and transferred CAR T cells on day 0. We decided to take blood on day three and harvest tissues on day 7. On day three CAR T cells which received NKTR-255 proliferated faster than control CAR T cells (Fig. 34B). We again observed a lower antitumor efficacy and radiance compared to controls (CAR T cells only) in the beginning.

Frequency of tumor cells in the blood was decreased for NKTR-255 treated mice. Interestingly, CAR T cell frequency in the bone marrow and $CD8^+$ CAR T cell frequency in the spleen was increased (Fig. 34B-D). In addition, especially $CD8^+$ CAR T cells supported by NKTR-255 showed a more activated phenotype on day 7, indicated by the frequency of PD-$1^+$/Lag-$3^+$ or PD-$1^+$/Tim-$3^+$ cell fraction in tissues pronounced in the bone marrow (Fig. 34E and F). These data indicate that the treatment with NKTR-255 might change the behavior of the CAR T cells early on.

Our data showed superior antitumor efficacy of CAR T cells treated with NKTR-255 *in vivo* in a dose dependent manner. Additionally, we observed better engraftment and persistence of CAR T cells in NKTR-255 treated mice. NKTR-255 supported the engraftment of adoptively transferred CAR T cells, especially $CD8^+$ CAR T cells. This is in line with the described mechanism of native IL-15 on T cells, maintaining $T_{MEM}$ cells, in particular $T_{CMs}$ [218]. Similar data were observed with NKTR-255 using human T cells and *in vivo* in an NHP model (NEKTAR, unpublished). Accordingly, after re-challenge we observed superior functionality of CAR T cells treated with NKTR-255 which might be caused be the maintenance of a higher fraction of $T_{CM}$ CAR T cells. Unfortunately, the aggressive lymphoma tumor model we used is not ideal to determine the exact phenotype of the transferred cells. Nevertheless, we believe that NKTR-255 maintains the $T_{CM}$ pool supporting the persistence and functionality even at later time points. Others could show that IL-15 can enhance *in vivo* function of tumor-reactive $CD8^+$ T cells as well [219]. However, the used mouse model was not ideal. Yet, clinical application is hard to be translated due to the low half-life of native IL-15. A first-in-human clinical trial using recombinant human IL-15 was performed. After administration of recombinant IL-15 a dramatic efflux of $CD8^+$ and NK cells was noted, which ultimately returned to baseline due to the short half-life. More importantly no toxicities were observed [220]. NKTR-255 can overcome these limitations by having an adequate serum half-life maintaining the physiological properties. In our study NKTR-255 infusion didn't provoke any adverse effects as well.

One of the most recent improvements in Immunotherapy is the preconditioning of the patients before adoptive cell transfer. It was found that additional infusion of IL-2 supported the engraftment of adoptively transferred cells. However, after infusing high doses of IL-2 life-

threatening side effects were observed [221]. By that IL-15 or more specifically NKTR-255 might have a greater therapeutic index and improved safety in humans compared with IL-2.

Interestingly, we observed a dose-dependent drawback on the antitumor effect infusing NKTR-255 early on day -1. Within the first week a lower antitumor efficacy was observed. The Riddell lab has described proliferation-linked apoptosis of adoptively transferred T cells after IL-15 administration in NHP. They described that T cells which proliferated in response to IL-15 expressed apoptosis markers like AnnexinV and activated caspases. In murine studies proliferation-linked apoptosis was described to regulate $CD8^+$ homeostasis [222]. In our model the mechanism described by the Riddell lab might be applicable. Administration of NKTR-255 accompanied by high tumor lysis might lead to severe activation and proliferation induced apoptosis indicated by a delayed peak of serum cytokines. We believe that mainly CAR high expressing T cells will undergo apoptosis whereas the lower expressing CAR T cells repopulate the organism. Another hypothesis could be that NKTR-255 treated CAR T cells might show an altered migration pattern delaying antitumor response initially. It has been described that IL-15 forces the initial migration of $CD8^+$ cells into mucosal tissues which could be true in our scenario as well [223].

However, we could overcome this problem by infusing NKTR-255 on day 6 after CAR T cell administration. We observed similar tumor burden compared to control mice. After NKTR-255 injection we, similarly to previous experiments, detected a drastic engraftment and rapid tumor clearance of CAR T cells. This argues for the hypothesis of proliferation-induced apoptosis.

Accordingly, we investigated the mechanism of proliferation-induced apoptosis. Indeed, we observed a faster proliferation of CAR T cells when NKTR-255 was injected. We also observed a significantly higher expression of activation/exhaustion markers on the cell surface in analyzed tissues. The highly activated cell status hints to an exhaustion phenotype after hyperactivation caused by the high amount of cytokines accumulating after tumor lysis. The exact mode of action must be further investigated to circumvent any harm on the CAR T cells decreasing the antitumor efficacy. Especially, regarding clinical translation, the optimal administration window of NKTR-

255 might be crucial to obtain the best engraftment, persistence and antitumor efficacy of even very low CAR T cell numbers.

Taken together, administration of NKTR-255 significantly improves antitumor efficacy and exhibits superior engraftment and persistence of CAR T cells, especially for $CD8^+$ CAR T cells *in-vivo*. Reduced antitumor efficacy when NKTR-255 was infused on day -1 could be completely overcome by infusing NKTR-255 on day 6 post CAR T cell administration. These data support previous data that NKTR-255 is a promising and safe antibody-like drug for immunotherapies to be confirmed in human clinical trials.

In summary, in this thesis we investigated on safeguard mechanisms and affinity modified CARs for the improvement of cellular therapies, as well enhancing engraftment of CAR T cells using NKTR-255. The astonishing results of CAR T cell therapy in clinical trials are very promising for cancer treatment. Nevertheless, major adverse effects such as CRS are still present and need to be addressed. With our results we could show that it is possible to terminate CAR T cell therapy after successful eradication of the malignant B cells and reverse B cell aplasia using the EGFRt safeguard mechanism. After CAR T cell transfer lower cytokine secretion and a reduced risk for CRS could be shown by using affinity modified CAR T cells in a pre-clinical model. The development of a novel cellular safeguard mechanism might be promising for the CAR T cell usage in solid tumors actively guard for unwanted target cells. The fact that initial complete remissions are higher than sustained remissions hints towards the need of persistent and CAR T cells maintaining in the patients' body. The development of polymer conjugated IL-15 (NKTR-255) having a superior plasma half-life and maintaining the biology of the IL-15 - IL15R$\alpha$ complex makes it possible to significantly improve the persistence, maintenance and efficacy of CAR T cells.

# 7 Summary

Adoptive cell therapy using genetically modified CAR T cells specific for a desired antigen is a promising approach in cancer immunotherapy. Outstanding pre-clinical and clinical results have been generated for anti-CD19 CARs. Recently, first CD19 specific CAR T cells were FDA approved for the treatment of B cell malignancies. However, the safety and efficiency of this new approach is highly dependent on the chosen target specificity and the structure of the CAR. High activity after target antigen encounter can lead to life threatening adverse effects. Furthermore, when transferring this approach to other (solid-) tumors, persistence and engraftment of CAR T cell manifests a major hurdle.

In this thesis, we mainly focused on how to improve the safety and efficacy of CAR T cell therapy. First, we studied safeguard mechanisms for CAR T cell depletion in case of short and long-term toxicities. For this purpose, we implemented and demonstrated the feasibility of using the EGFRt as safeguard mechanism showing a rapid and complete depletion of engineered CAR/EGFRt expressing cells with Cetuximab, a clinically approved antibody recognizing EGFRt. Importantly, by terminating CAR T cell therapy, we were able to reverse B cell aplasia without an increased risk of tumor relapse *in vivo* and the recovered B cell compartment was fully functional. As there are some disadvantages that limit the clinical use of Cetuximab, we developed a novel cellular safeguard mechanism, the so-called "aCAR-CAR approach" based on the StrepTag technology. We designed and expressed the aCAR-CAR in primary cells and showed recognition and elimination of StrepTagII containing CAR T cells as described [203] *in vitro*. Second, we explored strategies for reducing a priori the risk of severe acute side effects upon CAR T cell administration, specifically through the generation of lower affinity CD19 CARs. We designed and generated affinity modified scFvs and used the $K_{off}$-rate assay developed in our laboratory for providing preliminary data supporting differences in avidity [190]. We could implement these scFvs in current clinically relevant CAR constructs and demonstrate that affinity modified CARs lead to tumor regression accompanied with lower activation and cytokine secretion upon target cell encounter, reducing the risk of CRS and other adverse effects after CAR T cell transfer *in vitro* and *in vivo*. Unfortunately, affinity reducing mutations also affected the surface expression level of

recombinant receptor expressed on CAR T cells, which did not allow us to conclusively link affinity modulation to improved CAR T cell performance. Finally, we investigated the beneficial effect of exogeneous administration of IL-15 on the persistence, and in turn therapeutic efficacy, of adoptively transferred CAR T cell. Using a polymer conjugated IL-15 cytokine inheriting an increased plasma half-life (NKTR-255, NEKTAR therapeutics) we were able to stimulate $CD4^+$ and $CD8^+$ CAR T cells preserving a sustained IL-15 receptor pathway engagement and an improved IL-15 agonist exposure *in vitro*. Further we showed that we could significantly improve the engraftment, antitumor activity and persistence of clinically relevant anti-CD19 CAR T cells *in vivo* utilizing NKTR-255. Combining and implementing these improvements into the clinic might improve CAR T cell therapy.

# 8 Acknowledgements

At this place I want to thank all my colleagues, friends and my family for the support which was essential for the success to finish my doctoral thesis.

A very special thanks to Prof. Dirk Busch and my mentor and TUM associate Prof. Stan Riddell from the FHCRC in Seattle for their dedicated supervision of my doctoral thesis and their valuable and expedient advice at each stage of my thesis which pushed and advanced my work enormously. I am very grateful for the projects offered to me I could work on free and independently. All projects were ranging from basic research with a straight-forward perspective to clinical translation and relevance. By that I could deeply dive into basic biological mechanisms and relevant parameters for clinical development. Working in a very close collaboration with Prof. Dirk Busch and Prof. Stan Riddell was extremely motivating, helpful and an honor. Myriads of Skype conferences constantly supported my work and showed their extraordinary commitment to the projects. It was not only very helpful for the projects, discussing and exchanging ideas with Prof. Busch and Prof. Riddell was very inspiring, fun and made me able to sense relevant developments.

In addition, I am very grateful having the opportunity to join Prof. Stan Riddell's laboratory at the FHCRC in Seattle for unforgettable 8 months. It was a great learning experience scientifically, with a very close connection to the clinic where patients were treated, stressing out the importance of the science we do. It was also a personal enrichment working and living in Seattle getting to know and making friends with a lot of new and nice people. I further want to thank Prof. Busch and Prof. Riddell for giving me the opportunity to attend on international conferences being very inspiring and informative. During all the time the scientific exchange between Munich and Seattle was supported by the Institute for Advanced Studies (IAS).

As a part of my committee, I want to thank my second supervisor Prof. Vogel from Weihenstephan for very helpful discussions and support during my thesis.

I also want to thank Dr. Kilian Schober and Dr. Elvira D'Ippolito for a lots of helpful discussions and their help and advice all the time during my thesis. They also helped me a lot reviewing manuscripts and talks in detail what I really appreciated and helped me structuring manuscripts and talks.

Further I want to thank Dr. Paulina Paszkiewicz for her support, especially in the beginning, of my doctoral thesis and the nice and harmonic team-work resulting in our shared publication. She also helped me performing and handling mouse work.

In Seattle I received a lot of support from Alexander Salter and Shivani Srivastava who introduced me in a new environment the FHCRC. Additionally, they showed me how to work in a very structured and straight forward way, helping me a lot for the thesis as well as for future projects. Thanks to Dr. Cameron Turtle and Dr. Takahiro Miyazaki from NEKTAR therapeutics for their support and giving me the opportunity working on a great project. I also have to thank Don Parrilla for performing mouse work, Margot Pont, Isabelle Leung and Carla Jaeger for showing me Seattle which was always a lot of fun. The whole Riddell lab was very supportive all the time and it was a pleasure being part of the lab.

Many thanks to my cooperation partners from the former STAGE cell Therapeutics group (now Celgene), Dr. Lothar Germeroth, Dr. Christian Stemberger, Dr. Stefan Dreher, Dr. Herbert Stadler, Claudia Tschulik, Michaela Wagner, Mateusz Poltorak and Patricia Gräf for providing reagents, primary cells, and helping me with cloning, generation of constructs and critical discussions of my results.

A special thanks to the AG Busch Dr. Simon Grassmann, Marten Plambeck, Fabian Mohr, Manuel Effenberger for their support in all situations in the lab and beyond. Dr. Simon Grassmann supported me concerning cloning and cell engineering, Manuel Effenberger and Philipp Lückemeier helped me setting up the $K_{off}$-rate assay. I also want to thank all colleagues in the Busch lab for sharing their expertise and protocols, Katherine Molter, Anna Hochholzer, Monika Hammel, Franziska Graml for their technical know-how and the help with daily problems. It was a pleasure being part of the Busch lab and thank you all for generating a warm, trust worthfully working atmosphere.

Thanks to the AG Schiemann especially Immanuel Andrä and Lynette Henkel for performing endless sorts, helping with panel setups and fixing the flow cytometer machines even after working hours.

Thanks to Marvin Festag from the AG Protzer from the Virology department for helpful discussions and sharing knowledge to move our projects forward.

At that point I specifically want to mention Immanuel Andrä, Dr. Simon Grassmann, Marten Plambeck and Fabian Mohr with who I have shared all my ups and downs at work and beyond. They were becoming very good friends.

Of course, I could not have managed all the challenges without my family and friends from Freiburg, Freising and Munich. I want to specifically thank my Mum who accompanied me during the long way, not only of my thesis, during my whole academic career. She supported me at each stage and gave me the mental strength, I needed for completing my doctoral thesis.

Most special thanks to my wife Carina Fräßle for her love and endless support helped me stay calm and focused for the thesis. Thanks to her remarkable patience when working until night hours or on weekends. Thank you for everything, the wonderful time with each other and for just being there.

# 9 References:


1. Flajnik, M.F. and M. Kasahara, *Origin and evolution of the adaptive immune system: genetic events and selective pressures.* Nat Rev Genet, 2010. **11**(1): p. 47-59.
2. Robins, H.S., et al., *Comprehensive assessment of T-cell receptor beta-chain diversity in alphabeta T cells.* Blood, 2009. **114**(19): p. 4099-107.
3. Gajewski, T.F., et al., *Immune resistance orchestrated by the tumor microenvironment.* Immunol Rev, 2006. **213**: p. 131-45.
4. Hanahan, D. and R.A. Weinberg, *Hallmarks of cancer: the next generation.* Cell, 2011. **144**(5): p. 646-74.
5. Howlader N, N.A., Krapcho M, Garshell J, Neyman N, Altekruse SF, Kosary CL, Yu M, Ruhl J, Tatalovich Z, Cho H, Mariotto A, Lewis DR, Chen HS, Feuer EJ, Cronin KA (eds)., National Cancer Institute. Bethesda, MD, https://seer.cancer.gov/csr/1975_2010/, based on November 2012 SEER data submission, posted to the SEER web site, April 2013., *SEER Cancer Statistics Review, 1975-2010.* https://seer.cancer.gov/csr/1975_2010/, 2013.
6. Hurwitz, S., *The history of pediatric dermatology in the United States.* Pediatr Dermatol, 1988. **5**(4): p. 280-5.
7. Quintas-Cardama, A., W. Wierda, and S. O'Brien, *Investigational immunotherapeutics for B-cell malignancies.* J Clin Oncol, 2010. **28**(5): p. 884-92.
8. Cheever, M.A., et al., *The prioritization of cancer antigens: a national cancer institute pilot project for the acceleration of translational research.* Clin Cancer Res, 2009. **15**(17): p. 5323-37.
9. Davila, M.L., et al., *How do CARs work?: Early insights from recent clinical studies targeting CD19.* Oncoimmunology, 2012. **1**(9): p. 1577-1583.
10. Long, A.H., W.M. Haso, and R.J. Orentas, *Lessons learned from a highly-active CD22-specific chimeric antigen receptor.* Oncoimmunology, 2013. **2**(4): p. e23621.
11. Billingham, R.E., et al., *Quantitative studies on tissue transplantation immunity. I. The survival times of skin homografts exchanged between members of different inbred strains of mice.* Proc R Soc Lond B Biol Sci, 1954. **143**(910): p. 43-58.
12. Mitchison, N.A., *Studies on the immunological response to foreign tumor transplants in the mouse. I. The role of lymph node cells in conferring immunity by adoptive transfer.* J Exp Med, 1955. **102**(2): p. 157-77.
13. Cheever, M.A., R.A. Kempf, and A. Fefer, *Tumor neutralization, immunotherapy, and chemoimmmunotherapy of a Friend leukemia with cells secondarily sensitized in vitro.* J Immunol, 1977. **119**(2): p. 714-8.
14. Restifo, N.P., M.E. Dudley, and S.A. Rosenberg, *Adoptive immunotherapy for cancer: harnessing the T cell response.* Nat Rev Immunol, 2012. **12**(4): p. 269-81.
15. Moss, P. and A. Rickinson, *Cellular immunotherapy for viral infection after HSC transplantation.* Nat Rev Immunol, 2005. **5**(1): p. 9-20.
16. Coppin, C., et al., *Immunotherapy for advanced renal cell cancer.* Cochrane Database Syst Rev, 2005(1): p. CD001425.
17. Kolb, H.J., et al., *Donor leukocyte transfusions for treatment of recurrent chronic myelogenous leukemia in marrow transplant patients.* Blood, 1990. **76**(12): p. 2462-5.
18. Horowitz, M.M., et al., *Graft-versus-leukemia reactions after bone marrow transplantation.* Blood, 1990. **75**(3): p. 555-62.

19. Goldman, J.M., et al., *Bone marrow transplantation for chronic myelogenous leukemia in chronic phase. Increased risk for relapse associated with T-cell depletion.* Ann Intern Med, 1988. **108**(6): p. 806-14.
20. Kolb, H.J., et al., *Graft-versus-leukemia effect of donor lymphocyte transfusions in marrow grafted patients.* Blood, 1995. **86**(5): p. 2041-50.
21. Bleakley, M. and S.R. Riddell, *Molecules and mechanisms of the graft-versus-leukaemia effect.* Nat Rev Cancer, 2004. **4**(5): p. 371-80.
22. Warren, E.H., et al., *Therapy of relapsed leukemia after allogeneic hematopoietic cell transplantation with T cells specific for minor histocompatibility antigens.* Blood, 2010. **115**(19): p. 3869-78.
23. Biron, C.A., K.S. Byron, and J.L. Sullivan, *Severe herpesvirus infections in an adolescent without natural killer cells.* N Engl J Med, 1989. **320**(26): p. 1731-5.
24. Riddell, S.R., *Engineering antitumor immunity by T-cell adoptive immunotherapy.* Hematology Am Soc Hematol Educ Program, 2007: p. 250-6.
25. Feuchtinger, T., et al., *Detection of adenovirus-specific T cells in children with adenovirus infection after allogeneic stem cell transplantation.* Br J Haematol, 2005. **128**(4): p. 503-9.
26. Riddell, S.R. and P.D. Greenberg, *Principles for adoptive T cell therapy of human viral diseases.* Annu Rev Immunol, 1995. **13**: p. 545-86.
27. Neuenhahn, M., et al., *Transfer of minimally manipulated CMV-specific T cells from stem cell or third-party donors to treat CMV infection after allo-HSCT.* Leukemia, 2017. **31**(10): p. 2161-2171.
28. Heslop, H.E., et al., *Long-term outcome of EBV-specific T-cell infusions to prevent or treat EBV-related lymphoproliferative disease in transplant recipients.* Blood, 2010. **115**(5): p. 925-35.
29. Knabel, M., et al., *Reversible MHC multimer staining for functional isolation of T-cell populations and effective adoptive transfer.* Nat Med, 2002. **8**(6): p. 631-7.
30. Riddell, S.R., et al., *Restoration of viral immunity in immunodeficient humans by the adoptive transfer of T cell clones.* Science, 1992. **257**(5067): p. 238-41.
31. Gerdemann, U., et al., *Rapidly generated multivirus-specific cytotoxic T lymphocytes for the prophylaxis and treatment of viral infections.* Mol Ther, 2012. **20**(8): p. 1622-32.
32. Tzannou, I., et al., *Off-the-Shelf Virus-Specific T Cells to Treat BK Virus, Human Herpesvirus 6, Cytomegalovirus, Epstein-Barr Virus, and Adenovirus Infections After Allogeneic Hematopoietic Stem-Cell Transplantation.* J Clin Oncol, 2017. **35**(31): p. 3547-3557.
33. Berger, C., et al., *Adoptive transfer of effector CD8+ T cells derived from central memory cells establishes persistent T cell memory in primates.* J Clin Invest, 2008. **118**(1): p. 294-305.
34. Zhang, L., et al., *Intratumoral T cells, recurrence, and survival in epithelial ovarian cancer.* N Engl J Med, 2003. **348**(3): p. 203-13.
35. Uttenthal, B.J., et al., *Challenges in T cell receptor gene therapy.* J Gene Med, 2012. **14**(6): p. 386-99.
36. Atkins, M.B., et al., *High-dose recombinant interleukin 2 therapy for patients with metastatic melanoma: analysis of 270 patients treated between 1985 and 1993.* J Clin Oncol, 1999. **17**(7): p. 2105-16.
37. Rosenberg, S.A., et al., *Prospective randomized trial of high-dose interleukin-2 alone or in conjunction with lymphokine-activated killer cells for the treatment of patients with advanced cancer.* J Natl Cancer Inst, 1993. **85**(8): p. 622-32.
38. Xu, Y., et al., *Closely related T-memory stem cells correlate with in vivo expansion of CAR.CD19-T cells and are preserved by IL-7 and IL-15.* Blood, 2014. **123**(24): p. 3750-9.
39. Gargett, T. and M.P. Brown, *Different cytokine and stimulation conditions influence the expansion and immune phenotype of third-generation chimeric antigen receptor T cells specific for tumor antigen GD2.* Cytotherapy, 2015. **17**(4): p. 487-95.

40. Hinrichs, C.S., et al., *IL-2 and IL-21 confer opposing differentiation programs to CD8+ T cells for adoptive immunotherapy.* Blood, 2008. **111**(11): p. 5326-33.
41. Rosenberg, S.A., et al., *Use of tumor-infiltrating lymphocytes and interleukin-2 in the immunotherapy of patients with metastatic melanoma. A preliminary report.* N Engl J Med, 1988. **319**(25): p. 1676-80.
42. Rosenberg, S.A., et al., *Treatment of patients with metastatic melanoma with autologous tumor-infiltrating lymphocytes and interleukin 2.* J Natl Cancer Inst, 1994. **86**(15): p. 1159-66.
43. Rosenberg, S.A., et al., *Durable complete responses in heavily pretreated patients with metastatic melanoma using T-cell transfer immunotherapy.* Clin Cancer Res, 2011. **17**(13): p. 4550-7.
44. Clay, T.M., et al., *Efficient transfer of a tumor antigen-reactive TCR to human peripheral blood lymphocytes confers anti-tumor reactivity.* J Immunol, 1999. **163**(1): p. 507-13.
45. Miller, A.D., *Retrovirus packaging cells.* Hum Gene Ther, 1990. **1**(1): p. 5-14.
46. Sadelain, M., I. Riviere, and R. Brentjens, *Targeting tumours with genetically enhanced T lymphocytes.* Nat Rev Cancer, 2003. **3**(1): p. 35-45.
47. Ho, W.Y., et al., *Adoptive immunotherapy: engineering T cell responses as biologic weapons for tumor mass destruction.* Cancer Cell, 2003. **3**(5): p. 431-7.
48. Sadelain M, M.R., *International Congress of Immunology, editor. 8th International Congress of Immunology. Springer-Verlag; Budapest; Hungary:.* 1992.
49. Morris, E.C. and H.J. Stauss, *Optimizing T-cell receptor gene therapy for hematologic malignancies.* Blood, 2016. **127**(26): p. 3305-11.
50. Yang, Y., et al., *A dual AAV system enables the Cas9-mediated correction of a metabolic liver disease in newborn mice.* Nat Biotechnol, 2016. **34**(3): p. 334-8.
51. Eyquem, J., et al., *Targeting a CAR to the TRAC locus with CRISPR/Cas9 enhances tumour rejection.* Nature, 2017. **543**(7643): p. 113-117.
52. Dembic, Z., et al., *Transfer of specificity by murine alpha and beta T-cell receptor genes.* Nature, 1986. **320**(6059): p. 232-8.
53. Dossinger, G., et al., *MHC multimer-guided and cell culture-independent isolation of functional T cell receptors from single cells facilitates TCR identification for immunotherapy.* PLoS One, 2013. **8**(4): p. e61384.
54. Niklas, N., et al., *Qualifying high-throughput immune repertoire sequencing.* Cell Immunol, 2014. **288**(1-2): p. 31-8.
55. Schmitt, T.M., G.B. Ragnarsson, and P.D. Greenberg, *T cell receptor gene therapy for cancer.* Hum Gene Ther, 2009. **20**(11): p. 1240-8.
56. Obenaus, M., et al., *Identification of human T-cell receptors with optimal affinity to cancer antigens using antigen-negative humanized mice.* Nat Biotechnol, 2015. **33**(4): p. 402-7.
57. Mali, P., et al., *RNA-guided human genome engineering via Cas9.* Science, 2013. **339**(6121): p. 823-6.
58. Nauerth, M., et al., *TCR-ligand koff rate correlates with the protective capacity of antigen-specific CD8+ T cells for adoptive transfer.* Sci Transl Med, 2013. **5**(192): p. 192ra87.
59. Robbins, P.F., et al., *Single and dual amino acid substitutions in TCR CDRs can enhance antigen-specific T cell functions.* J Immunol, 2008. **180**(9): p. 6116-31.
60. Gross, G., et al., *Generation of effector T cells expressing chimeric T cell receptor with antibody type-specificity.* Transplant Proc, 1989. **21**(1 Pt 1): p. 127-30.
61. Eshhar, Z., et al., *Specific activation and targeting of cytotoxic lymphocytes through chimeric single chains consisting of antibody-binding domains and the gamma or zeta subunits of the immunoglobulin and T-cell receptors.* Proc Natl Acad Sci U S A, 1993. **90**(2): p. 720-4.

62. Vitale, M., et al., *HLA class I antigen down-regulation in primary ovary carcinoma lesions: association with disease stage.* Clin Cancer Res, 2005. **11**(1): p. 67-72.
63. Morgan, R.A., et al., *Cancer regression in patients after transfer of genetically engineered lymphocytes.* Science, 2006. **314**(5796): p. 126-9.
64. Johnson, L.A., et al., *Gene therapy with human and mouse T-cell receptors mediates cancer regression and targets normal tissues expressing cognate antigen.* Blood, 2009. **114**(3): p. 535-46.
65. Rosenberg, S.A., *Cell transfer immunotherapy for metastatic solid cancer--what clinicians need to know.* Nat Rev Clin Oncol, 2011. **8**(10): p. 577-85.
66. Robbins, P.F., et al., *Tumor regression in patients with metastatic synovial cell sarcoma and melanoma using genetically engineered lymphocytes reactive with NY-ESO-1.* J Clin Oncol, 2011. **29**(7): p. 917-24.
67. Kakarla, S., et al., *Antitumor effects of chimeric receptor engineered human T cells directed to tumor stroma.* Mol Ther, 2013. **21**(8): p. 1611-20.
68. Stanislawski, T., et al., *Circumventing tolerance to a human MDM2-derived tumor antigen by TCR gene transfer.* Nat Immunol, 2001. **2**(10): p. 962-70.
69. Cohen, C.J., et al., *Recognition of fresh human tumor by human peripheral blood lymphocytes transduced with a bicistronic retroviral vector encoding a murine anti-p53 TCR.* J Immunol, 2005. **175**(9): p. 5799-808.
70. Meij, P., et al., *Generation and administration of HA-1-specific T-cell lines for the treatment of patients with relapsed leukemia after allogeneic stem cell transplantation: a pilot study.* Haematologica, 2012. **97**(8): p. 1205-8.
71. Lamers, C.H., et al., *Treatment of metastatic renal cell carcinoma with autologous T-lymphocytes genetically retargeted against carbonic anhydrase IX: first clinical experience.* J Clin Oncol, 2006. **24**(13): p. e20-2.
72. Lamers, C.H., et al., *Immune responses to transgene and retroviral vector in patients treated with ex vivo-engineered T cells.* Blood, 2011. **117**(1): p. 72-82.
73. Riddell, S.R., et al., *T-cell mediated rejection of gene-modified HIV-specific cytotoxic T lymphocytes in HIV-infected patients.* Nat Med, 1996. **2**(2): p. 216-23.
74. Milone, M.C., et al., *Chimeric receptors containing CD137 signal transduction domains mediate enhanced survival of T cells and increased antileukemic efficacy in vivo.* Mol Ther, 2009. **17**(8): p. 1453-64.
75. Savoldo, B., et al., *CD28 costimulation improves expansion and persistence of chimeric antigen receptor-modified T cells in lymphoma patients.* J Clin Invest, 2011. **121**(5): p. 1822-6.
76. Ramos, C.A., B. Savoldo, and G. Dotti, *CD19-CAR trials.* Cancer J, 2014. **20**(2): p. 112-8.
77. Bradbury, L.E., et al., *The CD19/CD21 signal transducing complex of human B lymphocytes includes the target of antiproliferative antibody-1 and Leu-13 molecules.* J Immunol, 1992. **149**(9): p. 2841-50.
78. Uckun, F.M. and J.A. Ledbetter, *Immunobiologic differences between normal and leukemic human B-cell precursors.* Proc Natl Acad Sci U S A, 1988. **85**(22): p. 8603-7.
79. Porter, D.L., et al., *Chimeric antigen receptor-modified T cells in chronic lymphoid leukemia.* N Engl J Med, 2011. **365**(8): p. 725-33.
80. Kochenderfer, J.N., et al., *Eradication of B-lineage cells and regression of lymphoma in a patient treated with autologous T cells genetically engineered to recognize CD19.* Blood, 2010. **116**(20): p. 4099-102.
81. Kochenderfer, J.N., et al., *B-cell depletion and remissions of malignancy along with cytokine-associated toxicity in a clinical trial of anti-CD19 chimeric-antigen-receptor–transduced T cells.* Blood, 2012. **119**(12): p. 2709-2720.

82. Brentjens, R.J., et al., *CD19-targeted T cells rapidly induce molecular remissions in adults with chemotherapy-refractory acute lymphoblastic leukemia.* Sci Transl Med, 2013. **5**(177): p. 177ra38.
83. Kalos, M., et al., *T cells with chimeric antigen receptors have potent antitumor effects and can establish memory in patients with advanced leukemia.* Sci Transl Med, 2011. **3**(95): p. 95ra73.
84. Grupp, S.A., et al., *Chimeric antigen receptor-modified T cells for acute lymphoid leukemia.* N Engl J Med, 2013. **368**(16): p. 1509-1518.
85. Sommermeyer, D., et al., *Chimeric antigen receptor-modified T cells derived from defined CD8+ and CD4+ subsets confer superior antitumor reactivity in vivo.* Leukemia, 2016. **30**(2): p. 492-500.
86. Turtle, C.J., et al., *CD19 CAR-T cells of defined CD4+:CD8+ composition in adult B cell ALL patients.* J Clin Invest, 2016. **126**(6): p. 2123-38.
87. Teachey, D.T., et al., *Cytokine release syndrome after blinatumomab treatment related to abnormal macrophage activation and ameliorated with cytokine-directed therapy.* Blood, 2013. **121**(26): p. 5154-7.
88. Fitzgerald, J.C., et al., *Cytokine Release Syndrome After Chimeric Antigen Receptor T Cell Therapy for Acute Lymphoblastic Leukemia.* Crit Care Med, 2017. **45**(2): p. e124-e131.
89. *Tisagenlecleucel (Kymriah) for ALL.* Med Lett Drugs Ther, 2017. **59**(1532): p. 177-178.
90. Ying, Z., et al., *A safe and potent anti-CD19 CAR T cell therapy.* Nat Med, 2019. **25**(6): p. 947-953.
91. Pule, M.A., et al., *Virus-specific T cells engineered to coexpress tumor-specific receptors: persistence and antitumor activity in individuals with neuroblastoma.* Nat Med, 2008. **14**(11): p. 1264-70.
92. Ahmed, N., et al., *Human Epidermal Growth Factor Receptor 2 (HER2) -Specific Chimeric Antigen Receptor-Modified T Cells for the Immunotherapy of HER2-Positive Sarcoma.* J Clin Oncol, 2015. **33**(15): p. 1688-96.
93. Brown, C.E., et al., *Regression of Glioblastoma after Chimeric Antigen Receptor T-Cell Therapy.* N Engl J Med, 2016. **375**(26): p. 2561-9.
94. Louis, C.U., et al., *Antitumor activity and long-term fate of chimeric antigen receptor-positive T cells in patients with neuroblastoma.* Blood, 2011. **118**(23): p. 6050-6.
95. Kershaw, M.H., et al., *A phase I study on adoptive immunotherapy using gene-modified T cells for ovarian cancer.* Clin Cancer Res, 2006. **12**(20 Pt 1): p. 6106-15.
96. Joyce, J.A. and D.T. Fearon, *T cell exclusion, immune privilege, and the tumor microenvironment.* Science, 2015. **348**(6230): p. 74-80.
97. Klebanoff, C.A., L. Gattinoni, and N.P. Restifo, *Sorting through subsets: which T-cell populations mediate highly effective adoptive immunotherapy?* J Immunother, 2012. **35**(9): p. 651-60.
98. Sallusto, F., et al., *Two subsets of memory T lymphocytes with distinct homing potentials and effector functions.* Nature, 1999. **401**(6754): p. 708-12.
99. Masopust, D., et al., *Preferential localization of effector memory cells in nonlymphoid tissue.* Science, 2001. **291**(5512): p. 2413-7.
100. Gebhardt, T., et al., *Different patterns of peripheral migration by memory CD4+ and CD8+ T cells.* Nature, 2011. **477**(7363): p. 216-9.
101. Bottcher, J.P., et al., *Functional classification of memory CD8(+) T cells by CX3CR1 expression.* Nat Commun, 2015. **6**: p. 8306.
102. Kaneko, S., et al., *IL-7 and IL-15 allow the generation of suicide gene-modified alloreactive self-renewing central memory human T lymphocytes.* Blood, 2009. **113**(5): p. 1006-15.
103. Graef, P., et al., *Serial transfer of single-cell-derived immunocompetence reveals stemness of CD8(+) central memory T cells.* Immunity, 2014. **41**(1): p. 116-26.
104. Stemberger, C., et al., *A single naive CD8+ T cell precursor can develop into diverse effector and memory subsets.* Immunity, 2007. **27**(6): p. 985-97.

105. Hinrichs, C.S., et al., *Adoptively transferred effector cells derived from naive rather than central memory CD8+ T cells mediate superior antitumor immunity.* Proc Natl Acad Sci U S A, 2009. **106**(41): p. 17469-74.
106. Klebanoff, C.A., et al., *Determinants of successful CD8+ T-cell adoptive immunotherapy for large established tumors in mice.* Clin Cancer Res, 2011. **17**(16): p. 5343-52.
107. Oren, R., et al., *Functional comparison of engineered T cells carrying a native TCR versus TCR-like antibody-based chimeric antigen receptors indicates affinity/avidity thresholds.* J Immunol, 2014. **193**(11): p. 5733-43.
108. Hinrichs, C.S. and N.P. Restifo, *Reassessing target antigens for adoptive T-cell therapy.* Nat Biotechnol, 2013. **31**(11): p. 999-1008.
109. Bax, D.A., et al., *EGFRvIII deletion mutations in pediatric high-grade glioma and response to targeted therapy in pediatric glioma cell lines.* Clin Cancer Res, 2009. **15**(18): p. 5753-61.
110. Chekmasova, A.A., et al., *Successful eradication of established peritoneal ovarian tumors in SCID-Beige mice following adoptive transfer of T cells genetically targeted to the MUC16 antigen.* Clin Cancer Res, 2010. **16**(14): p. 3594-606.
111. Hudecek, M., et al., *The B-cell tumor-associated antigen ROR1 can be targeted with T cells modified to express a ROR1-specific chimeric antigen receptor.* Blood, 2010. **116**(22): p. 4532-41.
112. Zhang, T., A. Barber, and C.L. Sentman, *Generation of antitumor responses by genetic modification of primary human T cells with a chimeric NKG2D receptor.* Cancer Res, 2006. **66**(11): p. 5927-33.
113. Krenciute, G., et al., *Characterization and Functional Analysis of scFv-based Chimeric Antigen Receptors to Redirect T Cells to IL13Ralpha2-positive Glioma.* Mol Ther, 2016. **24**(2): p. 354-363.
114. Hudecek, M., et al., *Receptor affinity and extracellular domain modifications affect tumor recognition by ROR1-specific chimeric antigen receptor T cells.* Clin Cancer Res, 2013. **19**(12): p. 3153-64.
115. Ghorashian, S., et al., *Enhanced CAR T cell expansion and prolonged persistence in pediatric patients with ALL treated with a low-affinity CD19 CAR.* Nat Med, 2019. **25**(9): p. 1408-1414.
116. Liu, X., et al., *Affinity-Tuned ErbB2 or EGFR Chimeric Antigen Receptor T Cells Exhibit an Increased Therapeutic Index against Tumors in Mice.* Cancer Res, 2015. **75**(17): p. 3596-607.
117. Long, A.H., et al., *4-1BB costimulation ameliorates T cell exhaustion induced by tonic signaling of chimeric antigen receptors.* Nat Med, 2015. **21**(6): p. 581-90.
118. Fujiwara, K., et al., *Impact of scFv structure in chimeric antigen receptor on receptor expression efficiency and antigen recognition properties.* Biochem Biophys Res Commun, 2020.
119. Bridgeman, J.S., et al., *Building better chimeric antigen receptors for adoptive T cell therapy.* Curr Gene Ther, 2010. **10**(2): p. 77-90.
120. Guest, R.D., et al., *The role of extracellular spacer regions in the optimal design of chimeric immune receptors: evaluation of four different scFvs and antigens.* J Immunother, 2005. **28**(3): p. 203-11.
121. James, S.E., et al., *Antigen sensitivity of CD22-specific chimeric TCR is modulated by target epitope distance from the cell membrane.* J Immunol, 2008. **180**(10): p. 7028-38.
122. Hudecek, M., et al., *The nonsignaling extracellular spacer domain of chimeric antigen receptors is decisive for in vivo antitumor activity.* Cancer Immunol Res, 2015. **3**(2): p. 125-35.
123. Pule, M.A., et al., *A chimeric T cell antigen receptor that augments cytokine release and supports clonal expansion of primary human T cells.* Mol Ther, 2005. **12**(5): p. 933-41.
124. Kahlon, K.S., et al., *Specific recognition and killing of glioblastoma multiforme by interleukin 13-zetakine redirected cytolytic T cells.* Cancer Res, 2004. **64**(24): p. 9160-6.
125. Schambach, A., W.P. Swaney, and J.C. van der Loo, *Design and production of retro- and lentiviral vectors for gene expression in hematopoietic cells.* Methods Mol Biol, 2009. **506**: p. 191-205.

126. Tammana, S., et al., *4-1BB and CD28 signaling plays a synergistic role in redirecting umbilical cord blood T cells against B-cell malignancies.* Hum Gene Ther, 2010. **21**(1): p. 75-86.
127. Brocker, T. and K. Karjalainen, *Signals through T cell receptor-zeta chain alone are insufficient to prime resting T lymphocytes.* J Exp Med, 1995. **181**(5): p. 1653-9.
128. Jenkins, M.K., et al., *CD28 delivers a costimulatory signal involved in antigen-specific IL-2 production by human T cells.* J Immunol, 1991. **147**(8): p. 2461-6.
129. Torikai, H., et al., *A foundation for universal T-cell based immunotherapy: T cells engineered to express a CD19-specific chimeric-antigen-receptor and eliminate expression of endogenous TCR.* Blood, 2012. **119**(24): p. 5697-705.
130. Finney, H.M., et al., *Chimeric receptors providing both primary and costimulatory signaling in T cells from a single gene product.* J Immunol, 1998. **161**(6): p. 2791-7.
131. Krause, A., et al., *Antigen-dependent CD28 signaling selectively enhances survival and proliferation in genetically modified activated human primary T lymphocytes.* J Exp Med, 1998. **188**(4): p. 619-26.
132. Finney, H.M., A.N. Akbar, and A.D. Lawson, *Activation of resting human primary T cells with chimeric receptors: costimulation from CD28, inducible costimulator, CD134, and CD137 in series with signals from the TCR zeta chain.* J Immunol, 2004. **172**(1): p. 104-13.
133. Loskog, A., et al., *Addition of the CD28 signaling domain to chimeric T-cell receptors enhances chimeric T-cell resistance to T regulatory cells.* Leukemia, 2006. **20**(10): p. 1819-28.
134. Kawalekar, O.U., et al., *Distinct Signaling of Coreceptors Regulates Specific Metabolism Pathways and Impacts Memory Development in CAR T Cells.* Immunity, 2016. **44**(3): p. 712.
135. Carpenito, C., et al., *Control of large, established tumor xenografts with genetically retargeted human T cells containing CD28 and CD137 domains.* Proc Natl Acad Sci U S A, 2009. **106**(9): p. 3360-5.
136. Morgan, R.A., et al., *Case report of a serious adverse event following the administration of T cells transduced with a chimeric antigen receptor recognizing ERBB2.* Mol Ther, 2010. **18**(4): p. 843-51.
137. Dotti, G., et al., *Design and development of therapies using chimeric antigen receptor-expressing T cells.* Immunol Rev, 2014. **257**(1): p. 107-26.
138. Terakura, S., et al., *Generation of CD19-chimeric antigen receptor modified CD8+ T cells derived from virus-specific central memory T cells.* Blood, 2012. **119**(1): p. 72-82.
139. Salter, A.I., et al., *Phosphoproteomic analysis of chimeric antigen receptor signaling reveals kinetic and quantitative differences that affect cell function.* Sci Signal, 2018. **11**(544).
140. Guedan, S., et al., *Single residue in CD28-costimulated CAR T cells limits long-term persistence and antitumor durability.* J Clin Invest, 2020.
141. Grada, Z., et al., *TanCAR: A Novel Bispecific Chimeric Antigen Receptor for Cancer Immunotherapy.* Mol Ther Nucleic Acids, 2013. **2**: p. e105.
142. Ruella, M., et al., *Dual CD19 and CD123 targeting prevents antigen-loss relapses after CD19-directed immunotherapies.* J Clin Invest, 2016. **126**(10): p. 3814-3826.
143. Fedorov, V.D., M. Themeli, and M. Sadelain, *PD-1- and CTLA-4-based inhibitory chimeric antigen receptors (iCARs) divert off-target immunotherapy responses.* Sci Transl Med, 2013. **5**(215): p. 215ra172.
144. Hegde, M., et al., *Tandem CAR T cells targeting HER2 and IL13Ralpha2 mitigate tumor antigen escape.* J Clin Invest, 2016. **126**(8): p. 3036-52.
145. Tamada, K., et al., *Redirecting gene-modified T cells toward various cancer types using tagged antibodies.* Clin Cancer Res, 2012. **18**(23): p. 6436-45.
146. Kudo, K., et al., *T lymphocytes expressing a CD16 signaling receptor exert antibody-dependent cancer cell killing.* Cancer Res, 2014. **74**(1): p. 93-103.

147. Feldmann, A., et al., *Retargeting of T lymphocytes to PSCA- or PSMA positive prostate cancer cells using the novel modular chimeric antigen receptor platform technology "UniCAR".* Oncotarget, 2017. **8**(19): p. 31368-31385.
148. Stewart-Jones, G., et al., *Rational development of high-affinity T-cell receptor-like antibodies.* Proc Natl Acad Sci U S A, 2009. **106**(14): p. 5784-8.
149. Roybal, K.T., et al., *Engineering T Cells with Customized Therapeutic Response Programs Using Synthetic Notch Receptors.* Cell, 2016. **167**(2): p. 419-432 e16.
150. Roybal, K.T., et al., *Precision Tumor Recognition by T Cells With Combinatorial Antigen-Sensing Circuits.* Cell, 2016. **164**(4): p. 770-9.
151. Srivastava, S., et al., *Logic-Gated ROR1 Chimeric Antigen Receptor Expression Rescues T Cell-Mediated Toxicity to Normal Tissues and Enables Selective Tumor Targeting.* Cancer Cell, 2019. **35**(3): p. 489-503 e8.
152. Lynn, R.C., et al., *c-Jun overexpression in CAR T cells induces exhaustion resistance.* Nature, 2019. **576**(7786): p. 293-300.
153. Brentjens, R.J., et al., *Eradication of systemic B-cell tumors by genetically targeted human T lymphocytes co-stimulated by CD80 and interleukin-15.* Nat Med, 2003. **9**(3): p. 279-86.
154. Kochenderfer, J.N., et al., *Chemotherapy-refractory diffuse large B-cell lymphoma and indolent B-cell malignancies can be effectively treated with autologous T cells expressing an anti-CD19 chimeric antigen receptor.* J Clin Oncol, 2015. **33**(6): p. 540-9.
155. Scholler, J., et al., *Decade-long safety and function of retroviral-modified chimeric antigen receptor T cells.* Sci Transl Med, 2012. **4**(132): p. 132ra53.
156. Davila, M.L., et al., *Efficacy and toxicity management of 19-28z CAR T cell therapy in B cell acute lymphoblastic leukemia.* Sci Transl Med, 2014. **6**(224): p. 224ra25.
157. Lin, T.S., et al., *Phase II study of flavopiridol in relapsed chronic lymphocytic leukemia demonstrating high response rates in genetically high-risk disease.* J Clin Oncol, 2009. **27**(35): p. 6012-8.
158. Norelli, M., et al., *Monocyte-derived IL-1 and IL-6 are differentially required for cytokine-release syndrome and neurotoxicity due to CAR T cells.* Nat Med, 2018. **24**(6): p. 739-748.
159. Hay, K.A., et al., *Kinetics and biomarkers of severe cytokine release syndrome after CD19 chimeric antigen receptor-modified T-cell therapy.* Blood, 2017. **130**(21): p. 2295-2306.
160. Dutcher, J., et al., *Kidney cancer: the Cytokine Working Group experience (1986-2001): part II. Management of IL-2 toxicity and studies with other cytokines.* Med Oncol, 2001. **18**(3): p. 209-19.
161. Turtle, C.J., et al., *Immunotherapy of non-Hodgkin's lymphoma with a defined ratio of CD8+ and CD4+ CD19-specific chimeric antigen receptor-modified T cells.* Sci Transl Med, 2016. **8**(355): p. 355ra116.
162. Gust, J., et al., *Endothelial Activation and Blood-Brain Barrier Disruption in Neurotoxicity after Adoptive Immunotherapy with CD19 CAR-T Cells.* Cancer Discov, 2017. **7**(12): p. 1404-1419.
163. Curran, K.J., H.J. Pegram, and R.J. Brentjens, *Chimeric antigen receptors for T cell immunotherapy: current understanding and future directions.* J Gene Med, 2012. **14**(6): p. 405-15.
164. Doan, A. and M.A. Pulsipher, *Hypogammaglobulinemia due to CAR T-cell therapy.* Pediatr Blood Cancer, 2018. **65**(4).
165. Hacein-Bey-Abina, S., et al., *LMO2-associated clonal T cell proliferation in two patients after gene therapy for SCID-X1.* Science, 2003. **302**(5644): p. 415-9.
166. Lee, D.W., et al., *T cells expressing CD19 chimeric antigen receptors for acute lymphoblastic leukaemia in children and young adults: a phase 1 dose-escalation trial.* Lancet, 2015. **385**(9967): p. 517-528.

167. Park, S., et al., *Micromolar affinity CAR T cells to ICAM-1 achieves rapid tumor elimination while avoiding systemic toxicity.* Sci Rep, 2017. **7**(1): p. 14366.
168. Bordignon, C., et al., *Transfer of the HSV-tk gene into donor peripheral blood lymphocytes for in vivo modulation of donor anti-tumor immunity after allogeneic bone marrow transplantation.* Hum Gene Ther, 1995. **6**(6): p. 813-9.
169. Bonini, C., et al., *HSV-TK gene transfer into donor lymphocytes for control of allogeneic graft-versus-leukemia.* Science, 1997. **276**(5319): p. 1719-24.
170. Berger, C., et al., *Analysis of transgene-specific immune responses that limit the in vivo persistence of adoptively transferred HSV-TK-modified donor T cells after allogeneic hematopoietic cell transplantation.* Blood, 2006. **107**(6): p. 2294-302.
171. Di Stasi, A., et al., *Inducible apoptosis as a safety switch for adoptive cell therapy.* N Engl J Med, 2011. **365**(18): p. 1673-83.
172. Zhou, X., et al., *Long-term outcome after haploidentical stem cell transplant and infusion of T cells expressing the inducible caspase 9 safety transgene.* Blood, 2014. **123**(25): p. 3895-905.
173. Ando, M., et al., *Bortezomib sensitizes non-small cell lung cancer to mesenchymal stromal cell-delivered inducible caspase-9-mediated cytotoxicity.* Cancer Gene Ther, 2014. **21**(11): p. 472-482.
174. Mestermann, K., et al., *The tyrosine kinase inhibitor dasatinib acts as a pharmacologic on/off switch for CAR T cells.* Sci Transl Med, 2019. **11**(499).
175. Serafini, M., et al., *Characterization of CD20-transduced T lymphocytes as an alternative suicide gene therapy approach for the treatment of graft-versus-host disease.* Hum Gene Ther, 2004. **15**(1): p. 63-76.
176. Quast, I., B. Peschke, and J.D. Lunemann, *Regulation of antibody effector functions through IgG Fc N-glycosylation.* Cell Mol Life Sci, 2017. **74**(5): p. 837-847.
177. Vogler, I., et al., *An improved bicistronic CD20/tCD34 vector for efficient purification and in vivo depletion of gene-modified T cells for adoptive immunotherapy.* Mol Ther, 2010. **18**(7): p. 1330-8.
178. Philip, B., et al., *A highly compact epitope-based marker/suicide gene for easier and safer T-cell therapy.* Blood, 2014. **124**(8): p. 1277-87.
179. Introna, M., et al., *Genetic modification of human T cells with CD20: a strategy to purify and lyse transduced cells with anti-CD20 antibodies.* Hum Gene Ther, 2000. **11**(4): p. 611-20.
180. Kieback, E., et al., *A safeguard eliminates T cell receptor gene-modified autoreactive T cells after adoptive transfer.* Proc Natl Acad Sci U S A, 2008. **105**(2): p. 623-8.
181. Wang, X., et al., *A transgene-encoded cell surface polypeptide for selection, in vivo tracking, and ablation of engineered cells.* Blood, 2011. **118**(5): p. 1255-63.
182. Gibson, D.G., *Oligonucleotide assembly in yeast to produce synthetic DNA fragments.* Methods Mol Biol, 2012. **852**: p. 11-21.
183. Conti, C., et al., *Electrostatic interactions in the early events of VSV infection.* Res Virol, 1991. **142**(1): p. 17-24.
184. Arcasoy, S.M., et al., *Polycations increase the efficiency of adenovirus-mediated gene transfer to epithelial and endothelial cells in vitro.* Gene Ther, 1997. **4**(1): p. 32-8.
185. Parish, C.R., *Fluorescent dyes for lymphocyte migration and proliferation studies.* Immunol Cell Biol, 1999. **77**(6): p. 499-508.
186. Davila, M.L., et al., *CD19 CAR-targeted T cells induce long-term remission and B Cell Aplasia in an immunocompetent mouse model of B cell acute lymphoblastic leukemia.* PLoS One, 2013. **8**(4): p. e61338.
187. Brudno, J.N. and J.N. Kochenderfer, *Toxicities of chimeric antigen receptor T cells: recognition and management.* Blood, 2016. **127**(26): p. 3321-30.

188. Schropfer, S., et al., *A Single Effector Protein, AvrRpt2EA, from Erwinia amylovora Can Cause Fire Blight Disease Symptoms and Induces a Salicylic Acid-Dependent Defense Response.* Mol Plant Microbe Interact, 2018. **31**(11): p. 1179-1191.
189. Masuda, S., et al., *Nonlinear Viscoelasticity of Highly Ordered, Two-Dimensional Assemblies of Metal Nanoparticles Confined at the Air/Water Interface.* Langmuir, 2018. **34**(43): p. 13025-13034.
190. Nauerth, M., et al., *Flow cytometry-based TCR-ligand Koff -rate assay for fast avidity screening of even very small antigen-specific T cell populations ex vivo.* Cytometry A, 2016. **89**(9): p. 816-25.
191. Stemberger, C., et al., *Novel serial positive enrichment technology enables clinical multiparameter cell sorting.* PLoS One, 2012. **7**(4): p. e35798.
192. Busch, D.H., et al., *Role of memory T cell subsets for adoptive immunotherapy.* Semin Immunol, 2016. **28**(1): p. 28-34.
193. Sommermeyer, D., et al., *Fully human CD19-specific chimeric antigen receptors for T-cell therapy.* Leukemia, 2017. **31**(10): p. 2191-2199.
194. Guo, Y., et al., *Immunobiology of the IL-15/IL-15Ralpha complex as an antitumor and antiviral agent.* Cytokine Growth Factor Rev, 2017. **38**: p. 10-21.
195. Berger, C., et al., *Proliferation-linked apoptosis of adoptively transferred T cells after IL-15 administration in macaques.* PLoS One, 2013. **8**(2): p. e56268.
196. Mendelsohn, J., *Targeting the epidermal growth factor receptor for cancer therapy.* J Clin Oncol, 2002. **20**(18 Suppl): p. 1S-13S.
197. Hansel, T.T., et al., *The safety and side effects of monoclonal antibodies.* Nat Rev Drug Discov, 2010. **9**(4): p. 325-38.
198. Brentjens, R.J., et al., *Safety and persistence of adoptively transferred autologous CD19-targeted T cells in patients with relapsed or chemotherapy refractory B-cell leukemias.* Blood, 2011. **118**(18): p. 4817-28.
199. *<B cell charackterization.full (1).pdf>.*
200. Pontvert-Delucq S, B.-G.J., Schmitt C, Baillou C, Guichard J, Najman A, Lemoine FM, *Characterization and functional analysis of adult human bone marrow cell subsets in relation to B-lymphoid development.* Blood, 1993.
201. Linette, G.P., et al., *Cardiovascular toxicity and titin cross-reactivity of affinity-enhanced T cells in myeloma and melanoma.* Blood, 2013. **122**(6): p. 863-71.
202. Watanabe, K., et al., *Target antigen density governs the efficacy of anti-CD20-CD28-CD3 zeta chimeric antigen receptor-modified effector CD8+ T cells.* J Immunol, 2015. **194**(3): p. 911-20.
203. Liu, L., et al., *Inclusion of Strep-tag II in design of antigen receptors for T-cell immunotherapy.* Nat Biotechnol, 2016. **34**(4): p. 430-4.
204. Festag, M.M., et al., *Evaluation of a Fully Human, Hepatitis B Virus-Specific Chimeric Antigen Receptor in an Immunocompetent Mouse Model.* Mol Ther, 2019.
205. Yang, Y., et al., *TCR engagement negatively affects CD8 but not CD4 CAR T cell expansion and leukemic clearance.* Sci Transl Med, 2017. **9**(417).
206. Yewale, C., et al., *Epidermal growth factor receptor targeting in cancer: a review of trends and strategies.* Biomaterials, 2013. **34**(34): p. 8690-707.
207. Vazquez-Lombardi, R., et al., *Transient expression of human antibodies in mammalian cells.* Nat Protoc, 2018. **13**(1): p. 99-117.
208. Montoliu-Gaya, L., J.C. Martinez, and S. Villegas, *Understanding the contribution of disulfide bridges to the folding and misfolding of an anti-Abeta scFv.* Protein Sci, 2017. **26**(6): p. 1138-1149.
209. Effenberger, M., et al., *FLEXamers: A Double Tag for Universal Generation of Versatile Peptide-MHC Multimers.* J Immunol, 2019. **202**(7): p. 2164-2171.

210. Lynn, R.C., et al., *High-affinity FRbeta-specific CAR T cells eradicate AML and normal myeloid lineage without HSC toxicity.* Leukemia, 2016. **30**(6): p. 1355-64.
211. Zhong, S., et al., *T-cell receptor affinity and avidity defines antitumor response and autoimmunity in T-cell immunotherapy.* Proc Natl Acad Sci U S A, 2013. **110**(17): p. 6973-8.
212. Drent, E., et al., *A Rational Strategy for Reducing On-Target Off-Tumor Effects of CD38-Chimeric Antigen Receptors by Affinity Optimization.* Mol Ther, 2017. **25**(8): p. 1946-1958.
213. Kalergis, A.M., et al., *Efficient T cell activation requires an optimal dwell-time of interaction between the TCR and the pMHC complex.* Nat Immunol, 2001. **2**(3): p. 229-34.
214. Tian, S., et al., *CD8+ T cell activation is governed by TCR-peptide/MHC affinity, not dissociation rate.* J Immunol, 2007. **179**(5): p. 2952-60.
215. Sidaway, P., *Haematological cancer: Low-dose CAR T cells are safe and effective.* Nat Rev Clin Oncol, 2017. **14**(9): p. 524.
216. Drake, A., et al., *Interleukins 7 and 15 Maintain Human T Cell Proliferative Capacity through STAT5 Signaling.* PLoS One, 2016. **11**(11): p. e0166280.
217. Cieri, N., et al., *IL-7 and IL-15 instruct the generation of human memory stem T cells from naive precursors.* Blood, 2013. **121**(4): p. 573-84.
218. Munger, W., et al., *Studies evaluating the antitumor activity and toxicity of interleukin-15, a new T cell growth factor: comparison with interleukin-2.* Cell Immunol, 1995. **165**(2): p. 289-93.
219. Klebanoff, C.A., et al., *IL-15 enhances the in vivo antitumor activity of tumor-reactive CD8+ T cells.* Proc Natl Acad Sci U S A, 2004. **101**(7): p. 1969-74.
220. Conlon, K.C., et al., *Redistribution, hyperproliferation, activation of natural killer cells and CD8 T cells, and cytokine production during first-in-human clinical trial of recombinant human interleukin-15 in patients with cancer.* J Clin Oncol, 2015. **33**(1): p. 74-82.
221. Davar, D., et al., *High-dose interleukin-2 (HD IL-2) for advanced melanoma: a single center experience from the University of Pittsburgh Cancer Institute.* J Immunother Cancer, 2017. **5**(1): p. 74.
222. Nolz, J.C., et al., *Division-linked generation of death-intermediates regulates the numerical stability of memory CD8 T cells.* Proc Natl Acad Sci U S A, 2012. **109**(16): p. 6199-204.
223. Sowell, R.T., et al., *IL-15 Complexes Induce Migration of Resting Memory CD8 T Cells into Mucosal Tissues.* J Immunol, 2017. **199**(7): p. 2536-2546.